Acta Universitatis Tamperensis 2429

ROLLE RAHIKAINEN

Talin Mechanosensing in the Regulation of Adhesion Complex Composition and Function

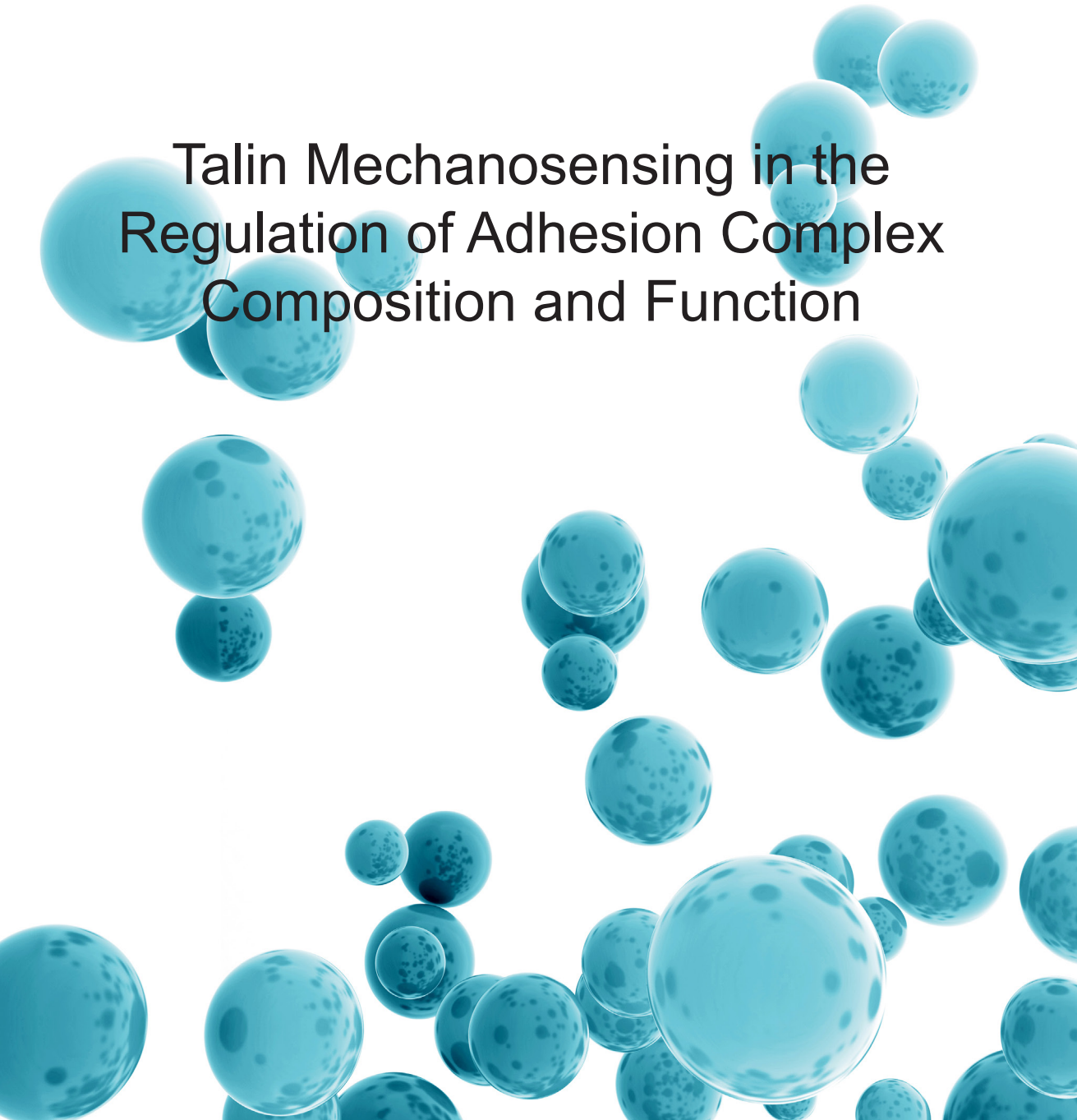

ROLLE RAHIKAINEN

Talin Mechanosensing in the Regulation of Adhesion Complex Composition and Function

ACADEMIC DISSERTATION
To be presented, with the permission of
the Faculty Council of the Faculty of Medicine and Life Sciences
of the University of Tampere,
for public discussion in the Yellow Hall F025
of the Arvo building, Arvo Ylpön katu 34, Tampere,
on 2 November 2018, at 12 o'clock.

UNIVERSITY OF TAMPERE

ROLLE RAHIKAINEN

Talin Mechanosensing in the Regulation of Adhesion Complex Composition and Function

Acta Universitatis Tamperensis 2429
Tampere University Press
Tampere 2018

UNIVERSITY
OF TAMPERE

ACADEMIC DISSERTATION
University of Tampere, Faculty of Medicine and Life Sciences
Finland

Supervised by
Associate Professor Vesa Hytönen
University of Tampere
Finland
Docent Teemu Ihalainen
University of Tampere
Finland

Reviewed by
Professor Pekka Lappalainen
University of Helsinki
Finland
Assistant Professor Haguy Wolfenson
Israel Institute of Technology
Israel

The originality of this thesis has been checked using the Turnitin OriginalityCheck service in accordance with the quality management system of the University of Tampere.

Cover design by
Mikko Reinikka

Acta Universitatis Tamperensis 2429
ISBN 978-952-03-0881-0 (print)
ISSN-L 1455-1616
ISSN 1455-1616

Acta Electronica Universitatis Tamperensis 1940
ISBN 978-952-03-0882-7 (pdf)
ISSN 1456-954X
http://tampub.uta.fi

Suomen Yliopistopaino Oy – Juvenes Print
Tampere 2018

ABSTRACT

All living organisms, and the cells they are composed of, are constantly subjected to a variety of mechanical forces. Some of these forces are external, such as the gravity of the Earth or sound waves transmitted through the air, while some forces are generated by the cells themselves. It is now acknowledged that all cells can sense mechanical forces, or signals, through a process called mechanotransduction. Accordingly, mechanical signals are known to regulate many cellular processes, including growth, proliferation and differentiation. However, many of the molecular mechanisms sensing these ubiquitous cellular signals are still poorly understood.

Talin is a central scaffold protein in integrin-mediated cell adhesions. Talin connects integrin adhesion receptors to the actin cytoskeleton and functions as a cellular mechanosensor. In the work presented here, we investigated the mechanisms mediating talin mechanosensing in cell-matrix adhesions. By modulating the structural and functional properties of talin R3 and R8 subdomains we were able to investigate the mechanisms by which talin rod domain unfolding regulates different cellular functions. We found that the mechanical stability of the R3 subdomain determines its activity in the regulation of many downstream processes, such as traction force generation and cell migration. In addition, we demonstrated that the force-regulated unfolding of the R8 subdomain regulates its interactions with Deleted in liver cancer-1 (DLC1) protein, and they thus constitute a novel force-regulated signaling switch in adhesion complexes. Furthermore, by designing modified talin forms with altered structural properties we dissected the roles of the talin rod domain as a structural scaffold and as a regulator of adhesion signaling. We found that both talin mechanotransmission and mechanotransduction contribute to the regulation of adhesion dynamics and phosphotyrosine signaling. The results presented in here demonstrate that talin mechanosensing is a robust process mediated by multiple parallel mechanisms.

In the last part of this work we investigated the expression levels of talin and vinculin transcripts in atherosclerotic plaques. We found that decreased talin and vinculin expression is a general feature of atherosclerotic plaques and may contribute to the progression of the disease. Furthermore, confocal microscope imaging revealed a loss of talin expression in the plaque *tunica intima*, which may compromise the mechanical stability of the plaque and make it susceptible to rupture.

TIIVISTELMÄ

Kaikkiin eläviin organismeihin ja niitä muodostaviin yksittäisiin soluihin kohdistuu jatkuvasti erilaisia mekaanisia voimia. Jotkut näistä voimista ovat ulkoisia, kuten maan painovoima tai ilmassa kulkevat ääniaallot, kun taas jotkut voimat ovat solujen itsensä tuottamia. Nykyään on selvää, että solut voivat aistia mekaanisia voimia, tai signaaleja, mekanotransduktioksi kutsutun prosessin avulla. Mekaanisten signaalien tiedetäänkin säätelevän useita keskeisiä solubiologian prosesseja, kuten solujen kasvua ja erilaistumista. Tästä huolimatta useimmat mekaanisia voimia aistivat solun rakenteet eli mekanosensorit ovat edelleen varsin huonosti tunnettuja.

Taliini on solun ja soluväliaineen välisten adheesioiden keskeinen rakenneproteiini. Taliini yhdistää adheesioreseptori integriinit solun aktiinitukirankaan, minkä lisäksi taliinin on osoitettu toimivan yhtenä solun mekanosensoreista. Tässä väitöskirjassa esitellyissä tutkimuksissa selvitettiin niitä mekanismeja, joiden avulla taliini osallistuu mekaanisten voimien aistimiseen soluissa. Havaitsimme, että taliinin R3 alayksikön rakenteellinen kestävyys säätelee sen signalointiaktiivisuutta solussa, mikä heijastuu edelleen muun muassa solun voimantuoton ja solumigraation säätelyyn. Lisäksi näytimme, että taliinin R8 alayksikön aukilaskostuminen säätelee sen vuorovaikutusta Deleted in liver cancer-1-proteiinin kanssa, muodostaen näin aiemmin tuntemattoman voimasäädellyn solun signalointikytkimen. Lisäksi tutkimme taliinin tehtäviä adheesion rakenneproteiinina ja mekanosensorina hyödyntämällä rakenteeltaan ja toiminnaltaan muokattuja taliiniproteiinin muotoja. Näiden työkalujen avulla havaitsimme, että sekä mekaanisten voimien välittäminen että taliinin aukilaskostuminen säätelevät adheesiodynamiikkaa ja solun signalointia. Nämä tulokset osoittavat, että taliinivälitteinen mekaanisten voimien aistiminen tapahtuu soluissa useilla rinnakkaisilla ja toisiaan täydentävillä mekanismeilla.

Työn viimeisessä osassa tutkimme taliini- ja vinkuliinigeenien ilmentymistä ateroskleroottisissa plakeissa. Havaitsimme, että taliinin alentunut ilmentyminen on yleinen piirre ateroskleroottisissa plakeissa ja voi osaltaan vaikuttaa taudin etenemiseen. Lisäksi konfokaalimikroskopian avulla havaitsimme taliinin ilmentymisen olevan erityisen alhaista plakin *tunica intimassa*, mikä saattaa vähentää plakin mekaanista kestävyyttä ja altistaa sen repeämiselle.

CONTENTS

LIST OF ORIGINAL COMMUNICATIONS

This thesis is based on the following original communications, referred to in the text by their Roman numerals I-IV:

I. **Rolle Rahikainen***, Magdaléna von Essen*, Markus Schaefer, Lei Qi, Latifeh Azizi, Conor Kelly, Teemu O. Ihalainen, Bernhard Wehrle-Haller, Martin Bastmeyer, Cai Huang, Vesa P. Hytönen (2017). Mechanical stability of talin rod controls cell migration and substrate sensing. Scientific Reports, 7, 3571 (* equal contribution)

II. Alexander William M. Haining*, **Rolle Rahikainen***, Ernesto Cortes, Dariusz Lachowski, Alistair Rice, Magdaléna von Essen, Vesa P. Hytönen†, Armando del Río Hernández† (2018). Mechanotransduction in talin through the interaction of the R8 domain with DLC1. PLoS Biology, 16(7): e2005599 (*, † equal contribution)

III. **Rolle Rahikainen**, Tiina Öhman*, Paula Turkki*, Markku Varjosalo, Vesa P. Hytönen. The transmission of mechanical forces through talin regulates adhesion complex composition and signaling independently of talin rod domain unfolding. Manuscript submitted. (* equal contribution)

IV. Magdaléna von Essen*, **Rolle Rahikainen***, Niku Oksala, Emma Raitoharju, Ilkka Seppälä, Ari Mennander, Thanos Sioris, Ivana Kholová, Norman Klopp, Thomas Illig, Pekka J. Karhunen Mika Kähönen, Terho Lehtimäki, Vesa P. Hytönen (2016). Talin and vinculin are downregulated in atherosclerotic plaque; Tampere Vascular Study. Atherosclerosis, 255, 43-53. (* equal contribution)

ABBREVIATIONS

aa	Amino acid (residue)
Akt	Protein kinase B
ALOX5	Arachidonate 5-lipoxygenase
AP-2	Adipocyte protein 2
ARH	Low density lipoprotein receptor adapter protein 1
CD68	Cluster of differentiation 68
Cdc42	Cell division control protein 42 homolog
cDNA	Complementary DNA
CNN1	Calponin-1
DAB2	Disabled homolog 2
DIC	Differential interference contrast microscopy
DMEM	Dulbecco's modified Eagle medium
Dock1	Dedicator of cytokinesis 1
ECM	Extracellular matrix
Ena	Enabled protein
FA	Focal adhesion
FAK	Focal adhesion kinase
FB	Fibrillar adhesion
FERM	Band 4.1, Ezrin, Radixin, Moesin-domain
Fn	Fibronectin
FX	Focal complex
GAP	GTPase activating protein
GEF	Guanine nucleotide exchange factor
IAC	Integrin adhesion complex
IF	Immunofluorescence
IHC	Immunohistochemistry
LITA	Left internal thoracic artery
MAPK	Mitogen-activated protein kinase
MD	Molecular dynamics
MEF	Mouse embryonic fibroblast

Mena	Mammalian Ena
MLC2	Myosin light chain 2
MS-MS	Tandem mass spectrometry
NA	Nascent adhesion
PCR	Polymerase chain reaction
PH-domain	Pleckstrin homology domain
$PI(4,5)P_2$	Phosphatidylinositol 4,5-bisphosphate
PI3K	Phosphoinositide 3-kinase
PIPK1γ	Phosphatidylinositol 4-phosphate 5-kinase 1γ
PKC	Protein kinase C
PTB	Phosphotyrosine-binding
pY	Phosphotyrosine
Rac1	Ras-related C3 botulinum toxin substrate 1
Ras	Ras GTPase
RGD	Arginine-glycine-aspartate tripeptide
RhoA	Ras homolog gene family, member A
RIAM	Rap1-GTP-interacting adapter molecule
ROCK	RhoA-kinase
RT	Room temperature
SAM	Sterile alpha motif
SDS-PAGE	Sodium dodecyl sulfate-polyacrylamide gel electrophoresis
SH2	Src homolog 2 –domain
smAFM	Single molecule atomic force microscopy
SMD	Steered molecular dynamics
SMTN	Smoothelin
Src	Src tyrosine kinase
START	Steroidogenic acute regulatory –related lipid transfer domain
TVS	Tampere Vascular Study
VASP	Vasodilator stimulated phosphoprotein
Vn	Vitronectin
VSMC	Vascular smooth muscle cell
WB	Western blot

1 INTRODUCTION

The astonishingly complex organization of multicellular organisms is dependent on the tightly coordinated interplay of cells. This interplay is controlled by cellular signaling, where cells transmit and receive messages to and from their neighboring cells. Some of these signals promote cellular processes such as cell survival, proliferation and differentiation, while some may be blunt requests for another cell to simply die (Elmore, 2007). Although possibly tragic from the perspective of an individual cell, strict adherence to this regulation is required for the functioning of the organism as a whole. Accordingly, alterations in the cellular signals can negatively affect the coordinated interplay of cells and may thus be manifested as various diseases such as cancer, where the cancer cells disregard the inhibiting signals sent by their concerned neighbors.

Traditionally, the signals mediating cellular communication have been considered to be either chemical or electrical. However, during the past two decades, mechanical signals have emerged as ubiquitous mediators of cellular signaling (Orr *et al.*, 2006; Wang and Thampatty, 2006). It is now clear that in most cell types, mechanical signals function in parallel with biochemical and electrical signals to regulate cellular functions. In comparison to chemical and electrical signals, the non-material nature of mechanical signals grants them some unique properties. As most tissues are naturally mechanically connected, the transmission of mechanical signals does not require specialized transmitting cells or molecules, like in the case of electrical signals transmitted by neurons or hormones secreted by endocrine cells. In addition, unlike biomolecules, mechanical signals are independent of the rate of diffusion and can therefore facilitate rapid signaling over long distances within a cell, a tissue or a complete organism (Ma *et al.*, 2013). Importantly, different types of cells can respond to mechanical signals of vastly different magnitudes and forms, which facilitates the concurrent regulation of different biological processes in different tissues.

The importance of mechanical signals in the regulation of cellular processes is highlighted by the wide spectrum of diseases associated with altered mechanosignaling (Jaalouk and Lammerding, 2009; Hoffman, Grashoff and

Schwartz, 2011). These 'mechanotransduction disorders' comprise a diverse group of diseases and pathological conditions ranging from congenital deafness to the development and progression of atherosclerosis or cancer (Jaalouk and Lammerding, 2009). Although many of these diseases share little similarities at first sight, the defective cellular mechanisms contributing to their development are often related to the same structures. Cellular mechanosignaling is critically dependent on both the transmission of mechanical cues and their integration with biochemical and electrical signals. Consequently, mutations in the proteins required for these processes or changes in their expression level can lead to defects in the sensing of mechanical signals. The wide variety of diseases caused by dysregulated mechanical signaling suggests that mechanical signals likely regulate the functions of most, if not all, types of cells in the human body. In the future, identifying the structures sensing mechanical signals in different cellular contexts and investigating the molecular details of their function may help to predict and prevent the development of various mechanotransduction disorders.

This thesis work aimed to shed light on the roles of a protein called talin in cellular mechanosignaling. Talin is one of the most central cell adhesion proteins and has been demonstrated to function as an intracellular sensor of mechanical tension. However, the structure-function relationship in the talin protein and the interlinked mechanisms acting in talin mechanosensing have remained incompletely understood. In this work, the mechanisms of talin mechanosensing were investigated *in cellulo* and *in silico* by modulating different structural and functional features of the talin protein. In addition, in an attempt to better understand the role of talin in vascular mechanobiology, we investigated the expression levels of talin-1, talin-2 and vinculin transcripts in atherosclerotic plaques.

2 REVIEW OF THE LITERATURE

2.1 Mechanosignaling

All cells and tissues are constantly subjected to a variety of mechanical stimuli. Some of these mechanical stimuli are external, while some are caused by the cells themselves. Importantly, all living organisms can sense different kinds of mechanical stimuli (Kung, 2005; Orr *et al.*, 2006). For example, plants can direct the growth of their sprouts and roots according to the gravity of the Earth or strengthen their stems in response to swinging in the wind (Fasano, Massa and Gilroy, 2002; Monshausen and Gilroy, 2009; Kurusu *et al.*, 2013). Many unicellular organisms can sense touch and react to it in a different ways, such as initiating cell division or swimming away from the point of contact (Perbal and Driss-Ecole, 2003; Ellison and Brun, 2015). In multicellular organisms, mechanical forces regulate a multitude of processes at the levels of individual cells, tissues, organs and complete organisms. For example, mechanical forces are known to be critical regulators of cell differentiation and tissue organization during the embryonic development of mammals (Discher, Janmey and Wang, 2005; Orr *et al.*, 2006). In adults, mechanical forces are involved in maintaining the homeostasis of tissues such as vasculature, muscles and bones (Hahn and Schwartz, 2009; Huang, Akaishi and Ogawa, 2012). Also many human senses, including hearing, touch and the sense of balance, are dependent on the sensing of mechanical forces in specialized mechanosensory cells (Kung, 2005; Delmas, Hao and Rodat-Despoix, 2011).

The cellular responses to mechanical forces generally function on two different timescales (Chiquet *et al.*, 2009). The long-term of effects of mechanical forces result from the integration of mechanical signals over long periods of time, leading to a slow gradual change in the functional or structural properties of the tissue. For example, as first found over a century ago, physical exercise affects the structure and mineralization density of bones (Wolff, 1892; Xiao and Quarles, 2015). Ultimately, many of these delayed responses to mechanical signals act to regulate tissue homeostasis and human physiology. Although this kind of long-term sensing of mechanical signals is most apparent in the case of bone and muscle remodeling,

similar regulation of tissue structure by mechanical forces has been discovered from other tissues as well (Hahn and Schwartz, 2009; Kolahi and Mofrad, 2010; Humphrey, Dufresne and Schwartz, 2014). In addition to these integrated responses, mechanical signals can affect cellular functions on a very short time scale, such as in the activation of the sensory neurons in response to sound, touch or change in balance (Chiquet *et al.*, 2009; Delmas, Hao and Rodat-Despoix, 2011). Although some of the effects of mechanical forces on human physiology have been known for decades, only recently the vast extent of mechanical regulation of cells has gained widespread attention (Chiquet *et al.*, 2009). The emerging field focusing on how mechanical forces regulate the functions of living cells and tissues is now collectively called mechanobiology, while the role of these forces in cellular signaling is studied on the field of mechanosignaling.

2.1.1 Mechanotransmission and mechanotransduction

Mechanosignaling is dependent on both the transmission and transduction of mechanical signals. Mechanotransmission covers the processes transmitting mechanical signals between tissues, cells or locations within individual cells. In multicellular organisms, mechanotransmission allows mechanical signals to simultaneously act on cells far away from each other (Ma *et al.*, 2013). Thus, mechanical forces can regulate both local and long-distance signaling and allow rapid responses to the signal in different parts of the tissue (Kolahi and Mofrad, 2010). This is most apparent in the case of endothelial cells, where alterations in the shear forces acting on the apical side of the cell can reorient the adhesion complexes connecting the basal side of the cell to the underlying extracellular matrix (Katoh, Kano and Ookawara, 2008). While mechanotransmission delivers the signal from place to place, mechanotransduction is the process of reading the message. The transduction of mechanical signal is dependent on cellular mechanosensors and mechanotransducers, i.e. biomolecules that are able to react to changes in the local mechanical tension or convert it into a biochemical form, respectively (Janoštiak *et al.*, 2014). After the mechanical signal has been transduced into a biochemical form, it is often integrated with signals from other sources. Accordingly, together with biochemical and electrical signals, mechanical signals contribute to the regulation of many critical cellular processes such as cell migration, proliferation and differentiation (Eyckmans *et al.*, 2011). As many mechanosensors can themselves activate downstream signaling, it is often difficult to make a clear distinction between

the sensors responding to the force and the transducers converting it. Furthermore, in the current literature the terms 'mechanotransduction' and 'mechanosensing' are often used interchangeably (Kaminski, Fedorchak and Lammerding, 2014). For simplicity, in this review of the literature, the phenomenon of signal conversion is referred as mechanotransduction, while the proteins acting in both sensing and transducing the signal are collectively called mechanosensors.

2.1.2 Proteins as cellular mechanosensors

Cellular mechanosensing is mediated by biomolecules whose conformation, dynamics or local concentration are modulated in response to mechanical forces. Mechanically induced changes in the conformation of proteins seem to be a general mechanism of mechanosensing and widely utilized in the nature (Hytönen and Wehrle-Haller, 2014). Accordingly, with the exception of glycocalyx proteoglycans and mechanosensory lipid bilayers, practically all of the currently known mechanosensors are either polypeptides, proteins or protein complexes (Janmey and Weitz, 2004; Tarbell and Pahakis, 2006; Eyckmans *et al.*, 2011). As the folding of proteins is driven by the minimization of free energy, the folded, active conformation of a protein typically represents a local energetic minimum. Conversely, external forces deflecting a protein away from this state are likely to affect the functionality of the protein. Therefore, most proteins are naturally mechanosensitive (Orr *et al.*, 2006). However, it seems that in most cases specialized force-sensitive proteins have evolved to function as cellular mechanosensors, rather than mechanically regulating the bulk of the cellular proteins.

Depending on the type of the tissue or cell, the mechanical forces acting on human cells can be largely different in nature. For example, the chondrocytes in cartilage can experience stresses up to 20 MPa and respond to them by regulating the expression of glycosaminoglycans, while endothelial cells must be able to sense changes in shear stresses below 1 Pa (Janmey and Weitz, 2004). Furthermore, mechanical signals can either be static (gravity), oscillating (blood pressure) or single pulses (touch) (Orr *et al.*, 2006; Chiquet *et al.*, 2009). Accordingly, the mechanosensory proteins sensing these signals are a diverse group of proteins that often share little structural similarities and no common evolutionary background. The responses of some mechanosensitive proteins are qualitative, such as the exposure of mechanically regulated protein interaction sites, while some are quantitative, such as the modulation of enzyme kinetics in response to mechanical

forces (Sukharev and Sachs, 2012). Mechanosensory proteins also differ in their sensitivity to different force ranges, the desensitization time during continued mechanical stimuli and regeneration after relaxation. Consequently, many mechanosensory proteins are able to sense only certain types of mechanical signals (Orr *et al.*, 2006). To satisfy the requirement of sensing different types of mechanical stimuli, cells typically express many different kinds of mechanosensory proteins (Eyckmans *et al.*, 2011). In addition, the same mechanical signal can be simultaneously transduced by different mechanosensors in different cellular locations, thus regulating different signaling pathways and responses (Eyckmans *et al.*, 2011).

Mechanosensitive ion channels are the most studied group of cellular mechanosensors and, as such, warrant closer attention (Gillespie and Walker, 2001). These large protein complexes respond to mechanical forces by the opening of a membrane-embedded ion channel. The resulting flow of specific ions between different cellular compartments causes rapid changes in the local ion concentrations and membrane potential. Accordingly, mechanosensitive ion channels are the fastest known class of cellular mechanosensors (Sukharev and Sachs, 2012). Although mechanosensitive ion channels are a diverse group of protein complexes with different biophysical properties, their activation seems to employ either of two distinct mechanisms: lipid bilayer stretching or tether-mediated channel opening (Delmas and Coste, 2013). Many of the ion channels sensitive for lipid bilayer stretching function to relieve excess osmotic pressure acting on cells (Martinac, 2004; Sukharev and Sachs, 2012). Osmotic swelling of cells causes stretching and thinning of the cell membrane, which exposes hydrophobic patches on the outer surfaces of the channel proteins (Martinac, 2004). This hydrophobic mismatch drives the reorganization of the channel subunits to reach a new energetic minimum, which opens the channel and initiates a flux of ions across the membrane. The second mechanism regulating the opening of mechanosensitive channels is dependent on extracellular or intracellular tethers attached to the channel subunits (Gillespie and Walker, 2001). The forces transmitted by these tethers affect the organization of the channel subunits and their relative positions within the lipid bilayer, resulting in the opening of the ion channel. For example, the mechanosensitive ion channels involved in the hearing sensation generated in the organ of Corti are thought to function in this way, although the current understanding of this specialized ion channel complex is still incomplete (Fuchs, 2015; Wu *et al.*, 2017).

Taken together, it is apparent that cells utilize a wide variety of mechanosensors to detect mechanical stimuli. While some of these mechanosensors are likely to function universally in most human cells, the expression of some specific mechanosensors is restricted to certain specialized cell types. Although the importance of mechanosignaling in the regulation of many cellular functions has gained widespread interest during the past few decades, the mechanisms of function for many mechanosensory proteins remain to be fully understood (Eyckmans *et al.*, 2011).

2.2 Cell-matrix adhesions as anchoring points and signaling hubs

2.2.1 The types of cell-matrix adhesions

The structural integrity of tissues is dependent on the attachment of cells to each other and to the surrounding extracellular matrix (ECM). This attachment is mediated by different kinds of cell adhesions. Cell adhesions are typically classified into four main classes based on their structural and functional properties: (1) anchoring junctions, (2) occluding junctions, (3) channel forming junctions and (4) signal relaying junctions (Alberts *et al.*, 2002). Adhesions belonging to each class are specialized in different functions in the body. For example, anchoring junctions (focal adhesions, adherens junctions, desmosomes and hemidesmosomes) are specialized in the transmission of mechanical forces, while occluding junctions act to form an impermeable barrier between neighboring epithelial cells (Gumbiner, 1996). In addition to their important function in mechanically anchoring cells, cell adhesions are signaling hubs transmitting chemical and mechanical signals between cells and their surroundings. Cell adhesions also modulate these signals and they are typically sites of convergence for different signaling pathways. In the case of signal relaying junctions, such as synapses in the nervous system, intercellular signaling is the main function of the cell adhesion. Because of the vastly different properties of the different types of cell adhesions, most cells form multiple types of adhesions to facilitate their attachment to different extracellular ligands. On the other hand, some adhesion structures are only present in certain specialized types of cells. For example, epithelial cells express E-cadherin adhesion receptors to facilitate their attachment to neighboring cells, while non-epithelial cells express different kinds of adhesion

receptors (Meng and Takeichi, 2009). The expression of specific adhesion molecules in different types of cells restricts their ability to attach to each other or to different matrix proteins. This selective attachment of cells is required for the coordinated formation of tissues during embryonic development and for maintaining the separation of tissues in adults (Fagotto, 2014).

Cell-matrix adhesions are attachment points between cells and the surrounding ECM. As opposed to some types of cell-cell interactions, cell-matrix adhesions are always asymmetrical. Two main types of cell-matrix adhesions are present in humans: hemidesmosomes and focal adhesions. Hemidesmosomes mediate the attachment of epithelial cells to the basal membrane underlying skin epidermis and intestine epithelium (Walko, Castañón and Wiche, 2015). Hemidesmosomes are small and dynamic adhesion complexes that form around specialized α6β4 integrin adhesion receptors bound to basal membrane matrix proteins such as laminins (Tsuruta, Hopkinson and Jones, 2003; Margadant *et al.*, 2008). On the cytosolic side of the cell membrane, scaffolding hemidesmosome proteins link β4-integrins to intermediate filaments, such as the keratin filaments in basal skin keratinocytes. This mechanical linkage completed by the hemidesmosome complex is critical for the integrity of skin and intestine, as illustrated by various skin-blistering disorders where mutations in the proteins constituting the complex prevent its correct assembly and function (Fine *et al.*, 2014). Although recently hemidesmosome complexes have been reported to respond to mechanical forces, the current literature mostly describes hemidesmosomes as mediators of structural cell attachment (Zhang *et al.*, 2011; Walko, Castañón and Wiche, 2015; Ohashi, Fujiwara and Mizuno, 2017).

Focal adhesions are the second type of integrin-mediated cell-ECM adhesions found in many animal cells. Focal adhesions are large and highly dynamic complexes with up to 200 proteins involved in their assembly, maturation and disassembly (Zaidel-Bar and Geiger, 2010; Horton, Astudillo, *et al.*, 2016). The complex structure and the highly dynamic nature of focal adhesions makes it difficult to reliably determine the exact protein composition of the adhesion complex in its different maturation stages. Therefore, the different forms of focal adhesions are usually considered as a continuum of related structures rather than distinct types of protein complexes (Zamir and Geiger, 2001; Parsons, Horwitz and Schwartz, 2010). Nevertheless, four maturation stages of focal adhesions are commonly recognized: nascent adhesions (NA), focal complexes (FX), focal adhesions (FA) and fibrillar adhesions (FB) (Wehrle-Haller, 2012a). Although each of these four maturation stages has its

characteristic structural and functional features, they are often all collectively referred to as focal adhesions to distinguish them from the other types of cell-matrix adhesions, such as hemidesmosomes.

From a structural point of view, focal adhesions connect cytosolic actin filaments to ECM proteins and form a mechanical linkage between the actincytoskeleton and the surrounding tissue (Wehrle-Haller, 2012b). Focal adhesions actively regulate the dynamics of the actin cytoskeleton and can rapidly adapt it to the current requirements of the cell. Focal adhesions are also known to interact with microtubules and intermediate filaments, making focal adhesions convergence points for the regulation of all the three main types of cytoskeletal filaments (Palazzo *et al.*, 2004; Leube, Moch and Windoffer, 2015). In addition to their function as mechanical attachment points, focal adhesions are convergence points of the regulation of many, if not most, cytosolic signaling pathways. In the following sections, the structural and functional properties of integrin adhesion receptors and the formation of integrin-mediated adhesion complexes are described.

2.2.2 The structural features of integrin subunits

The assembly of focal adhesion complexes takes place around adhesion receptors called integrins. Integrins are a group of transmembrane proteins expressed in all human cell types except erythrocytes (De Franceschi *et al.*, 2015). Integrins belong to either of two classes, namely α- and β-integrins, each having its own characteristic features. Both α- and β-class integrins are composed of a large, highly glycosylated extracellular ectodomain, a single helical transmembrane domain and a short cytosolic tail domain. However, the α- and β-classes are structurally and functionally distinct and only partially homologous (Johnson *et al.*, 2009). The functional unit of an integrin is a heterodimer composed of one α-integrin and one β-integrin subunit. In humans, there are 18 α-integrin and 8 β-integrin subunits forming in total 24 functional integrin dimers (Figure 1) (Danen and Sonnenberg, 2003). Each integrin dimer has its characteristic binding affinities for different ECM proteins, which facilitates the selective use of integrin adhesion receptors in different cell types and tissues (Hynes, 2002). In most cases the functions of specific integrin dimers are non-redundant, as demonstrated by the many severe defects caused by the knockouts of specific integrin genes in mice (Hynes, 2002).

The integrin ectodomains are composed of globular subdomains (4-5 in α-integrins, 8 in β-integrins) organized into an elongated structure. Depending on the type of the α-subunit, the main ligand-binding site is located in either of two positions. In integrin dimers containing α1, α2, α10, α11, αL, αM, αX or αD subunits, the ligand binding site is located in the α-I domain of the α-subunit. All other α-subunits lack this domain, thus the integrin dimers containing these subunits bind to their ligands through a homologous β-I domain located in the β-subunit (Shattil, Kim and Ginsberg, 2010). In addition to these binding sites, ECM ligands can interact with other domains in the dimer, such as the β-propeller domain in the α-subunit (Campbell and Humphries, 2011). These synergistic interactions contribute to the ligand specificity and binding affinity of the integrin dimer. The molecular mechanisms of integrin-ligand interactions are classified into four main groups based on the nature of the interaction (Campbell and Humphries, 2011). Of these groups, the best characterized are the interactions with the arginine-glycine-aspartate (RGD)-tripeptide motif present in many ECM proteins including fibronectin and vitronectin. Eight (αVβ1, αVβ3, αVβ5, αVβ6, αVβ8, α5β1, α8β1 and αIIbβ3) of the 24 integrin heterodimers bind to the RGD motif (Humphries, Byron and Humphries, 2006). Due to differences in the fit of the RGD motif to its binding pocket and the synergistic interactions of integrins subunits with other binding sites in the ligand, each of the eight RGD-binding integrin dimers has its characteristic RGD affinity and ligand specificity. Other integrin-ligand interactions belong to one of the following three groups: leucine-aspartate-valine (LDV)-binding integrins, A-domain laminin/collagen binding integrins and Non-A-domain laminins-binding integrins (Humphries, Byron and Humphries, 2006). While the interactions of the LDV-binding integrins are mechanistically similar to the interactions of the RGD-binding integrins, the mechanisms of action for the A-domain-laminin/collagen-binding integrins and the Non-A-domain laminin-binding integrins are still not completely understood (Campbell and Humphries, 2011).

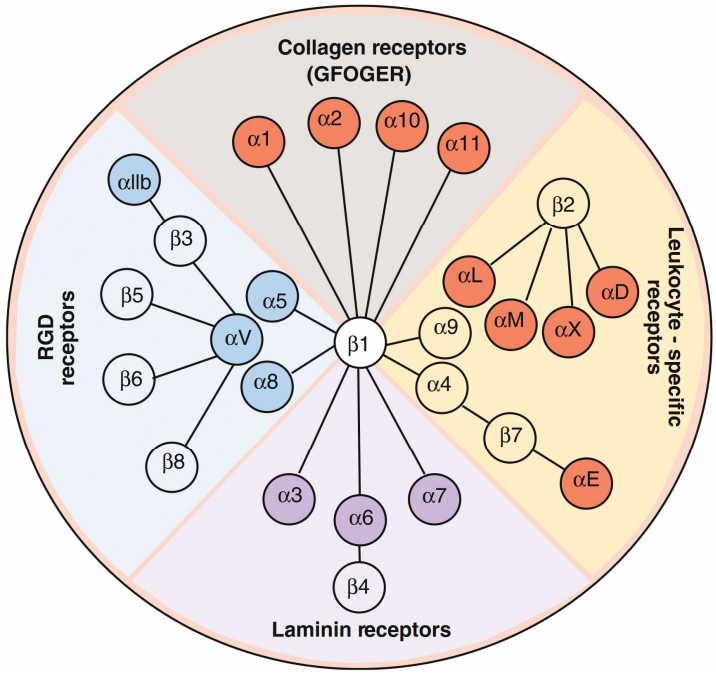

Figure 1. The integrin receptor family. Integrin heterodimers classified according to their major ligand specificity. The RGD motif is the key integrin binding site in many multivalent ECM proteins such as fibronectin and vitronectin. Figure from (Barczyk, Carracedo and Gullberg, 2010) and reproduced with permission from the publisher.

2.2.3 Integrin outside-in and inside-out activation

Integrin dimers can adopt three main conformations regulating their ligand binding and downstream signaling. In their inactive bent conformation, the ectodomains of both α and β integrins are bent back towards the cell plasma membrane (Figure 2) (Campbell and Humphries, 2011). An interaction between glycine residues in the transmembrane helices of the α- and β-subunits (called outer membrane clasp) and an ionic interaction between charged arginine and aspartate residues (called inner membrane clasp) stabilize this bent conformation and inhibit spontaneous integrin activation (Lau *et al.*, 2009; Shattil, Kim and Ginsberg, 2010). Although some integrins may be able to interact with ECM ligands even in their bent conformation, their ligand binding affinity in this conformation is low and the access of large ECM ligands into the binding site likely sterically restricted (Adair *et al.*, 2005). Before their activation, integrin dimers remain at the cell membrane in this inactive conformation ready to be activated and clustered into adhesion sites. The intermediate integrin

conformation is usually referred to as the 'extended-closed' conformation (Wehrle-Haller, 2012a). In this state, both α- and β-ectodomains are in their extended conformation, which allows ECM-ligands to bind to the ligand-binding sites. However, interactions between the transmembrane helices keep the integrin 'legs' closely together, preventing the full activation of the ligand binding sites. This allosteric regulation of integrins by the transmembrane helices and the cytosolic tail domains is a critical mechanism limiting integrin activity (Ginsberg, 2014). Accordingly, full activation of the integrin ligand-binding site is achieved only after the dissociation of the transmembrane helices. Tight spatial and temporal regulation of integrin activation is critical for the correct adhesiveness of many cell types. For example, blood clotting during hemorrhage is dependent on the rapid activation of integrins on the plasma membrane of platelets, while inappropriate activation elsewhere in the vasculature would cause uncontrolled platelet thrombus and result in a stroke (Ginsberg, 2014).

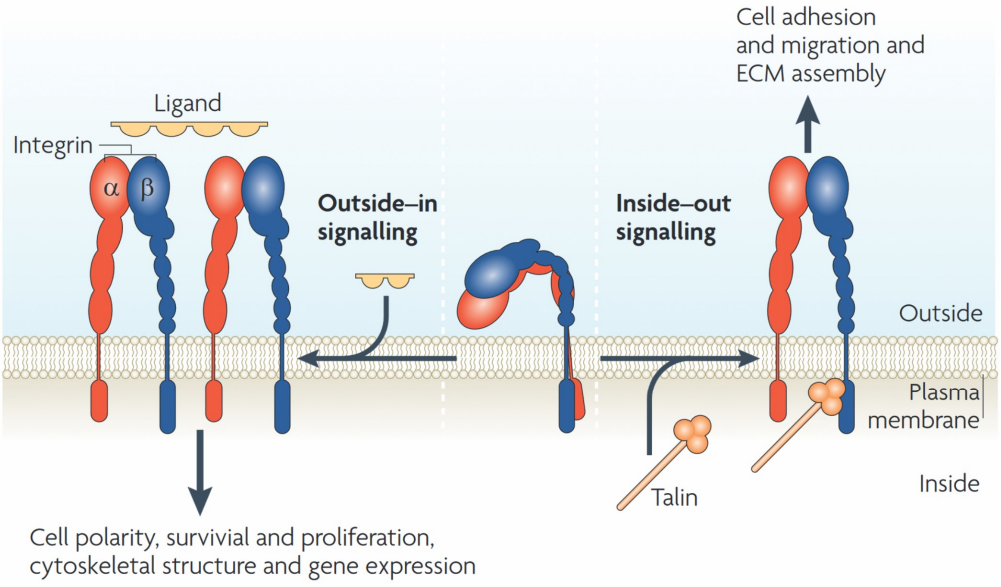

Figure 2. The two mechanisms of integrin activation. Outside-in activation is triggered by the binding of an extracellular ligand to the integrin ligand-binding site (left-hand side). Inside-out activation is dependent on the interactions of integrin tail domains and cytosolic adapter proteins such as talin and kindlin (right-hand side). Figure from (Shattil, Kim and Ginsberg, 2010) and reproduced with permission from the publisher.

Much of the current understanding of integrin activation comes from studies with αIIbβ3 integrins. Although the overall mechanisms governing the activation of different integrin heterodimers seem to be largely similar, some integrin heterodimers are activated through different mechanisms or show different dependence on the activating and inactivating factors (Roca-Cusachs *et al.*, 2009). As an example, the integrins expressed in some adherent cell types (such as α5β1 in fibroblasts) may predominantly be active, while the integrins expressed in the cells in the circulatory system (such as αIIbβ3 in platelets) are inactive by default (Anthis and Campbell, 2011).

Integrin activation can take place through two mechanisms, known as outside-in and inside-out pathways (Figure 2). Although these mechanisms are often described in the literature as separate processes, integrin activation should rather be considered as a dynamic equilibrium with both intracellular and extracellular factors contributing to the overall level of integrin activity (Ye *et al.*, 2013). In some cases, such as at the tips of filopodia in migrating fibroblasts, the inside-out activation dominates, while in other cases the outside-in pathway is more important for the regulation of the overall integrin activity (Galbraith, Yamada and Galbraith, 2007). Moreover, the relative importance of the inside-out and outside-in mechanisms also seems to vary depending on the specific integrin heterodimer (Wehrle-Haller, 2012a). In the outside-in pathway, binding of an extracellular ligand to the integrin ligand-binding site stabilizes the integrin subunits in their extended conformation. This results in the dissociation of the transmembrane helices and allows the recruitment of intracellular adapter proteins (Shattil, Kim and Ginsberg, 2010). As many ECM proteins contain multiple binding sites for integrins, the binding of an extracellular ligand also facilitates integrin clustering and adhesion complex formation (Ye *et al.*, 2013). Although the outside-in activation primes integrins for further activation, it cannot mediate efficient cell adhesion in the absence of the correct intracellular proteins (Wehrle-Haller, 2012a; Theodosiou *et al.*, 2016). In the inside-out activation mechanism, the dissociation of the transmembrane helices is induced by the recruitment of intracellular adapter proteins such as talin and kindlin. Talin and kindlin interact with the cytosolic β-integrin tail domain and contribute to the integrin inside-out activation in a cooperative manner (Theodosiou *et al.*, 2016). Furthermore, talin structurally completes the ligand–integrin–adapter–actin linkage, which allows force transmission between ECM and the cytoskeleton. The transmission of mechanical force contributes to the maintained activation of some β-integrin isoforms through the so-called catch-bond mechanism, where mechanical

tension induces a transition of the integrin headpiece from a low-affinity conformation to a high-affinity conformation (Kong *et al.*, 2009). As explained in detail in the next section, the initial adhesion complex formed by integrins, talin and kindlin either further matures into focal complexes or is rapidly disassembled, depending on the integrated outcome of the local intracellular and extracellular signals.

To maintain the fine balance between inactive and active integrin species, integrin activation is also negatively regulated. Many of the proteins inhibiting integrin activation interact with the cytosolic domains of either α or β-integrins, thus preventing the recruitment of talin and kindlin (Shattil, Kim and Ginsberg, 2010). Proteins interacting with β-integrins typically contain a phosphotyrosine binding domain (PTB-domain) and compete with talin and kindlin for binding to two so-called NxxY motifs in the β-integrin tail domain (Pouwels *et al.*, 2012). Some of these interactions are regulated by the phosphorylation of the NxxY motifs, decreasing the affinity of talin and kindlin and typically increasing the affinity of other β-integrin binding proteins such as DOK1 or tensin (Pouwels *et al.*, 2012). In addition, proteins interacting with α-integrin subunits can also regulate the activation of integrin dimers. For example, SHARPIN and MDGI interact with highly conserved regions in the α-integrin tail domains and prevent the recruitment of talin and/or kindlin proteins to the β-integrin tail domain within the same integrin heterodimer (Nevo *et al.*, 2010; Rantala *et al.*, 2011). In addition to the proteins limiting the activation of integrins at the plasma membrane, integrin endocytosis and selective recycling of inactive integrins effectively regulate the overall level of integrin activity. As mainly inactive integrins are recycled back to the plasma membrane, the level of integrin activity on the cellular scale is dependent on the current level of integrin endocytosis and degradation (Bouvard *et al.*, 2013).

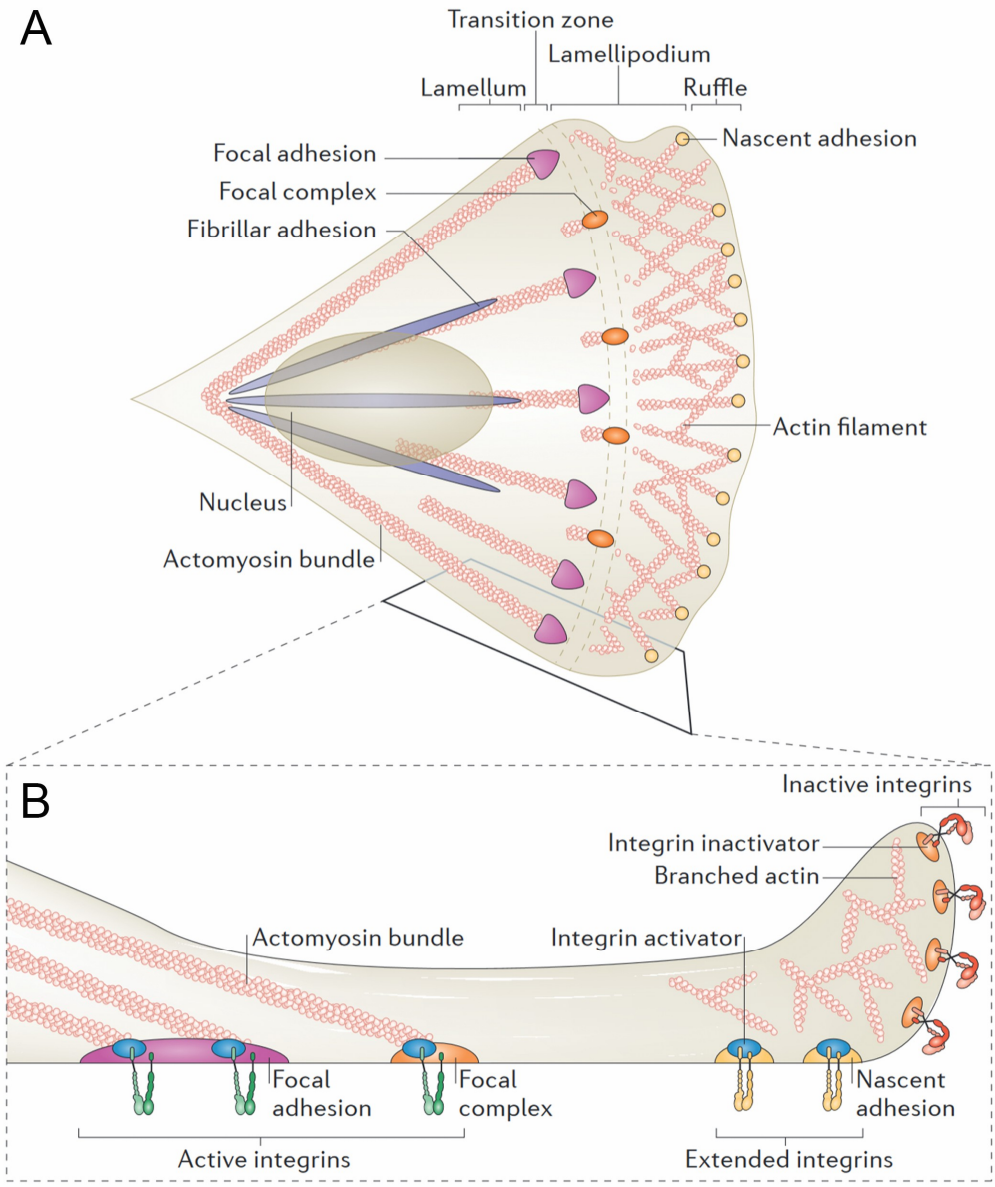

Figure 3. Adhesion complex maturation stages. (A) Nascent adhesions form around activated integrin receptors at the leading edge of the cell lamellipodium. Nascent adhesion maturation to focal complexes, focal adhesions and fibrillar adhesions is tightly controlled by numerous factors, including the level of mechanical tension. (B) The level of integrin activation is controlled by the binding of the integrin ectodomains to extracellular ligands and by recruitment of cytosolic positive and negative regulators. Figure adapted from (Bouvard *et al.*, 2013) and reproduced with permission from the publisher.

2.2.4 Nascent adhesions and adhesion maturation

Nascent adhesions are small, dot-like adhesion complexes that form around the tail domains of activated β-integrins. Nascent adhesions form in an actin polymerization-dependent manner, but independently of myosin activity (Wehrle-Haller, 2012b). In fibroblasts, the formation of nascent adhesion complexes usually takes place either at the front of the lamellipodium or at the tips of protruding filopodia (Figure 3). Nascent adhesions contain a limited set of core adhesion proteins, such as talin, kindlin, Arp2/3, paxillin and focal adhesion kinase (FAK), and they exhibit active adhesion signaling especially through Rac1-dependent mechanisms (Vicente-Manzanares and Horwitz, 2011; Böttcher *et al.*, 2017). Many of the signaling proteins present in nascent adhesions are regulated by tyrosine phosphorylation, which affects their activity and creates docking sites for the recruitment of additional adaptor proteins. The turnover rate of nascent adhesions is typically rapid, and they soon either disassemble or mature into focal complexes. This takes place at a region of active actin depolymerization, located 1-2 μm behind the leading edge of the cell lamellipodium (Figure 3) (Zaidel-Bar, 2003). Various structural and chemical factors can locally regulate the maturation and disassembly of nascent adhesions. These factors include the level of phosphotyrosine signaling and local actin depolymerization by cofilin (Vicente-Manzanares and Horwitz, 2011). In addition, the local phospholipid composition of the cell membrane, especially the presence of $PI(4,5)P_2$ and $PI(3,4)P_2$ phosphoinositides, regulates the recruitment of additional adhesion proteins into nascent adhesions. During nascent adhesion maturation, the adhesion complex grows in size and elongates in the direction perpendicular to the edge of the lamellipodium. This initial maturation stage is called focal complex (FX). Unlike nascent adhesions, focal complexes are bound to contractile actomyosin filaments and they can further mature into focal adhesions (FA) in a process dependent on active myosin contraction (Ballestrem *et al.*, 2001; Zaidel-Bar, 2003; Choi *et al.*, 2008). Focal complexes and focal adhesions are heterogeneous groups of adhesion structures along the adhesion maturation continuum, making it difficult to make a clear distinction between these adhesion classes (Vicente-Manzanares and Horwitz, 2011). However, as focal adhesion proteins vinculin, zyxin and tensin are generally absent from focal complexes, they are considered to be specific markers of mature focal adhesions (Zaidel-Bar, 2003).

2.2.5 Focal adhesions and adhesion signaling

Similarly to focal complexes, focal adhesions are highly dynamic and variable intracellular structures. The core adhesome of focal adhesions contains nearly 200 different proteins (Zaidel-Bar and Geiger, 2010). However, altogether the number of adhesion-associated proteins in the different structural states well exceeds 2000, underscoring the complexity of these adhesion structures (Horton *et al.*, 2015). The molecular composition of focal adhesions is constantly changing to facilitate the rapid spatiotemporal regulation of cell attachment and force generation. Accordingly, even in apparently static adhesions, most adhesion proteins exhibit rapid turnover with protein exchange half times in the range of seconds to tens of seconds (Wehrle-Haller, 2012b). The proteins constituting focal adhesions can be broadly classified into either structural or signaling proteins (Stutchbury *et al.*, 2017). However, many of the structural proteins also execute a variety of signaling functions, and it is often impossible to draw a clear line between these classes.

The structural adhesion proteins such as integrins, talin, vinculin, α-actinin, filamin and tensin form the backbone of the adhesion. By directly or indirectly linking β-integrin tail domains to the actin cytoskeleton, they resist the retrograde flow of actin filaments and allow cells to exert force on the underlying substrate (Parsons, Horwitz and Schwartz, 2010). The engagement of this so-called adhesion clutch causes the polymerization of actin to propel the edge of the lamellipodium forward, which is required for cell spreading and migration (Elosegui-Artola *et al.*, 2016). The transmission of mechanical forces also modulates the dynamics of the structural adhesion proteins, increasing their residence time in the adhesion complex, and thus contributes to adhesion stability (Geiger and Yamada, 2011; Stutchbury *et al.*, 2017). In addition to this regulation of adhesion turnover by mechanical tension, many of the structural adhesion proteins are substrates of various kinases. The phosphorylation and dephosphorylation of the structural proteins typically regulates their recruitment and release, providing a tension-independent way for the regulation of adhesion turnover (Oxley *et al.*, 2008; Anthis, Haling, *et al.*, 2009; Huang *et al.*, 2009; Bays *et al.*, 2014). Conversely, many of the structural adhesion proteins function as scaffolds for adhesion signaling proteins, which mediates the interplay between the structural and signaling functions of the adhesion complex. Of especially high interest are the cases where the application of mechanical tension regulates the interaction between structural and signaling proteins, as in the case of the talin protein. As explained in detail in the following sections, many of the

interactions of talin can only take place in a specific, mechanically-regulated conformation, making talin both a structural protein and a regulator of adhesion signaling.

Focal adhesions are convergence points of both extracellular and intracellular signals and contribute to the regulation of many different signaling pathways. At the heart of adhesion signaling are the non-receptor tyrosine kinases FAK and Src (Geiger and Yamada, 2011). The phosphorylation of specific tyrosine residues in many structural adhesion proteins by FAK and Src creates docking sites for proteins containing phosphotyrosine binding (PTB) and Src homology 2 (SH2) domains. This initiates the tightly controlled and hierarchical recruitment of additional proteins into the adhesion complex. In addition, tyrosine phosphorylation by FAK and Src also directly regulates the activities of many adhesion signaling proteins (Huveneers and Danen, 2009). Many of the target proteins of FAK and Src function as either activators (guanine nucleotide exchange factors, GEFs) or inhibitors (GTPase activating proteins, GAPs) of Rho-family GTPases (Vicente-Manzanares and Horwitz, 2011). Different Rho GEFs and GAPs form a complex network of interacting proteins effectively regulating the actin cytoskeleton. The activation of Rac1 and Cdc42 promotes actin polymerization through the Arp2/3-complex and Ena/VASP-proteins, respectively, while the activation of RhoA increases myosin activity through the phosphorylation of the myosin regulatory light chain by Rho associated protein kinase (ROCK) (Etienne-Manneville and Hall, 2002). Thus, the regulation of adhesion complexes and the cytoskeleton is bidirectional: while the cytoskeletal filaments and their mechanical tension are critical regulators of the structural and functional features of the adhesions complexes, the signals generated by these adhesions are required for the maintenance of the cytoskeleton.

In addition to tyrosine kinases, focal adhesions contribute to the regulation of most, if not all, major signaling pathways. For example, protein kinase C (PKC), phosphatidylinositol 3-kinase (PI3K), mitogen-activated protein kinases (MAP-kinases) and Wnt signaling are all in part regulated by the adhesion complex (Woods and Couchman, 1992; Xia *et al.*, 2004; Geiger and Yamada, 2011; Amin and Vincan, 2012). Together, these pathways regulate many central cellular processes such as cell survival, growth and proliferation. However, the mechanisms of their regulation by the adhesion complex are beyond the scope of this literature review.

2.2.6 Fibrillar adhesions and adhesion complex disassembly

Fibrillar adhesions (FB) are the most matured form of integrin-based cell-matrix adhesions. Compared to focal adhesions, fibrillar adhesions are relatively stable and usually absent from rapidly migrating cells (Parsons, Horwitz and Schwartz, 2010). These large and streak-like adhesions are areas of active ECM remodeling, including fibronectin fibrillogenesis (Vicente-Manzanares and Horwitz, 2011). Accordingly, fibrillar adhesions are enriched in α5β1 integrins specific for fibronectin binding. Many of the adhesion components recruited into focal adhesions are also present in fibrillar adhesions. However, their stoichiometry and spatial distribution may be different (Vicente-Manzanares and Horwitz, 2011). Moreover, the active phosphotyrosine-signaling seen in focal complexes and focal adhesions is largely absent from fibrillar adhesions. Mature fibrillar adhesions are often rich in tensin and contain decreased levels of talin (Geiger and Yamada, 2011). During adhesion maturation from focal adhesion to fibrillar adhesion, talin is likely replaced by tensin, which may reflect the changed requirements for the structural and functional properties of these adhesions types (Georgiadou *et al.*, 2017). Similarly to talin in focal adhesions, tensin functions as both a structural scaffold and as a signaling hub in fibrillar adhesions. Accordingly, adhesion-localized tensin can drive the recruitment of various mediators of phosphotyrosine signaling, such as FAK, Src, p130Cas and paxillin into the adhesion complex (Lo, 2017). Although both talin and tensin contribute to the recruitment of the same signaling proteins, the cellular effects of their recruitment into focal adhesions and fibrillar adhesions seems to be somewhat different. Interestingly, tensin proteins have been recently suggested to function as fibrillar adhesion-specific mechanosensors through the force-regulated activation of integrins (Georgiadou *et al.*, 2017). However, the mechanisms mediating tensin mechanosensing remain to be fully understood.

In contrast to the extensively studied mechanisms regulating adhesion formation and maturation, the mechanisms mediating adhesion disassembly have gained relatively little attention. The prevailing view is that depending on the cellular localization and the maturation stage of the adhesion, its disassembly can proceed through one of a few different mechanisms (Vicente-Manzanares and Horwitz, 2011). The initial trigger for adhesion disassembly typically consists of multiple factors, including local changes in the ratios of activated RhoA and Rac1 GTPases, as well as increased $PI(4,5)P_2$ and decreased $PI(3,4,5)P_3$ concentrations at the plasma membrane (Wehrle-Haller, 2012a). Also contractile forces acting on adhesions are known to be

a major regulator to adhesion stability, as illustrated by the classical experiments where the inhibition of myosin motor proteins leads to a rapid disassembly of adhesion complexes (Parsons, Horwitz and Schwartz, 2010; Carisey *et al.*, 2013). In addition to myosin-II activity, other factors, such as actin filament crosslinking and stress fiber formation, locally regulate cell contractility and contribute to adhesion stability (Elkhatib *et al.*, 2014). One of the most studied mechanisms of adhesion disassembly is the calpain-mediated cleavage of adhesion complex proteins including β-integrins, talin, FAK, Src and filamin (Pfaff, Du and Ginsberg, 1999; Franco *et al.*, 2004; Chan, Bennin and Huttenlocher, 2010; Xu *et al.*, 2010; Saxena *et al.*, 2017). Calpain cleavage of the structural adhesion proteins releases the tension across the adhesion complex and promotes the dissociation of its protein components. Although calpain cleavage typically accounts only for a fraction of the total turnover of adhesion proteins, it may have a high significance especially in the disassembly of adhesion at the retracting parts of the cell (Huttenlocher *et al.*, 1997; Franco *et al.*, 2004; Chan, Bennin and Huttenlocher, 2010). In contrast, adhesion disassembly in the central parts of the cell typically proceeds through microtubule-dependent mechanisms (Kaverina, Krylyshkina and Small, 1999; Vicente-Manzanares and Horwitz, 2011). Microtubule-induced adhesion disassembly is known to be dependent on the recruitment of FAK and dynamin, which promotes clathrin-dependent endocytosis of integrins and other adhesion complex proteins (Ezratty, Partridge and Gundersen, 2005). In this process, microtubules likely function to target clathrin and endocytosis adapters such as AP-2, DAB2 and ARH to the adhesion complex (Chao and Kunz, 2009; Ezratty *et al.*, 2009). Targeting of the endosome components to the adhesion sites is also regulated by the spatially restricted production of $PI(4,5)P_2$ through adhesion-localized PIPKIβ (De Franceschi *et al.*, 2015). Endocytosis of integrin receptors serves as a way to recycle them and other adhesion proteins, such as talin and FAK, back to the leading edge of the cell, where they can be used as building blocks for the formation of nascent adhesions (Nader, Ezratty and Gundersen, 2016). Interestingly, different integrin isoforms are recycled differently, which may serve as a way to regulate their relative fractions at the plasma membrane (De Franceschi *et al.*, 2015). Moreover, endocytosed integrins have been shown to remain in their active conformation and to activate FAK-mediated downstream signaling (Alanko *et al.*, 2015). However, the exact mechanisms of the endosomal integrin signaling and its role in the regulation of adhesion turnover and cell migration are not yet completely understood (Alanko and Ivaska, 2016; Nader, Ezratty and Gundersen, 2016).

2.3 Talin as an integrin activator and a mechanosensor

Talin is one of the most central proteins in cell-matrix adhesions. It forms a direct mechanical linkage between integrin adhesion receptors and the cytoskeleton and thus critically contributes to the integrity of the tissue. Talin is also an important scaffold protein capable of recruiting at least 20 other adhesion proteins to the adhesion complex. Importantly, some of these interactions between talin and other proteins are regulated by mechanical force, making talin a *bona fide* mechanosensor in cell-matrix adhesions. The signals initiated by talin mechanosensing regulate many cellular processes with implications on the levels of both individual cells and complete tissues. The structural and functional features of this true molecular master of adhesion functions are discussed in the following sections.

2.3.1 The discovery of talin proteins

Talin was first identified in 1983 by Burridge and Connell from lysates of chicken gizzard smooth muscle cells (Burridge and Connell, 1983). Because of its apparent molecular weight of 215 kDa on SDS-PAGE gels, talin was originally called 215K. Antibodies raised in rabbits against this newly identified protein revealed its localization at the termini of actin stress fibers and co-localization with the previously identified adhesion protein vinculin (known as 130K at that time) (Geiger, 1979; Burridge and Connell, 1983). The 215K protein was also found to partially co-localize with fibronectin fibrils on the surface of the cell, leading the authors to the conclusion that 215K is a cell adhesion protein that regulates the organization of actin filaments or mediates their attachment to the cell membrane (Burridge and Connell, 1983). The authors found the prominent localization of the 215K protein in the interface of actin filaments and adhesion complexes reminiscent of an ankle connecting leg and foot. Therefore, they proposed the name "talin" for the 215K protein, derived from the Latin word *talus* meaning an ankle (Burridge and Connell, 1983).

The apparent co-localization of intracellular actin filaments and extracellular fibronectin fibrils led to the idea that specific transmembrane proteins or protein complexes must mediate a connection between actin and fibronectin (Horwitz *et al.*, 1985). However, the proteins mediating this interaction remained unknown until the identification of a fibronectin-specific cell adhesion receptor, called cell-substrate

attachment antigen (CSAT, later found to represent a complete integrin heterodimer) in 1985 (Horwitz *et al.*, 1985; Buck and Horwitz, 1987). Further studies demonstrated that talin directly interacts with both CSAT and actin, thus completing the mechanical linkage from ECM to the cell cytoskeleton and filling the missing piece of the puzzle (Horwitz *et al.*, 1986; Muguruma, Matsumura and Fukazawa, 1990). During the following decade, the rapid development of tools for the genetic modification of animals provided new methods for investigating the functions of talin both in cell culture and in complete model organisms (Critchley, 2005). As discussed next, these studies established the role of talin as a central adhesion protein regulating both the structural composition and signaling of the adhesion complex.

2.3.2 Mammalian talin isoforms and their expression patterns

Talin proteins are widely present in eukaryotes ranging from the slime mold *Dictyostelium discoideum* to multicellular animals such as *Caenorhabditis elegans* and humans. While most animal genomes contain only one talin gene, vertebrate genomes contain two homologous talin genes originating from a gene duplication early in the chordate lineage (McCann and Craig, 1998; Senetar and McCann, 2005). The two talin genes in vertebrates share conserved intron-exon boundaries, but differ in the size and complexity of the intron sequences. The proteins encoded by human *TLN1* and *TLN2* genes share 74% amino acid identity and 84% similarity (Monkley, Pritchard and Critchley, 2001). Most of the less conserved areas are located in the unstructured loops and linkers connecting different talin domains, while many of the known interaction sites of talin are highly conserved between the two human talins (Monkley, Pritchard and Critchley, 2001). Despite the high degree of sequence conservation between talin-1 and talin-2, their functions in the body seem to be non-redundant. Talin-1 is ubiquitously expressed in most human tissues except brain and striated muscle, while talin-2 is predominantly expressed in brain, striated muscle and cardiac muscle (Critchley, 2005; Senetar and McCann, 2005). The gene encoding talin-2 was identified more than 15 years after the discovery of talin-1, mainly because of the more restricted tissue specific expression of talin-2 and the lack of suitable expressed sequence tag libraries available at that time (Monkley, Pritchard and Critchley, 2001). Therefore, all of the initial efforts to understand talin function were unaware of the presence of two closely related and partially complementary talin proteins in mammalian cells. After the identification of talin-2 in 2001 by Susan Monkley and her co-workers, the understanding of the distinct

functions and biochemical properties of talin-1 and talin-2 has steadily accumulated (Monkley, Pritchard and Critchley, 2001; Conti *et al.*, 2009; Debrand *et al.*, 2009; Manso *et al.*, 2013, 2017; Austen *et al.*, 2015).

As demonstrated by early talin-1 knockout experiments with non-differentiated mouse embryonic stem cells, talin-1 is required for normal adhesion complex formation, cell spreading and polarization (Priddle *et al.*, 1998). Accordingly, further studies aiming at breeding homozygous talin-1 knockout mice were unsuccessful due to the embryonal lethality of the knockout mice at 8.5 days after fertilization. This indicated that the loss of talin-1 compromises the correct functionality of integrins during gastrulation (Monkley *et al.*, 2000). In contrast to talin-1 knockout mice, homozygous talin-2 knockout mice were viable and fertile (Debrand *et al.*, 2009, 2012). However, the talin-2 null mice were found to suffer from mild muscular dystrophies, indicating that talin-2 may be specifically required for the development and remodeling of muscle tissue. (Debrand *et al.*, 2012). Accordingly, the expression of the *TLN2* gene has been demonstrated to be induced during muscle cell differentiation. Furthermore, talin-2 localizes into intercalated discs and myotendinous junctions in striated muscle cells of adult mice, suggesting it has muscle-specific functions (Senetar, Moncman and McCann, 2007). Interestingly, talin-2 has also been found to have an unusually high binding affinity for both the muscle-specific type of actin and the integrin β1D isoform expressed in muscle cells (Senetar and McCann, 2005; Anthis *et al.*, 2010; Qi *et al.*, 2016). These high binding affinities may have evolved to withstand the high mechanical tension in the myotendinous junctions. More recent studies have demonstrated that while talin-2 is likely the main talin isoform expressed in adult myocardium, expression of talin-1 is still required for efficient recovery of the tissue after mechanical or pharmacological stress (Manso *et al.*, 2013, 2017).

Taken together, talin-1 and talin-2 share many structural and functional properties. However, they seem to execute somewhat different, isoform-specific functions both during the embryonic development and in adult tissues. Although recent studies have discovered the biochemical basis for some of these isoform-specific functions, additional studies will be required to completely understand the roles of talin-1 and talin-2 at the levels of both individual cells and complete tissues (Austen *et al.*, 2015; Qi *et al.*, 2016). As a large majority of the studies focusing on the biochemical properties of talin proteins have been conducted by using talin-1, in the following sections the term 'talin' refers to the talin-1 protein unless otherwise stated.

2.3.3 The domain structure of talin

Human talin-1 is a 2541 amino-acid protein with molecular mass of roughly 270 kDa. Talin comprises a globular head domain (~430 amino acid residues) and an elongated rod domain (~2000 residues) (Critchley, 2009). The talin head domain is divided into four subdomains called F0, F1, F2 and F3 (Figure 4). The head domain binds to β-integrin cytosolic tail domains and interacts with numerous adhesion proteins, including focal adhesion kinase (FAK), layilin, phosphatidylinositol 4-phosphate 5-kinase type Iγ (PIPKIγ), T lymphoma invasion and metastasis protein 1 (TIAM1), Rap1, Rap1-GTP interacting adaptor molecule (RIAM) and F-actin (Figure 4) (Di Paolo *et al.*, 2002; Ling *et al.*, 2002; Han *et al.*, 2006; Goult *et al.*, 2010; Lawson *et al.*, 2012; Wang *et al.*, 2012; Yang *et al.*, 2014). In addition, the talin head domain interacts with $PI(4,5)P_2$ phospholipids at the inner leaflet of the plasma membrane (Saltel *et al.*, 2009). As discussed in detail below, many of the proteins interacting with the talin head domain regulate its activation and recruitment to β-integrin tail domains. The head domain is connected to the rod domain by an unstructured linker of around 80 residues. The entirely α-helical talin rod domain consists of 62 amphipathic α-helices organized into 13 helical bundles (called R1-R13) with 4-5 α-helices in each bundle (Figure 4) (Goult, Zacharchenko, *et al.*, 2013). The last C-terminal α-helix mediates the antiparallel dimerization of two talin molecules and contributes to actin filament binding together with the actin binding site 3 (ABS3) located in the R13 subdomain (Gingras *et al.*, 2008).

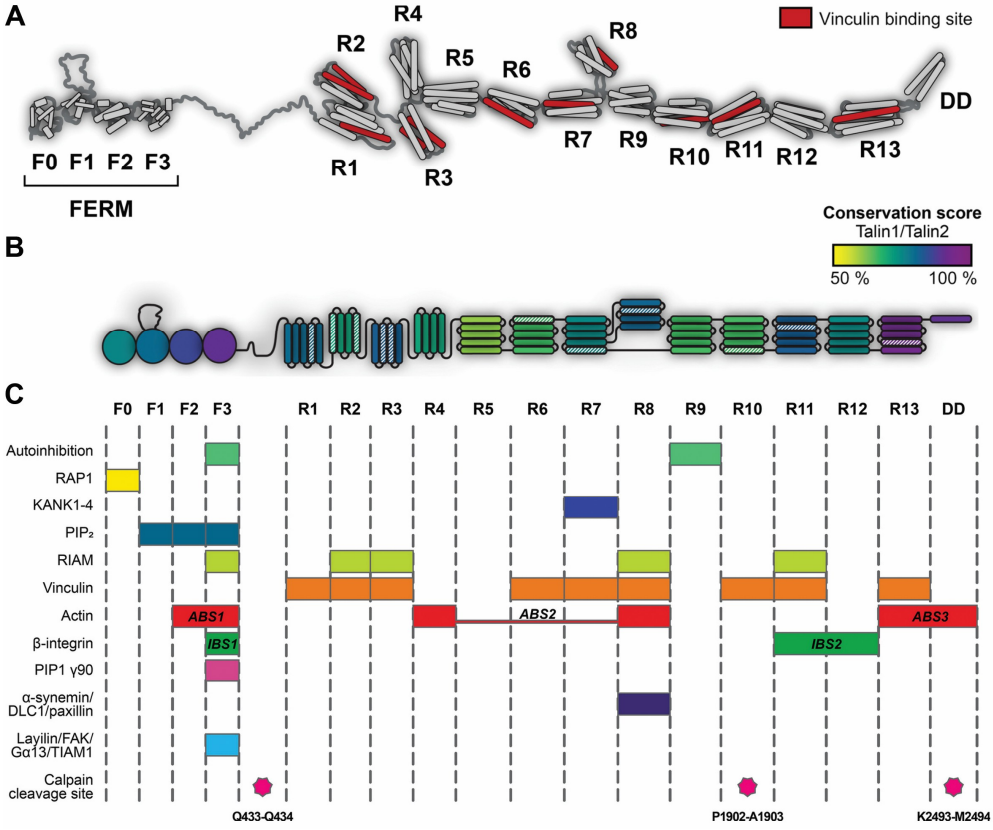

Figure 4. The domain structure and the known interaction partners of talin-1. (A) The talin head domain belongs to the family of FERM proteins and is composed of F0-F3 subdomains. The talin rod is composed of subdomains R1-R13, each of which consists of 4-5 amphipathic α-helices. Vinculin binding helices are colored in red. (B) Sequence conservation for mouse talin-1 and talin-2. The head F3 subdomain (integrin binding site) and the rod R13 (actin binding site ABS3) subdomain are highly conserved. (C) The known interaction partners of talin-1. The interactions of many adhesion proteins binding to the same domain in talin are mutually exclusive. Figure adapted from (Gough and Goult, 2018) and reproduced with permission from the publisher.

2.3.4 Talin autoinhibition and activation

The interaction between the talin head domain and β-integrin tail domain is regulated at multiple levels, including intramolecular autoinhibition of talin. Talin autoinhibition is known to be required for the correct morphogenesis of Drosophila embryos, suggesting that the activation of talin by its release from the autoinhibited conformation is the rate-limiting step of adhesion formation (Ellis *et al.*, 2013; Klapholz and Brown, 2017). In its autoinhibited conformation, talin exists as an

antiparallel dimer folded into a compact, circular structure. The head domains of both talin molecules are likely buried in the center of the doughnut-shaped structure (Goult, Xu, *et al.*, 2013). This interaction masks both the C-terminal actin binding site and the talin head β-integrin binding site and thus simultaneously inhibits actin and integrin binding. The intramolecular interaction stabilizing this autoinhibited conformation takes place between the F3 subdomain of the talin head and specific negatively charged residues in the talin rod R9 subdomain (Goksoy *et al.*, 2008; Goult *et al.*, 2009; Zhang *et al.*, 2016). Accordingly, a single point mutation in either the talin rod domain (E1770A) or the head domain (M319A) disrupts this autoinhibition and activates talin (Goksoy *et al.*, 2008; Goult *et al.*, 2009; Ellis *et al.*, 2013; Zhang *et al.*, 2016). In addition to this well-characterized interaction, talin contains other intramolecular interactions regulating its functions. For example, the head domain has been shown to interact with the talin rod R2-3 subdomains, which may regulate the recruitment of talin to the plasma membrane (Banno *et al.*, 2012). As discussed in detail in the following paragraphs, also many of the interactions of the talin rod domain are negatively regulated by their flanking α-helices or complete rod subdomains (Critchley, 2005; Atherton *et al.*, 2015).

For talin to activate integrins, it must be brought close to the plasma membrane and released from its autoinhibited conformation. It seems probable that before its activation, talin is first recruited to the plasma membrane to avoid its binding randomly to cytosolic actin filaments (Klapholz and Brown, 2017). The best understood mechanism of talin activation is an electrostatic interaction between acidic phospholipids, specifically $PI(4,5)P_2$, and positively charged patches in the talin head F2 and F3 subdomains (Martel *et al.*, 2001; Anthis, Wegener, *et al.*, 2009; Goult *et al.*, 2010; Song *et al.*, 2012). Importantly, PIPKIγ, the kinase responsible for the local production of $PI(4,5)P_2$, directly binds to the talin head F3 subdomain (Di Paolo *et al.*, 2002; Ling *et al.*, 2002). Although the recruitment of PIPKIγ to the talin head does not activate talin itself, it induces the local production of $PI(4,5)P_2$ at the inner leaflet of the plasma membrane (Goksoy *et al.*, 2008). The negative charge of the $PI(4,5)P_2$ phospholipids attracts the positively charged patches in the talin head F1, F2 and F3 subdomains and simultaneously repels negatively charged areas in the talin rod R9 subdomain (Song *et al.*, 2012). This push-pull mechanism forces the extension of the talin rod domain and activates talin in response to an increased concentration of $PI(4,5)P_2$ at the plasma membrane. Indeed, $PI(4,5)P_2$ has been shown to be a potent activator of talin and to greatly enhance the interaction between the talin head domain and β-integrins tail domains also *in vitro* (Martel *et al.*, 2001).

Another mechanism of talin recruitment is *via* its interactions with the Mig10/RIAM/Lamellipodia-family (MRL) protein RIAM. Talin contains multiple RIAM binding sites along its length. Specifically, the F3 subdomain in the talin head and the R2, R3, R8 and R11 subdomains in the rod are known to interact with RIAM (Han *et al.*, 2006; Lee *et al.*, 2009; Goult, Zacharchenko, *et al.*, 2013; Yang *et al.*, 2014). Talin-bound RIAM interacts with GTP-bound Rap1 GTPase, whose membrane-targeting motif directs the entire talin-RIAM-Rap1 complex to the plasma membrane. This typically takes place at sites of active adhesion formation, including the leading edge of the cell lamellipodium and the tips of protruding filopodia (Lee *et al.*, 2009; Lagarrigue *et al.*, 2015). Similarly to talin, also RIAM directly interacts with $PI(4,5)P_2$ phospholipids through its pleckstrin homology (PH) domain, which contributes to the targeting of the complex formed by RIAM, talin and Rap1 to the sites of adhesion formation (Wynne *et al.*, 2012). It is not yet known if the talin rod domain is able to interact with RIAM in its autoinhibited compact conformation (Goult, Xu, *et al.*, 2013; Goult, Zacharchenko, *et al.*, 2013; Zhang *et al.*, 2016). Interestingly, the binding of RIAM to the talin head F3 subdomain has been found to displace the autoinhibition between the F3 subdomain and rod R9 subdomain (Yang *et al.*, 2014). Therefore, it seems possible that RIAM functions both in the recruitment of talin to the plasma membrane and in its release from its intramolecular autoinhibition.

Additional to the mechanisms presented above, FAK and Kank proteins contribute to the recruitment and activation of talin. However, both FAK and Kank are also known to negatively regulate the stability of the adhesion complex (Lawson *et al.*, 2012; Sun *et al.*, 2016). The C-terminal focal adhesion targeting (FAT) domain in FAK interacts with the talin head F3 subdomain and facilitates the recruitment of talin into nascent adhesions (Chen *et al.*, 1995; Lawson *et al.*, 2012; Serrels and Frame, 2012). However, FAK is also required for the correct regulation of adhesion turnover and for the disassembly of mature focal adhesions (Lawson *et al.*, 2012). Kank proteins exhibit similar dual functions in the regulation of adhesion dynamics. During adhesion formation, Kank-2 binds to the talin rod R7 subdomain and promotes the activation of integrins. On the other hand, in mature adhesions, Kank-2 interferes with the binding of actin filaments to the actin binding site 2 (ABS2) in the talin rod subdomains R4-R8, which leads to decreased traction force generation and increased adhesion sliding (Sun *et al.*, 2016).

2.3.5 Talin head domain as an integrin activator

The talin head domain is an atypical FERM (Band 4.1 Ezrin Radixin Moesin) domain with four globular subdomains, called F0 – F3, and a 30 residue-long unstructured loop inserted into the F1 domain (Figure 4A) (Goult *et al.*, 2010). Although the talin head F3 subdomain is the only subdomain directly interacting with β-integrin tail domains, the F0, F1 and F2 subdomains are also required for efficient integrin activation (Bouaouina, Lad and Calderwood, 2008; Goult *et al.*, 2010). According to a currently recognized model, the talin head domain folds into an atypical extended FERM fold, where positively charged patches in the F1, F2 and F3 subdomains make extensive contacts with negatively charged phospholipids (Elliott *et al.*, 2010). In this model, interactions of the F1 loop with membrane phospholipids promote the folding of the loop into an α-helical conformation, which contributes to talin activation (Goult *et al.*, 2010). However, recent unpublished results suggest that the talin head may adopt a more traditional FERM fold with a cloverleaf arrangement of the F1-F3 subdomains (Kukkurainen et al. manuscript). In this novel model, the negatively charged residues in the F1 loop cleave open the ionic inner membrane clasp between the integrin α- and β-subunits. This promotes the separation of the integrin tail domains and results in the activation of integrins (Kukkurainen et al. manuscript).

The F3 subdomain of the talin head adopts a phosphotyrosine binding domain (PTB)-like conformation and mediates most of the interactions of the head domain. During the initial inside-out activation of integrins, the head F3 subdomain binds to the β-integrin membrane-proximal NPxY motif, which induces elongation of the β-integrin transmembrane helix and allows additional interactions between the talin head F3 subdomain and the β-integrin tail domain (Figure 5) (Wegener *et al.*, 2007). This binding of talin to the NPxY-motif disrupts the ionic inner membrane clasp between integrin α- and β-subunits and allows the separation of α- and β-integrin transmembrane domains (Goult *et al.*, 2009). However, the complete activation of integrins and the stabilization of the nascent complex requires the recruitment of other integrin-binding proteins (Pinon *et al.*, 2014; Theodosiou *et al.*, 2016). Of these, the three members of the kindlin protein family are the most important. Kindlin proteins are structurally related to the talin head domain, although they contain a pleckstrin homology domain (PH domain) inserted into the F2 subdomain. After the talin-dependent separation of integrin transmembrane domains, kindlin proteins bind to the membrane-distal NxxY motif *via* their PTB domain and function as co-

activators of integrins together with talin (Calderwood, Campbell and Critchley, 2013; Theodosiou *et al.*, 2016). Importantly, the PTB domains in the talin head domain and kindlin can only bind integrin in the absence of tyrosine phosphorylation of the NxxY motifs. In contrast, phosphorylation of these motifs by tyrosine kinase Src enhances the binding of other integrin-binding proteins such as DOK1 and 14-3-3 (Oxley *et al.*, 2008; Takala *et al.*, 2008; Anthis, Haling, *et al.*, 2009). Thus, the tyrosine phosphorylation of the NxxY motifs effectively regulates the ability of talin and kindlin to bind to β-integrin tail domains and provides another layer of regulation for fine-tuning the level of integrin activation.

Talin and kindlin interact with numerous adhesion proteins regulating the assembly of the nascent adhesion complex. Although the presence of both is required for efficient activation of β1-integrins, kindlin seems to be more important for the recruitment of additional proteins into the initial adhesion complex (Theodosiou *et al.*, 2016). Kindlin is recruited to the plasma membrane together with the Arp2/3 complex, and, once bound to the NxxY-motif in the β-integrin tail domain, recruits additional adhesion proteins including paxillin, FAK, p130Cas and Dock180 (Theodosiou *et al.*, 2016; Böttcher *et al.*, 2017). This initial signaling complex activates actin polymerization and membrane protrusion through Rac1-dependent mechanisms (Böttcher *et al.*, 2017). However, as discussed next, the maturation of the initial adhesion complex is dependent on the talin rod domain and its downstream signaling.

2.3.6 Talin rod domain as an adhesion scaffold

The talin rod domain is composed of 13 α-helical bundles, in here referred to as rod subdomains or R1-R13. Each subdomain consists of 4-5 amphipathic α-helices tightly packed into a compact bundle (Goult, Zacharchenko, *et al.*, 2013). The subdomains are connected with short flexible linkers and form an elongated structure resembling beads on a string. The only exception to this structure is the R8 subdomain, which is inserted into the R7 subdomain and likely has a special role in mediating the interactions between talin and other adhesion proteins (Figure 4) (Goult, Zacharchenko, *et al.*, 2013; Yao *et al.*, 2016). The R1 and R2 subdomains are closely packed into a staggered double domain by hydrophobic packing, while the folding of the other subdomains is likely less dependent on their flanking subdomains (Papagrigoriou *et al.*, 2004; Goult, Zacharchenko, *et al.*, 2013). The final C-terminal helix in the talin rod domain mediates talin dimerization by forming an

antiparallel dimer with another talin molecule and contributes to actin binding through the actin binding site in the R13 subdomain (Gingras *et al.*, 2008; Goult *et al.*, 2008). In addition to the ABS3 in the R13 subdomain, talin head domain and talin rod subdomains R4-R8 contain actin binding regions, termed ABS1 and ABS2, respectively (Hemmings *et al.*, 1996; Lee *et al.*, 2004; Atherton *et al.*, 2015). The C-terminal ABS3 is likely required for the initial mechanical activation of talin. Indeed, mutations either in the dimerization domain or in the R13 subdomain affect adhesion complex stability and cell spreading (Atherton *et al.*, 2015; Austen *et al.*, 2015). In the absence of mechanical force, the central ABS2 is negatively regulated by the flanking R3 and R9 subdomains (Atherton *et al.*, 2015). Mechanical force transmitted through the ABS3 can activate the ABS2, thus strengthening the adhesion. Accordingly, ABS2 likely functions as the main force-bearing ABS in talin, while the main role of ABS3 may be to regulate the activation of ABS2 (Austen *et al.*, 2015; Kumar *et al.*, 2016). The function of the ABS1 in the talin head domain is unclear at the moment.

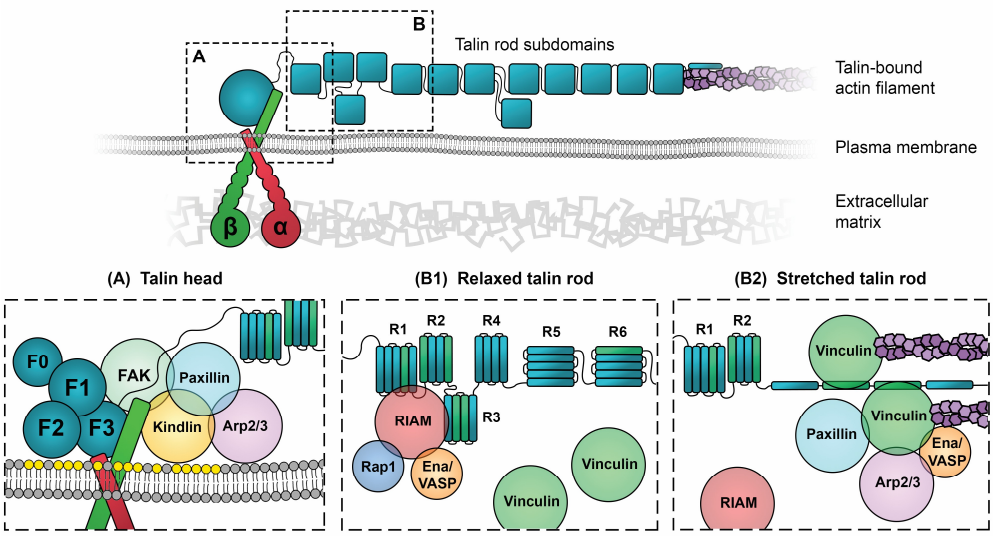

Figure 5. Schematic representations of the key interactions of the talin head domain and rod subdomains. (A) The talin head domain interacts with the membrane proximal NxxY motif in the β-integrin tail domain and promotes the separation of α- and β-integrin transmembrane helices. Interactions of the talin F2 and F3 domains with acidic phospholipids (yellow dots) are required for efficient talin recruitment and integrin activation. Kindlin acts as an integrin coactivator with talin and recruits other adhesion proteins including paxillin and the Arp2/3 complex. (B1) In the relaxed talin rod, the R2-R3 subdomains can interact with RIAM and mediate the Rap1-dependent recruitment of talin to the plasma membrane. (B2) The force-induced unfolding of talin rod subdomains promotes the dissociation of RIAM and exposes cryptic binding sites for vinculin (green bars). Vinculin structurally reinforces the adhesion complex and recruits additional adhesion proteins such as paxillin and VASP.

In addition to its actin binding sites, the talin rod domain contains numerous binding sites for other adhesion proteins. Most importantly, the talin rod subdomains R1, R2, R3, R6. R7, R8, R10, R11 and R13 harbor in total 11 vinculin binding sites (VBS), each consisting of a single amphipathic α-helix (Critchley, 2005; Gingras *et al.*, 2005). However, in a relaxed talin molecule, the VBS-helices are closely packed with non-VBS helices to form α-helical bundles, i.e. talin rod subdomains. This packing renders the VBSs structurally inaccessible, or *cryptic*. Therefore, unfolding of the helix bundle is required for vinculin binding (Figure 5). Accordingly, mechanical stretching of the rod subdomains activates vinculin binding both *in vitro* and *in vivo* (Hytönen and Vogel, 2008; del Rio *et al.*, 2009; Ciobanasu, Faivre and Le Clainche, 2014; Hirata *et al.*, 2014). Vinculin binding to unfolded talin rod subdomains prevents their refolding and locks them into their open conformation (Carisey *et al.*, 2013; Yao *et al.*, 2014). Similarly to talin, the activity of vinculin is regulated by an intramolecular interaction between the vinculin head and tail domains (Bakolitsa *et al.*, 2004). In solution, the equilibrium between inactive and active vinculin species lies strongly on the side of the autoinhibited, inactive conformation (Cohen *et al.*, 2005). Mechanical activation of the talin rod VBSs allows vinculin binding and promotes a shift in the equilibrium towards the open, active vinculin conformation. Talin-bound vinculin can bind to actin filaments through its C-terminal actin binding domain, which further shifts the equilibrium towards the open conformation. Although vinculin itself does not possess any enzymatic activity, talin-bound vinculin can interact with nearly 20 adhesion proteins and regulate their recruitment into the adhesion complex (Carisey and Ballestrem, 2011; Carisey *et al.*, 2013).

In addition to their interactions with vinculin, the talin rod subdomains R2, R3, R8 and R11 can interact with RIAM and mediate the recruitment of talin to the plasma membrane. Interestingly, RIAM is able to bind to these subdomains only in their intact, folded conformation (Goult, Zacharchenko, *et al.*, 2013). Therefore, it seems that the initial RIAM-talin interaction required for the recruitment of talin is later disrupted by the unfolding of the talin rod subdomains. This unfolding simultaneously exposes talin VBSs and allows vinculin binding (Figure 5). This switch from RIAM-bound talin to vinculin-bound talin likely occurs early during the force-dependent maturation of the adhesion complex and it may function as an important trigger for downstream signaling (Calderwood, Campbell and Critchley, 2013; Goult, Zacharchenko, *et al.*, 2013).

The talin rod domain also contains binding sites for Kank-1 (R7) and Kank-2 (R7), Deleted in liver cancer-1 (DLC1, R8), α-synemin (R8), paxillin (R8) and β-integrin (R11) (Sun *et al.*, 2008, 2016; Gingras *et al.*, 2009; Li *et al.*, 2011; Bouchet *et al.*, 2016; Zacharchenko *et al.*, 2016). The second integrin binding site (IBS2) in the talin rod subdomain R11 binds to the membrane-proximal helix in the β-integrin tail domain with relatively high affinity, but is unable to activate integrins by itself (Rodius *et al.*, 2008; Calderwood, Campbell and Critchley, 2013). The different binding sites of talin IBS1 and IBS2 in the β-integrin tail domains suggest that both IBS1 and IBS2 can simultaneously bind to a single β-integrin tail domain. Although this model of integrin binding would nicely explain how talin mediates the crosslinking and clustering activated integrins, at the moment many open questions regarding the formation of this talin-based intracellular meshwork remain to be answered (Klapholz and Brown, 2017).

2.3.7 Talin in the recruitment of DLC1

While the interactions of talin and vinculin have been extensively characterized, many of the interactions of the rod subdomains are still relatively poorly understood. Among these is the interaction of the R8 subdomain with Deleted in liver cancer-1 (DLC1), a RhoGAP frequently downregulated in various cancers. Human DLC1 belongs to a family of three homologous proteins (DLC1, DLC2 and DLC3) with similar structural and functional characteristics. Each of these proteins is roughly 1100 amino acids in size and composed of three conserved functional domains, namely the N-terminal sterile alpha motif (SAM) domain, the central RhoGAP domain and the C-terminal steroidogenic acute regulatory –related lipid transfer (START) domain. In addition to these three functional domains, a serine-rich linker region connecting the SAM domain and the RhoGAP domain is required for the complete functionality of the protein. This mostly unstructured region harbors various interaction sites such as the LD-like motif and regulates the cellular localization of the DLC1 protein (Li *et al.*, 2011; Ko and Ping Yam, 2014). Despite the structural similarity of the three human DLC proteins, their functions in cells seems to be non-redundant. While both DLC2 and DLC3 are dispensable for embryonic development, DLC1-deficient embryos are not viable. (Durkin *et al.*, 2005; Yau *et al.*, 2009; Wang *et al.*, 2016) Furthermore, DLC1 is extensively expressed both during embryonic development and in adults tissues, suggesting it to be required for central cellular functions in many cell types (Durkin *et al.*, 2002; Seng *et*

al., 2007). DLC1 participates in the regulation of cytoskeleton organization and adhesion function through multiple, currently only partly understood mechanisms. Although the different domains present in DLC1 interact with numerous adhesion proteins and regulate their localization and function, the central RhoGAP domain is considered to be the key domain for its biological activity (Wong *et al.*, 2008). The RhoGAP domain exhibits high GAP activity towards RhoA and its homologs RhoB and RhoC and weak GAP activity towards Cdc42 (Healy *et al.*, 2008). Accordingly, fibroblast cell lines derived from DLC1 knockout embryos have severe defects in the organization of actin cytoskeleton and focal adhesions, demonstrating the importance of DLC1 in the regulation of different Rho-family GTPases (Durkin *et al.*, 2005).

As its name implies, DLC1 was originally identified as a gene frequently lost in liver cancer (Yuan *et al.*, 1998). Later studies have demonstrated that the loss of DLC1 is not specific for liver cancer, but a general feature of many human cancers (Feng *et al.*, 2013). In fact, the frequency of DLC1 loss in liver, colon, lung and breast cancers is close to that of the well-established tumor suppressor protein p53, underscoring the relevance of DLC1 as a tumor suppressor (Xue *et al.*, 2008). The mechanisms of DLC1 downregulation or inactivation in cancer include deletions of entire chromosomal regions from the chromosome 8, DLC1 promoter hypermethylation and mutations in the serine-rich linker region of the DLC1 protein (Liao, Shih and Lo, 2008; Ko and Ping Yam, 2014). The loss of DLC1 activity in cancer cells has been associated with facilitated cell migration and increased metastatic potential of the cells, indicating that DLC1 generally acts to inhibit cell migration (Xue *et al.*, 2008; Barras and Widmann, 2014). Accordingly, in cultured cancer cells, the loss of DLC1 promotes anchorage independent growth and colony formation in soft-agar, while the re-expression of DLC1 rescues these effects and limits the tumorigenic potential of the cells in mice xenografts (Healy *et al.*, 2008; Feng *et al.*, 2013). How DLC1 orchestrates the cytoskeleton and adhesion complexes in normal cells and why its loss in cancer activates cell mobility remain to be thoroughly understood. While the functionality of the RhoGAP domain is known to be critical for the correct regulation of the cell cytoskeleton, the overall activity of DLC1 in the regulation of cell mobility and invasiveness likely results from the combined effects of multiple RhoGAP-dependent and RhoGAP-independent mechanisms (Barras and Widmann, 2014). The currently known RhoGAP-independent mechanisms include the local activation of phosphoinositide signaling, regulation of caveolin-dependent

endocytosis and the recruitment of specific protein phosphatases into the adhesion complex (Barras and Widmann, 2014).

In adhesion complexes, DLC1 interacts with many canonical adhesion proteins including talin, FAK and tensin (Qian *et al.*, 2007; Li *et al.*, 2011). The interaction of DLC1 with talin is mediated by the LD-like motif in DLC1 and the groove between helices H2 and H3 in the talin R8 subdomain (Zacharchenko *et al.*, 2016). This talin R8-DLC1 interaction, as well as the interaction of an adjacent motif in DLC1 with tensin are both required for the efficient recruitment of DLC1 into the adhesion complex (Qian *et al.*, 2007; Li *et al.*, 2011). Importantly, the presence of the talin-binding LD-like motif in DLC1 has been found to be required for its activity in the suppression of cell migration, anchorage-independent cell growth and cancer cell invasiveness. As both the deletion of this motif and the co-expression of soluble talin R7-R8 fragments are sufficient to inhibit DLC1 activity, it seems that the correct talin-mediated recruitment of DLC1 into focal adhesions is critical for its functionality in cells (Zacharchenko *et al.*, 2016). However, biochemical analyses have demonstrated that the presence of the LD-like motif is not necessary for the activity of the RhoGAP domain in DLC1, suggesting that talin may regulate DLC1 activity mainly through its altered cellular localization (Kim *et al.*, 2009; Li *et al.*, 2011). Interestingly, talin and FAK are both known to interact with the same LD-like motif in DLC1 (Li *et al.*, 2011). This suggests that the interactions of talin and FAK with DLC1 are likely to be mutually exclusive. Furthermore, the LD-motif in paxillin competes with DLC1 for binding to the FAT domain in FAK and with DLC1 and RIAM for binding to the R8 subdomain in talin (Li *et al.*, 2011; Kaushik *et al.*, 2014; Zacharchenko *et al.*, 2016). Thorough investigation of how this complex network of mutually exclusive interactions regulates the localization and biological activities of talin, FAK, paxillin and DLC1 will be an interesting challenge for future studies. As explained in detail in the Results- and Discussion-sections of this thesis, the force-regulated unfolding of the talin R8 subdomain is likely to function as the master switch in the regulation of this interaction network and DLC1 activity.

2.3.8 The mechanical features of the rod subdomains

As explained in the previous sections, the force-regulated unfolding of talin rod subdomains is an important regulator of their interactions and activity. Studies utilizing *in vitro* systems with purified proteins and *in silico*-steered molecular dynamics (SMD) simulations have demonstrated that all 13 subdomains can unfold

under forces acting in the physiological force range (Haining *et al.*, 2016; Yao *et al.*, 2016). Therefore, all 13 talin subdomains may, in theory, contribute to cellular force sensing. Each subdomain has its characteristic mechanical stability, and thus the magnitude of mechanical tension required for their unfolding varies from bundle to bundle (Haining *et al.*, 2016). Together with the unique combination of interaction sites in each subdomain, this creates a sensitive, multi-step mechanosensory system, where mechanical forces operating at different magnitudes activate different protein interactions and downstream signaling pathways. The gradual unfolding of the talin rod subdomains may also serve a molecular shock absorber, buffering any sudden mechanical impacts on the cell cytoskeleton (Yao *et al.*, 2014).

The key determinants of talin rod subdomain stability seem to be the number of individual α-helices in the bundle and the fit of the hydrophobic packing of the bundle core (Goult, Zacharchenko, *et al.*, 2013; Haining *et al.*, 2016; Mykuliak *et al.*, 2018). The bundles composed of four helices are generally less stable than the bundles with five helices. This is due to their unzipping geometry, where both of the connecting linkers are at the same end of the bundle (Yan *et al.*, 2015; Yao *et al.*, 2016). Interestingly, unfolding of both five-helix and four-helix subdomains seems to proceed through a stable 3-helix intermediate state, which may function to recruit additional adhesion proteins to the transiently exposed helix interfaces (Mykuliak *et al.*, 2018). The hydrophobic cores of the four-helix bundles of R3 and R8 contain polar residues that mechanically destabilize these bundles (Goult, Zacharchenko, *et al.*, 2013). Accordingly, the R3 subdomain has relatively low mechanical stability in *in vitro* and *in silico* experiments and it is likely to be the first subdomain to unfold under mechanical tension (Haining *et al.*, 2016; Yao *et al.*, 2016). Mutagenesis of the destabilizing threonine residues to hydrophobic isoleucine and leucine residues increases the mechanical stability of the R3 subdomain *in vitro* and also affects cellular responses to substrate stiffness *in cellulo* (Goult, Zacharchenko, *et al.*, 2013; Yao *et al.*, 2014; Elosegui-Artola *et al.*, 2016). Similarly to the R3 subdomain, the R8 subdomain is mechanically relatively unstable. However, its position in the middle of the R7 subdomain protects it from mechanical tension until the unfolding of the R7 subdomain (Haining *et al.*, 2016; Yao *et al.*, 2016).

The forces experienced by individual adhesion-localized talin molecules have been studied by talin tension sensors based on stretchable peptides connecting fluorophore pairs in a Förster resonance energy transfer (FRET) system (Austen *et al.*, 2015; Kumar *et al.*, 2016; Ringer *et al.*, 2017). Based on these studies, it seems that

in mature adhesions, the N-terminal side (FRET-pair in the linker region) of the rod domain experiences higher forces than the C-terminal side (FRET-pair in the R10-R11 interface) (Ringer *et al.*, 2017). This effect was found to be dependent on the presence of vinculin, suggesting that talin VBS-bound vinculin proteins mediate the transmission of forces between the actin cytoskeleton and the talin rod domain (Ringer *et al.*, 2017). Accordingly, maximal force through the flexible linker connecting talin head and rod domain was only observed in the presence of vinculin (Austen *et al.*, 2015; Kumar *et al.*, 2016). Moreover, in the absence of vinculin, the mechanical stress experienced by the N-terminal side of the talin rod was equal to the stress experienced by the C-terminal side. These results support the model, where ABS3 mediates the initial mechanical activation of talin ABS2 and VBSs, while in mature adhesions forces are mainly transmitted through the β-integrin-talin-vinculin-actin linkages (Atherton *et al.*, 2015; Austen *et al.*, 2015).

2.3.9 Talin as a mechanosensor and a molecular ruler

The regulation of adhesion dynamics and signaling by the mechanical properties of the ECM was first discovered already two decades ago (Pelham *et al.*, 1997; Solon *et al.*, 2007). Although it was soon apparent that integrin-mediated adhesions can sense the magnitude of force transmitted through the adhesion complex, the molecular mechanisms sensing these forces were unknown at that time. Several different focal adhesion proteins, including p130Cas, α-actinin, filamin, FAK and actin have since been proposed to function as cellular mechanosensors (Sawada *et al.*, 2006; Hampton, Taylor and Taylor, 2007; Hayakawa, Tatsumi and Sokabe, 2011; Razinia *et al.*, 2012; Trichet *et al.*, 2012; Janoštiak *et al.*, 2014; Zhou *et al.*, 2015). However, to date, extensive evidence has accumulated suggesting that talin functions as the key mechanosensor in integrin-mediated cell adhesions. Importantly, talin rod domain mechanosensing is known to be dependent on the rate of its mechanical loading (Elosegui-Artola *et al.*, 2016). On soft substrates, mechanical load through the ECM-integrin-talin-actin linkage builds up too slowly and the complex dissociates before the unfolding of the talin rod domain. On rigid substrates, however, the loading rate of the complex is high enough to allow talin rod unfolding and adhesion complex reinforcement before its disassembly. Thus, the activation of talin rod-mediated mechanosensing exhibits a threshold that is modulated by the substrate rigidity, the level of myosin contractility, the integrin-ligand affinity and the mechanical stability of the individual talin rod subdomains (Elosegui-Artola *et al.*, 2016).

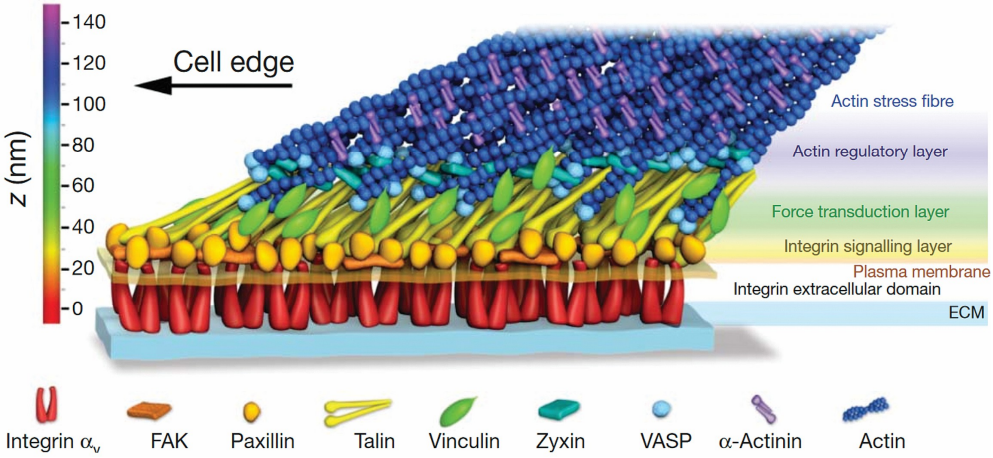

Figure 6. The nanoscale layering of the adhesion complex. The cytosolic integrin tail domains serve as attachment points for many signaling proteins (Integrin signaling layer). The elongated talin rod domain and actin filaments reach further away from the cell membrane and act as scaffolds for the proteins transducing mechanical forces (force transduction layer) or regulating actin polymerization and bundling (actin regulatory layer). Figure from (Kanchanawong *et al.*, 2010) and reproduced with permission from the publisher.

In living cells, the molecular clutch between integrin-mediated adhesions and retrograde actin flow is constantly engaged and disengaged to allow precise regulation of traction force generation and rapid adaptation to changing cellular conditions (Margadant *et al.*, 2011). This is reflected on the stretching state of talin, which shows repeated extension and relaxation phases in the adhesion complex at the time scale of seconds (Margadant *et al.*, 2011). The length of a relaxed, non-autoinhibited talin molecule is around 80 nm, while mechanical stretching can increase its length to over 350 nm (Margadant *et al.*, 2011; Goult, Xu, *et al.*, 2013; Liu *et al.*, 2015). Because of this elongated structure of the extended talin rod domain, integrin-bound talin spans a considerable distance across the adhesion complex. The talin head domain interacts with the adhesion complex proteins recruited around integrin tail domains, while the C-terminal actin binding site in talin reaches far away from the plasma membrane (Liu *et al.*, 2015). Consequently, the adhesion proteins interacting with talin are distributed into different layers along the extended talin molecule (Figure 6) (Kanchanawong *et al.*, 2010). The proteins interacting with the talin head domain are considered to form an adhesion signaling layer actively regulating adhesion structure and function especially through phosphotyrosine signaling. The layers further away from the plasma membrane participate in mechanotransduction and in the regulation of actin dynamics (Figure 6) (Kanchanawong *et al.*, 2010). As predicted by this model, truncation of the talin rod

domain has been demonstrated to cause a downward shift in the position of actin-binding proteins in the adhesion complex (Liu *et al.*, 2015). Interestingly, the dynamics of the proteins constituting the different layers, or adhesion modules, seem to be rather independent of the other modules (Horton, Humphries, *et al.*, 2016; Stutchbury *et al.*, 2017). While the stiffness of the extracellular matrix regulates the dynamics of many structural adhesion proteins, it has little effect on the proteins of the signaling layer (Stutchbury *et al.*, 2017). Conversely, the activity of the signaling proteins has surprisingly little effect on the dynamics of the structural proteins (Horton, Humphries, *et al.*, 2016). Nevertheless, proteins of both structural and signaling modules are required for the coordinated regulation of adhesion assembly and disassembly during cell polarization and migration.

3 AIMS OF THE STUDY

Experiments with talin knockout model organisms and cell lines have demonstrated the critical role of talin in the regulation of adhesion reinforcement and signaling. However, as talin mechanotransduction is mediated by multiple interlinked mechanisms, a more detailed analysis of the structural and functional features of individual talin domains is required to fully understand the versatile functions of talin in cell adhesions. Specifically, the structure-function relationship of the different talin rod subdomains and the contributions of talin rod domain mechanotransmission and mechanotransduction in the regulation of adhesion reinforcement and signaling have remained incompletely understood.

Due to the important roles of talin and vinculin in the development and homeostasis of most tissues, changes in their expression levels are likely to be reflected on the functionality of the tissue. This seems especially likely in those tissues where integrin-mediated adhesions are critical for the integrity of the tissue, such as heart and vasculature. However, so far the expression levels and patterns of talin and vinculin transcripts in cardiovascular diseases have not been investigated.

The specific aims of this thesis were:

I. To study the structure-function relationship of the talin R3 subdomain.

II. To investigate the mechanical regulation of the interaction between the talin R8 subdomain and DLC1.

III. To dissect the roles of talin rod domain mechanotransmission and mechanotransduction in adhesion complex reinforcement and signaling.

IV. To analyze the expression levels and patterns of talin and vinculin transcripts in atherosclerotic plaques.

4 MATERIALS AND METHODS

4.1 DNA expression constructs (I, II, III)

Expression constructs for mouse talin and vinculin proteins were created by subcloning PCR-amplified cDNA fragments into pEGFP-C1 or pEGFP-C3 plasmid backbones containing the cytomegalovirus promoter and the SV40 polyadenyation site (Clontech, USA). See Table 1 for the structures of the used expression constructs. All expression constructs contained either a N- or C-terminal EGFP or mCherry fluorescent protein to allow fluorescence live-cell imaging, analysis of subcellular protein localization and comparison of expression levels at single cell level. Destabilizing point mutations in talin were created by PCR using overlapping mutagenesis primers and natural restriction sites in the talin cDNA sequence. All cDNA constructs were authenticated by sequencing. The talin-1, vinculin, paxillin and DLC1 cDNA constructs used as PCR templates and for cell transfections were kindly provided by Professor Michael Sheetz, Dr. Wolfgang Ziegler, Dr. Chinten James Lim, Professor Susan Craig, Professor Irene Ng and Professor Anna Huttenlocher.

Table 1. The expression constructs used in studies I, II and III

DNA construct	Structure	Mutations	Study
WT Talin	1-2541 + mCherry or EGFP		I, II,III
Talin (1S)	1-2541 + mCherry or EGFP	I812S	I
Talin (2S)	1-2541 + mCherry or EGFP	I812S, I805S	I
Talin (3S)	1-2541 + mCherry or EGFP	I812S, I805S, L890S	I
Talin (4S)	1-2541 + mCherry or EGFP	I812S, I805S, L890S, L897S	I
Talin R8 clamp	EGFP + Talin	Q1459C, S1583C	II
Talin C1	EGFP + Talin	Q1459C	II
Talin C2	EGFP + Talin	S1583C	II
Talin head	mCherry or EGFP + 1-490		III
ΔR1-12	1-490 + 2296-2541 + mCherry or EGFP		III
ΔR1-12 + C-terminal R1-3	1-490 + 2296-2541 + 487-913 + mCherry		III

ΔR1-10	1-490 + 1974-2541 + mCherry or EGFP		III
ΔR4-12	1-913 + 2296-2541 + mCherry or EGFP		I, III
ΔR4-12 (4S)	1-913 + 2296-2541 + mCherry or EGFP	I812S, I805S, L890S, L897S	I, III
ΔR4-12 (4S) + R1-3	1-913 + 2296-2541 + 487-913 + mCherry	I812S, I805S, L890S, L897S	III
ΔR4-12 (4S) + 2x R1-3	1-913 + 2296-2541 + 2x 487-913 + mCherry	I812S, I805S, L890S, L897S	III
WT Vinculin	EGFP + Vinculin 1-1066		III
Vinculin T12	EGFP + Vinculin 1-1066	D974A, K975A, R976A, R978A	III
Vinculin head	EGFP + Vinculin 1-255		III
Talin head + WT Vinculin	EGFP + Talin 1-490 + Vinculin 1-1066		III
Talin head + Vinculin T12	EGFP + Talin 1-490 + Vinculin 1-1066	D974A, K975A, R976A, R978A	III

4.2 Cell lines and cell culture methods (I, II, III)

The wild type MEF cell line was a kind gift from Dr. Wolfgang Ziegler, Hannover Medical School, Germany, and has been previously described by Xu & Baribault (Xu and Baribault, 1998). The *Tln1-/-Tln2-/-* MEF cell line has been previously described by Theodosiou et al. (Theodosiou *et al.*, 2016) and was kindly provided by Dr. Carsten Grashoff, Max Plank Institute of Biochemistry, Germany. Both cell lines were maintained in high-glucose DMEM supplemented with 10% FBS and 1% GlutaMax (Thermo Fisher Scientific, USA). Standard cell culture methods and a 37 °C incubator with 5% CO_2 were used to culture both cell lines.

Wild type and *Tln1-/-Tln2-/-* mouse embryonic fibroblast (MEF) cells were transfected with the Neon transfection system according to the manufacturer's recommendations (Thermo Fisher Scientific, USA). For all plasmid constructs, 5 μg of endotoxin-free plasmid DNA was used per 10^6 cells. The following electroporation parameters were used for wild type and talin-null MEF cells: 1350 V, 30 ms, 1 pulse and 1400 v, 30 ms, 1 pulse, respectively. Transfected cells were allowed to recover for a minimum of 24 h before they were used in any experiments.

4.3 Sample preparation for microscope imaging (I, II, III, IV)

4.3.1 Immunocytochemistry (I, II, III)

For immunocytochemistry, coverslips were washed with 2% Hellmanex-III (Merck) in a bath sonicator (40 °C, 20 min), rinsed with water and attached to perforated 35 mm polystyrene dishes (MatTek). Coverslips were coated with 25 μg/ml gelatin affinity-purified human fibronectin (Fn) for 1 h at 37 °C and washed two times with PBS. *Tln1-/-Tln2-/-* MEF cells were transfected with talin expression constructs and allowed to recover for 24 h. Transfected cells were plated at a low confluency on fibronectin coated coverslips for 120 min, after which media was aspirated from the wells and the cells were fixed with 4% PFA in PBS (pH 7.4) for 15 min at the room temperature (RT). Fixed cells were washed two times with PBS and permeabilized with 0.2% Triton X100 in PBS for 5 min at RT. Nonspecific antibody binding was blocked by incubation of the samples in 5% FCS, 1% BSA and 0.05% Triton-X100 in PBS for 30 min at RT. Both primary and secondary antibodies were diluted in the blocking buffer. The antibodies and dilutions used are presented in Table 2. Immunostained coverslips were washed with PBS (3 x 10 min) and stored at 4 °C until imaged. In studies I and IV, immunostained samples were mounted with Prolong mounting reagent (Thermo Fisher Scientific, USA).

Table 2. The antibodies and actin or DNA binding dyes used in studies I, II, III and IV

Antibody	Manufacturer	Catalogue No.	Dilution	Study
Vinculin	Merck	V9131	1:400 IF	I, III
Paxillin	BD Biosciences	610051	1:100 IF	I, III
Paxillin pY31	Thermo Fisher	44-720G	1:200 IF	III
FAK	BD Biosciences	610088	1:100 IF	III
FAK pY397	Abcam	ab81298	1:200 IF	III
p190RhoGAP pY1105	Merck	SAB4503875	1:100 IF	III
VASP	Merck	HPA005724	1:100 IF	III
MLC2	Millipore	MABT180	1:200 IF	II
MLC2 pT18/pS19	Cell Signaling	3674	1:200 IF	II
MLC2 pS19	Cell Signaling	3675	1:200 IF	III
DLC1	SantaCruz	sc-271915	1:100 IF	II
mCherry	Sicgen	AB0040-200	1:1000 WB	I, III

GFP	Merck	G1546	1:1000 WB	I, III
Actin	Millipore	MAB1501R	1:5000 WB	I, III
PECAM-1	Dako Agilent	JC70A	1:20 IHC	IV
Talin 1	Abcam	ab71333	1:80 IHC	IV
Talin 2	Cancer Research	68E7	1:100 IHC	IV
Vinculin	Abcam	ab61186	1:80 IHC	IV
Anti-mouse AlexaFluor 405	Thermo Fisher	A31553	1:250 IF	I, III
Anti-mouse AlexaFluor 488	Thermo Fisher	A21202	1:250 IF	I, II, III, IV
Anti-mouse AlexaFluor 568	Thermo Fisher	A11004	1:250 IF 1:100 IHC	I, III, IV
Anti-mouse AlexaFluor 633	Thermo Fisher	A21050	1:250 IF	I, III
Anti-rabbit AlexaFluor 405	Thermo Fisher	A31556	1:250 IF	I, III
Anti-rabbit AlexaFluor 488	Thermo Fisher	A21206	1:250 IF 1:100 IHC	I, III, IV
Anti-rabbit AlexaFluor 568	Thermo Fisher	A11011	1:250 IF	I, III, IV
Anti-rabbit AlexaFluor 633	Thermo Fisher	A21071	1:250 IF	I, III
Phalloidin AlexaFluor 488	Thermo Fisher	A12379	1:40 IF	I, III
Phalloidin AlexaFluor 568	Thermo Fisher	A12380	1:40 IF	I, III
Prolong Diamond with DAPI	Thermo Fisher	P36962		I, IV

4.3.2 Microcontact printing of patterned substrates (I)

Microcontact printing of patterned cell culture substrates was performed by our collaborators at the Karlsruhe Institute of Technology under the supervision of Professor Martin Bastmeyer. Briefly, stamps were incubated for 10 min with a fibronectin (Fn) solution consisting of 45 μg/ml inactive human Fn (thermal denaturation), 5 μg/ml active human Fn (Merck) and 1 μg/ml Alexa Fluor 647-labeled bovine Fn (Thermo Fisher Scientific). Fn molecules adsorbed to the stamp were transferred to a glass coverslip for 10 min. Stamped structures were incubated with 5 μg/ml human Vn (Merck) for 1 h to coat protein-free regions. Micropatterned substrates were rinsed once with PBS before they were used for cell culture. Transiently transfected wild type MEF cells were seeded and cultured for 2 h on the Fn/Vn substrates in serum-free DMEM. After 2h of cultivation, cells were fixed and immunostained using anti-paxillin primary antibody (BD Biosciences, Table 2) and fluorophore-labeled secondary antibody.

4.3.3 Immunohistochemistry (IV)

For immunofluorescence labeling of frozen tissue sections (Study IV), vascular samples from left internal thoracic artery (LITA) and from atherosclerotic carotid artery were embedded into TissueTek O.C.T. compound (Sakura Finetek), frozen in liquid nitrogen and cut into 6 μm sections. Air-dried tissue sections were fixed with acetone at -20°C for 10 min. The fixed samples were immersed into PBS (pH 7.4) and transferred to Shandon Sequenza (Thermo Fisher Scientific) immunostaining cassettes. Nonspecific antibody binding was blocked by preincubation of the tissue sections in blocking buffer containing 1% BSA and 0.3% Triton-X100 diluted in PBS (pH 7.4). All antibodies were diluted into the blocking buffer. The samples were incubated with diluted primary antibodies at +4°C overnight, followed by three washes with PBS (pH 7.4). Secondary antibodies (Table II) were incubated on the samples for 1 h at room temperature. Immunostained samples were washed five times with PBS (pH 7.4), followed by one wash with deionized water. Immunostained stamples were mounted by using Prolong Diamond mounting reagent (Thermo Fisher Scientific) with DAPI for nuclear staining.

For immunofluorescence staining of formalin-fixed and paraffin-embedded (FFPE) samples (Study IV), 4 μm sections were cut from FFPE samples of LITA, healthy carotid artery and abdominal aorta. Hematoxylin-eosin (HE)-stained tissue sections were used to confirm typical tissue morphology of the samples. All tissue sections were deparaffinized and rehydrated by incubation in xylene and 99%, 95%, 70% and 50% ethanol solution for 10 min, respectively. For antigen retrieval, tissue sections were boiled in 10 mM sodium citrate buffer (pH 6) with 0.05% Tween-20 for 20 min in a microwave oven and allowed to slowly cool down to room temperature. Samples were washed three times with PBS (pH 7.4) and treated with 0.1% Sudan Black B for 20 min at RT to quench tissue autofluorescence. Samples were washed with PBS (3 x 10 min) and immunostained using the same methods used for frozen tissue sections. Antibody specificity was confirmed by using control samples with no primary antibodies.

4.4 Microscopy methods (I, II, III, IV)

4.4.1 Live cell imaging (I, II, III)

Polystyrene well plates were coated with 10 μg/ml fibronectin at 37 °C for 1 h and washed two times with PBS (pH 7.4). Transfected *Tln1-/-Tln2-/-* cells were allowed to recover for 24 h, trypsinized and plated onto fibronectin-coated well plates at a low confluency. Cells were allowed to attach for 1 h, followed by a wash with warm PBS (pH 7.4) to remove dead or non-transfected cells. Cells were incubated in fresh media for 30 min before imaging was started. The EVOS FL Auto microscope (Thermo Fisher Scientific) equipped with a 37 °C and 5% CO_2 incubator was used for live cell imaging for 12 h at 120 or 360 s intervals. For the diamide treatment of cells in the study II, diamide reagent (Merck) was dissolved in 1x PBS to a stock concentration of 50 mM and further diluted in cell culture media to a final concentration of 50 μM. Diamide media was added to the wells 15 min before the start of the experiment. The resulting image stacks were analyzed with ImageJ version 1.50e (Schneider, Rasband and Eliceiri, 2012) and MTrackJ plugin (Meijering, Dzyubachyk and Smal, 2012).

4.4.2 Confocal microscopy (I, III, IV)

For protein co-localization analysis in single cells (Studies I and III), immunostained samples were imaged with a Nikon Eclipse Ti inverted microscope (Nikon Instruments) equipped with a CFI Plan Apo VC 60x/1.40 Oil immersion objective (Nikon instruments), a Yokogawa CSU10 spinning disk confocal unit (Yokogava, Japan) and an Andor NEO sCMOS camera (Andor Technology). 488 nm, 561 nm and 640 nm lasers were used to excite fluorescent GFP and mCherry proteins or AlexaFluor 488, 568 and 633 fluorophores, respectively. All imaging parameters were kept constant for all samples to allow quantitative image analysis.

For the analyses of cell area and polarity (Studies I and III), PFA-fixed cells were stained with Phalloidin-AlexaFluor 488 (Thermo Fisher Scientific) and imaged with a Zeiss CellObserver.Z1 equipped with a 25X/0.8 oil immersion objective and an LSM780 confocal unit (Carl Zeiss Microscopy). Zeiss Zen Black software and ImageJ 1.50e were used in image analysis (Schneider, Rasband and Eliceiri, 2012).

Immunostained tissue sections (Study IV) were imaged with a Zeiss Cell Observer.Z1 equipped with a 63x/NA 1.4 oil immersion objective and Zeiss LSM780 confocal unit (Carl Zeiss Microscopy). For fluorophore excitation, a 480 nm argon laser and 405 nm and 561 nm diode lasers were used together with suitable filter sets. For comparative analysis the laser intensities, PMT gains and other settings were kept constant for all samples. Serial plane images were collected throughout the whole thickness of the sample at 200 nm intervals. During image processing, maximum intensity projections were used to collect the areas of maximum intensity from the image stacks into single images.

4.4.3 Fluorescence recovery after photobleaching (I, II, III)

For fluorescence recovery after photobleaching (FRAP) analysis, *Tln1-/-Tln2-/-* cells were transfected with EGFP- or mCherry-fused talin, vinculin, paxillin and DLC1 constructs. Transfected cells were plated on fibronectin-coated (25 μg/ml) glass-bottom dishes 2 h before imaging. In studies I and III, a Zeiss Cell Observer.Z1 microscope equipped with an LSM780 confocal unit, 37°C/ 5% CO2 incubator and 63x/1.4 Oil immersion objective was used for imaging. Circular regions with a diameter of 2.6 μm were photobleached with a 488 nm argon laser operated at a high intensity. In study II, a Nikon Eclipse Ti microscope equipped with a TIRF prism and a FRAP module was used to capture images at 5 s intervals for 100 s. Only one region in each cell was selected to be bleached. Confocal microscope images were captured at 500 ms intervals for 5 s before photobleaching and for 90 s after photobleaching. Fluorescence recovery was analyzed by the equation

$$F = \frac{\mathrm{B(t)/B(t<0)}}{\mathrm{Cell(t)/Cell(t<0)}}$$

where B(t<0) and Cell(t<0) are the average fluorescence intensities of the bleached area and the entire cell, respectively, before bleaching and B(t) and Cell(t) the intensities of the same regions at each time point after bleaching. The resulting F-values were normalized to zero. EasyFRAP (Rapsomaniki *et al.*, 2012) FRAP analysis software was used for the fitting of single exponential curves to each data series to determine the mobile fraction and the half-recovery time for each FRAP curve.

4.5 Collagen gel contraction assay (III)

For the collagen-I gel contraction assay, ring-shaped PDMS casts placed at the bottom of 6-well plate wells were coated with 1% BSA in PBS for 1 h at 37 °C, washed twice with PBS, air-dried and sterilized by a UV-light source. Transfected *Tln1-/-Tln2-/-* cells were cultured for 24 h, trypsinized and counted. The number of cells in the complete polymerized collagen-I matrix was 312,000 cells per 100 µl of the matrix mixture. Cells were resuspended in DMEM in one third of the final volume of the mixture, while the rest of the mixture was composed of the following components: 1/10 of 10x DMEM, 1/10 of 0.5 M NaOH and 8/10 of 3 mg/ml rat tail collagen-I (Thermo Fisher Scientific). All components were carefully mixed on ice and the matrix mixture was cast into the BSA coated PDMS wells. The collagen-I matrixes were allowed to polymerize for 30 min at 37 °C, after which the PDMS casts were released and the wells filled with warm complete media. The macroscopic contraction of the collagen-I matrices was followed at 24 h intervals for 72 h by a gel imager.

4.6 Steered molecular dynamics simulations (I, II)

All molecular dynamics (MD) and steered molecular dynamics (SMD) simulations (Studies I and II) were performed using Gromacs version 4.6.7. (Hess *et al.*, 2008) on the Sisu supercomputer, CSC, Espoo, Finland. All models were built with an explicit TIP3P water model in 0.15 M KCl neutralized solution and placed into a 10*10*30 nm rectangular box. The system was minimized with 100,000 steps and equilibrated for 10 ns before applying pulling force. The equilibration was performed with a 2 fs step size at NTP conditions. Simulations of the domain stability assessment were performed at equilibration conditions with 2 fs step size for 20 ns. Pulling simulations were performed with a 2 fs step size for 10 ns and recorded at 500 frames/ns. Simulations for domain refolding were performed at equilibration conditions for 20 ns starting from the structure coordinates after 10 ns pulling. Pulling simulations were repeated five times for each structure. All trajectories were analyzed with VMD (Humphrey, Dalke and Schulten, 1996) at 100 frames/ns.

4.7 Mass spectrometry (III)

The mass spectrometry analysis of the cell phosphoproteome (Study III) was performed by our collaborators at the University of Helsinki, Finland, under the supervision of Docent Markku Varjosalo. Briefly, transfected *Tln1-/-Tln2-/-* cells were lysed with 50 mM NH_4HCO_3 buffer supplemented with 8 M urea and homogenized with a bath sonicator. 400 μg of total protein per sample was reduced with Tris(2-carboxyethyl)phosphine (TCEP; Sigma Aldrich), alkylated with iodoacetamide and trypsin digested with sequencing grade trypsin (Promega, USA) and desalted with C18 microspin columns (Nest Group). Phosphopeptide enrichment was performed using Ti^{4+}-IMAC. The IMAC material was prepared and used as previously described (Zhou *et al.*, 2013). The LC-MS/MS analysis was performed using a Q Exactive ESI-quadrupole-orbitrap mass spectrometer coupled to an EASY-nLC 1000 nanoflow LC (Thermo Fisher Scientific). Three fully independent replicates were performed for each talin protein and control transfection. Raw data were processed with MaxQuant version 1.6.0.16 (Cox and Mann, 2008). MS spectra were compared against the mouse component of the UniProtKB database (release 2017_09 with 16970 entries) using the Andromeda search engine (Cox *et al.*, 2011).

4.8 Patient sample material (IV)

The arterial samples (Study IV) were collected as a part of the Tampere Vascular Study (TVS). The study has been approved by the Ethics Committee of Tampere Hospital District. The study was conducted according to the declaration of Helsinki with the informed consent from the individual patients involved.

Samples from femoral, carotid and abdominal aortic regions were obtained during open vascular procedures. The left internal thoracic artery (LITA) controls were obtained during coronary artery bypass surgery due to coronary artery disease. The samples were collected from patients subjected to vascular surgery in the Division of Vascular Surgery and Heart Center, Tampere University Hospital. The patient's denial to participate in the study was used as a measure of exclusion. The vascular samples were classified according to American Heart Association recommendation (Stary *et al.*, 1994). The type V and VI atherosclerotic lesions were further histologically classified as stable and unstable according to the presence of fissure,

rupture, hemorrhage or thrombosis. The healthy carotid artery and abdominal aorta samples were collected from a corpse of a person with no coronary artery disease.

4.9 Microarrays and qRT-PCR (IV)

The analysis of the expression levels of TLN1, TLN2 and VCL genes in arterial tissue samples was performed by our collaborators at the University of Tampere, Finland, under the supervision of Professor Terho Lehtimäki. Briefly, RNA was isolated from fresh tissue samples using Trizol reagent and the RNAEasy kit (Qiagen, USA). Gene expression levels in arterial samples were analyzed by Illumina HumanHT-12 v3 Expression BeadChip (Illumina, USA) analyzing 47 000 transcripts of all known genes, gene candidates and splice variants. Arrays were run according to the manufacturer's instructions and scanned with the Illumina iScan system (Illumina). The raw gene expression data were background-subtracted, log2 transformed and normalized using the R/Bioconductor package Lumi (Du, Kibbe and Lin, 2008). Probes were considered robustly expressed if the detection was $p<0.05$ for at least 50% of the samples in the data set. The TLN1 (probe ILMN_1696643), TLN2 (probe ILMN_1700042) and VCL (probes ILMN_1795429; probe ILMN_2413527) genes were selected for differential expression and correlation analyses.

Quantitative real-time polymerase chain reaction (qRT-PCR) was performed with the TaqMan low-density array (Applied Biosystems) according to the manufacturer's instructions to confirm the results of the microarray analysis. Sufficient RNA for the qRT-PCR analysis was available from 19 out of 24 (79.2%) LITA samples and from 64 out of 68 (94.2%) plaque samples. The qRT-PCR data was analyzed with Expression suite software (Applied Biosystems) using the 2-ΔΔCT method.

4.10 Statistical analyses (I, II, III, IV)

For studies I, II and III all statistical analyses were performed using GraphPad Prism version 5.02 (GraphPad Software). Student's t-test and one-way analysis of variance (ANOVA) with Bonferroni post-test were used to assess the statistical significance of the results. Differences were considered statistically significant with $p<0.05$. For study IV, statistical analyses were performed using R version 2.15.0. The statistical

significance of gene expression differences in the microarray analysis was assessed using the nonparametric Wilcoxon signed-rank test and log2-transformed data. For analyzing the associations between TLN1, TLN2 and VCL expression levels and vascular smooth muscle cell and macrophage markers the Spearman correlation coefficient was used.

5 SUMMARY OF THE RESULTS

5.1 Modulating the stability of the rod subdomains (I)

5.1.1 SMD simulations and the strategy for talin R3 destabilization (I)

The talin rod R3 subdomain has been shown to be the mechanically most vulnerable rod subdomain and it is likely the first subdomain to unfold under mechanical tension (Haining *et al.*, 2016; Yao *et al.*, 2016). Therefore, the force-regulated unfolding of the R3 bundle may have a key role in the regulation of adhesion structure and signaling. To investigate the intramolecular interactions contributing to the mechanical stability of the talin rod R3 subdomain, we utilized computational molecular dynamics (MD) and steered molecular dynamics (SMD) simulations. Talin R3 unfolding was simulated in a 150 pN constant-force simulation for 10 ns. Based on the recorded unfolding trajectories, we designed a panel of mutations gradually further destabilizing the structure of the R3 subdomain (Figure 7A). The designed isoleucine-serine and leucine-serine mutations affect the hydrophobic packing of the α-helix bundle core and are likely to mechanically destabilize its structure. However, the designed mutations do not affect the VBS helices in this subdomain and are therefore unlikely to negatively affect its interactions with vinculin or RIAM.

The four mutations designed were computationally analyzed as a series of 1-4 mutations (referred to as 1S, 2S, 3S and 4S) by constant-force SMD simulations at 150 pN for 10 ns. Talin mutagenesis was found to decrease the mechanical stability of the bundle, as indicated by the increased penetration of water molecules into the bundle core (Figure 7B). The degree of water penetration was found to be dependent on the number of destabilizing mutations, with most penetrated water molecules observed for the 4S mutant. Importantly, in the absence of mechanical force the destabilizing mutations did not affect the folding of the helix bundle. Furthermore, relaxation of the stretched molecules resulted in the return of the individual helices close to their original positions within 10 ns, indicating that the observed reorganization of the helix bundle under mechanical force is reversible.

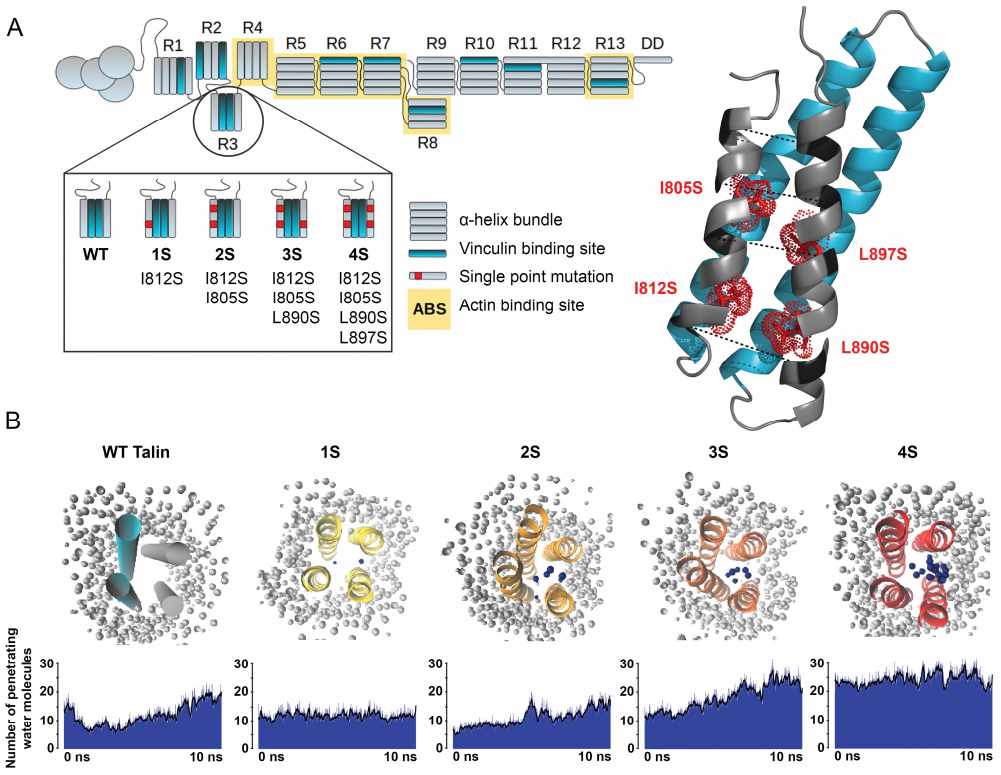

Figure 7. Talin rod R3 subdomain destabilization by mutagenesis of selected residues. (A) In total four isoleucine and leucine residues were mutated to more hydrophilic serine residues. All mutated residues are located in the hydrophobic core of the R3 subdomain and do not affect the functionality of the two VBS helices (colored in light blue). (B) Water penetration into the bundle core during an SMD simulation at a constant force of 150 pN. The molecular models represent the endpoints of 10 ns simulations. Water molecules at each end of the bundle are omitted from the molecular models to allow unobstructed view into the bundle core.

5.2 Talin mechanosensing regulates adhesion structure and function (I, II, III)

5.2.1 Destabilization of the R3 subdomain drives adhesion protein accumulation and increases adhesion turnover rate (I)

The effects of talin rod domain destabilization *in cellulo* were investigated using wild type mouse embryonic fibroblast (MEF) cells and talin-deficient *Tln1-/-Tln2-/-* MEF cells. The destabilizing 1S-4S mutations were generated in talin-1-mCherry and

talin-1-GFP expression constructs by site-directed mutagenesis. Talin R3 subdomain destabilization was found to dramatically increase the accumulation of talin into adhesion sites in wild type MEF cells (Figure 8A). Importantly, the level of talin accumulation was dependent on the level of talin destabilization with the highest accumulation observed for the 4S mutant. The increased accumulation of talin was also reflected on the recruitment of vinculin (Figure 8A). However, the increase in the recruitment of vinculin was smaller than the increase of talin, indicating that the vinculin/talin ratio in the adhesion was decreased.

The binding of vinculin to talin is known to regulate talin dynamics in the adhesion complex (Carisey *et al.*, 2013; Stutchbury *et al.*, 2017). Therefore, we hypothesized that the facilitated vinculin binding caused by talin destabilization would decrease talin turnover in adhesion sites. The dynamics of the destabilized talin proteins and co-expressed GFP-vinculin were studied in *Tln1-/-Tln2-/-* cells by fluorescence recovery after photo bleaching (FRAP). Surprisingly, talin R3 subdomain destabilization resulted in an increase, rather than decrease, in the mobile fractions of both talin-GFP and GFP-vinculin (Figure 8B, C). The observed increase in protein mobility was larger for talin than vinculin, likely due to the faster initial turnover rate of vinculin (Figure 8C). For both talin and vinculin, the maximal increase in mobile fraction was seen already on the 1S mutant with a single destabilizing point mutation (I812S), while the 4S mutant yielded similar results. In addition to the increased mobile fraction of the co-expressed vinculin, also its halftime (t_{half}) of recovery was increased. This suggests that despite the increased vinculin mobility after talin destabilization, the initial rate of vinculin exchange in the adhesion complex was decreased.

Taken together, these results indicate that the mechanical stability of the talin rod subdomains is a critical regulator of both talin and vinculin accumulation and mobility. The increased accumulation of talin after its structural destabilization likely decreases the level of mechanical loading experienced by each individual talin molecule. Because mechanical tension is required for the activation of the talin-vinculin interaction, this results in a decrease in the vinculin/talin ratio and in an increase in the mobility of both talin and vinculin proteins.

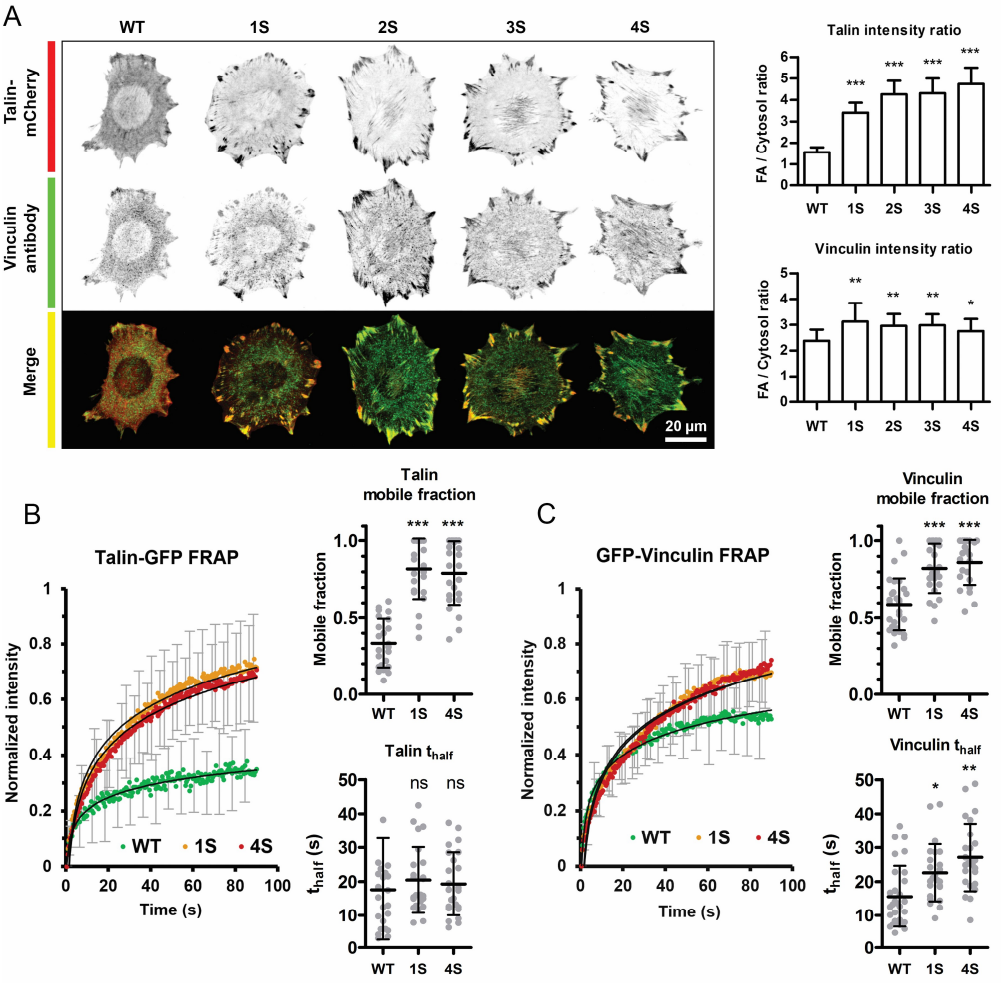

Figure 8. Destabilization of the R3 subdomain increases adhesion protein accumulation and adhesion turnover rate. (A) Analysis of talin and vinculin accumulation into adhesion sites in wild type MEF cells. Asterisks indicate statistical significance compared to wild type talin. (B) Talin-GFP FRAP in *Tln1-/-Tln2-/-* cells. (C) GFP-Vinculin FRAP in *Tln1-/-Tln2-/-* cells. In all graphs bars and horizontal lines represent the mean ± sd. * $p < 0.01$, ** $p < 0.001$, *** $p < 0.0001$. Statistical testing by one-way ANOVA and Bonferroni test. Figure adapted from study I.

5.2.2 The mechanical stability of the R3 subdomain regulates traction force generation and the rate of cell migration (I, III)

In collaboration with the Huang group at the University of Kentucky, USA, we used traction force microscopy to investigate if the increased accumulation of talin and vinculin into adhesion complexes is reflected onto the level cellular traction force generation. Interestingly, expression of the destabilized 4S talin form in talin-1/2 knockout U2OS cells significantly decreased the traction force generation compared to cells expressing wild type talin (Figure 9A). In contrast, the 1S mutant did not significantly alter the level of traction force generation compared to wild type talin, despite the increased turnover rate and accumulation of talin and vinculin in the cells expressing this talin form.

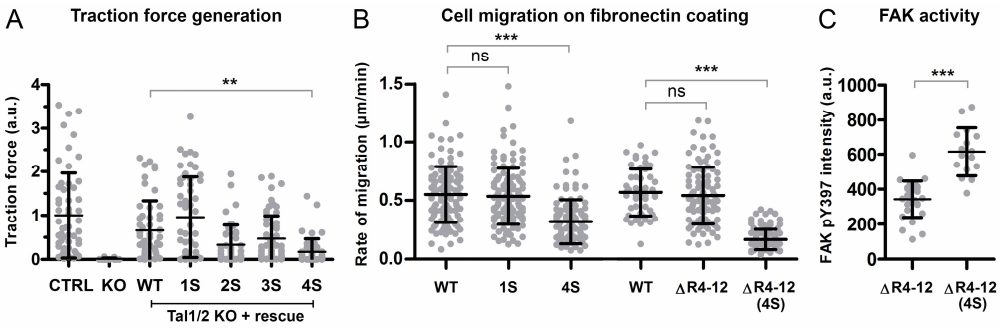

Figure 9. The stability of the talin R3 subdomain regulates traction force generation and the rate of cell migration. (A) Traction force generation of talin-1/2 knockout (KO) U2OS cells expressing destabilized talin proteins. (B) The rate of cell migration for *Tln1-/-Tln2-/-* cells expressing destabilized talin proteins. (C) The intensity of FAK pY397 immunostaining in adhesion sites. In all graphs horizontal lines represent the mean ± sd. ** p <0.001, *** p < 0.0001. Statistical testing by one-way ANOVA and Bonferroni test. Figure adapted from studies I and III.

Cell migration is dependent on the correct spatiotemporal coordination of adhesion formation, maturation and disassembly. Talin R3 subdomain destabilization by one mutation (1S) did not affect the rate of cell migration, while destabilization by all four mutations (4S) resulted in a significant decrease in the rate of cell migration on a fibronectin coated surface (Figure 9B). However, despite the increased adhesion turnover and decreased traction force generation, cells expressing the 4S protein retained their ability to migrate on fibronectin. In contrast, talin destabilization in the context of a truncated ΔR4-12 talin protein lacking rod subdomains R4-R12 resulted in a complete loss of cell migration (Figure 9B). This suggests that in the destabilized full-length protein, the presence of the other rod subdomains can compensate the

altered R3 subdomain mechanosensitivity. Indeed, cloning of additional talin R1-3 fragments into the destabilized ΔR4-12 (4S) protein in tandem configuration restored cell polarization and migration (not shown). These results indicate that the presence of talin rod subdomains with correct mechanical stability is critical for the spatiotemporal regulation of adhesion structure during cell migration. The local talin-dependent adhesion reinforcement and signaling generates cellular anisotropy that is a prerequisite for cell polarization and migration. In contrast, the facilitated unfolding of the destabilized talin 4S mutant prevents the correct spatiotemporal control of adhesion reinforcement and abolishes cellular signaling anisotropy.

The observed decrease in the overall traction force generation by the 4S mutant suggested, that the facilitated unfolding of the R3 subdomain may activate signaling pathways downregulating cell contractility. To investigate the signaling responses downstream of talin rod unfolding, we analyzed the level of focal adhesion kinase (FAK) activation in the adhesion complexes. Destabilization of the ΔR4-12 protein resulted in a significant increase in the level of adhesion-localized active (pY397) FAK (Figure 9C). FAK acts as a master switch regulating both cell contractility and the maturation and disassembly of adhesion complexes. Moreover, activated FAK is known to limit cell contractility by downregulating RhoA activity (Arthur and Burridge, 2001; Tsubouchi *et al.*, 2002; Mitra, Hanson and Schlaepfer, 2005). The results presented here indicate that the unfolding state of the talin R3 subdomain regulates FAK activity, adhesion maturation and cell contractility in response to the mechanical loading of the adhesion complex. However, we do not know yet how talin rod domain unfolding is coupled to the activation of FAK and regulation of its downstream targets.

5.2.3 Unfolding of the R3 subdomain differentially regulates the clustering of β1 and β3 integrins (I)

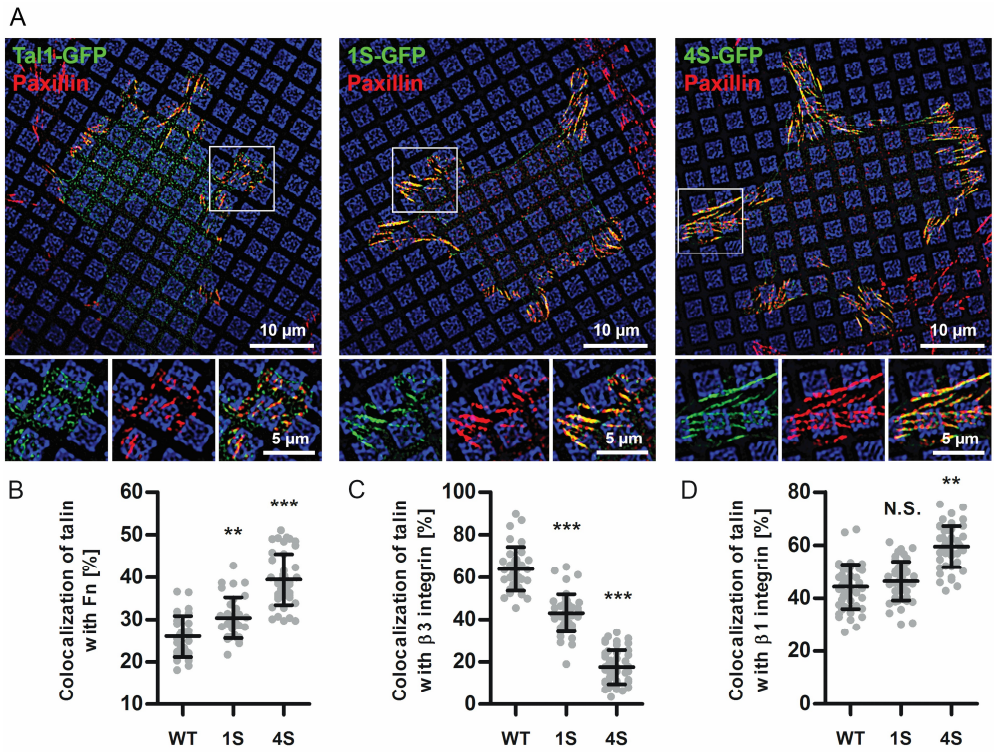

Figure 10. Talin rod domain unfolding regulates the clustering of different integrin isoforms. (A-B) Co-localization of talin with fibronectin (blue squares, 56% of total area) or vitronectin (black background, 44% of total area). Paxillin antibody staining was used as a marker of mature focal adhesions. (C-D) Co-localization of destabilized talin proteins with β3 or β1 integrins, respectively. In all graphs * $p < 0.01$, ** $p < 0.001$, *** $p < 0.0001$. Statistical testing by one-way ANOVA and Bonferroni test. Figure adapted from study I.

The increased FAK activation caused by talin destabilization suggested, that talin rod domain unfolding can regulate many different aspects of adhesion complex protein composition and function. In collaboration with the Bastmeyer group at the Karlsruhe Institute of Technology, Germany, we analyzed the substrate preference (fibronectin and vitronectin) of adhesions formed by cells expressing modified talin proteins (Figure 10A). In this analysis, adhesions formed around wild type talin strongly preferred vitronectin coated areas (Figure 10B). However, talin destabilization by the 1S or 4S mutations resulted in a shift in the adhesion substrate preference towards the fibronectin coating. As adhesion substrate specificity is

determined by the differential clustering of integrin isoforms, it seemed probable that the force-regulated unfolding of talin rod subdomains regulates the clustering of integrin heterodimers. To investigate this, we analyzed the co-localization of destabilized talin proteins with β3-integrins (fibronectin and vitronectin receptor) and β1-integrins (fibronectin receptor) in cells cultured on a fibronectin coating. Interestingly, talin destabilization (1S or 4S) resulted in a large decrease in the co-localization of talin with β3-integrins (Figure 10C) and in a concurrent increase in the co-localization of talin and β1-integrins (Figure 10D). The level of both effects followed the degree of talin destabilization on the WT - 1S - 4S continuum. Taken together, these results indicate that the unfolding of talin rod subdomains differentially regulates the clustering of β-integrin isoforms in the adhesion complex. Due to the different ligand specificities of different integrin isoforms, this talin rod-mediated regulation of integrin clustering is reflected onto the ECM substrate specificity of the entire adhesion complex.

5.2.4 The R8 subdomain regulates adhesion dynamics and cell migration through its interaction with DLC1 (II)

The R8 subdomain in talin contains many unique interaction sites not found in the other rod subdomains (see Figure 4). Therefore, the force-regulated unfolding of the R8 subdomain may function as an important trigger in the regulation of adhesion structure and signaling. In a collaborative effort with the del Rio group at the Imperial College London, UK, we set out to investigate the functional role of the R8 subdomain in talin mechanosensing. For this, we designed two cysteine mutations in the flexible linkers connecting the R7 and R8 subdomains (Figure 11A). The covalent disulphide bond formed by these cysteine residues prevents the separation of the linkers under mechanical force, and thus protects the R8 subdomain from unfolding. Accordingly, stretching of the clamped molecule with a single molecule atomic force microscope (smAFM) setup resulted in a decreased molecule unfolding length compared to wild type talin, confirming that the chosen strategy is capable of restricting the force-regulated unfolding of the R8 subdomain. Importantly, the presence of the disulphide clamp did not affect the unfolding force of the R7 bundle.

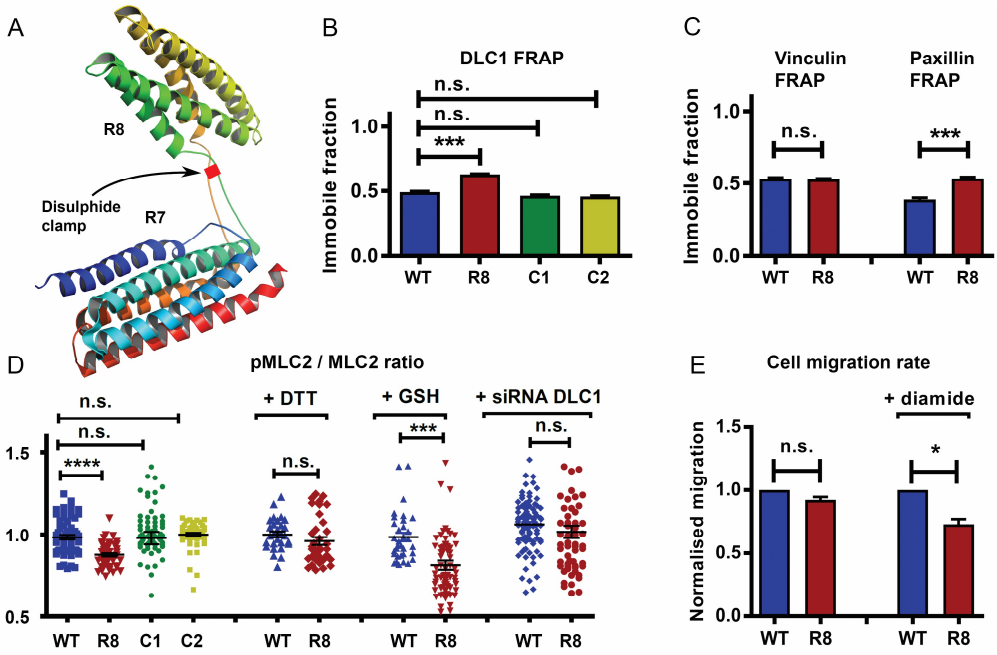

Figure 11 Unfolding of the R8 subdomain regulates adhesion dynamics, myosin activity and the rate of cell migration. (A) The strategy for restricting the unfolding of the R8 subdomain. The disulphide clamp was generated by Q1459C and S1583C mutations in the flexible R7-R8 linkers. (B-C) FRAP immobile fractions for DLC1, vinculin and paxillin in cells expressing wild type talin, talin with disulphide clamped R8 or control constructs with single cysteine mutations. (D) MLC2 activation (pS19) analysis for cells expressing modified talin proteins. DTT: dithiothreitol, cell-permeable reducing agent, GSH: glutathione, cell-impermeable reducing agent. (E) Normalized rate of cell migration in the presence and absence of 50 µM diamide. In all graphs, bars represent the mean ± SEM. In all graphs * $p < 0.05$, *** $p < 0.001$, **** $p < 0.0001$. Figure adapted from study II.

To investigate the processes regulated by the unfolding of the R8 subdomain in living cells, we expressed wild type talin or the R8 clamped mutant in *Tln1-/-Tln2-/-* MEF cells. As DLC1 and paxillin are known to interact with the R8 subdomain only in its folded conformation, we hypothesized that the restricted unfolding of the R8 subdomain in the clamped mutant would affect the dynamics of paxillin and DLC1 in the adhesion complex. Accordingly, the presence of both cysteine residues significantly increased the immobile fraction of both DLC1 and paxillin in FRAP experiments (Figure 11B, C), while single cysteine residues (C1 and C2) did not have an effect on paxillin or DLC1 dynamics. Although a single VBS is present in the talin R8 subdomain, we did not observe changes in vinculin dynamics (Figure 11C), possibly because of the presence of many other VBSs in the talin rod domain.

To investigate if the restricted unfolding of the talin R8 subdomain is reflected onto the regulation of RhoA by the RhoGAP DLC1, we analyzed the level of myosin light chain-2 (MLC2) phosphorylation in cells expressing wild type or R8 clamped talin. As expected, cells expressing the R8 clamped protein exhibited decreased myosin activity compared to wild type talin or control constructs (Figure 11D). This effect was abolished by the cell permeable reducing agent dithiothreitol, but not by cell impermeable glutathione, indicating that the observed effect is indeed dependent on the formation of the disulphide clamp in the R7-R8 linker (Figure 11D). To further investigate the role of adhesion-localized DLC1 in the regulation of myosin activity, we repeated the experiment in the presence of a siRNA silencing DLC1 expression. Silencing of DLC1 abolished the effect of the R8 clamp on myosin activity (Figure 11D), indicating that the observed effect was mediated by the interaction of the R8 subdomain with DLC1. As expected, the observed decrease in MLC2 activity was also reflected onto the level of cell contractility in traction force microscopy and collagen gel contraction assays (not shown). In *Tln1-/-Tln2-/-* cells, the R8 clamp caused a small, statistically insignificant decrease in the mean rate of cell migration (Figure 11E). To facilitate the formation of the R8 clamp in the cell cytosol, we repeated the experiment in the presence of the cell permeable oxidizing agent diamide. In the presence of 50 μM diamide, the R8 clamp resulted in a significant decrease in the rate of cell migration compared to cells expressing wild type talin (Figure 11E). Taken together, these results indicate that the force-dependent unfolding of the R8 subdomain regulates the cellular localization and activity of DLC1 and present a novel force-regulated signaling switch in adherent cells.

5.2.5 Talin mechanotransmission facilitates cell spreading, while talin rod subdomains are critically required for adhesion reinforcement (III)

Talin is the key force-bearing scaffold protein in the adhesion complex. Thus, the forces transmitted through talin are likely to regulate many force-dependent processes, such actin dynamics and fibronectin fibrillogenesis also independently of talin rod domain unfolding (Hayakawa, Tatsumi and Sokabe, 2011; Weinberg, Mair and Lemmon, 2017). However, while the concept of talin rod domain unfolding in adhesion mechanosensing is well established, the contribution of talin mechanotransmission in the regulation of adhesion stability and signaling has remained unknown. To investigate the roles of talin mechanotransmission and mechanotransduction in adhesion stabilization and signaling, we created a panel of expression constructs (Figure 12A) lacking different parts of the talin rod domain and expressed them in *Tln1-/-Tln2-/-* cells.

Expression of the talin head domain in talin-null cells promoted cell attachment to ECM proteins and facilitated isotropic cell spreading, but did not allow cell polarization or migration (Figure 12B-D). In contrast to the talin head domain, the ΔR1-12 protein allows simultaneous binding to both β-integrin tail domains and actin filaments and thus restores the transmission of mechanical forces between ECM and the actin cytoskeleton. Expression of this talin form dramatically increased the mean cell area compared to talin head-expressing cells. However, cells expressing this talin form were unable to polarize or migrate, suggesting that the mechanical coupling of ECM to the actin cytoskeleton cannot mediate the reinforcement of adhesion complexes in the absence of talin rod subdomains. In contrast, expression of either ΔR1-10 or Δ4-12 proteins containing 2 or 3 mechanosensitive talin rod subdomains, respectively, largely restored cell polarization and migration.

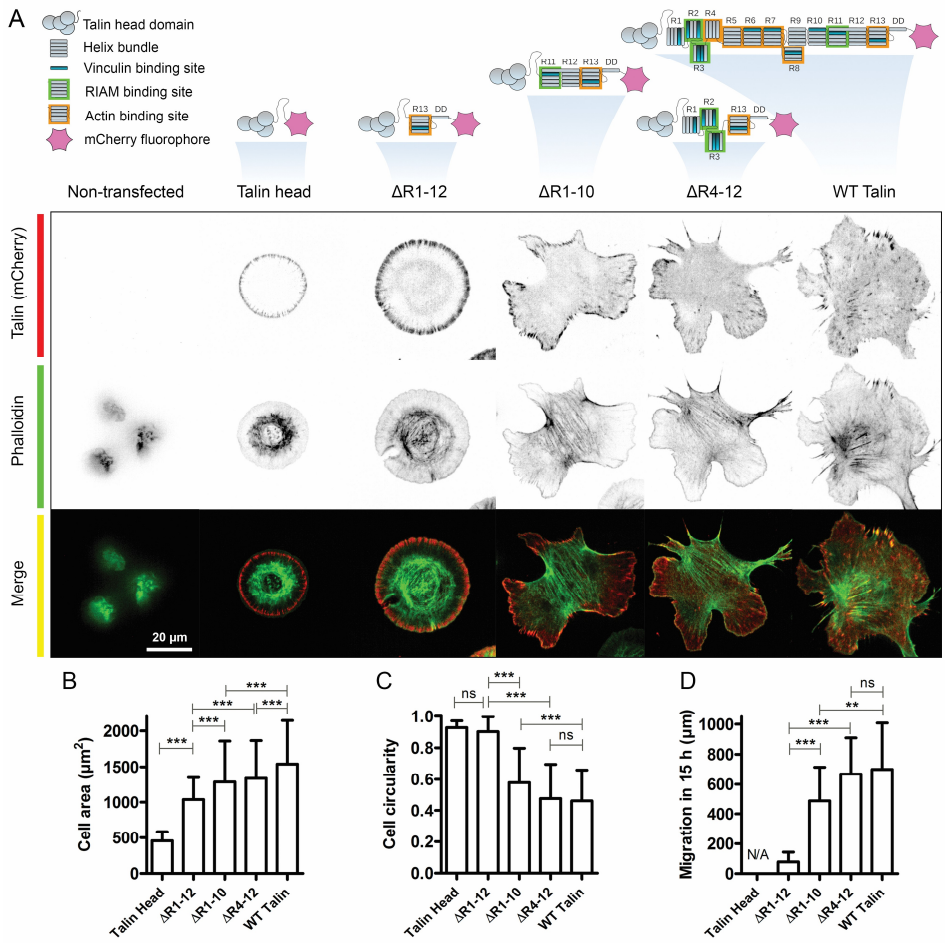

Figure 12. The presence of the rod subdomains is required for adhesion reinforcement and cell migration. (A) Schematic models of the analyzed modified talin forms and representative images of *Tln1-/-Tln2-/-* cells expressing them. (B-C) Cell area and cell circularity analysis. A circularity value of 1 corresponds to a perfectly circular cell. (D) Migration analysis on fibronectin coating. In all graphs * $p < 0.05$, ** $p < 0.01$, *** $p < 0.001$. Statistical testing by one-way ANOVA and Bonferroni test. Figure adapted from study III.

To estimate the level of traction force generation by the modified talin forms, we used a 3D collagen gel contraction assay (Robinson *et al.*, 2016). While the cells expressing either the ΔR4-12 protein or WT talin were able to macroscopically contract the collagen gel in 72 hours, cells expressing the ΔR1-12 protein exhibited only a small increase in gel contractility compared to non-transfected *Tln1-/-Tln2-/-* cells. This indicates that despite the mechanical connectivity of the ΔR1-12 protein, adhesion reinforcement by rod domain unfolding is required for efficient traction force generation. However, the cells expressing the ΔR1-12 protein were able to

reorganize fluorescent fibronectin coated on glass coverslips. This indicates that despite the lack of talin rod-dependent adhesion reinforcement, the fibronectin-integrin-talin-actin linkages can transiently withstand the high-magnitude forces required for the reorganization of the fibronectin molecules adsorbed to the surface of the glass coverslip.

5.2.6 Talin mechanotransmission regulates adhesion dynamics and the rate of actin retrograde flow (III)

The talin-mediated engagement of the adhesion clutch is known to regulate the rate of actin retrograde flow in the cell lamellipodium (Thievessen *et al.*, 2013). To investigate the rate of actin retrograde flow in the presence and absence of rod-mediated adhesion reinforcement, we used DIC imaging to analyze cells expressing talin head, ΔR1-12 and wild type talin. As expected, the ΔR1-12 protein was sufficient to decrease the rate of actin retrograde flow compared to the talin head domain (Figure 13A). As the expression of wild type talin caused only a small further reduction, it seems that the interaction between talin ABS3 and actin is critical for the engagement of the adhesion clutch in cell lamellipodia. Importantly, this initial engagement of the clutch seems to be largely independent of the functions of talin ABS2 or vinculin.

To investigate if the mechanical connectivity of the ΔR1-12 protein is reflected onto its turnover in the adhesions, we analyzed the dynamics of the talin head, ΔR1-12 and wild type talin by FRAP. As expected, the ΔR1-12 protein exhibited decreased FRAP mobility compared to the talin head domain (Figure 13B). This indicates that even in the absence of talin rod domain unfolding, the transmission of mechanical forces through talin regulates its dynamics. However, the expression of wild type talin resulted in a further decrease in the mobile fraction of talin (Figure 13B), indicating that the talin rod-mediated adhesion reinforcement significantly contributes to the regulation of talin mobility in the adhesion complex. In addition, the t_{half} of wild type talin in FRAP was decreased compared to the talin head domain or the ΔR1-12 protein (Figure 13B). This suggests that despite the decreased overall mobility of wild type talin, a fraction of the talin molecules may exhibit rapid turnover in the adhesion complex.

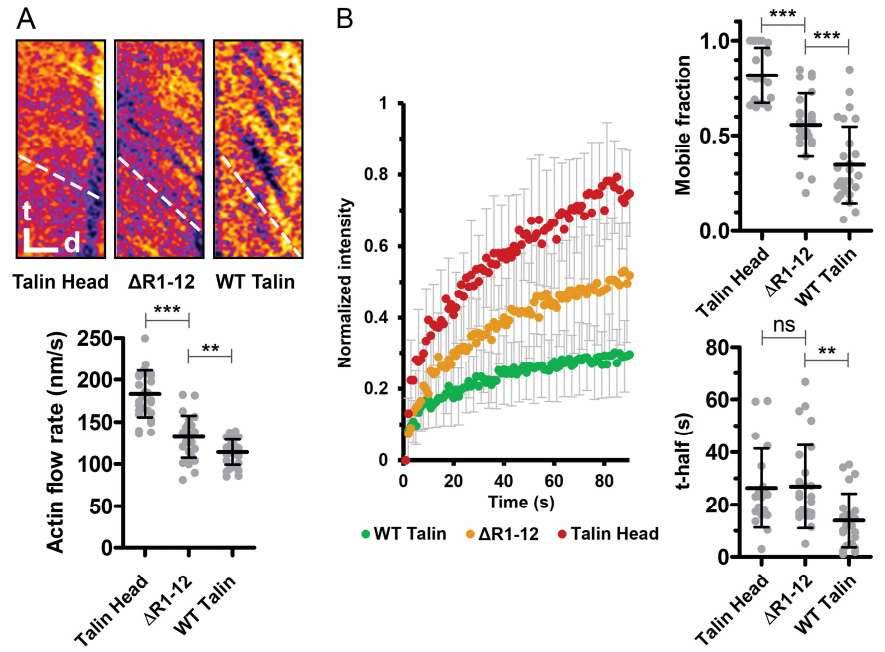

Figure 13. Mechanotransmission through talin ABS3 decreases the rate of actin retrograde flow in the lamellipodium and contributes to adhesion stability. (A) The rate of actin retrograde flow in lamellipodia. In the kymograms, the vertical and horizontal scale bars are 10 s and 2 µm, respectively. (B) FRAP analysis of different talin proteins. In all graphs, ** $p < 0.01$, *** $p < 0.001$. Statistical testing by one-way ANOVA and Bonferroni test. Figure adapted from study III.

5.2.7 Both talin mechanotransmission and mechanotransduction contribute to adhesion signaling (III)

As both talin mechanotransmission and mechanotransduction were found to contribute to adhesion stability, we were curious to investigate their relative contributions in adhesion signaling. In collaboration with the Varjosalo group at the University of Helsinki, Finland, we performed high-resolution quantitative MS-MS phosphoproteome analysis for lysates of cells expressing the talin head domain, ΔR1-12 or wild type talin. Pairwise comparison of the head domain and the ΔR1-12 protein revealed that the expression of the ΔR1-12 protein modulates the phosphorylation status of many proteins associated with the structure or signaling of the adhesion complex. Many of the differentially phosphorylated proteins, such as paxillin, p120Catenin and p190RhoGAP are known to interact with the central adhesion tyrosine kinases FAK and Src. The differential phosphorylation of these proteins suggests that the transmission of mechanical forces through the ΔR1-12

protein may regulate adhesion phosphotyrosine signaling independently of talin rod domain unfolding. In comparison to ΔR1-12, the expression of wild type talin caused further changes in the phosphorylation status of many adhesion proteins. Importantly, these proteins included many regulators of actin polymerization and bundling (e.g. vinculin, zyxin, Evl and palladin), suggesting that talin rod domain is required for the correct regulation of various actin binding proteins.

To investigate this further, we used activation-specific antibodies against different adhesion signaling proteins in confocal microscopy. Analysis of the mCherry intensity of the modified talin proteins indicated that although the turnover, shape and size of the adhesion complexes were largely different, all studied talin proteins accumulated into adhesions roughly to the same extent (Figure 14A). The recruitment of adhesion signaling proteins, in contrast, was found to be dependent on the domain composition of the expressed talin proteins. In cells expressing the talin head domain, small punctate foci of activated FAK were observed at the front of the cell lamella. However, these sites of FAK activation did not co-localize with the talin head domain (Figure 14B). In contrast, the ΔR1-12 protein induced the recruitment of activated FAK into the adhesion sites (Figure 14B, C), indicating that the mechanical tension transmitted through the ΔR1-12 protein regulates adhesion signaling independently of talin rod domain unfolding. However, the co-localization of the ΔR1-12 protein and FAK was only partial, suggesting that the lateral layering of the adhesion complex was somewhat abnormal in these cells. Expression of any of the talin forms containing force-regulated rod subdomains significantly increased the level of adhesion-localized FAK (Figure 14B, C). As expected, the activity (pY31) of paxillin closely followed the activity of FAK (Figure 14D), indicating that the talin-dependent activation of FAK is reflected onto its substrate proteins. Of the known FAK and Src-substrates, p190RhoGAP is the major negative regulator of RhoA and myosin activity in adhesion complexes (Arthur, Petch and Burridge, 2000; Arthur and Burridge, 2001; Holinstat et al., 2006). As expected, expression of the ΔR1-12 protein promoted the recruitment of activated (pY1105) p190RhoGAP into the adhesion complex (Figure 14E). However, in these cells, the region of activated MLC2 extended all the way to the edge of the cell lamellipodium (Figure 14F), indicating that the level of FAK and p190RhoGAP activity was insufficient to correctly downregulate the activity of RhoA in the cell lamellipodium. In contrast, the expression of either the ΔR4-12 protein or wild type talin resulted in the formation of a distinct zone lacking MLC2 activity close to the leading edge of the lamellipodium (Figure 14F). This indicates that although the ΔR1-12 protein is able

to mediate the recruitment and activation of FAK and its downstream target proteins, either the low level of FAK activity or the lack of parallel talin rod-dependent mechanisms prevent the correct regulation of RhoA and myosin activity in the cell lamellipodium.

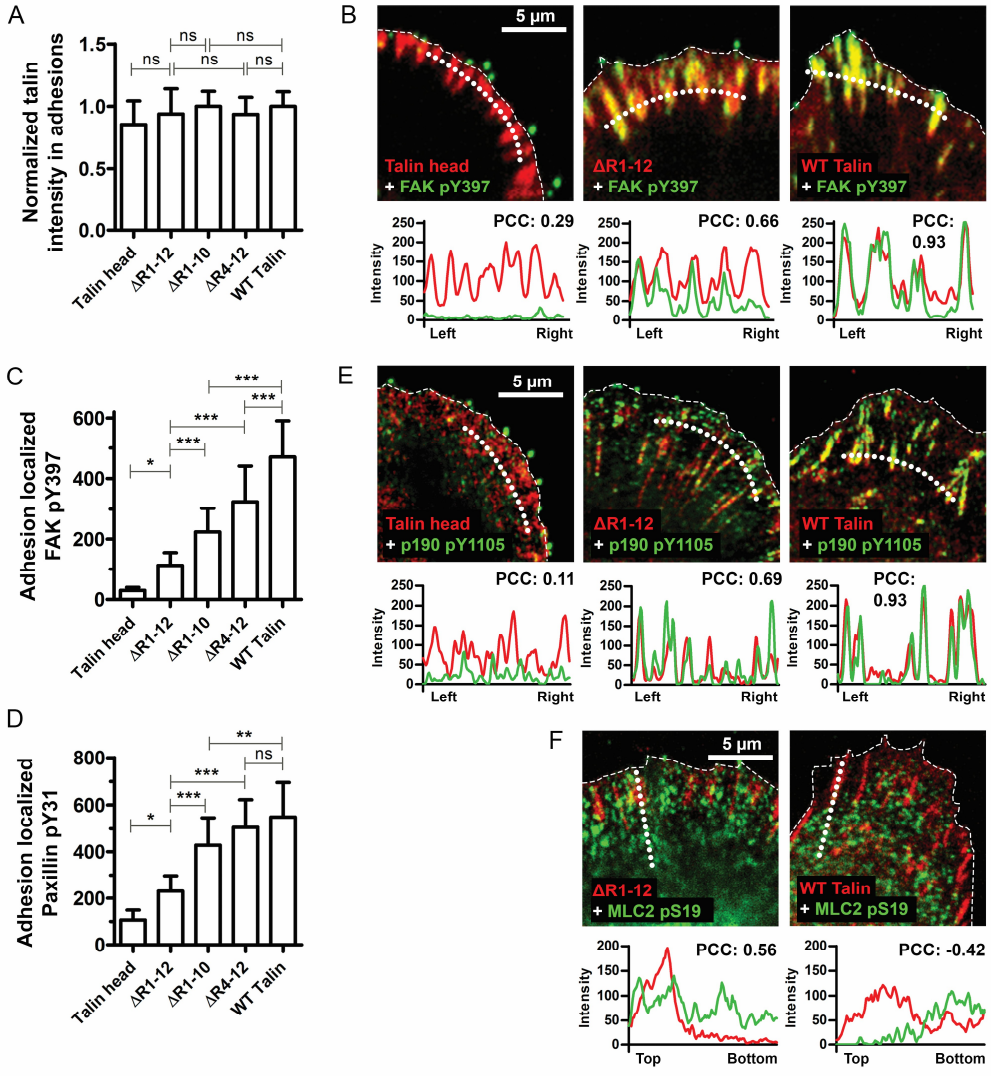

Figure 14. Talin mechanotransmission activates phosphotyrosine signaling. (A) Background-normalized intensities of the studied talin proteins in adhesion sites. Intensity values normalized to wild type talin. (B) Co-localization analysis for activated (pY397) FAK. PCC = Pearson's correlation coefficient. (C-D) Intensity analyses for activated FAK and paxillin. (E-F) Co-localization analyses for activated p190RhoGAP and MLC2. In all graphs * $p < 0.05$, ** $p < 0.01$, *** $p < 0.001$. Statistical testing by one-way ANOVA and Bonferroni test. Figure adapted from study III.

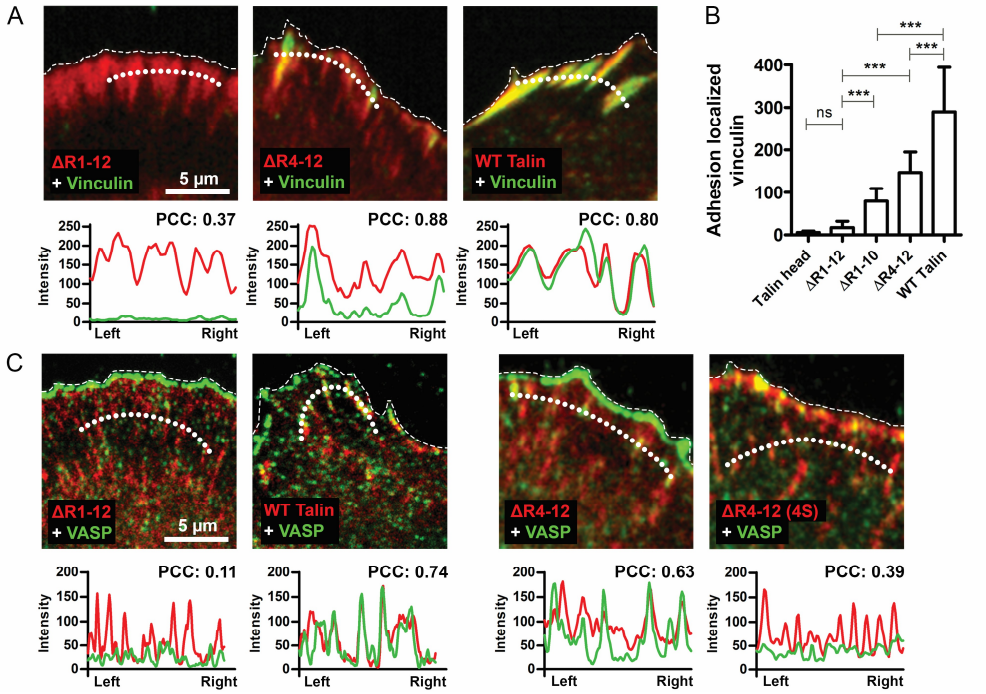

Figure 15. The presence and the force-regulated unfolding of talin rod subdomains are required, but not sufficient for VASP recruitment into the adhesion complex. (A-B) Co-localization and intensity analyses for vinculin. *** $p < 0.001$. Statistical testing by one-way ANOVA and Bonferroni test. (C) Co-localization analysis for VASP. Figure adapted from study III.

As expected, the recruitment of vinculin into adhesion sites was found to be fully dependent on the presence of force-regulated talin rod subdomains (Figure 15A, B). The degree of vinculin recruitment roughly followed the number of cryptic vinculin binding sites in each talin construct, indicating that multiple vinculin binding sites are concurrently activated in each talin protein (Figure 15B). To test if the recruitment of vinculin is reflected onto its interaction partners regulating actin dynamics, we used an antibody against actin regulatory protein VASP. In line with the lack of vinculin recruitment, the ΔR1-12 protein failed to recruit any VASP into adhesion sites, while both the ΔR4-12 protein and wild type talin induced robust recruitment of VASP (Figure 15C left side). Despite the increased recruitment of vinculin by the destabilized ΔR4-12 (4S) protein (Figure 8A), it largely failed to recruit VASP into the adhesion complexes in these cells (Figure 15C right side). This indicates that although talin rod subdomains are required for the recruitment of VASP into adhesions, presumably through their interactions with vinculin and RIAM proteins, also other factors are required for the efficient recruitment of VASP.

Such factors may include the presence of specific adhesion proteins, the correct nanoscale organization of the adhesion complex or its sufficient mechanical loading (Lafuente *et al.*, 2004; Carisey *et al.*, 2013; Liu *et al.*, 2015).

Taken together, these results demonstrate that the transmission of mechanical forces through talin contributes to the activation of adhesion phosphotyrosine signaling independently of the talin rod subdomains. However, the presence of the rod subdomains and their mechanical activation are required for the correct regulation of the adhesion complex composition and signaling in response to its mechanical loading.

5.3 Altered expression of talin and vinculin in atherosclerosis (IV)

5.3.1 Atherosclerotic plaques show decreased expression of talin-1, talin-2 and vinculin transcripts (IV)

Mechanical forces act as important regulators of artery homeostasis. Accordingly, defects in artery mechanosensing have been associated with various human diseases. In collaboration with the Lehtimäki group at the University of Tampere, Finland, we set out to investigate the expression levels of talin-1, talin-2 and vinculin transcripts in atherosclerotic plaques. Samples from the left internal thoracic artery (LITA), known to be resistant for the development of atherosclerosis, were used as control samples. Microarray analysis revealed significantly decreased expression of both talin and vinculin transcripts in atherosclerotic plaques of the carotid artery, abdominal aorta and femoral artery (Figure 16). Further analysis revealed a negative trend, albeit statistically insignificant, in the expression levels of talin and vinculin transcripts in plaques histologically classified as unstable, compared to stable plaques (Figure 16). The results of the microarray analysis were confirmed by qRT-PCR analysis yielding similar results.

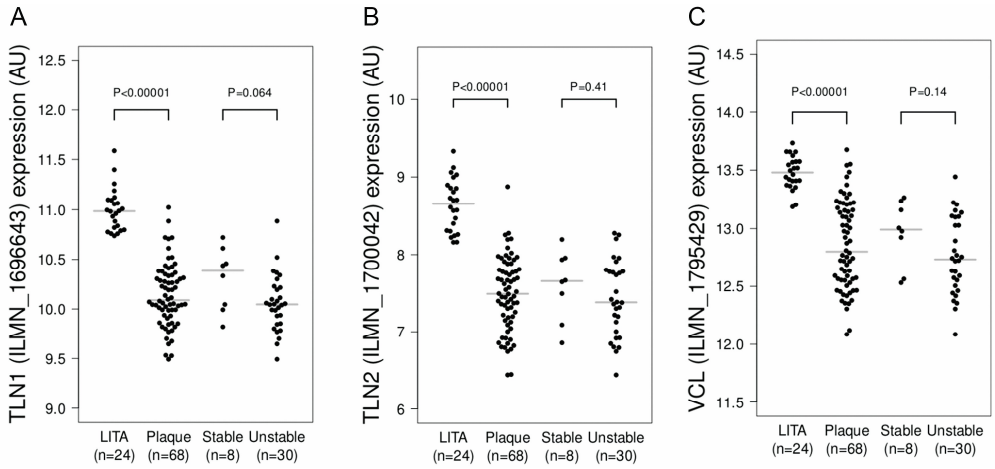

Figure 16. Expression of talin (TLN1, TLN2) and vinculin (VCL) transcripts in the microarray analysis. (A-C) The expression levels of the studied transcripts presented on a log2 scale. The analyzed plaque samples were further classified as either stable or unstable according to the presence of fissure, rupture, hemorrhage or thrombosis. Figure adapted from study IV.

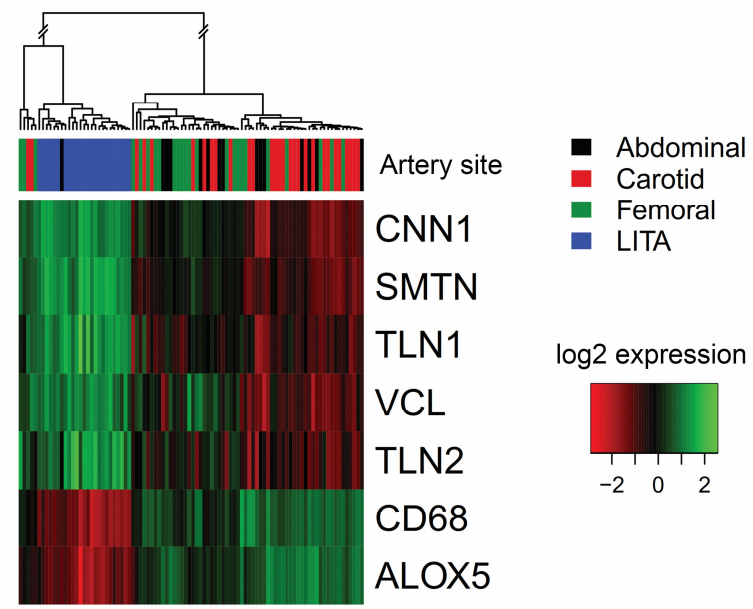

Figure 17. Hierarchical clustering analysis of the log2 expression values of talin and vinculin transcripts and tissue-specific markers. CNN1 (Calponin-1) and SMTN (Smoothelin) were used as markers of mature vascular smooth muscle cells. CD68 (Cluster of differentiation 68) and ALOX5 (Arachidonate 5-Lipoxygenase) were used as markers of macrophage and leukocyte maturation. Figure adapted from study IV.

Hierarchical clustering analysis was used to classify the samples according to the expression levels of talin and vinculin transcripts, markers of vascular smooth muscle cells (VSMC)(Smoothelin (SMTN), Calponin-1 CNN1)) and markers of leukocyte maturation and inflammation (Cluster of differentiation 68 (CD68), arachidonate 5-lipoxygenase (ALOX5)). Hierarchical clustering revealed a clear separation of the samples of LITA from the samples of all three studied plaque sites (Figure 17). Concurrently with the decreased expression of talin and vinculin transcripts, the expression of VSMC markers was downregulated and the expression of inflammation markers upregulated. All LITA samples clustered together and showed robust expression of VSMC markers and low expression of inflammation markers (Figure 17).

5.3.2 Talin-1, talin-2 and vinculin have altered expression patterns in atherosclerotic plaques (IV)

The microarray and qRT-PCR analyses indicated that the expression levels of talin (talin-1, talin-2) and vinculin transcripts were downregulated in atherosclerotic plaques. To investigate the expression patterns of talin and vinculin at the protein level, we stained frozen tissue sections with talin- and vinculin-specific antibodies. Talin-1, talin-2 and vinculin were all found to be robustly expressed in the *tunica intima* and *tunica media* of the LITA sections representing healthy tissue (Figure 18A, B). In contrast, in the sections of atherosclerotic plaques from carotid artery, we observed a dramatic loss of talin-1 expression in the *tunica intima*. This was especially noticeable in endothelial cells, marked by PECAM-1 antibody staining. While talin-1 was completely absent from the endothelial cells in the plaque samples, its expression in the thickened *tunica intima* exhibited a gradual increase towards the *tunica media*. Immunostaining for talin-2 revealed a similar loss of talin-2 expression in endothelial cells (Figure 18B). However, we did not observe a gradient of talin-2 expression in the thickened *tunica intima* (Figure 18B). As seen for talin-1 and talin-2, also vinculin expression was found to be decreased in endothelial cells. However, vinculin was robustly expressed in the lower parts of the thickened *tunica intima*.

To confirm that the tissue morphology and the expression patterns of talin in LITA accurately represent healthy artery wall, tissue sections of formalin-fixed and paraffin-embedded samples of healthy carotid artery and abdominal aorta were stained with a talin-1 antibody and hematoxylin-eosin (HE) staining. We observed a similar intense talin-1 staining in both LITA and healthy carotid artery and

abdominal aorta. Unlike in atherosclerotic plaques, we did not observe a gradient of talin expression in the healthy tissue. Furthermore, HE staining revealed a similar tissue morphology for LITA and healthy tissue samples, confirming the suitability of LITA as a healthy control tissue when investigating the expression patterns of adhesion proteins in atherosclerotic plaques.

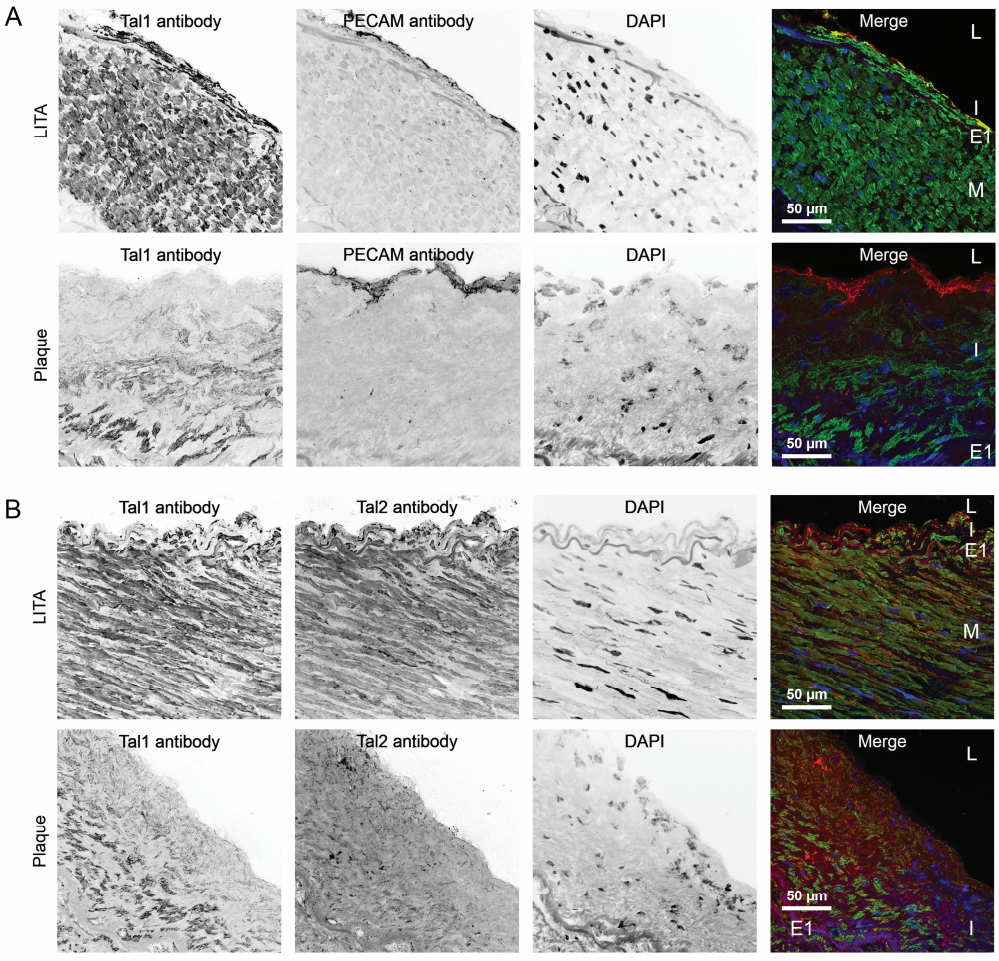

Figure 18. Localization of talin proteins in samples of carotid artery plaques and LITA. (A) Talin-1 and platelet endothelial cell adhesion molecule 1 (PECAM-1) staining for carotid artery plaque and LITA control. PECAM-1 staining is used as a marker of endothelial cells. L, lumen; I, *tunica intima*; E1, internal elastic lamina; M, *tunica media*. (B) Talin-1 and talin-2 immunostaining. Figure adapted from study IV.

6 DISCUSSION

6.1 The structure-function relationship of the talin rod subdomains

Talin proteins are ubiquitously expressed in most human cell types. This suggests that in different tissues, talin is subjected to mechanical forces of vastly different magnitudes and forms. It seems possible that the "beads in a string"-like structure of the talin rod domain has evolved to allow efficient talin-mediated mechanosensing in the different tissue contexts. As previously demonstrated, each talin rod subdomain has its characteristic mechanical and biochemical properties (Haining *et al.*, 2016; Yao *et al.*, 2016; Klapholz and Brown, 2017; Gough and Goult, 2018). Due to the elongated structure of the rod domain, the unfolding of a single rod subdomain is largely independent of the conformational state of its flanking domains (with the exception of the R7-R8 double domain). Therefore, high magnitude forces are likely to activate different protein interactions and signaling pathways than low magnitude forces (Gough and Goult, 2018). Although in dynamic systems, the key determinant of talin activation is likely to be its *loading rate*, and not the magnitude of the force *per se*, this simplified model helps to investigate the structural features determining the mechanical properties of the talin rod subdomains (Elosegui-Artola *et al.*, 2016; Elosegui-Artola, Trepat and Roca-Cusachs, 2018).

Since the R3 subdomain has the lowest mechanical stability of all talin rod subdomains, its force-regulated unfolding is likely to function as the initial signal of mechanical tension through the talin protein. To investigate the structure-function relationship of the R3 subdomain, we analyzed the structural determinants contributing to its mechanical stability by utilizing computational SMD simulations (Study I). Based on these analyses, it seemed probable that the fit of the α-helix packing in the R3 subdomain, and in talin subdomains in general, is the key determinant of their mechanical stability. Accordingly, in the R3 subdomain, we identified four leucine and isoleucine residues, whose mutagenesis to more hydrophilic serine was likely to decrease the mechanical stability of the bundle. As expected, in biochemical analysis, we observed a gradual decrease in the thermal

stability of R3 subdomain fragments containing one to four destabilizing mutations, confirming the feasibility of the chosen destabilization strategy. In contrast to the destabilized talin proteins investigated in the study I, mutations stabilizing the talin R3 subdomain have been previously described (Goult, Zacharchenko, *et al.*, 2013). In line with the results presented in the study I, also the stabilization of the R3 subdomain through the improved packing of its hydrophobic core was demonstrated to affect cellular mechanosensing (Goult, Zacharchenko, *et al.*, 2013; Elosegui-Artola *et al.*, 2016). In addition to the fit of the hydrophobic packing of the α-helix bundle core, the configuration of the force application, namely shear or zipper configuration, has been recently proposed to affect the mechanical stability of the rod subdomains (Mykuliak *et al.*, 2018). Thus, it seems that multiple factors contribute to the mechanical and biochemical properties of the individual talin rod subdomains.

6.2 Unfolding of the R3 subdomain regulates multiple aspects of adhesion structure and function

In study I, we found that the destabilization of the R3 subdomain increased the accumulation of both talin and vinculin into adhesion sites (Figure 8A). This was expected, as the mechanical stability of the talin subdomains has been proposed to regulate the activity of the cryptic VBSs (Hytönen and Vogel, 2008; Yao *et al.*, 2016). As vinculin binding to the exposed VBSs is known to regulate refolding and mobility of talin in the adhesion complex, it seems likely that the increased accumulation of talin resulted from the facilitated vinculin binding. (Humphries *et al.*, 2007; Carisey *et al.*, 2013). Surprisingly, despite the increased accumulation of talin and vinculin, the destabilization of the R3 subdomain also increased their mobility in the adhesion complex (Figure 8B, C). Although this finding seems counterintuitive at first, it may be explained by the altered distribution of mechanical tension between multiple talin molecules and by the decreased vinculin/talin ratio. As the amount of talin in the adhesion complex is increased by talin destabilization, the cytoskeletal tension is distributed to a larger number of talin molecules, resulting in a decrease in the tension acting on each individual protein. Furthermore, while talin destabilization increased the recruitment of vinculin into the adhesion complex, the overall vinculin/talin ratio was decreased. As the dissociation of vinculin from talin likely precedes the dissociation of talin itself from the adhesion complex, the low vinculin/talin ratio increases the mobility of talin in the adhesion complex.

In addition to the altered adhesion protein accumulation and mobility, talin destabilization was found to downregulate cellular traction force generation. Although we cannot fully distinguish the contributions of cellular contractility and adhesion stability to the overall level of traction force generation, this finding suggests that talin rod domain unfolding may act to downregulate myosin activity. Talin destabilization also induced the recruitment of activated FAK into the adhesion complex. FAK is known to regulate multiple aspects of adhesion maturation and turnover through RhoA-dependent mechanisms, and its activation is critical for the coordinated disassembly of the adhesion complex (Orr *et al.*, 2004; Webb *et al.*, 2004; Lawson *et al.*, 2012). Thus, it seems possible that the facilitated unfolding of the R3 subdomain activates a FAK-dependent negative feedback loop limiting myosin activity and adhesion growth. This kind of negative feedback would prevent the indefinite growth of the adhesion complex under mechanical tension and set a limit for the maximum adhesion size. Accordingly, cells are known to control adhesion complex stability and traction force generation also independently of the transmitted mechanical force, which facilitates the disassembly of mechanically loaded adhesions at the trailing edge of the cell (Stricker *et al.*, 2011; Oakes *et al.*, 2012). How the force-regulated unfolding of the talin rod subdomains regulates this negative feedback loop remains to be investigated in detail.

Destabilization of the R3 subdomain was also found to affect the co-localization of talin with different integrin isoforms (Figure 10). This indicates that talin rod domain unfolding not only regulates the recruitment of talin rod-binding proteins, but also the substrate specificity of the entire adhesion complex. As the rod R3 subdomain does not directly interact with β-integrins, it seems likely that the increased clustering of β1 integrins is mediated by talin-rod activated adhesion signaling. Interestingly, β1 and β3 integrins have been associated with different functions in the cell, namely structural strength and adhesion mechanotransduction (Roca-Cusachs *et al.*, 2009; Schiller *et al.*, 2013). It seems possible that the force-regulated unfolding of the talin rod domain facilitates the recruitment of β1-integrins to reinforce the ECM-β-integrin interaction. As α5β1- and αVβ3-integrins, the major types of integrin heterodimers present in fibroblast cells, have different affinities for fibronectin and vitronectin, their relative levels in the adhesion complex determines its ECM substrate specificity. However, whether this talin rod-dependent regulation of integrin clustering is mediated by an active signaling response (e.g. increased activation of FAK), or results from changes in adhesion protein dynamics and traction force generation remains to be investigated in future studies.

6.3 The R8 subdomain acts as a switch regulating DLC1 recruitment and myosin activity

Although the force-regulated interaction of vinculin with talin VBSs is well characterized, only little is known about how mechanical tension regulates the recruitment and release of the other talin rod-binding proteins (Goult, Zacharchenko, *et al.*, 2013; Atherton *et al.*, 2015). The unusual structural position of the R8 subdomain and its many interaction partners raise an interesting question about its functionality as a mechanosensor. Although the R8 subdomain has been demonstrated to be mechanically relatively unstable (Haining *et al.*, 2016, 2018; Yao *et al.*, 2016), its position in the middle of the R7 subdomain protects it from mechanical tension until the unfolding of the R7 subdomain. Thus, the structural properties of the R8 domain are not restricted by the requirement for sufficient mechanical stability, which may have contributed to the development of its many specific interactions during the evolution of talin. Interestingly, the R8 subdomain is more conserved in mouse talin proteins than the rod subdomains flanking it (Figure 4), suggesting that its correct structure is critical for the functionality the talin protein (Gough and Goult, 2018).

In collaboration with the del Rio group at the Imperial College London, we aimed to investigate the role of the talin R8 subdomain in talin mechanosensing. To achieve this, we introducing two cysteine mutations into specific, closely positioned residues within the flexible R7-R8 linkers. Experiments with smAFM demonstrated that the cysteine residues readily form a disulphide bond *in vitro* and confirmed the suitability of the chosen R8 clamping strategy. In fibroblast cells, co-expression of the R8-clamped talin was found to decrease the mobility of both GFP-DLC1 and GFP-paxillin compared to cells expressing wild type talin (Figure 11). This indicates that the unfolding of the R8 subdomain under mechanical force regulates the dynamics of proteins interacting with it in its folded conformation. Importantly, previous studies have demonstrated that the biological activity of the RhoGAP protein DLC1 is dependent on its interaction with the R8 subdomain (Li *et al.*, 2011; Zacharchenko *et al.*, 2016). This suggests that the conformation of the R8 subdomain regulates both DLC1 recruitment and its activity in the adhesion complex. Indeed, we observed decreased MLC2 activity and traction force generation in cells expressing the R8-clamped talin constitutively interacting with the DLC1 protein (Figure 11). This talin- and force-dependent regulation of DLC1 activity presents a novel mechanism of mechanotransduction in adhesion complexes.

As explained in the section 2.3.7 of this thesis, DLC1 is best known for its role as a tumor suppressor protein. The loss of the genes encoding DLC1 and their decreased expression are known to be general features of a wide range of human cancers (Durkin *et al.*, 2007; Kim *et al.*, 2009). Importantly, the identification of the talin- and force-dependent regulation of DLC1 sheds light on the mechanisms regulating its functions both in normal cell physiology and in cancer cells. While the altered mechanical stiffness of solid tumors has been associated with increased metastatic potential of the tumor cells (Zaman *et al.*, 2006; Swaminathan *et al.*, 2011; Reid *et al.*, 2017), the roles of talin and DLC1 mechanosensing in the regulation of cancer cell migration are still poorly understood. In the future, it will be interesting to investigate how the positive feedback loop comprising the force-regulated R8-DLC1 interaction, RhoA and myosin contributes to the regulation of contractility and metastatic potential of cancer cells.

The use of disulphide bonds to regulate the conformational state of cytosolic proteins (study II) presents a novel strategy for investigating protein functions in living cells. Despite the generally reducing conditions of the cell cytosol (López-Mirabal and Winther, 2008), the cellular effects observed in the presence of two, but not one, cysteine mutations indicate that the disulphide bond formed as planned. Although it is likely that only a certain fraction of all possible disulphide bonds are formed in living cells, the results of study II demonstrate the suitability of disulphide clamps as tools for regulating protein conformation within the cytosol. Importantly, the extent of the observed effects could be modulated by the use of cell-permeable reducing and oxidizing agents, such as dithiothreitol and diamide (Figure 11D, E). However, it is not currently known if disulphide clamps could be utilized as a general strategy to regulate the conformation of cytosolic proteins, or if the formation of the clamp is dependent on the specific cellular localization of the studied protein. Importantly, the results of a recently published study suggest that cellular redox balance is affected by the proximity to membrane structures and vesicular compartments within the cell. This indicates that cellular redox balance is a much more complicated matter than what was previously thought (Hatori *et al.*, 2018).

6.4 The different roles of talin in adhesion mechanosensing

6.4.1 Talin mechanosensing is a robust process mediated by multiple parallel mechanisms

The sensing of mechanical forces by cells is dependent on biomolecules whose conformation, dynamics or local concentration are modulated in response to their mechanical loading. To date, many different mechanisms have been proposed to transduce mechanical forces in integrin-mediated adhesions. These mechanisms include force-regulated phosphorylation of p130Cas (Sawada *et al.*, 2006; Janoštiak *et al.*, 2014), force-regulated cleavage of talin by calpain (Saxena *et al.*, 2017), force-regulated conformational changes in filamin proteins (Razinia *et al.*, 2012) and direct FAK-mediated mechanosensing (Zhou *et al.*, 2015), to name a few. Nevertheless, talin is commonly considered to function as the key mechanosensor of the adhesion complex. Accordingly, experiments with fibroblast cells, both in the studies comprising this thesis and elsewhere, have demonstrated the critical role of talin in the force-regulated reinforcement and maturation of integrin-mediated adhesions (Zhang *et al.*, 2008; Theodosiou *et al.*, 2016). In a simplified model of talin functions, the talin head domain mediates the recruitment of talin to the plasma membrane and the activation of integrins (Zhang *et al.*, 2008; Pinon *et al.*, 2014), while the rod domain forms a mechanical connection between actin filaments and β-integrins (Chan and Odde, 2008; Elosegui-Artola *et al.*, 2016). This talin-dependent engagement of the adhesion clutch has been demonstrated to be required for the substrate sensing and downstream signaling of fibroblast cells (Austen *et al.*, 2015; Elosegui-Artola *et al.*, 2016). However, as many parallel talin-dependent and talin-independent mechanisms mediate focal adhesion mechanosensing, the contributions of each mechanism in the regulation of cellular functions have remained incompletely understood.

Based on the studies I-III and previously published results, it seems likely that talin participates in the regulation of adhesion structure and function through at least three general mechanisms (Table 3, Figure 19). These mechanisms are (1) the force-regulated structural reinforcement of the adhesion complex, (2) the force-regulated interactions of the talin rod domain with signaling proteins and (3) the regulation of other cellular mechanosensors by the transmission of mechanical forces through the talin protein, i.e. talin mechanotransmission. Although these three mechanisms are

here described as independent processes, it is noteworthy that in most cases they are tightly functionally interlinked. For example, the force-regulated binding of vinculin to talin rod subdomains simultaneously modulates talin turnover, mechanically reinforces the adhesion complex and recruits multiple signaling proteins. The details of each of these three general mechanisms are briefly discussed in the following sections and the proteins and talin domains involved in them listed in the Table 3.

Table 3. The talin-dependent mechanisms of cellular mechanosensing

Mechanism	Mode of action	Cellular response	Talin domains required	Experimental evidence	Key references
Force-regulated structural reinforcement of the adhesion complex	Vinculin-mediated actin binding	Regulation of adhesion stability and force transmission	Rod domain VBSs	Yes	**Study I** (Thievessen *et al.*, 2013; Ciobanasu, Faivre and Le Clainche, 2014)
	Synemin-mediated intermediate filament binding	Regulation of adhesion stability and force transmission	R8 subdomain	Hypothesis	(Sun *et al.*, 2008)
	ABS2-mediated actin binding	Regulation of adhesion stability and force transmission	R4-R8 subdomains	Yes	(Atherton *et al.*, 2015)
Force-regulated interactions of the talin rod domain with signaling proteins	Increased vinculin binding	Regulation of actin dynamics, regulation of phosphotyrosine signaling	Rod domain VBSs	Yes	**Study I** (Hytönen and Vogel, 2008; del Rio *et al.*, 2009; Yao *et al.*, 2016)
	Decreased RIAM binding	Regulation of adhesion signaling	R2-R3, R8 and R11 subdomains	Yes	(Goult, Zacharchenko, *et al.*, 2013)
	Decreased DLC1 binding	Regulation of local RhoA activity	R8 subdomain	Yes	**Study II** (Li *et al.*, 2011; Zacharchenko *et al.*, 2016)
	Decreased paxillin binding	Regulation of phosphotyrosine signaling	R8 subdomain	Indirect	(Zacharchenko *et al.*, 2016)
	Decreased Kank-protein binding	Regulation of ABS2 activity and traction force generation	R7 subdomain	Hypothesis	(Bouchet *et al.*, 2016; Sun *et al.*, 2016)
Regulation of other mechanosensors by talin mechanotransmission	Regulation of tyrosine kinase activity	Regulation of phosphotyrosine signaling	Head domain and the mechanical linkage to actin	Yes	**Study III** (Zhou *et al.*, 2015)
	Regulation of actin dynamics and cellular tension	Depends on the mechanosensitive protein	ABSs, VBSs and the mechanical connection to β-integrins	Indirect	(Hayakawa, Tatsumi and Sokabe, 2011; Weinberg, Mair and Lemmon, 2017; Yamashiro *et al.*, 2018)

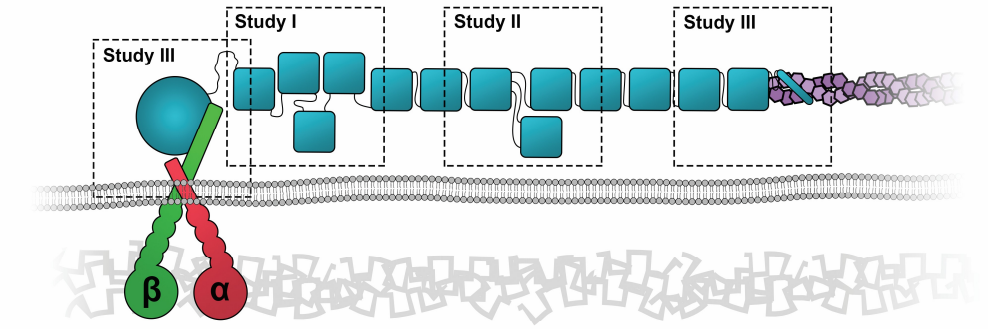

Study I. Talin R3 subdomain as a regulator of adhesion structure and function

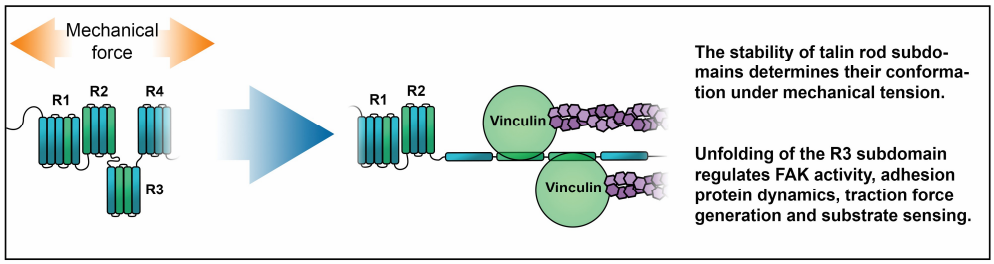

Study II. Talin R8 subdomain as a regulator of DLC1 localization and activity

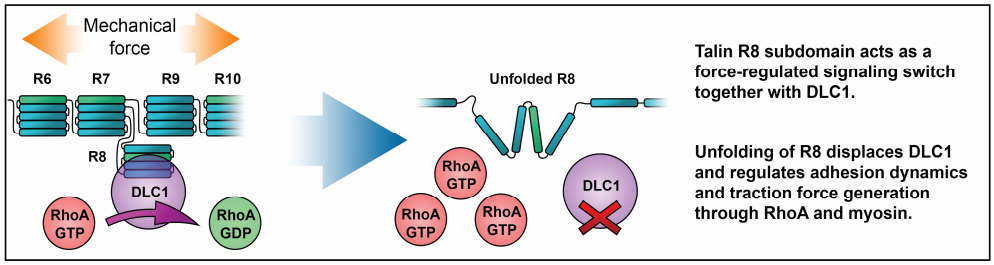

Study III. Talin mechanotransmission as a regulator of phosphotyrosine signaling and actin dynamics

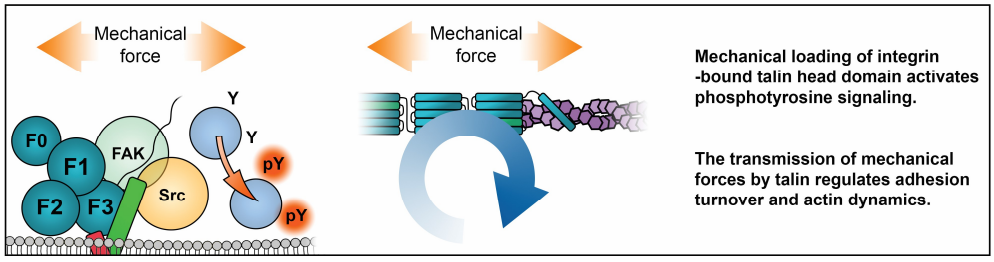

Figure 19 The different mechanisms of talin mechanosensing investigated in studies I-III. Top part: the mechanisms of talin mechanosensing mapped to different parts of the talin protein. Talin mechanotransmission (Study III) is dependent on both the talin head domain and the actin binding sites. Bottom part: schematic models of the studied mechanisms of talin mechanosensing.

6.4.2 Talin in the structural reinforcement of the adhesion complex

The role of vinculin in talin-mediated mechanosensing is well established (Critchley, 2005; Hytönen and Vogel, 2008; del Rio *et al.*, 2009; Carisey *et al.*, 2013; Thievessen *et al.*, 2013; Ciobanasu, Faivre and Le Clainche, 2014; Austen *et al.*, 2015; Elosegui-Artola *et al.*, 2016). In the canonical model of adhesion reinforcement, the force regulated unfolding of the talin rod subdomains exposes cryptic VBSs and activates vinculin binding, which allows connections with additional actin filaments and results in the structural reinforcement of the adhesion complex. The increased recruitment of vinculin and actin results in an increase in the mechanical loading of the adhesion complex, which promotes further recruitment of talin, vinculin and actin, thus activating a positive feedback loop strengthening the adhesion complex. Interestingly, experiments with an *in vitro* setup utilizing purified proteins indicate that this vinculin-dependent positive feedback mediates the reinforcement of the adhesion complex independently of other adhesion proteins (Ciobanasu, Faivre and Le Clainche, 2014). Furthermore, experiments with talin force sensors have demonstrated that vinculin is required for the transmission of maximal force through talin, confirming the role of vinculin as a structural component in integrin-mediated adhesions (Austen *et al.*, 2015; Thievessen *et al.*, 2015; Kumar *et al.*, 2016; Ringer *et al.*, 2017). However, as demonstrated by the relatively normal spreading and migration of vinculin-null cells, vinculin is not critically required for the reinforcement of the adhesion complex (Coll *et al.*, 1995; Xu and Baribault, 1998). This striking finding indicates that other, vinculin-independent mechanisms must be able regulate adhesion reinforcement and signaling in vinculin-null cells. Interestingly, the force gradient normally seen across the talin rod domain (See section 2.3.8) is not observed in vinculin-null cells (Ringer *et al.*, 2017). Thus, it seems that in these cells, adhesion reinforcement is primarily mediated by adhesion signaling, rather than by the direct structural reinforcement of the adhesion complex through other talin-rod binding proteins. Moreover, the lack of the force gradient in vinculin-null cells indicates that the talin ABS3 alone is responsible for talin force transmission in these cells. However, the results of study III demonstrate that the ABS3 alone cannot mediate adhesion reinforcement or traction force generation in the absence of the talin rod subdomains (Figure 12). Taken together, these results indicate that the force-regulated signaling of the talin rod domain is in some cases more important for adhesion reinforcement than its structural connectivity through ABS2 and vinculin. However, for the maximal adhesion strength, the presence and correct functionality of the talin ABS2 and VBSs is likely always required.

6.4.3 Talin rod-dependent recruitment and release of signaling proteins

As explained in the section 2.3.6, the unfolding of the talin rod domain regulates the recruitment and release of a number of adhesion proteins. Some of these proteins (Kank-proteins, DLC1, paxillin and α-synemin) interact with a single binding site in the talin rod, while others (vinculin, MRL-proteins and actin) can bind to multiple talin rod subdomains (Figure 4). The truncated talin forms developed in study III allowed us to investigate the importance of these interactions in talin rod-dependent adhesion reinforcement and signaling. Intriguingly, we found that although the ΔR1-12 protein did not allow adhesion reinforcement, both ΔR1-10 or ΔR4-12 proteins did, as indicated by cell polarization, migration and traction force generation (Figure 12C, D). This indicates that at least *in vitro*, talin rod domain-mediated adhesion reinforcement is a robust process independent of any single talin rod subdomain or interaction site. The rod subdomains present in these truncated talin forms contain mechanically regulated binding sites for vinculin (rod subdomains R1, R2, R3, R12, R13) and MRL-proteins such as RIAM (R1-2, R11). Both vinculin and MRL-proteins interact with a large number of adhesion proteins and can directly contribute to the regulation of both actin polymerization (through Ena/VASP proteins and Arp2/3 complex) and phosphotyrosine signaling (through paxillin and PLCγ). As VASP can interact with both vinculin and MRL-proteins and contributes to the regulation of actin dynamics in the adhesion complex, we investigated the force- and talin-dependent recruitment of VASP into adhesion sites (Figure 15). As expected, the recruitment of VASP was found to depend on the presence of talin rod subdomains, and its intensity in the adhesion sites closely followed the intensity of vinculin. However, as talin destabilization almost completely abolished VASP recruitment despite the increased vinculin recruitment, it seems that also other factors are required for the recruitment of VASP. Such factors may include other adapter proteins such as zyxin or sufficient mechanical tension of the actin cytoskeleton (Moody *et al.*, 2009; Carisey *et al.*, 2013).

In addition to vinculin and RIAM, also the interactions of other talin rod-binding proteins are likely to be regulated by mechanical force. Importantly, the unfolding of the R8 subdomain is known to regulate the recruitment and release of RIAM (Goult, Zacharchenko, *et al.*, 2013), DLC1 and paxillin (Study II)(Li *et al.*, 2011) and likely affects the interaction of R8 with α-synemin (Sun *et al.*, 2008). Moreover, the interaction of the R7 subdomain with Kank-proteins is likely displaced by the unfolding of the subdomain, although experimental evidence of it is still lacking

(Bouchet *et al.*, 2016; Sun *et al.*, 2016). Altogether, it seems that the multiple force-regulated interactions of the rod domain and the concurrent activation of many different signaling pathways grant talin mechanosensing a high level of resistance against the loss of individual rod subdomains or protein interactions. However, it is likely that in living tissues, all these parallel mechanisms are be required to allow tight spatio-temporal regulation over adhesion formation, maturation and disassembly.

6.4.4 Talin mechanotransmission in the regulation of other cellular mechanosensors

In addition to its role as a cellular mechanosensor, talin acts as a central force-bearing protein in integrin-mediated adhesions. While also other proteins such as filamins (Razinia *et al.*, 2012), tensins (Lo, 2004) and α-actinin (Otey, Pavalko and Burridge, 1990) can mediate the β-integrin-actin linkage in different cellular contexts, talin seems to have a critical role in the transmission of mechanical forces. As many adhesion proteins are known to respond to force transmitted through the adhesion complex, it seems likely that talin mechanotransmission regulates these processes independently of talin rod mechanotransduction. Examples of such talin mechanotransmission-dependent but talin rod-independent processes include force-regulated assembly of fibronectin fibrils (Weinberg, Mair and Lemmon, 2017), force-regulated actin polymerization by formins (Courtemanche *et al.*, 2013), force-regulated severing of actin filaments by cofilin (Hayakawa, Tatsumi and Sokabe, 2011), force-dependent stabilization of actin filaments (Yamashiro *et al.*, 2018) and force-regulated chromatin packing in the nucleus (Miroshnikova, Nava and Wickström, 2017). Moreover, the forces transmitted through talin regulate the stability of the interactions between force-bearing proteins, thus regulating their dynamics in the cell. Interestingly, many of the interactions transmitting mechanical loads in the cell such as the fibronectin-β1-integrin, vinculin-actin and actin-myosin interactions are catch-bonds, whose stability is increased in a response to their mechanical loading (Guo and Guilford, 2006; Kong *et al.*, 2009; Huang *et al.*, 2017). However, the concurrent activation of multiple force-regulated cellular processes makes it difficult to dissect the contribution of any single mechanosensor. To investigate adhesion dynamics and signaling in the absence of talin rod domain, we created the ΔR1-12 protein (Figure 12A). In study III, expression of this modified talin in talin-null cells increased the cell spreading area (Figure 12B), decreased the rate of actin retrograde flow (Figure 13A) and slowed down adhesion turnover

compared to the talin head domain (Figure 13B). However, cells expressing the ΔR1-12 protein were unable to polarize, migrate or macroscopically contract 3D collagen matrices (Figure 12C, D). This indicates that in the absence of talin rod-mediated adhesion reinforcement, the mechanical connection through the ΔR1-12 protein repeatedly fails under mechanical tension, exemplifying the previously proposed frictional slippage of unstable adhesion complexes (Atherton *et al.*, 2015; Elosegui-Artola *et al.*, 2016). Altogether, both talin mechanotransmission and rod mechanotransduction contribute to the regulation of adhesion functions. However, the presence of the force-regulated talin rod subdomains is required for adhesion reinforcement and efficient force transmission. It is obvious that the different mechanisms transmitting and transducing mechanical forces in cells function in a tight co-operation and are dependent on the completeness of the structural protein network.

The FAK-Src signaling module is considered to be the central axis of adhesion signaling and known to regulate both adhesion assembly and disassembly (Hamadi *et al.*, 2005; Tomar and Schlaepfer, 2009; Lawson *et al.*, 2012). In study III, all studied talin proteins, regardless of the presence of rod subdomains, were found to localize into adhesion sites in *Tln1-/-Tln2-/-* cells to the same extent. However, their expression resulted in vastly different levels of FAK activity. Although the talin head domain can directly interact with FAK, it thus seems that mechanisms independent of the sheer talin level in the adhesion complex must regulate the recruitment and activation of FAK. In the case of the talin proteins containing rod subdomains, such mechanisms could be mediated by the force-dependent regulation of the talin-vinculin-paxillin-FAK (Subauste *et al.*, 2004; Pasapera *et al.*, 2010) and talin-DLC1-paxillin-FAK (Zacharchenko *et al.*, 2016) signaling modules. This model is supported by the observed concurrent increase in the recruitment of vinculin and activated FAK in the cells expressing the destabilized talin protein (Figure 9C). The ΔR1-12 protein, however, cannot interact with vinculin, paxillin or DLC1. Thus, the mechanisms mediating the increased FAK activation in the cells expressing this construct must be independent of these proteins. Interestingly, recent molecular dynamics simulations suggest that mechanical force could directly activate adhesion-localized FAK, although biochemical evidence of this mechanism is still largely lacking (Zhou *et al.*, 2015; Bell and Terentjev, 2017). Alternatively, the talin-mediated mechanical tension may function to orient β-integrin tail domains, and thus, regulate the availability of its binding sites for cytosolic signaling proteins. Although the activation of FAK by the ΔR1-12 protein was found to be reflected onto its

substrates paxillin and p190RhoGAP, it failed to correctly downregulate the activity of MLC2 in lamellipodia (Figure 14F). This indicates that either the level of FAK activation by the ΔR1-12 protein is insufficient for the downregulation of myosin activity in lamellipodia, or that the concurrent activation of other, talin rod-dependent signaling pathways is required for the correct regulation of local myosin activity. However, the observed force-dependent but talin rod subdomain-independent activation of FAK may play a significant role in certain conditions, such as during the initial assembly of the adhesion complex. Taken together, the level of adhesion phosphotyrosine signaling is regulated by multiple talin-dependent mechanisms. While the complete activation of FAK signaling is dependent on the mechanical regulation of the talin rod domain, the results of study III demonstrate that also mechanisms independent of talin rod domain unfolding contribute to the overall level of phosphotyrosine signaling in the adhesion complex.

6.5 The roles of talin in artery homeostasis and atherosclerosis

6.5.1 Mechanosignaling in the regulation of artery homeostasis

The contribution of mechanical signals in the development and homeostasis of mammalian tissues has been studied the most in the context of the vasculature. It is now well acknowledged that the mechanical signals generated by blood shear stress, blood pressure and smooth muscle contraction regulate many structural and functional processes within the artery wall. Examples of such processes include the regulation of vascular permeability, leukocyte recruitment during inflammation and stem cell differentiation (Tarbell, Simon and Curry, 2014). Importantly, laminar blood flow is known to activate atheroprotective cellular responses, characterized by low cell proliferation rate, low inflammatory activity, low oxidative stress and low thrombogenicity (Chiu and Chien, 2011). Conversely, branches and sharp curvatures in arteries create areas of disturbed blood flow, which has been associated with increased local inflammatory response and increased formation of atherosclerotic lesions (Caro, Fitz-Gerald and Schroter, 1969; Glagov *et al.*, 1988; Chiu and Chien, 2011). Thus, both hemodynamics and the mechanical properties of the vascular wall seem to affect the generation and transmission of the mechanical signals regulating vascular homeostasis (Davies *et al.*, 2001).

Due to their direct contact with the blood flow, endothelial cells have been considered the prime candidates for general transducers of mechanical signals in the vasculature. As a result, studies investigating artery mechanosignaling have mostly focused on the mechanisms functioning in endothelial cells (Givens and Tzima, 2016). In addition to the shear forces generated by the blood flow, endothelial cells are subjected to cyclic stretching caused by the beating of the heart. These mechanical forces are transmitted through the cytoskeleton to different parts of the cell. To date, a large number of endothelial cell mechanosensors acting in different cellular contexts have been identified (Ali and Schumacker, 2002; Deng, Huo and Luo, 2014; Givens and Tzima, 2016). Importantly, integrin-mediated adhesions at the basal side of endothelial cells are known to respond to the shear forces acting on the apical side (Davies, Robotewskyj and Griem, 1994; Shyy and Chien, 2002; Katoh, Kano and Ookawara, 2008). As different integrin receptors can activate different signaling pathways, the exact signaling response depends on the protein composition and the mechanical properties of the underlying extracellular matrix (Finney *et al.*, 2017). Many of the mechanisms mediating mechanosensing in the vascular endothelium are likely to be functionally similar to those acting in fibroblast cells (Katoh, Kano and Ookawara, 2008). For example, the exposure to fluid shear forces and the mechanical stretching of endothelial cells have been found to induce stress fiber formation and FAK activation, indicating a common functional basis with the mechanisms acting in fibroblasts (Katoh, Kano and Ookawara, 2008; Deng, Huo and Luo, 2014).

In addition to the endothelial cells in the *tunica intima*, also the other layers of artery walls are subjected to cyclic stretching and compressing forces. Vascular smooth muscle cells (VSMC) residing in the *tunica media* are firmly attached to the surrounding ECM by integrin-mediated adhesions. This mechanical connectivity allows VSMCs to accurately modulate blood pressure through the contraction of the circumferential layers of ECM around the artery lumen (Lacolley *et al.*, 2012). Conversely, the tensional state of the ECM regulates VSMC proliferation, adhesion formation and the secretion of ECM proteins (Lacolley *et al.*, 2012). In addition, fibroblasts and specialized myofibroblasts residing in the *tunica adventitia* are activated by both chemical and mechanical stimuli during wound healing and vascular remodeling (Forte *et al.*, 2010). Taken together, it is clear that all major cell types in artery walls can sense mechanical signals and respond to them.

6.5.2 The structural and functional roles of talin in the artery wall

Although both the nature of mechanical signals and the type of cells transducing them vary between the different layers of the artery wall, integrin-mediated adhesions seem to function as universal mediators of force transmission and transduction. Due to the critical role of talin as a cytosolic adapter in integrin-mediated adhesions, it is likely that talin is required for both the formation and function of the adhesion complexes in the artery wall. Importantly, the β-integrin isoforms interacting with talin, for example β1 and β3, are known to be abundantly expressed in endothelial cells and VSMCs, especially during tissue remodeling (Kim, Harris and Varner, 2000; Moiseeva, 2001; Baranska *et al.*, 2005; Lei *et al.*, 2008; Finney *et al.*, 2017).

It is conceivable that talin has a dual role in the integrin-mediated adhesions of the artery wall. Firstly, as a major force-bearing component in integrin-mediated adhesions, talin is required for the structural integrity of the artery wall. The constant cyclic stressing of the artery wall sets high requirements for the strength of the cell-matrix adhesions, while cell migration during tissue remodeling requires rapid, yet controlled, disassembly of these adhesions. Therefore, the functionality of the talin-mediated linkage from ECM to the actin cytoskeleton is important for the structural integrity of the artery wall, as well as for its efficient remodeling. Secondly, it seems likely that talin functions as a cellular mechanosensor in vascular endothelial cells and VSMCs through the same molecular mechanisms studied in the context of fibroblasts. Accordingly, the importance of talin-1 expression in the vasculature has been demonstrated by a tissue-specific knockout of talin-1 in mouse vascular endothelium, which resulted in embryonal lethality due to defects in angiogenesis (Monkley *et al.*, 2011). Similarly to talin-1, also the loss of kindlin proteins has been shown to lead to defects early in the development of heart and vasculature, demonstrating the importance of the correct regulation of integrin activation during embryonic development (Malinin, Pluskota and Byzova, 2012).

6.5.3 Altered expression of talin-1 and talin-2 in atherosclerosis

Atherosclerosis is a chronic inflammatory disease of large arteries. It is characterized by the thickening of the artery *tunica intima*, accumulation of lipids, infiltration of monocytes and excessive proliferation of VSMCs (Singh *et al.*, 2002). The development of an atherosclerotic plaque results in major changes in the mechanical and biochemical properties of the artery wall. Furthermore, the local inflammation

in the artery wall induces the secretion of fibronectin, fibrinogen and collagen by endothelial cells and VSMCs (Finney *et al.*, 2017). This is reflected onto the activation of different integrin isoforms and onto the mechanotransduction by the integrin-adhesion complexes (Finney *et al.*, 2017). The changes in the biochemical and mechanical properties of the adhesion complex can, in turn, modulate the secretion of cytokines and growth factors maintaining the local inflammation of the plaque.

In study IV, we observed a large reduction in the levels of talin-1, talin-2 and vinculin transcripts in atherosclerotic plaques (Figure 16). The consistently reduced expression of talin and vinculin transcripts across all studied arterial beds (carotid artery, femoral artery, abdominal aorta) suggests that the decreased expression of these genes is a general feature of atherosclerotic plaques. Although we do not yet know the root cause of the reduced expression of talin and vinculin, it seems possible that initial changes in the mechanical properties of the artery wall can modulate the expression of different adhesion proteins (Peyton and Putnam, 2005; Lv *et al.*, 2015). Accordingly, the level of cellular tension has been found to regulate the expression of talin-1, talin-2 and vinculin transcripts through YAP/TAZ-signaling (Nardone *et al.*, 2017). The decreased expression of structural adhesion proteins such as talin and vinculin may compromise the integrity of the tissue and render cells unable to sense the mechanical signals required for the normal atheroprotective responses. In addition to the altered sensing of external signals, the loss of talin expression is likely to affect the deposition and remodeling of vascular ECM. Because of the mechanically tensioned structure of the arterial wall, ECM proteins deposited into the extracellular space must be mechanically pre-stressed after their secretion (Humphrey *et al.*, 2014). Talin mechanosensing is required for this coordinated, integrin-mediated assembly of ECM proteins and the loss of talin expression likely prevents the correct remodeling of the artery wall.

In previous studies, the expression levels of specific adhesion proteins were found to be downregulated in VSMCs residing in atherosclerotic plaques (Meyer *et al.*, 1994; de la Cuesta *et al.*, 2013). In these studies, the decreased expression of adhesion proteins was associated with the phenotypic switch of the VSMCs from their typical contractile phenotype to a motile, proliferative phenotype. This phenotypic switch is required for the migration of VSMC from the *tunica media* to the *tunica intima* during vascular injury and also for the increased secretion of ECM proteins during plaque development (Gomez and Owens, 2012). In the motile phenotypically switched VSMC cells, the strong integrin-mediated attachments between ECM and the

cytoskeleton are disassembled and the expression levels of many adhesion proteins downregulated. The observed overall decrease in the expression of talin and vinculin transcripts (study IV) may thus reflect the local fractions of phenotypically switched and non-switched VSMCs in the artery wall. Indeed, together with the decreased expression of talin and vinculin transcripts, we observed a concurrent decrease in the expression of smoothelin and calponin-1 (Figure 17). Smoothelin and calponin-1 are typically robustly expressed in mature VSMC with contractile phenotype and downregulated during the phenotypic switch (Duband *et al.*, 1993; van Eys, Niessen and Rensen, 2007). However, due to the heterogeneous structure of the analyzed tissue samples, it is difficult to associate the decreased expression of talin and vinculin with any specific cell type or tissue layer. In the future, direct analysis of adhesion protein expression in the different layers of the artery wall and in the different stages of the disease could help to answer these open questions.

Confocal microscope imaging of carotid artery plaques revealed a complete loss of talin-1 expression in the endothelial cells (Figure 18). This suggests that the structural integrity granted by integrin-mediated adhesions is compromised in the atherosclerotic plaque. Intact endothelium is known to be critical for the protection of the plaque site from the attachment of circulating platelets (Xu *et al.*, 2009). Conversely, the loss of endothelial integrity may lead to its erosion or plaque rupture, which results in the rapid aggregation of activated platelets and possibly to a life-threatening thrombosis (Singh *et al.*, 2002; Xu *et al.*, 2009). Interestingly, the expression of talin-1 in the *tunica intima* was found to be low near the artery lumen and to gradually increase towards the *tunica media*. In advanced atherosclerotic plaques, a fibrous cap composed of ECM proteins and phenotypically switched VSMCs develops beneath the endothelium. Thus, the low expression of talin in the *tunica intima* may contribute to the decreased stability of this fibrous cap, increasing its susceptibility to rupture. In the expression analysis, we observed a clear, albeit statistically insignificant, negative trend in the expression of talin and vinculin transcripts in unstable *versus* stable atherosclerotic plaques (Figure 16). This suggests that the expression of talin is further downregulated during the progression of the disease. However, we cannot yet conclude whether some plaques are unstable because of the low expression of talin or if currently unknown factors act to downregulate talin expression specifically in unstable plaques. In the future, it will be interesting to investigate the causality between the low talin expression in the plaque endothelium and fibrous cap and their mechanical stability in more detail.

7 SUMMARY AND CONCLUSIONS

During the past two decades, mechanical signals have emerged as ubiquitous regulators of many cellular processes including cell migration, proliferation and differentiation. Accordingly, correct cellular mechanosignaling is known to be required for both embryogenesis and tissue remodeling. It is now clear that mechanical forces of different magnitudes and frequencies can induce different cellular responses, resembling the functions of different biochemical signaling molecules in cellular signaling. However, the multiple mechanisms transmitting and transducing mechanical signals in cells are still incompletely understood.

In the first part of the work presented here, we investigated the structure-function relationship of the adhesion protein talin. Talin is a central scaffold protein in integrin-mediated adhesions and functions as a mechanosensor in many types of cells. By expression of genetically modified versions of the talin protein in talin-null cells, we were able to investigate the mechanisms of talin mechanosensing in adhesion complexes. Specifically, we demonstrated that the mechanical stability of the talin R3 subdomain regulates its activity in cell adhesions. The increased activity of a destabilized R3 subdomain was found to reflect onto multiple aspects of adhesion structure and function, including adhesion complex composition, isoform-specific integrin activation and the level of phosphotyrosine signaling. These findings demonstrate that the mechanical stability of the talin rod subdomains directly regulates their signaling activity and provide interesting insights into the processes regulated by talin rod domain unfolding.

In the second part, we investigated the mechanical regulation of the interaction between the talin R8 subdomain and adhesion signaling protein DLC1. By restricting the unfolding of the R8 subdomain, we demonstrated that the R8-DLC1 interaction is regulated by mechanical tension and thus constitutes a novel mechanically-regulated signaling switch in adherent cells. Furthermore, the restricted unfolding of the R8 subdomain was found to affect many different aspects of adhesion function, including adhesion protein dynamics, the level of traction force generation and the rate of cell migration. These findings shed light on the mechanisms by which

adhesion-localized DLC1 regulates different cellular processes and indicate that talin rod domain functions as a cellular mechanotransducer through a larger variety of mechanisms than what was previously thought.

In the third part, we investigated the mechanisms of talin-dependent adhesion reinforcement and signaling. Utilizing talin forms with modified rod domain structure, we dissected the roles of talin mechanotransmission and mechanotransduction in the regulation of adhesion structure and function. We demonstrated that the transmission of mechanical forces through talin regulates multiple aspects of adhesion function independently of talin rod subdomains, but is not sufficient for adhesion reinforcement in the absence of talin rod domain unfolding. The results of this study deepen our understanding of the roles of talin in the regulation of cellular signaling and indicate that talin-mediated adhesion reinforcement and signaling are robust processes mediated by many parallel mechanisms.

In the last part of this work, we investigated the expression levels of talin and vinculin transcripts in atherosclerotic plaques. We observed a significant reduction in the expression of talin and vinculin in atherosclerotic plaques compared to healthy artery wall. Furthermore, immunostaining and confocal microscope imaging of tissue sections revealed that talin proteins are largely absent from the *tunica intima* of atherosclerotic plaques. This loss of talin expression likely prevents the correct cellular responses to mechanical signals and negatively affects the integrity of the plaque epithelial layer. The compromised structural integrity of the plaque may make it susceptible to rupture and contribute to the progression of the disease. However, the mechanisms downregulating talin and vinculin expression in atherosclerotic plaques remain to be investigated in detail.

In conclusion, the studies described in this thesis provide novel insights into the many roles played by the talin protein in integrin-mediated cell adhesions. In the future, detailed knowledge of the complex mechanisms mediating talin mechanotransduction will help us to understand the mechanical regulation of tissue development and remodeling. Furthermore, better understanding of these mechanisms may reveal how the failure of cells to sense mechanical signals contributes to the onset and progression of human diseases such as atherosclerosis and cancer.

8 ACKNOWLEDGEMENTS

This study was carried out at the University of Tampere in the research group of Protein Dynamics. I would like to thank the Academy of Finland and the Finnish Cultural Foundation for the financial support making this work possible. I also want to acknowledge the Faculty of Medicine and Life Sciences for providing excellent facilities and research infrastructure.

I wish to express my deepest gratitude to our group leader, Associate Professor Vesa Hytönen for the opportunity to delve into the world of cell adhesions and mechanosensitive proteins. Your optimism and out-of-the-box thinking so many times kept us moving forward when we faced unexpected turns along the journey. I am also grateful for always trusting my judgement and highly valuing my opinion. I also highly appreciate the chance to participate in so many interesting projects alongside my thesis work. I want to sincerely thank my other thesis supervisor, Docent Teemu Ihalainen for the countless tips with imaging systems and for the many enlightening discussions about science in general. I am also thankful to the other members of my thesis committee, Professor Olli Silvennoinen and Professor Bernhard 'Berni' Wehrle-Haller for all the valuable comments during the thesis project. I am also very grateful to Berni for the opportunity to visit his lab during my thesis project. Likewise, I would like to thank Professor Armando del Rio and his group at the Imperial College for being excellent collaborators and welcoming me to their lab in London. I also want to warmly thank all my collaborators and coauthors, especially Magdaléna von Essen, who provided the much-needed atomistic level understanding of the structure of the talin rod subdomains. I also want to thank my external reviewers, Professor Pekka Lappalainen and Professor Haguy Wolfenson for the valuable comments of the thesis manuscript.

I want to thank Professor Emeritus Markku 'Kuku' Kulomaa for the guidance and help especially during my Master's project. Your positive attitude towards undergraduate students and appreciation of their contribution has certainly left a positive effect on an entire generation of biotechnology students at the University of Tampere. I also want to thank Professor Tapio Visakorpi for the opportunity to

work at his lab and to contribute to many interesting projects during my undergraduate studies.

I am very thankful to all my colleagues, both present and former, who have always made the PD (and MBT) group the most enjoyable place to work at. I especially want to thank Juha for his friendship and for making sure we every now and then have had fun together also outside the lab. Whether it was board game nights, hiking through a swamp, curling or Megazone combined with fine dining, you always had it covered. I am thankful to Soili, Tiia, Tiina, Jenni, Magda, Paula, Lati, Minna, Sanna, Laura, Elina, Sampo, Niila, Nikke, Vili, Janne, Anssi and to the many other members of our traditional '10:30 lunch club' for the most entertaining conversations and great company. I also want to thank Magda, Sampo and Lati for sharing the struggle of thesis writing and for all the great time during our conference trips. I also want to warmly thank Ulla, Outi, Merja and Nikke for the excellent technical assistance and for sharing your expert knowledge.

I would like to express my gratitude to my family and friends for their support and help during all my studies. First, I want to express my gratitude to my dad for slowly but steadily guiding me into the world of life sciences. Without your everlasting enthusiasm towards science and natural phenomena, I could have ended up doing something much less exciting. I also want to most warmly thank my mom for all the support, encouragement and help during my studies and the thesis project. I am also thankful to Heljä and Jokke for all the help and for organizing so many great celebrations for reasons both big and small. I also want thank the Hammarén family, Moona, Janne, Leevi, Sonja, Aleksi, Tanu, Annika and the FPV Manse crew for the great company and all the excitement outside the lab.

I want to thank our sons Urho and Sisu for all the great time we have had together during the past few years. You have made sure I get to take my thoughts completely away from the lab work every now and then. Finally, I want to express my deepest gratitude to my wonderful wife Iida, who has enabled me to work with the thesis project, always supported me along the journey and helped me to put things into the right perspective. Your support and encouragement made this possible.

Tampere, September 2018

Rolle Rahikainen

9 REFERENCES

Adair, B. D. *et al.* (2005) "Three-dimensional EM structure of the ectodomain of integrin αVβ3 in a complex with fibronectin," *Journal of Cell Biology*, 168(7), pp. 1109–1118.

Alanko, J. *et al.* (2015) "Integrin endosomal signalling suppresses anoikis," *Nature Cell Biology*, 17(11), pp. 1412–1421.

Alanko, J. and Ivaska, J. (2016) "Endosomes: Emerging Platforms for Integrin-Mediated FAK Signalling," *Trends in Cell Biology*, 26(6), pp. 391–398.

Alberts *et al.* (2002) "Chapter 19: Cell Junctions," in *Molecular Biology of the Cell,* Garland Science, New York.

Ali, M. H. and Schumacker, P. T. (2002) "Endothelial responses to mechanical stress: where is the mechanosensor?," *Critical care medicine*, 30(5), pp. 198–206.

Amin, N. and Vincan, E. (2012) "The Wnt signaling pathways and cell adhesion.," *Frontiers in bioscience*, 17, pp. 784–804.

Anthis, N. J., Haling, J. R., *et al.* (2009) "Beta integrin tyrosine phosphorylation is a conserved mechanism for regulating talin-induced integrin activation.," *The Journal of biological chemistry*, 284(52), pp. 36700–36710.

Anthis, N. J., Wegener, K. L., *et al.* (2009) "The structure of an integrin/talin complex reveals the basis of inside-out signal transduction.," *The EMBO journal*, 28(22), pp. 3623–3632.

Anthis, N. J. *et al.* (2010) "Structural Diversity in Integrin/Talin Interactions," *Structure*, 18(12), pp. 1654–1666.

Anthis, N. J. and Campbell, I. D. (2011) "The tail of integrin activation," *Trends in Biochemical Sciences*, 36(4), pp. 191–198.

Arthur, W. T. and Burridge, K. (2001) "RhoA inactivation by p190RhoGAP regulates cell spreading and migration by promoting membrane protrusion and polarity.," *Molecular biology of the cell*, 12(9), pp. 2711–20.

Arthur, W. T., Petch, L. A. and Burridge, K. (2000) "Integrin engagement suppresses RhoA activity via a c-Src-dependent mechanism," *Current Biology*, 10(12), pp. 719–722.

Atherton, P. *et al.* (2015) "Vinculin controls talin engagement with the actomyosin machinery," *Nature communications*, 6, p. e10038.

Austen, K. *et al.* (2015) "Extracellular rigidity sensing by talin isoform-specific mechanical linkages.," *Nature cell biology*, 17(12), pp. 1597–1606.

Bakolitsa, C. *et al.* (2004) "Structural basis for vinculin activation at sites of cell adhesion," *Nature*, 430(6999), pp. 583–586.

Ballestrem, C. *et al.* (2001) "Marching at the front and dragging behind: Differential aVb3-integrin turnover regulates focal adhesion behavior," *Journal of Cell Biology*, 155(7), pp. 1319–1332.

Banno, A. *et al.* (2012) "Subcellular localization of talin is regulated by inter-domain interactions," *Journal of Biological Chemistry*, 287(17), pp. 13799–13812.

Baranska, P. *et al.* (2005) "Expression of Integrins and Adhesive Properties of Human Endothelial Cell Line EA.hy 926," *Cancer genomics & proteomics*, 2(5), pp. 265–269.

Barczyk, M., Carracedo, S. and Gullberg, D. (2010) "Integrins," *Cell and Tissue Research*, 339(1), pp. 269–280.

Barras, D. and Widmann, C. (2014) "GAP-independent functions of DLC1 in metastasis," *Cancer and Metastasis Reviews*, 33(1), pp. 87–100.

Bays, J. L. *et al.* (2014) "Vinculin phosphorylation differentially regulates mechanotransduction at cell-cell and cell-matrix adhesions.," *The Journal of cell biology*, 205(2), pp. 251–63.

Bell, S. and Terentjev, E. M. (2017) "Focal Adhesion Kinase: The Reversible Molecular Mechanosensor," *Biophysical Journal*, 112(11), pp. 2439–2450.

Böttcher, R. T. *et al.* (2017) "Kindlin-2 recruits paxillin and Arp2/3 to promote membrane protrusions during initial cell spreading," *Journal of Cell Biology*, 216(11), pp. 3785–3798.

Bouaouina, M., Lad, Y. and Calderwood, D. A. (2008) "The N-terminal domains of talin cooperate with the phosphotyrosine binding-like domain to activate beta1 and beta3 integrins.," *The Journal of biological chemistry*, 283(10), pp. 6118–6125.

Bouchet, B. P. *et al.* (2016) "Talin-KANK1 interaction controls the recruitment of cortical microtubule stabilizing complexes to focal adhesions," *eLife*, 5, e18124.

Bouvard, D. *et al.* (2013) "Integrin inactivators: Balancing cellular functions in vitro and in vivo," *Nature Reviews Molecular Cell Biology*, 14(7), pp. 432–444.

Buck, C. A. and Horwitz, A. F. (1987) "Integrin, a Transmembrane Glycoprotein Complex Mediating Cell-Substratum Adhesion," *Journal of Cell Science*, 1987(8), pp. 231–250.

Burridge, K. and Connell, L. (1983) "A New Protein of Adhesion and Ruffling Membranes Plaques," *The Journal of Cell Biology*, 97, pp. 359–367.

Calderwood, D. A., Campbell, I. D. and Critchley, D. R. (2013) "Talins and kindlins: partners in integrin-mediated adhesion.," *Nature reviews. Molecular cell biology*, 14(8), pp. 503–517.

Campbell, I. D. and Humphries, M. J. (2011) "Integrin structure, activation, and interactions," *Cold Spring Harbor Perspectives in Biology*, 3(3), p. a004994.

Carisey, A. *et al.* (2013) "Vinculin regulates the recruitment and release of core focal adhesion proteins in a force-dependent manner," *Current Biology*, 23(4), pp. 271–281.

Carisey, A. and Ballestrem, C. (2011) "Vinculin, an adapter protein in control of cell adhesion signalling," *European Journal of Cell Biology*, 90(2–3), pp. 157–163.

Caro, C. G., Fitz-Gerald, J. M. and Schroter, R. C. (1969) "Arterial Wall Shear and Distribution of Early Atheroma in Man," *Nature*, 223(5211), pp. 1159–1161.

Chan, C. E. and Odde, D. J. (2008) "Traction dynamics of filopodia on compliant substrates.," *Science*, 322(5908), pp. 1687–1691.

Chan, K. T., Bennin, D. A. and Huttenlocher, A. (2010) "Regulation of adhesion dynamics by calpain-mediated proteolysis of focal adhesion kinase (FAK)," *Journal of Biological Chemistry*, 285(15), pp. 11418–11426.

Chao, W. T. and Kunz, J. (2009) "Focal adhesion disassembly requires clathrin-dependent endocytosis of integrins," *FEBS Letters*, 583(8), pp. 1337–1343.

Chen, H.-C. *et al.* (1995) "Interaction of Focal Adhesion Kinase with Cytoskeletal Protein Talin," *Journal of Biological Chemistry*, 270(28), pp. 16995–16999.

Chiquet, M. *et al.* (2009) "From mechanotransduction to extracellular matrix gene expression in fibroblasts.," *Biochimica et biophysica acta*, 1793(5), pp. 911–920.

Chiu, J.-J. and Chien, S. (2011) "Effects of disturbed flow on vascular endothelium: pathophysiological basis and clinical perspectives.," *Physiological reviews*, 91(1), pp. 327–387.

Choi, C. K. *et al.* (2008) "Actin and α-actinin orchestrate the assembly and maturation of nascent adhesions in a myosin II motor-independent manner," *Nature Cell Biology*, 10(9), pp. 1039–1050.

Ciobanasu, C., Faivre, B. and Le Clainche, C. (2014) "Actomyosin-dependent formation of the mechanosensitive talin-vinculin complex reinforces actin anchoring.," *Nature communications*, 5, p. 3095.

Cohen, D. M. *et al.* (2005) "Two Distinct Head-Tail Interfaces Cooperate to Suppress Activation of Vinculin by Talin," *Journal of Biological Chemistry*, 280(17), pp. 17109–17117.

Coll, J. L. *et al.* (1995) "Targeted disruption of vinculin genes in F9 and embryonic stem cells changes cell morphology, adhesion, and locomotion.," *Proceedings of the National Academy of Sciences of the United States of America*, 92(20), pp. 9161–9165.

Conti, F. J. *et al.* (2009) "Talin 1 and 2 are required for myoblast fusion, sarcomere assembly and the maintenance of myotendinous junctions.," *Development*, 136(21), pp. 3597–3606.

Courtemanche, N. *et al.* (2013) "Tension modulates actin filament polymerization mediated by formin and profilin.," *Proceedings of the National Academy of Sciences of the United States of America*, 110(24), pp. 9752–9757.

Cox, J. *et al.* (2011) "Andromeda: A Peptide Search Engine Integrated into the MaxQuant Environment," *Journal of Proteome Research*, 10(4), pp. 1794–1805.

Cox, J. and Mann, M. (2008) "MaxQuant enables high peptide identification rates, individualized p.p.b.-range mass accuracies and proteome-wide protein quantification," *Nature Biotechnology*, 26(12), pp. 1367–1372.

Critchley, D. R. (2009) "Biochemical and Structural Properties of the Integrin-Associated Cytoskeletal Protein Talin," *Annual review of biophysics*, 38, pp. 235–254.

Critchley, D. R. R. (2005) "Genetic, biochemical and structural approaches to talin function.," *Biochemical Society transactions*, 33(6), pp. 1308–1312.

Danen, E. H. J. and Sonnenberg, A. (2003) "Integrins in regulation of tissue development and function," *Journal of Pathology*, 200(4), pp. 471–480.

Davies, P. F. *et al.* (2001) "Hemodynamics and the Focal Origin of Atherosclerosis," *Annals of the New York Academy of Sciences*, 947(1), pp. 7–17.

Davies, P. F., Robotewskyj, A. and Griem, M. L. (1994) "Quantitative studies of endothelial cell adhesion. Directional remodeling of focal adhesion sites in response to flow forces.," *The Journal of clinical investigation*, 93(5), pp. 2031–2038.

Debrand, E. *et al.* (2009) "Talin 2 is a large and complex gene encoding multiple transcripts and protein isoforms," *FEBS Journal*, 276(6), pp. 1610–1628.

Debrand, E. *et al.* (2012) "Mice carrying a complete deletion of the talin2 coding sequence are viable and fertile," *Biochemical and Biophysical Research Communications*, 426(2), pp. 190–195.

Delmas, P. and Coste, B. (2013) "Mechano-gated ion channels in sensory systems," *Cell*, 155(2), pp. 278–284.

Delmas, P., Hao, J. and Rodat-Despoix, L. (2011) "Molecular mechanisms of mechanotransduction in mammalian sensory neurons," *Nature Reviews Neuroscience*, 12(3), pp. 139–153.

Deng, Q., Huo, Y. and Luo, J. (2014) "Endothelial mechanosensors: the gatekeepers of vascular homeostasis and adaptation under mechanical stress," *Science China Life Sciences*, 57(8), pp. 755–762.

Discher, D. E., Janmey, P. and Wang, Y.-L. (2005) "Tissue Cells Feel and Respond to the Stiffness of Their Substrate," *Science*, 310(5751), pp. 1139–1143.

Du, P., Kibbe, W. A. and Lin, S. M. (2008) "lumi: a pipeline for processing Illumina microarray," *Bioinformatics*, 24(13), pp. 1547–1548.

Duband, J. L. *et al.* (1993) "Calponin and SM 22 as differentiation markers of smooth muscle: spatiotemporal distribution during avian embryonic development.," *Differentiation*, 55(1), pp. 1–11.

Durkin, M. E. *et al.* (2002) "Gene structure, tissue expression, and linkage mapping of the mouse DLC-1 gene (Arhgap7)," *Gene*, 288(1–2), pp. 119–127.

Durkin, M. E. *et al.* (2005) "DLC-1, a Rho GTPase-activating protein with tumor suppressor function, is essential for embryonic development," *FEBS Letters*, 579(5), pp. 1191–1196.

Durkin, M. E. *et al.* (2007) "DLC-1:a Rho GTPase-activating protein and tumour suppressor," *Journal of Cellular and Molecular Medicine*, 11(5), pp. 1185–1207.

Elkhatib, N. *et al.* (2014) "Fascin plays a role in stress fiber organization and focal adhesion disassembly," *Current Biology*, 24(13), pp. 1492–1499.

Elliott, P. R. *et al.* (2010) "The Structure of the Talin Head Reveals a Novel Extended Conformation of the FERM Domain," *Structure*, 18(10), pp. 1289–1299.

Ellis, S. J. J. *et al.* (2013) "Talin autoinhibition is required for morphogenesis," *Current Biology*, 23(18), pp. 1825–1833.

Ellison, C. and Brun, Y. V. (2015) "Mechanosensing: A regulation sensation," *Current Biology*, 25(3), pp. 113–115.

Elmore, S. (2007) "Apoptosis: A Review of Programmed Cell Death," *Toxicologic Pathology*, 35(4), pp. 495–516.

Elosegui-Artola, A. *et al.* (2016) "Mechanical regulation of a molecular clutch defines force transmission and transduction in response to matrix rigidity.," *Nature cell biology*, 18(5), pp. 540–548.

Elosegui-Artola, A., Trepat, X. and Roca-Cusachs, P. (2018) "Control of Mechanotransduction by Molecular Clutch Dynamics," 28(5), pp. 356–367.

Etienne-Manneville, S. and Hall, A. (2002) "Rho GTPases in cell biology," *Nature*, 420(6916), pp. 629–635.

Eyckmans, J. *et al.* (2011) "A Hitchhiker's Guide to Mechanobiology," *Developmental Cell*, 21(1), pp. 35–47.

van Eys, G. J., Niessen, P. M. and Rensen, S. S. (2007) "Smoothelin in vascular smooth muscle cells.," *Trends in cardiovascular medicine*, 17(1), pp. 26–30.

Ezratty, E. J. *et al.* (2009) "Clathrin mediates integrin endocytosis for focal adhesion disassembly in migrating cells," *Journal of Cell Biology*, 187(5), pp. 733–747.

Ezratty, E. J., Partridge, M. A. and Gundersen, G. G. (2005) "Microtubule-induced focal adhesion disassembly is mediated by dynamin and focal adhesion kinase," *Nature Cell Biology*, 7(6), pp. 581–590.

Fagotto, F. (2014) "The cellular basis of tissue separation," *Development*, 141(17), pp. 3303–3318.

Fasano, J. M., Massa, G. D. and Gilroy, S. (2002) "Ionic Signaling in Plant Responses to Gravity and Touch," *Journal of Plant Growth Regulation*, 21(2), pp. 71–88.

Feng, X. *et al.* (2013) "DLC-1, a candidate tumor suppressor gene, inhibits the proliferation, migration and tumorigenicity of human nasopharyngeal carcinoma cells.," *International journal of oncology*, 42(6), pp. 1973–1984.

Fine, J. D. *et al.* (2014) "Inherited epidermolysis bullosa: Updated recommendations on diagnosis and classification," *Journal of the American Academy of Dermatology*, 70(6), pp. 1103–1126.

Finney, A. C. *et al.* (2017) "Integrin signaling in atherosclerosis," *Cellular and Molecular Life Sciences*, 74(12), pp. 2263–2282.

Forte, A. *et al.* (2010) "Role of myofibroblasts in vascular remodelling: focus on restenosis and aneurysm," *Cardiovascular Research*, 88(3), pp. 395–405.

De Franceschi, N. *et al.* (2015) "Integrin traffic - the update," *Journal of Cell Science*, 128(5), pp. 839–852.

Franco, S. J. *et al.* (2004) "Calpain-mediated proteolysis of talin regulates adhesion dynamics.," *Nature Cell Biology*, 6(10), pp. 977–983.

Fuchs, P. A. (2015) "How many proteins does it take to gate hair cell mechanotransduction?," *Proceedings of the National Academy of Sciences*, 112(5), pp. 1254–1255.

Galbraith, C. G., Yamada, K. M. and Galbraith, J. A. (2007) "Polymerizing actin fibers position integrins primed to probe for adhesion sites," *Science*, 315(5814), pp. 992–995.

Geiger, B. (1979) "A 130K protein from chicken gizzard: Its localization at the termini of microfilament bundles in cultured chicken cells," *Cell*, 18(1), pp. 193–205.

Geiger, B. and Yamada, K. M. (2011) "Molecular Architecture and Function of Matrix Adhesions," *Cold Spring Harbor Perspectives in Biology*, 3(5), a005033.

Georgiadou, M. *et al.* (2017) "AMPK negatively regulates tensin-dependent integrin activity," *Journal of Cell Biology*, 216(4), pp. 1107–1121.

Gillespie, P. G. and Walker, R. G. (2001) "Molecular basis of mechanosensory transduction," *Nature*, 413(6852), pp. 194–202.

Gingras, A. R. *et al.* (2005) "Mapping and consensus sequence identification for multiple vinculin binding sites within the talin rod," *Journal of Biological Chemistry*, 280(44), pp. 37217–37224.

Gingras, A. R. *et al.* (2008) "The structure of the C-terminal actin-binding domain of talin.," *The EMBO journal*, 27(2), pp. 458–69.

Gingras, A. R. *et al.* (2009) "Structural determinants of integrin binding to the talin rod.," *The Journal of biological chemistry*, 284(13), pp. 8866–8876.

Ginsberg, M. H. (2014) "Integrin activation," *BMB Reports*, 47(12), pp. 655–659.

Givens, C. and Tzima, E. (2016) "Endothelial Mechanosignaling: Does One Sensor Fit All?," *Antioxidants & Redox Signaling*, 25(7), pp. 373–388.

Glagov, S. *et al.* (1988) "Hemodynamics and Atherosclerosis," *Pathology and Laboratory Medicine*, 112, pp. 1018–1031.

Goksoy, E. *et al.* (2008) "Structural Basis for the Autoinhibition of Talin in Regulating Integrin Activation," *Molecular Cell*, 31(1), pp. 124–133.

Gomez, D. and Owens, G. K. (2012) "Smooth muscle cell phenotypic switching in atherosclerosis," *Cardiovascular Research*, 95(2), pp. 156–164.

Gough, R. E. and Goult, B. T. (2018) "The tale of two talins - two isoforms to fine-tune integrin signalling," *FEBS Letters*, 592(12), pp. 2108–2125.

Goult, B. T. *et al.* (2008) "NMR assignment of the C-terminal actin-binding domain of talin," *Biomolecular NMR Assignments*, 2(1), pp. 17–19.

Goult, B. T. *et al.* (2009) "The structure of an interdomain complex that regulates Talin activity," *Journal of Biological Chemistry*, 284(22), pp. 15097–15106.

Goult, B. T. *et al.* (2010) "Structure of a double ubiquitin-like domain in the talin head: a role in integrin activation.," *The EMBO journal*, 29(6), pp. 1069–1080.

Goult, B. T., Zacharchenko, T., *et al.* (2013) "RIAM and vinculin binding to talin are mutually exclusive and regulate adhesion assembly and turnover," *Journal of Biological Chemistry*, 288(12), pp. 8238–8249.

Goult, B. T., Xu, X.-P. P., *et al.* (2013) "Structural studies on full-length talin1 reveal a compact auto-inhibited dimer: Implications for talin activation," *Journal of Structural Biology*, 184(1), pp. 21–32.

Gumbiner, B. M. (1996) "Cell adhesion: The molecular basis of tissue architecture and morphogenesis," *Cell*, 84(3), pp. 345–357.

Guo, B. and Guilford, W. H. (2006) "Mechanics of actomyosin bonds in different nucleotide states are tuned to muscle contraction.," *Proceedings of the National Academy of Sciences of the United States of America*, 103(26), pp. 9844–9849.

Hahn, C. and Schwartz, M. A. (2009) "Mechanotransduction in vascular physiology and atherogenesis," *Nature Reviews Molecular Cell Biology*, 10(1), pp. 53–62.

Haining, A. W. M. *et al.* (2016) "All Subdomains of the Talin Rod Are Mechanically Vulnerable and May Contribute to Cellular Mechanosensing," *ACS Nano*, 10(7), pp. 6648–6658.

Haining, A. W. M. *et al.* (2018) "Mechanotransduction in talin through the interaction of the R8 domain with DLC1," *PLOS Biology*, 16(7), e2005599.

Hamadi, A. *et al.* (2005) "Regulation of focal adhesion dynamics and disassembly by phosphorylation of FAK at tyrosine 397.," *Journal of cell science*, 118(19), pp. 4415–4425.

Hampton, C. M., Taylor, D. W. and Taylor, K. A. (2007) "Novel Structures for α-Actinin:F-Actin Interactions and their Implications for Actin–Membrane

Attachment and Tension Sensing in the Cytoskeleton," *Journal of Molecular Biology*, 368(1), pp. 92–104.

Han, J. *et al.* (2006) "Reconstructing and Deconstructing Agonist-Induced Activation of Integrin αIIbβ3," *Current Biology*, 16(18), pp. 1796–1806.

Hatori, Y. *et al.* (2018) "Local redox environment beneath biological membranes probed by palmitoylated-roGFP," *Redox Biology*, 14, pp. 679–685.

Hayakawa, K., Tatsumi, H. and Sokabe, M. (2011) "Actin filaments function as a tension sensor by tension-dependent binding of cofilin to the filament.," *The Journal of cell biology*, 195(5), pp. 721–727.

Healy, K. D. *et al.* (2008) "DLC-1 suppresses non-small cell lung cancer growth and invasion by RhoGAP-dependent and independent mechanisms," *Molecular Carcinogenesis*, 47(5), pp. 326–337.

Hemmings, L. *et al.* (1996) "Talin contains three actin-binding sites each of which is adjacent to a vinculin-binding site.," *Journal of Cell Science*, 109(1), pp. 2715–2726.

Hess, B. *et al.* (2008) "GROMACS 4: Algorithms for highly efficient, load-balanced, and scalable molecular simulation," *Journal of Chemical Theory and Computation*, 4(3), pp. 435–447.

Hirata, H. *et al.* (2014) "Force-dependent vinculin binding to talin in live cells: a crucial step in anchoring the actin cytoskeleton to focal adhesions.," *American journal of physiology, Cell physiology*, 306(6), pp. 607–620.

Hoffman, B. D., Grashoff, C. and Schwartz, M. A. (2011) "Dynamic molecular processes mediate cellular mechanotransduction.," *Nature*, 475(7356), pp. 316–323.

Holinstat, M. *et al.* (2006) "Suppression of RhoA Activity by Focal Adhesion Kinase-induced Activation of p190RhoGAP," *Journal of Biological Chemistry*, 281(4), pp. 2296–2305.

Horton, E. R. *et al.* (2015) "Definition of a consensus integrin adhesome and its dynamics during adhesion complex assembly and disassembly," *Nature Cell Biology*, 17(12), pp. 1577–1587.

Horton, E. R., Astudillo, P., *et al.* (2016) "Mechanosensitivity of integrin adhesion complexes: Role of the consensus adhesome," *Experimental Cell Research*, 343(1), pp. 7–13.

Horton, E. R., Humphries, J. D., *et al.* (2016) "Modulation of FAK and Src adhesion signaling occurs independently of adhesion complex composition," *Journal of Cell Biology*, 212(3), pp. 349–364.

Horwitz, A. *et al.* (1985) "The cell substrate attachment (CSAT) antigen has properties of a receptor for laminin and fibronectin.," *The Journal of cell biology*, 101(6), pp. 2134–44.

Horwitz, A. *et al.* (1986) "Interaction of plasma membrane fibronectin receptor with talin- a transmembrane linkage," *Nature*, 320(6062), pp. 531–533.

Huang, C. *et al.* (2009) "Talin phosphorylation by Cdk5 regulates Smurf1-mediated talin head ubiquitylation and cell migration," *Nature Cell Biology*, 11(5), pp. 624–630.

Huang, C., Akaishi, S. and Ogawa, R. (2012) "Mechanosignaling pathways in cutaneous scarring," *Archives of Dermatological Research*, 304(8), pp. 589–597.

Huang, D. L. *et al.* (2017) "Vinculin forms a directionally asymmetric catch bond with F-actin.," *Science*, 357(6352), pp. 703–706.

Humphrey, J. D. *et al.* (2014) "Cell biology. Dysfunctional mechanosensing in aneurysms.," *Science*, 344(6183), pp. 477–479.

Humphrey, J. D., Dufresne, E. R. and Schwartz, M. A. (2014) "Mechanotransduction and extracellular matrix homeostasis," *Nature Reviews Molecular Cell Biology*, 15, pp. 802–812.

Humphrey, W., Dalke, A. and Schulten, K. (1996) "VMD: Visual molecular dynamics," *Journal of Molecular Graphics*, 14(1), pp. 33–38.

Humphries, J. D. *et al.* (2007) "Vinculin controls focal adhesion formation by direct interactions with talin and actin," *Journal of Cell Biology*, 179(5), pp. 1043–1057.

Humphries, J. D., Byron, A. and Humphries, M. J. (2006) "Integrin ligands at a glance," *Journal of Cell Science*, 119(19), pp. 3901–3903.

Huttenlocher, A. *et al.* (1997) "Regulation of cell migration by the calcium-dependent protease calpain," *J. Biol. Chem.*, 272, pp. 32719–31221.

Huveneers, S. and Danen, E. H. J. (2009) "Adhesion signaling - crosstalk between integrins, Src and Rho," *Journal of Cell Science*, 122(8), pp. 1059–1069.

Hynes, R. O. (2002) "Integrins : Bidirectional , Allosteric Signaling Machines," 110, pp. 673–687.

Hytönen, V. P. and Vogel, V. (2008) "How Force Might Activate Talin's Vinculin Binding Sites: SMD Reveals a Structural Mechanism," *PLOS Computational Biology*, 4(2), e24.

Hytönen, V. P. and Wehrle-Haller, B. (2014) "Protein conformation as a regulator of cell–matrix adhesion," *Phys. Chem. Chem. Phys.*, 16(14), pp. 6342–6357.

Jaalouk, D. E. and Lammerding, J. (2009) "Mechanotransduction gone awry," *Nature Reviews Molecular Cell Biology*, 10(1), pp. 63–73.

Janmey, P. A. and Weitz, D. A. (2004) "Dealing with mechanics: mechanisms of force transduction in cells," *Trends in Biochemical Sciences*, 29(7), pp. 364–370.

Janoštiak, R. *et al.* (2014) "Mechanosensors in integrin signaling: The emerging role of p130Cas," *European Journal of Cell Biology*, 93(10–12), pp. 445–454.

Johnson, M. S. *et al.* (2009) "Integrins during evolution: Evolutionary trees and model organisms," *Biochimica et Biophysica Acta - Biomembranes*, 1788(4), pp. 779–789.

Kaminski, A., Fedorchak, G. and Lammerding, J. (2014) "The Cellular Mastermind(?)—Mechanotransduction and the Nucleus," in *Mechanotransduction*, pp. 157–203.

Kanchanawong, P. *et al.* (2010) "Nanoscale architecture of integrin-based cell adhesions.," *Nature*, 468(7323), pp. 580–584.

Katoh, K., Kano, Y. and Ookawara, S. (2008) "Role of stress fibers and focal adhesions as a mediator for mechano-signal transduction in endothelial cells in situ.," *Vascular health and risk management*, 4(6), pp. 1273–1282.

Kaushik, S. *et al.* (2014) "Concerted modulation of paxillin dynamics at focal adhesions by deleted in liver cancer-1 and focal adhesion kinase during early cell spreading," *Cytoskeleton*, 71(12), pp. 677–694.

Kaverina, I., Krylyshkina, O. and Small, J. V. (1999) "Microtubule targeting of substrate contacts promotes their relaxation and dissociation," *Journal of Cell Biology*, 146(5), pp. 1033–1043.

Kim *et al.* (2009) "Role of DLC-1, a tumor suppressor protein with RhoGAP activity, in regulation of the cytoskeleton and cell motility," *Cancer and Metastasis Reviews*, 28(1–2), pp. 77–83.

Kim, S., Harris, M. and Varner, J. A. (2000) "Regulation of integrin alphaVbeta3-mediated endothelial cell migration and angiogenesis by integrin alpha5beta1 and protein kinase A.," *The Journal of biological chemistry*, 275(43), pp. 33920–33928.

Klapholz, B. and Brown, N. H. (2017) "Talin – the master of integrin adhesions," *Journal of Cell Science*, 130(15), pp. 2435–2446.

Ko, F. C. F. and Ping Yam, J. W. (2014) "Regulation of deleted in liver cancer 1 tumor suppressor by protein-protein interactions and phosphorylation," *International Journal of Cancer*, 135(2), pp. 264–269.

Kolahi, K. S. and Mofrad, M. R. K. (2010) "Mechanotransduction: a major regulator of homeostasis and development," *Wiley Interdisciplinary Reviews: Systems Biology and Medicine*, 2(6), pp. 625–639.

Kong, F. *et al.* (2009) "Demonstration of catch bonds between an integrin and its ligand," *Journal of Cell Biology*, 185(7), pp. 1275–1284.

Kukkurainen, S. *et al.* (2018) "The F1 loop of talin head acts as a gatekeeper in integrin activation and clustering," *Manuscript*.

Kumar, A. *et al.* (2016) "Talin tension sensor reveals novel features of focal adhesion force transmission and mechanosensitivity.," *The Journal of cell biology*, 213(3), pp. 371–383.

Kung, C. (2005) "A possible unifying principle for mechanosensation," *Nature*, 436(7051), pp. 647–654.

Kurusu, T. *et al.* (2013) "Plant mechanosensing and Ca2+ transport," *Trends in Plant Science*, 18(4), pp. 227–233.

de la Cuesta, F. *et al.* (2013) "Deregulation of smooth muscle cell cytoskeleton within the human atherosclerotic coronary media layer," *Journal of Proteomics*, 82, pp. 155–165.

Lacolley, P. *et al.* (2012) "The vascular smooth muscle cell in arterial pathology: a cell that can take on multiple roles," *Cardiovascular Research*, 95(2), pp. 194–204.

Lafuente, E. M. *et al.* (2004) "RIAM, an Ena/VASP and Profilin Ligand, Interacts with Rap1-GTP and Mediates Rap1-Induced Adhesion," *Developmental Cell*, 7(4), pp. 585–595.

Lagarrigue, F. *et al.* (2015) "A RIAM/lamellipodin–talin–integrin complex forms the tip of sticky fingers that guide cell migration," *Nature Communications*, 6(1), pp. 8492–8505.

Lau, T.-L. *et al.* (2009) "The structure of the integrin alphaIIbbeta3 transmembrane complex explains integrin transmembrane signalling.," *The EMBO journal*, 28(9), pp. 1351–1361.

Lawson, C. *et al.* (2012) "FAK promotes recruitment of talin to nascent adhesions to control cell motility," *Journal of Cell Biology*, 196(2), pp. 223–232.

Lee, H.-S. S. *et al.* (2004) "Characterization of an actin-binding site within the talin FERM domain," *Journal of Molecular Biology*, 343(3), pp. 771–784.

Lee, H.-S. S. *et al.* (2009) "RIAM activates integrins by linking talin to Ras GTPase membrane-targeting sequences," *Journal of Biological Chemistry*, 284(8), pp. 5119–5122.

Lei, L. *et al.* (2008) "Endothelial expression of β1 integrin is required for embryonic vascular patterning and postnatal vascular remodeling.," *Molecular and cellular biology*, 28(2), pp. 794–802.

Leube, R. E., Moch, M. and Windoffer, R. (2015) "Intermediate filaments and the regulation of focal adhesion," *Current Opinion in Cell Biology*, 32, pp. 13–20.

Li, G. *et al.* (2011) "Full activity of the deleted in liver cancer 1 (DLC1) tumor suppressor depends on an LD-like motif that binds talin and focal adhesion kinase (FAK).," *Proceedings of the National Academy of Sciences*, 108(41), pp. 17129–17134.

Liao, Y.-C., Shih, Y.-P. and Lo, S. H. (2008) "Mutations in the focal adhesion targeting region of deleted in liver cancer-1 attenuate their expression and function.," *Cancer research*, 68(19), pp. 7718–7722.

Ling, K. *et al.* (2002) "Type Iγ phosphatidylinositol phosphate kinase targets and regulates focal adhesions," *Nature*, 420(6911), pp. 89–93.

Liu, J. *et al.* (2015) "Talin determines the nanoscale architecture of focal adhesions," *Proceedings of the National Academy of Sciences*, 112(35), pp. 4864–4873.

Lo, S. H. (2004) "Tensin," *The International Journal of Biochemistry & Cell Biology*, 36(1), pp. 31–34.

Lo, S. H. (2017) "Tensins.," *Current biology*, 27(9), pp. 331–332.

López-Mirabal, H. R. and Winther, J. R. (2008) "Redox characteristics of the eukaryotic cytosol," *Biochimica et Biophysica Acta - Molecular Cell Research*, 1783(4), pp. 629–640.

Lv, H. *et al.* (2015) "Mechanism of regulation of stem cell differentiation by matrix stiffness," *Stem Cell Research & Therapy*, 6(1), pp. 103–118.

Ma, X. *et al.* (2013) "Fibers in the Extracellular Matrix Enable Long-Range Stress Transmission between Cells," *Biophysical Journal*, 104(7), pp. 1410–1418.

Malinin, N. L., Pluskota, E. and Byzova, T. V (2012) "Integrin signaling in vascular function.," *Current opinion in hematology*, 19(3), pp. 206–211.

Manso, A. M. *et al.* (2013) "Talini has unique expression versus talin 2 in the heart and modifies the hypertrophic response to pressure overload," *Journal of Biological Chemistry*, 288(6), pp. 4252–4264.

Manso, A. M. *et al.* (2017) "Loss of mouse cardiomyocyte talin-1 and talin-2 leads to β1 integrin reduction, costameric instability, and dilated cardiomyopathy.," *Proceedings of the National Academy of Sciences*, 114(30), pp. 6250–6259.

Margadant, C. *et al.* (2008) "Regulation of hemidesmosome disassembly by growth factor receptors," *Current Opinion in Cell Biology*, 20(5), pp. 589–596.

Margadant, F. *et al.* (2011) "Mechanotransduction in vivo by repeated talin stretch-relaxation events depends upon vinculin," *PLOS Biology*, 9(12), e1001223.

Martel, V. *et al.* (2001) "Conformation, localization, and integrin binding of talin depend on its interaction with phosphoinositides.," *The Journal of biological chemistry*, 276(24), pp. 21217–21227.

Martinac, B. (2004) "Mechanosensitive ion channels: molecules of mechanotransduction," *Journal of Cell Science*, 117(12), pp. 2449–2460.

McCann, R. and Craig, S. (1998) "Identification of a novel isoform of the focal adhesion protein talin," *Molecular Biology of the Cell*, 9, p. 138.

Meijering, E., Dzyubachyk, O. and Smal, I. (2012) "Methods for cell and particle tracking," *Methods in Enzymology*, 504, pp. 183–200.

Meng, W. and Takeichi, M. (2009) "Adherens junction: molecular architecture and regulation.," *Cold Spring Harbor perspectives in biology*, 1(6), a002899.

Meyer, T. *et al.* (1994) "Expression of meta-vinculin in human coronary arteriosclerosis is related to the histological grade of plaque formation.," *Atherosclerosis*, 111(1), pp. 111–119.

Miroshnikova, Y. A., Nava, M. M. and Wickström, S. A. (2017) "Emerging roles of mechanical forces in chromatin regulation.," *Journal of cell science*, 130(14), pp. 2243–2250.

Mitra, S. K., Hanson, D. A. and Schlaepfer, D. D. (2005) "Focal adhesion kinase: In command and control of cell motility," *Nature Reviews Molecular Cell Biology*, pp. 56–68.

Moiseeva, E. P. (2001) "Adhesion receptors of vascular smooth muscle cells and their functions.," *Cardiovascular research*, 52(3), pp. 372–386.

Monkley, S. J. *et al.* (2000) "Disruption of the talin gene arrests mouse development at the gastrulation stage," *Developmental Dynamics*, 219(4), pp. 560–574.

Monkley, S. J. *et al.* (2011) "Endothelial cell talin1 is essential for embryonic angiogenesis," *Developmental Biology*, 349(2), pp. 494–502.

Monkley, S. J., Pritchard, C. A. and Critchley, D. R. (2001) "Analysis of the mammalian talin2 gene TLN2," *Biochemical and Biophysical Research Communications*, 286(5), pp. 880–885.

Monshausen, G. B. and Gilroy, S. (2009) "Feeling green: mechanosensing in plants," *Trends in Cell Biology*, 19(5), pp. 228–235.

Moody, J. D. *et al.* (2009) "A zyxin head–tail interaction regulates zyxin–VASP complex formation," *Biochemical and Biophysical Research Communications*, 378(3), pp. 625–628.

Muguruma, M., Matsumura, S. and Fukazawa, T. (1990) "Direct interactions between talin and actin," *Biochemical and Biophysical Research Communications*, 171(3), pp. 1217–1223.

Mykuliak, V. V. *et al.* (2018) "Mechanical unfolding reveals stable 3-helix intermediates in talin and α-catenin," *PLOS Computational Biology*, 14(4), e1006126.

Nader, G. P. F., Ezratty, E. J. and Gundersen, G. G. (2016) "FAK, talin and PIPKI 3 regulate endocytosed integrin activation to polarize focal adhesion assembly," *Nature Cell Biology*, 18(5), pp. 491–503.

Nardone, G. *et al.* (2017) "YAP regulates cell mechanics by controlling focal adhesion assembly," *Nature Communications*, 8, e15321.

Nevo, J. *et al.* (2010) "Mammary-derived growth inhibitor (MDGI) interacts with integrin α-subunits and suppresses integrin activity and invasion," *Oncogene*, 29(49), pp. 6452–6463.

Oakes, P. W. *et al.* (2012) "Tension is required but not sufficient for focal adhesion maturation without a stress fiber template," *Journal of Cell Biology*, 196(3), pp. 363–374.

Ohashi, K., Fujiwara, S. and Mizuno, K. (2017) "Roles of the cytoskeleton, cell adhesion and rho signalling in mechanosensing and mechanotransduction," *Journal of Biochemistry*, 161(3), pp. 245–254.

Orr, A. *et al.* (2006) "Mechanisms of mechanotransduction," *Developmental Cell*, 10(1), pp. 11–20.

Orr, A. W. *et al.* (2004) "Thrombospondin induces RhoA inactivation through FAK-dependent signaling to stimulate focal adhesion disassembly," *Journal of Biological Chemistry*, 279(47), pp. 48983–48992.

Otey, C. A., Pavalko, F. M. and Burridge, K. (1990) "An interaction between α-actinin and the β1 integrin subunit in vitro," *The Journal of cell biology*, 111(2), pp. 721–729.

Oxley, C. L. *et al.* (2008) "An integrin phosphorylation switch: the effect of β3 integrin tail phosphorylation on Dok1 and talin binding.," *The Journal of biological chemistry*, 283(9), pp. 5420–5426.

Palazzo, A. F. *et al.* (2004) "Localized Stabilization of Microtubules by Integrin- and FAK-Facilitated Rho Signaling," *Science*, 303(5659), pp. 836–839.

Di Paolo, G. *et al.* (2002) "Recruitment and regulation of phosphatidylinositol phosphate kinase type 1γ by the FERM domain of talin," *Nature*, 420(6911), pp. 85–89.

Papagrigoriou, E. *et al.* (2004) "Activation of a vinculin-binding site in the talin rod involves rearrangement of a five-helix bundle.," *The EMBO journal*, 23(15), pp. 2942–2951.

Parsons, J. T., Horwitz, A. R. and Schwartz, M. A. (2010) "Cell adhesion: integrating cytoskeletal dynamics and cellular tension.," *Nature reviews. Molecular cell biology*, 11(9), pp. 633–643.

Pasapera, A. M. *et al.* (2010) "Myosin II activity regulates vinculin recruitment to focal adhesions through FAK-mediated paxillin phosphorylation.," *The Journal of cell biology*, 188(6), pp. 877–890.

Pelham, R. J. *et al.* (1997) "Cell locomotion and focal adhesions are regulated by substrate flexibility.," *Proceedings of the National Academy of Sciences of the United States of America*, 94(25), pp. 13661–13665.

Perbal, G. and Driss-Ecole, D. (2003) "Mechanotransduction in gravisensing cells," *Trends in Plant Science*, 8(10), pp. 498–504.

Peyton, S. R. and Putnam, A. J. (2005) "Extracellular matrix rigidity governs smooth muscle cell motility in a biphasic fashion," *Journal of Cellular Physiology*, 204(1), pp. 198–209.

Pfaff, M., Du, X. and Ginsberg, M. H. (1999) "Calpain cleavage of integrin β cytoplasmic domains," *FEBS Letters*, 460(1), pp. 17–22.

Pinon, P. *et al.* (2014) "Talin-bound NPLY motif recruits integrin-signaling adapters to regulate cell spreading and mechanosensing," *Journal of Cell Biology*, 205(2), pp. 265–281.

Pouwels, J. *et al.* (2012) "Negative regulators of integrin activity," *Journal of Cell Science*, 125(14), pp. 3271–3280.

Priddle, H. *et al.* (1998) "Disruption of the talin gene compromises focal adhesion assembly in undifferentiated but not differentiated embryonic stem cells," *Journal of Cell Biology*, 142(4), pp. 1121–1133.

Qi, L. *et al.* (2016) "Talin2-mediated traction force drives matrix degradation and cell invasion," *Journal of Cell Science*, 129(19), pp. 3661–3674.

Qian, X. *et al.* (2007) "Oncogenic inhibition by a deleted in liver cancer gene requires cooperation between tensin binding and Rho-specific GTPase-activating protein activities.," *Proceedings of the National Academy of Sciences*, 104(21), pp. 9012–9017.

Rantala, J. K. *et al.* (2011) "SHARPIN is an endogenous inhibitor of β1-integrin activation," *Nature Cell Biology*, 13(11), pp. 1315–1324.

Rapsomaniki, M. A. *et al.* (2012) "easyFRAP: an interactive , easy-to-use tool for qualitative and quantitative analysis of FRAP data," *Bioinformatics*, 28(13), pp. 1800–1801.

Razinia, Z. *et al.* (2012) "Filamins in Mechanosensing and Signaling," *Annual Review of Biophysics*, 41(1), pp. 227–246.

Reid, S. E. *et al.* (2017) "Tumor matrix stiffness promotes metastatic cancer cell interaction with the endothelium.," *The EMBO journal*, 36(16), pp. 2373–2389.

Ringer, P. *et al.* (2017) "Multiplexing molecular tension sensors reveals piconewton force gradient across talin-1," *Nature Methods*, 14(11), pp. 1090–1096.

del Rio, A. *et al.* (2009) "Stretching single talin rod molecules activates vinculin binding.," *Science*, 323(5914), pp. 638–641.

Robinson, B. K. *et al.* (2016) "Quantitative analysis of 3D extracellular matrix remodelling by pancreatic stellate cells," *Biology Open*, 5(6), pp. 875–882.

Roca-Cusachs, P. *et al.* (2009) "Clustering of α5β1 integrins determines adhesion strength whereas αvβ3 and talin enable mechanotransduction.," *Proceedings of the National Academy of Sciences of the United States of America*, 106(38), pp. 16245–16250.

Rodius, S. *et al.* (2008) "The talin rod IBS2 alpha-helix interacts with the β3 integrin cytoplasmic tail membrane-proximal helix by establishing charge complementary salt bridges," *The Journal of biological chemistry*, 283(35), pp. 24212–24223.

Saltel, F. *et al.* (2009) "New PI(4,5)P2- and membrane proximal integrin-binding motifs in the talin head control β3-integrin clustering," *Journal of Cell Biology*, 187(5), pp. 715–731.

Sawada, Y. *et al.* (2006) "Force Sensing by Mechanical Extension of the Src Family Kinase Substrate p130Cas," *Cell*, 127(5), pp. 1015–1026.

Saxena, M. *et al.* (2017) "Force-Induced Calpain Cleavage of Talin Is Critical for Growth, Adhesion Development, and Rigidity Sensing," *Nano Letters*, 17(12), pp. 7242–7251.

Schiller, H. B. *et al.* (2013) "β1- and αv-class integrins cooperate to regulate myosin II during rigidity sensing of fibronectin-based microenvironments," *Nature Cell Biology*, 15(6), pp. 625–636.

Schneider, C. A., Rasband, W. S. and Eliceiri, K. W. (2012) "NIH Image to ImageJ: 25 years of image analysis," *Nature Methods*, 9(7), pp. 671–675.

Senetar, M. A. and McCann, R. O. (2005) "Gene duplication and functional divergence during evolution of the cytoskeletal linker protein talin," *Gene*, 362, pp. 141–152.

Senetar, M. A., Moncman, C. L. and McCann, R. O. (2007) "Talin2 is induced during striated muscle differentiation and is targeted to stable adhesion complexes in mature muscle," *Cell Motility and the Cytoskeleton*, 64(3), pp. 157–173.

Seng, T. J. *et al.* (2007) "The major 8p22 tumor suppressor DLC1 is frequently silenced by methylation in both endemic and sporadic nasopharyngeal, esophageal and cervical carcinomas and inhibits tumor cell colony formation," *Oncogene*, 26(6), pp. 934–944.

Serrels, B. and Frame, M. C. (2012) "FAK and talin: Who is taking whom to the integrin engagement party?," *Journal of Cell Biology*, 196(2), pp. 185–187.

Shattil, S. J., Kim, C. and Ginsberg, M. H. (2010) "The final steps of integrin activation: The end game," *Nature Reviews Molecular Cell Biology*, 11(4), pp. 288–300.

Shyy, J. Y.-J. and Chien, S. (2002) "Role of integrins in endothelial mechanosensing of shear stress.," *Circulation research*, 91(9), pp. 769–75.

Singh, R. B. *et al.* (2002) "Pathogenesis of atherosclerosis: A multifactorial process.," *Experimental and clinical cardiology*, 7(1), pp. 40–53.

Solon, J. *et al.* (2007) "Fibroblast Adaptation and Stiffness Matching to Soft Elastic Substrates," *Biophysical Journal*, 93(12), pp. 4453–4461.

Song, X. *et al.* (2012) "A novel membrane-dependent on/off switch mechanism of talin FERM domain at sites of cell adhesion," *Cell Research*, 22(11), pp. 1533–1545.

Stary, H. C. *et al.* (1994) "A definition of initial, fatty streak, and intermediate lesions of atherosclerosis. A report from the Committee on Vascular Lesions of the Council on Arteriosclerosis, American Heart Association.," *Circulation*, 89(5), pp. 2462–2478.

Stricker, J. *et al.* (2011) "Spatiotemporal constraints on the force-dependent growth of focal adhesions," *Biophysical Journal*, 100(12), pp. 2883–2893.

Stutchbury, B. *et al.* (2017) "Distinct focal adhesion protein modules control different aspects of mechanotransduction," *Journal of Cell Science*, 130(9), pp. 1612–1624.

Subauste, M. C. *et al.* (2004) "Vinculin modulation of paxillin-FAK interactions regulates ERK to control survival and motility," *Journal of Cell Biology*, 165(3), pp. 371–381.

Sukharev, S. and Sachs, F. (2012) "Molecular force transduction by ion channels – diversity and unifying principles," *Journal of Cell Science*, 125(13), pp. 3075–3083.

Sun, N. *et al.* (2008) "Identification of a repeated domain within mammalian α-synemin that interacts directly with talin," *Experimental Cell Research*, 314(8), pp. 1839–1849.

Sun, Z. *et al.* (2016) "Kank2 activates talin, reduces force transduction across integrins and induces central adhesion formation," *Nature Cell Biology*, 18(9), pp. 941–953.

Swaminathan, V. *et al.* (2011) "Mechanical stiffness grades metastatic potential in patient tumor cells and in cancer cell lines.," *Cancer research*, 71(15), pp. 5075–5080.

Takala, H. *et al.* (2008) "β2 integrin phosphorylation on Thr758 acts as a molecular switch to regulate 14-3-3 and filamin binding.," *Blood*, 112(5), pp. 1853–1862.

Tarbell, J. M. and Pahakis, M. Y. (2006) "Mechanotransduction and the glycocalyx," *Journal of Internal Medicine*, 259(4), pp. 339–350.

Tarbell, J. M., Simon, S. I. and Curry, F.-R. E. (2014) "Mechanosensing at the Vascular Interface," *Annual Review of Biomedical Engineering*, 16(1), pp. 505–532.

Theodosiou, M. *et al.* (2016) "Kindlin-2 cooperates with talin to activate integrins and induces cell spreading by directly binding paxillin," *eLife*, 5, e10130.

Thievessen, I. *et al.* (2013) "Vinculin-actin interaction couples actin retrograde flow to focal adhesions, but is dispensable for focal adhesion growth," *Journal of Cell Biology*, 202(1), pp. 163–177.

Thievessen, I. *et al.* (2015) "Vinculin is required for cell polarization, migration, and extracellular matrix remodeling in 3D collagen," *The FASEB Journal*, 29(11), pp. 4555–4567.

Tomar, A. and Schlaepfer, D. D. (2009) "Focal adhesion kinase: switching between GAPs and GEFs in the regulation of cell motility," *Current Opinion in Cell Biology*, 21(5), pp. 676–683.

Tsubouchi, A. *et al.* (2002) "Localized suppression of RhoA activity by Tyr31/118-phosphorylated paxillin in cell adhesion and migration," *Journal of Cell Biology*, 159(4), pp. 673–683.

Tsuruta, D., Hopkinson, S. B. and Jones, J. C. (2003) "Characterization of Hemidesmosome protein dynamics in live cells," *Cell Motility and the Cytoskeleton*, 54(1), pp. 122–134.

Vicente-Manzanares, M. and Horwitz, A. R. (2011) "Adhesion dynamics at a glance," *Journal of Cell Science*, 124(23), pp. 3923–3927.

Walko, G., Castañón, M. J. and Wiche, G. (2015) "Molecular architecture and function of the hemidesmosome," *Cell and Tissue Research*, 360(2), pp. 363–378.

Wang, D. *et al.* (2016) "DLC1 is the principal biologically-relevant down-regulated DLC family member in several cancers," *Oncotarget*, 7(29), pp. 45144–45157.

Wang, J. H.-C. and Thampatty, B. P. (2006) "An Introductory Review of Cell Mechanobiology," *Biomechanics and Modeling in Mechanobiology*, 5(1), pp. 1–16.

Wang, S. *et al.* (2012) "Tiam1 interaction with the PAR complex promotes talin-mediated Rac1 activation during polarized cell migration.," *The Journal of cell biology*, 199(2), pp. 331–345.

Webb, D. J. *et al.* (2004) "FAK–Src signalling through paxillin, ERK and MLCK regulates adhesion disassembly," *Nature Cell Biology*, 6(2), pp. 154–161.

Wegener, K. L. *et al.* (2007) "Structural Basis of Integrin Activation by Talin," *Cell*, 128(1), pp. 171–182.

Wehrle-Haller, B. (2012a) "Assembly and disassembly of cell matrix adhesions," *Current Opinion in Cell Biology*, 24(5), pp. 569–581.

Wehrle-Haller, B. (2012b) "Structure and function of focal adhesions," *Current Opinion in Cell Biology*, 24(1), pp. 116–124.

Weinberg, S. H., Mair, D. B. and Lemmon, C. A. (2017) "Mechanotransduction Dynamics at the Cell-Matrix Interface," *Biophysical Journal*, 112(9), pp. 1962–1974.

Wolff, Y. (1892) "Das Gesetz der Transformation der Knochen," Publishing house August Hirschwald, Berlin.

Wong, C. C.-L. *et al.* (2008) "Deleted in Liver Cancer 1 (DLC1) Negatively Regulates Rho/ROCK/MLC Pathway in Hepatocellular Carcinoma," *PLOS One*, 3(7), p. e2779.

Woods, A. and Couchman, J. R. (1992) "Protein kinase C involvement in focal adhesion formation," *Journal of Cell Science*, 101(2), pp. 277–290.

Wu, Z. *et al.* (2017) "Mechanosensory hair cells express two molecularly distinct mechanotransduction channels," *Nature Neuroscience*, 20(1), pp. 24–33.

Wynne, J. P. *et al.* (2012) "Rap1-interacting adapter molecule (RIAM) associates with the plasma membrane via a proximity detector.," *The Journal of cell biology*, 199(2), pp. 317–330.

Xia, H. *et al.* (2004) "Focal adhesion kinase is upstream of phosphatidylinositol 3-kinase/Akt in regulating fibroblast survival in response to contraction of type I collagen matrices via a β1 integrin viability signaling pathway," *Journal of Biological Chemistry*, 279(31), pp. 33024–33034.

Xiao, Z. and Quarles, L. D. (2015) "Physiological mechanisms and therapeutic potential of bone mechanosensing," *Reviews in Endocrine and Metabolic Disorders*, 16(2), pp. 115–129.

Xu, F. *et al.* (2009) "Endothelial cell apoptosis is responsible for the formation of coronary thrombotic atherosclerotic plaques.," *The Tohoku journal of experimental medicine*, 218(1), pp. 25–33.

Xu, W. and Baribault, H. (1998) "Vinculin knockout results in heart and brain defects during embryonic development," *Development*, 125(2), pp. 327–337.

Xu, Y. *et al.* (2010) "Filamin A regulates focal adhesion disassembly and suppresses breast cancer cell migration and invasion," *The Journal of Experimental Medicine*, 207(11), pp. 2421–2437.

Xue, W. *et al.* (2008) "DLC1 is a chromosome 8p tumor suppressor whose loss promotes hepatocellular carcinoma.," *Genes & development*, 22(11), pp. 1439–1444.

Yamashiro, S. *et al.* (2018) "Myosin-dependent actin stabilization as revealed by single-molecule imaging of actin turnover," *Molecular Biology of the Cell*, 29(16), pp. 1941–1947.

Yan, J. *et al.* (2015) "Talin Dependent Mechanosensitivity of Cell Focal Adhesions," *Cellular and Molecular Bioengineering*, 8(1), pp. 151–159.

Yang, J. *et al.* (2014) "Conformational activation of talin by RIAM triggers integrin-mediated cell adhesion," *Nature Communications*, 5, e5880.

Yao, M. *et al.* (2014) "Mechanical activation of vinculin binding to talin locks talin in an unfolded conformation," *Scientific Reports*, 4, pp. 4610–4617.

Yao, M. *et al.* (2016) "The mechanical response of talin," *Nature Communications*, 7, e11966.

Yau, T. O. *et al.* (2009) "Deleted in Liver Cancer 2 (DLC2) Was Dispensable for Development and Its Deficiency Did Not Aggravate Hepatocarcinogenesis," *PLOS One*, 4(8), e6566.

Ye, F. *et al.* (2013) "The Mechanism of Kindlin-Mediated Activation of Integrin αIIbβ3," *Current Biology*, 23(22), pp. 2288–2295.

Yuan, B. Z. *et al.* (1998) "Cloning, characterization, and chromosomal localization of a gene frequently deleted in human liver cancer (DLC-1) homologous to rat RhoGAP.," *Cancer research*, 58(10), pp. 2196–2199.

Zacharchenko, T. *et al.* (2016) "LD Motif Recognition by Talin: Structure of the Talin-DLC1 Complex," *Structure*, 24(7), pp. 1130–1141.

Zaidel-Bar, R. (2003) "Early molecular events in the assembly of matrix adhesions at the leading edge of migrating cells," *Journal of Cell Science*, 116(22), pp. 4605–4613.

Zaidel-Bar, R. and Geiger, B. (2010) "The switchable integrin adhesome," *Journal of Cell Science*, 123(9), pp. 1385–1388.

Zaman, M. H. *et al.* (2006) "Migration of tumor cells in 3D matrices is governed by matrix stiffness along with cell-matrix adhesion and proteolysis.," *Proceedings of the National Academy of Sciences of the United States of America*, 103(29), pp. 10889–10894.

Zamir, E. and Geiger, B. (2001) "Molecular complexity and dynamics of cell-matrix adhesions.," *Journal of cell science*, 114(Pt 20), pp. 3583–3590.

Zhang, H. *et al.* (2011) "A tension-induced mechanotransduction pathway promotes epithelial morphogenesis," *Nature*, 471(7336), pp. 99–103.

Zhang, H. *et al.* (2016) "Structural and Functional Analysis of a Talin Triple-Domain Module Suggests an Alternative Talin Autoinhibitory Configuration," *Structure*, 24(5), pp. 721–729.

Zhang, X. *et al.* (2008) "Talin depletion reveals independence of initial cell spreading from integrin activation and traction.," *Nature cell biology*, 10(9), pp. 1062–1068.

Zhou, H. *et al.* (2013) "Robust phosphoproteome enrichment using monodisperse microsphere–based immobilized titanium (IV) ion affinity chromatography," *Nature Protocols*, 8(3), pp. 461–480.

Zhou, J. *et al.* (2015) "Mechanism of Focal Adhesion Kinase Mechanosensing," *PLOS Computational Biology*, 11(11), e1004593.

10 ORIGINAL COMMUNICATIONS

SCIENTIFIC REPORTS

OPEN

Mechanical stability of talin rod controls cell migration and substrate sensing

Received: 23 January 2017
Accepted: 26 April 2017
Published online: 15 June 2017

Rolle Rahikainen[1], Magdaléna von Essen[1], Markus Schaefer[2], Lei Qi[3], Latifeh Azizi[1], Conor Kelly[1], Teemu O. Ihalainen[1], Bernhard Wehrle-Haller[4], Martin Bastmeyer[2], Cai Huang[3] & Vesa P. Hytönen[1]

Cells adhere to the surrounding tissue and probe its mechanical properties by forming cell-matrix adhesions. Talin is a critical adhesion protein and participates in the transmission of mechanical signals between extracellular matrix and cell cytoskeleton. Force induced unfolding of talin rod subdomains has been proposed to act as a cellular mechanosensor, but so far evidence linking their mechanical stability and cellular response has been lacking. Here, by utilizing computationally designed mutations, we demonstrate that stepwise destabilization of the talin rod R3 subdomain decreases cellular traction force generation, which affects talin and vinculin dynamics in cell-matrix adhesions and results in the formation of talin-rich but unstable adhesions. We observed a connection between talin stability and the rate of cell migration and also found that talin destabilization affects the usage of different integrin subtypes and sensing of extracellular matrix proteins. Experiments with truncated forms of talin confirm the mechanosensory role of the talin R3 subdomain and exclude the possibility that the observed effects are caused by the release of talin head-rod autoinhibition. In conclusion, this study provides evidence into how the controlled talin rod domain unfolding acts as a key regulator of adhesion structure and function and consequently controls central cellular processes such as cell migration and substrate sensing.

Cell-matrix adhesions are large and dynamic membrane spanning protein complexes that physically anchor animal cells to their environment. These complexes connect integrin adhesion receptors to actin fibers providing a mechanical link between the cytoskeleton and the extracellular matrix. In addition to mechanical force, cell-matrix adhesions transmit biochemical signals across the plasma membrane and they have an important role in the regulation of cell anchorage, spreading and migration. The central role of cell-matrix adhesions in force transmission also makes them hotspots for cellular mechanotransduction. Mechanotransduction describes the cellular processes that translate mechanical tension or forces into a chemical or electrical signal. These processes allow cells to probe the mechanical properties of the surrounding tissue and to react to forces exerted on them[1]. Mechanotransduction regulates many processes on the levels of individual cells and complete tissues and it is involved in the development and progression of various diseases[2]. Despite the intense research focusing on the mechanotransduction of cell-matrix adhesions, the primary mechanosensory proteins in these adhesions remain largely unknown.

Talin is a 270 kDa adhesion protein containing a globular N-terminal head domain and a C-terminal rod domain composed of a series of alpha-helical bundles. The head domain (47 kDa) contains binding sites for multiple adhesion proteins and its binding to the β-integrin tail is one of the first steps in the formation of nascent cell-matrix adhesions. The head domain is linked to the rod domain by an unstructured linker region (9 kDa) which, when fully extended, increases the length of the protein by 20 nm and contains a protease cleavage site involved in adhesion turnover[3,4]. Talin rod domain (~210 kDa) consists solely of alpha-helices, assembled into

[1]Faculty of Medicine and Life Sciences and BioMediTech, University of Tampere, Finland and Fimlab Laboratories, Tampere, Finland. [2]Zoological Institute, Cell- and Neurobiology, Karlsruhe Institute of Technology (KIT), Institute of Functional Interfaces (IFG), Karlsruhe, Germany. [3]Markey Cancer Center and Department of Molecular and Biomedical Pharmacology, University of Kentucky, Lexington, KY, USA. [4]Department of Cell Physiology and Metabolism, University of Geneva, Geneva, Switzerland. Rolle Rahikainen and Magdaléna von Essen contributed equally to this work. Correspondence and requests for materials should be addressed to V.P.H. (email: vesa.hytonen@uta.fi)

13 subdomains. Each subdomain contains 4 to 5 amphipathic helixes folded into a compact helix bundle with a hydrophobic core. Talin rod subdomains have binding sites for other adhesion proteins, including vinculin, Rap1-GTP-interacting adapter molecule (RIAM), Deleted in liver cancer 1 (DLC1), β-integrins and actin, as reviewed by Calderwood *et al.*[5]. The most numerous binding sites are for vinculin, with a total of 11 binding sites located in 9 of the 13 rod subdomains. Many of these vinculin binding sites (VBS) are cryptic, which means that vinculin can only bind to them after the subdomain has partially unfolded. This unfolding event is thought to be initiated by mechanical force transmitted across the rod domain[6,7]. Different talin rod subdomains have been shown to unfold at different forces, ranging from 5–10 pN to 25–40 pN in *in vitro* experiments[8–10]. The gradual force-induced exposure of the talin VBSs creates a system where higher force causes more rod subdomains to unfold, exposing more VBSs. Vinculin accumulation is known to not only mechanically strengthen the adhesion, but also to initiate downstream signaling cascades. In addition, such multi-step unfolding of the talin rod domain has been suggested to create a force buffer that can smooth out sudden fluctuations in the cellular traction forces[9].

Talin is among the first proteins involved in integrin-mediated adhesion formation[11]. Therefore, mechanotransduction by the force-induced unfolding of talin rod subdomains may have an important role in promoting either maturation or disassembly of nascent adhesions[11,12]. The R3 subdomain of talin has been found to be the first subdomain to open under mechanical load, unfolding in *in vitro* experiments already at a 5 pN pulling force[8–10]. This low mechanical stability of the R3 subdomain makes it especially suitable for acting as a mechanosensor during adhesion maturation, where low magnitude forces are transmitted through the talin rod domain. If the force-induced unfolding of the talin R3 subdomain is a key step in adhesion maturation, mechanically stabilizing or destabilizing mutations should affect cellular mechanosensing and mechanosignaling. In a previous study, mechanically stabilized talin R3 subdomain was found to affect fibroblast substrate rigidity sensing and YAP signaling, highlighting the importance of talin R3 subdomain in mechanosensing[13,14]. However, this experiment does not give any indication about whether also destabilization of talin R3 subdomain would result in altered mechanosignaling and changes in cell phenotype.

In this study, we present a series of talin point mutations that destabilize the talin rod R3 subdomain. Steered molecular dynamics simulations were used to confirm that these mutations decreased the mechanical stability of the R3 subdomain. Expression of these talin mutants in fibroblast cells enabled us to study the importance of this rod subdomain for talin recruitment into cell-matrix adhesions. Importantly, we show that even a single destabilizing mutation affected adhesion protein composition and adhesion dynamics. On a cellular level, talin destabilization decreased both the cell migration rate and traction force generation and affected integrin subtype usage and ECM sensing. This study demonstrates that a controlled decrease in the stability of talin rod domain affects several cellular functions and sheds light into the importance of talin stability as a key regulator of adhesion mechanosignaling.

Results

Stepwise mutagenesis destabilizes the talin R3 subdomain in steered molecular dynamics simulations and affects subdomain folding *in vitro*. Talin-1 subdomain R3 is a four helix bundle located within the compact N-terminal end of the talin rod domain. It contains 2 vinculin binding sites in the helices 2 and 3 (Fig. 1b,c). Due to the presence of hydrophilic threonine residues in the hydrophobic core, the mechanical stability of the R3 subdomain helix bundle is relatively low[8]. With our mutagenesis design, we aimed to further destabilize the R3 subdomain by mutating conserved isoleucine and leucine residues within the hydrophobic core of the helix bundle to a small polar amino acid, serine. This addition of hydrophilic residues into the core of the helix bundle makes its tertiary structure thermodynamically less favorable, and thus facilitates its unfolding when the helix bundle is subjected to mechanical stretching. The multiple sequence alignment presented in Fig. 1c shows that the residues selected for mutagenesis are highly conserved over animal species. The side chains of the selected hydrophobic residues are oriented towards the core of the helix bundle (Fig. 1b). Furthermore, the residues targeted for mutagenesis are in a belt or ladder-like assembly through the hydrophobic core at sufficient distance from each other as well as from other polar residues in the core, so that stabilization of the mutated helix bundle through the organization of polar planes is unlikely. After the identification of the potential target residues for mutagenesis, a panel of mutants containing one to four single point mutations I805S, I812S, L890S and L897S in each construct was prepared (Fig. 1a).

The destabilized point mutations were investigated by using constant force steered molecular dynamics (SMD) simulations. The bundle behavior was assessed by analyzing the number of water molecules penetrating into the hydrophobic core of the R3 subdomain (Fig. 2). SMD simulations showed decreasing mechanical stability under mechanical load with the increasing number of single point mutations in the talin R3 bundle, as can be observed on the penetrating water count in Fig. 2g. The increase in the number of the penetrating water molecules reflects an increase in the total volume of the bundle due to the acting force and correlates with the number of destabilizing mutations. With the increased volume and area, also the number of water molecules that comply with the penetrated water selection criteria increases. The effect of the mutations on the R3 subdomains ability to withstand mechanical forces was also analyzed by observing the distance between the helix 1 (H1) and the helix 4 (H4) (Supplementary Figure S1). The H1-H4 displacement over time was followed on four vectors, drawn between the α-carbons of residues Gln800 – Ala904, Thr804 – Ala900, Val808 – Gly896, and Ser815 – Gln888. During 10 ns simulations at 150 pN, WT and 1S mutant subdomains underwent only negligible changes in the range of approximately 0.2 nm. For the 2S mutant, we recognized increasing distance between Gln800 – Ala904 at the top of the bundle. At the same time, the distance between Ser815 – Gln888 at the bottom of the bundle was decreasing, pointing at closing the bottom of the bundle. Similar, yet more intensive, helix reorganization was observed for the 3S and 4S mutants especially during the last 2 ns of the pulling simulation. This suggests that these bundles are opening from the top, making H3 VBS more accessible for vinculin binding (Supplementary Figure S1).

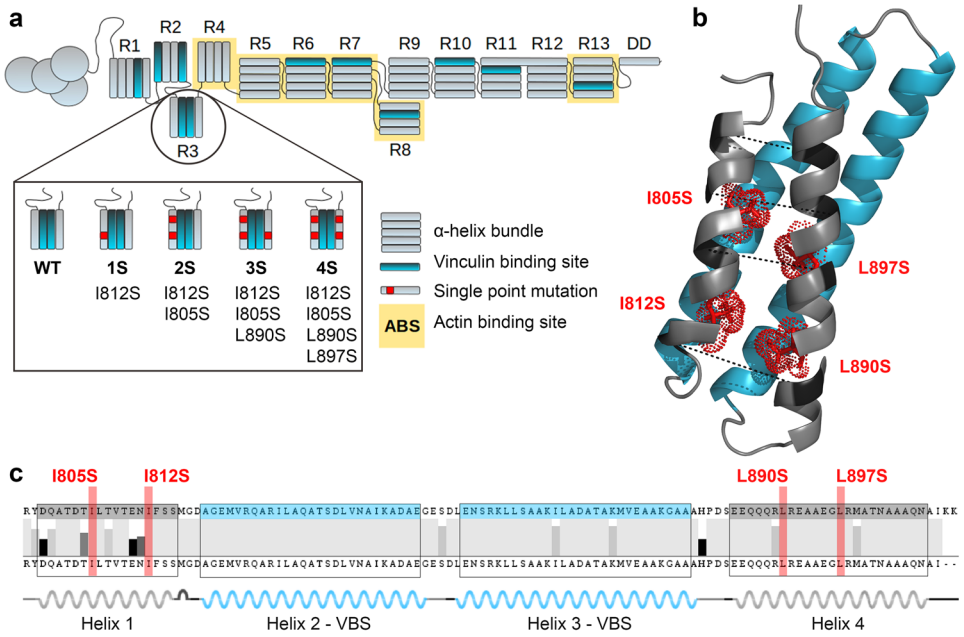

Figure 1. Talin-1 R3 domain destabilization by mutagenesis. (**a**) Schematic illustration of wild-type talin-1 and the locations of the mechanically destabilizing point mutations in the R3 subdomain in mutants 1S, 2S, 3S and 4S. (**b**) A cartoon model (PDB ID: 2L7A[14]) of mouse talin-1 R3 domain. The four mutated residues are shown as stick models colored in red and indicated with red labels. The pulling vectors in the SMD simulations are marked with a dashed black line and respective amino acids are indicated with dark coloring. The two vinculin binding helices in the R3 subdomain are colored in blue. (**c**) Talin-1 R3 domain helix boundaries and sequence conservation across 13 animal species (Human gi6739602, Mouse gi227116327, Rat gi189181726, Hamster gi344251776, Naked mole rat gi351707040, Threeshrew gi444729903, Bat gi432110771, Flying fox gi431902812, Cattle gi296484714, Turtle gi465952424, Quail gi667665823, Chicken gi45383127, Zebrafish gi57222259). The positions of the two VBS helices and four destabilizing point mutations are colored in blue and red, respectively.

To computationally investigate the stability of the mutated helix bundles in the absence of force, we compared the structural differences of wild-type R3 subdomain and the 4S mutant during subdomain refolding (Supplementary Figure S2). The refolding ability was measured on the Val808 – Gly896 vector located in the middle of the bundle. Although the 4S mutant showed increased Val808 – Gly896 distance during mechanical stretching, this distance returned to its original length within 7 ns of the relaxation simulation. This suggests that even the most heavily modified 4S mutant readily refolds to its equilibrated state and that the mechanically destabilizing mutations do not prevent refolding of the subdomain helix bundle.

In order to evaluate the effects of the mechanically destabilizing mutations on R3 subdomain thermal stability and secondary structure, we produced the corresponding His6-tagged talin fragments (amino acids 795 – 911) in *E. coli*. We observed robust protein expression and good solubility of the fragments. Because of surprisingly large differences in the electrophoretic mobility of the fragments in SDS-PAGE even in the presence of 8 M urea (Fig. 2h), we confirmed the molecular weights of the purified proteins by mass spectrometry. Size exclusion chromatography (SEC) was used to analyze solubility and size of the produced talin fragments. All studied fragments were found to be soluble and no protein aggregation was observed in SEC (Fig. 2i). However, 3S and 4S mutants showed faster penetration time, suggesting oligomeric structure. This was confirmed by inline right angle light scattering (RALS) analysis, where molecular weights for WT and 1S – 4S mutants were 12.7 kDa, 13.7 kDa, 14.2 kDa, 29.5 kDa and 27.6 kDa, respectively.

Circular dichroism (CD) spectroscopy was used to analyze folding and thermal stability of the purified talin fragments. In CD spectroscopy, wild-type talin R3 and 1S mutant showed closely matching spectra, while the 2S showed signs of decreased subdomain helicity. This decrease in the subdomain helicity was especially apparent for the 3S and 4S mutants. After deconvolution at 205–260 nm, the observed helical contents of WT, 1S, 2S, 3S and 4S were 79.7%, 77.4%, 51.2%, 25.8% and 26.4%, respectively (Fig. 2j). Similarly, in CD spectroscopy melting analysis (Fig. 2k) the 1S mutant was found to have a moderately decreased thermal stability (T_m 52.6 °C) as compared to the wild-type fragment (T_m 66.9 °C), while the 2S, 3S and 4S mutations resulted in a further decrease in T_m value (48.0 °C, 40.7 °C and 40.9 °C, respectively). These results suggest that that at least in the conditions used during the analysis and in the absence of the surrounding talin domains, extensive mutagenesis of the hydrophobic core of the R3 helix bundle reduces the helical content and may expose hydrophobic patches, leading to dimerization in the case of 3S and 4S. Some indications of such behavior were also observed in MD simulations, where the mutated site was found to bend away from its original position, causing torsion of the helix.

Overall, the biochemical analyses indicate that 1S mutant resembles WT in all the characteristics while having decreased stability. The 3S and 4S mutants have severely affected folding and represent significantly destabilized

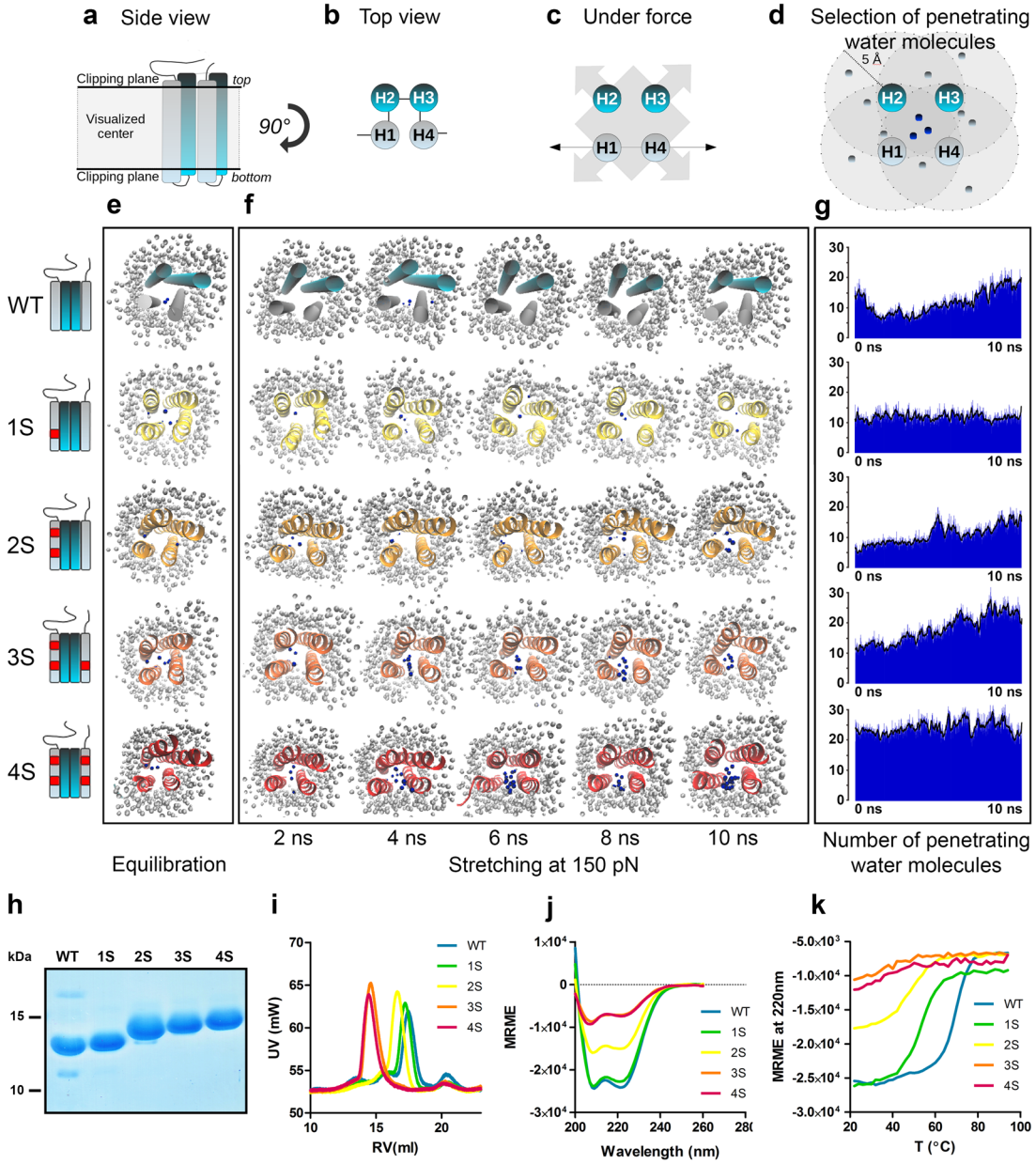

Figure 2. Simulated mechanical stretching and biochemical characteristics of destabilized mouse talin-1 fragments. Talin R3 subdomain stability during simulated mechanical stretching was analyzed by observing water penetration into the hydrophobic core of the subdomain. VBS in cyan color, point mutations in red, non-penetrating water in gray, penetrating water in blue. (**a–d**) Schematics of talin R3 subdomain helix positions and the criteria for selecting water molecules penetrated into the bundle core. The clippings planes used in visualizations in (**e**,**f**) are shown in (**a**). In (**d**), water molecules within 5 Å of each helix are marked in blue. (**e**) Snapshot images of the destabilized talin-1 R3 subdomains after a 20 ns equilibration without pulling force. The planes above and below the bundle ends are hidden to allow unobstructed view into the bundle core (schematics in (**a**)). Penetrating water molecules are colored in blue while water molecules outside the bundle are colored in gray. (**f**) Representative serial snapshot images of talin-1 R3 subdomain opening during a 10 ns simulation with a constant force of 150 pN. (**g**) The number of penetrating water molecules during a 10 ns pulling simulation as an average count of 5 experiments at each time point. Black lines represent sliding averages of 10 frames. Water molecules at the ends of the bundle are included in this total count, although they are hidden from the snapshot images in (**e**,**f**). (**h**) PageBlue staining for destabilized talin R3 subdomain fragments (amino acids 795 – 911) expressed in *E. coli*, affinity purified and separated by SDS-PAGE in the presence of 8 M urea. Apparent differences in fragment sizes result from differential SDS binding to purified talin forms. (**i**) Size exclusion chromatography analysis for the R3 subdomain fragments. RV = Retention volume (**j**) Circular dichroism spectroscopy scanning for the talin R3 fragments at wavelengths 200 nm–260 nm. MRME = Mean residue molar ellipticity. (**k**) Circular dichroism spectroscopy melting curves at 220 nm wavelength. Temperature was increased in 2 °C steps at a rate of 1 °C/min. Determined melting points for WT and 1S – 4S mutants were 66.9 °C, 51.6 °C, 48.0 °C, 40.7 °C and 40.9 °C, respectively.

R3 subdomains. The 2S mutant appears an intermediate between 1S and 3S. Therefore, we were keen to evaluate how these mutants would affect cellular talin-mediated functions.

Talin R3 subdomain destabilization induces talin accumulation into adhesions independently of the presence of talin R4 - R12 subdomains. The destabilizing talin mutations were introduced into full-length talin expression constructs to study their effects on talin and vinculin recruitment into cell-matrix adhesions. Wild-type mouse embryonic fibroblast (MEF) cells were transfected with the talin constructs, fixed and immunostained for vinculin. Based on captured microscope images, fluorescence intensity ratios between adhesions and cytosolic areas were determined to minimize the bias caused by cell-to-cell variance in the expression levels of the talin proteins. Interestingly, even a single point mutation (1S mutant) in the R3 subdomain was enough to significantly increase this ratio, indicating increased talin partitioning into cell-matrix adhesions (Fig. 3c). Further mutagenesis increased the ratio up to three-fold (for the 4S construct) as compared to the wild-type talin construct. Similar increase in the intensity ratio was also observed for vinculin staining (Fig. 3d). However, the fold increase in this ratio for vinculin was smaller than that observed for talin, resulting in a decrease in the vinculin/talin ratio for the destabilized talin mutants (Fig. 3e). Also the maximal increase in vinculin intensity ratio was already achieved by introducing one destabilizing point mutation (1S mutant). Consequently, the highest vinculin/talin ratio was observed for wild type talin-1 and the ratio gradually decreased when additional point mutations were introduced into the construct. The observed decrease in the vinculin/talin ratio likely resulted from vinculin binding to the abnormally active VBS in talin R3, which activates downstream signaling cascades, whilst decreasing cellular traction forces generation. This, in turn, decreased the force applied on individual talin and results in a decrease in the number of activated VBSs (overall, there are 11 VBSs in talin rod and only two of them are within R3). Similar increase in talin accumulation and decrease in vinculin/talin ratio was also observed in TLN1−/−TLN2−/− cells, confirming that the results are not dependent on the presence of endogenous talin proteins (Supplementary Figure S3c,e). To confirm similar expression levels and the expression of intact talin protein for all talin constructs, lysates of TLN1−/−TLN2−/− cells expressing the studied talin proteins were analyzed by using Western blot with anti-mCherry antibody (Supplementary Figure S3b).

In a previous study, a cryptic actin binding site (ABS2) in talin-1 rod R4-R8 subdomains was proposed to be a key factor in controlling the incorporation of talin into adhesion structures[15]. To rule out the possibility that the increased accumulation of the destabilized talin constructs would result from altered regulation of talin autoinhibition or talin ABS2, we also studied the 4S mutations in the context of a truncated talin-1 mutant lacking subdomains R4 - R12. This centrally truncated talin–1 (Tal1 ΔR4-12) accumulated only very weakly into cell-matrix adhesions, resulting in a low adhesion/cytosol intensity ratio and poorly visible adhesions (Fig. 3f). However, introduction of the four destabilizing mutations (Tal1 ΔR4-12 4S) into this construct caused a similar increase in the adhesion/cytosol intensity ratio as was seen with the full length talin (Fig. 3f,g), indicating that other talin rod subdomains are not required for the enhanced cell-matrix adhesion recruitment caused by the destabilizing mutations. This suggests that the increase in talin-1 adhesion localization was indeed dependent on the unfolding of the talin-1 R3 subdomain and not as a result from disturbed autoinhibition of talin-1 ABS2[15]. In addition, because both Tal1 ΔR4-12 and Tal1 ΔR4-12 4S lack the R9 subdomain needed in the talin autoinhibitory interaction between the talin-1 head F3 domain and the rod R9 subdomain[16,17], these results confirm that increased accumulation of destabilized full length talin is not caused by disrupted talin autoinhibition.

Talin R3 subdomain destabilization affects traction force generation, talin and vinculin mobility in adhesions and the rate of cell migration. Cell-matrix adhesions are important signaling hubs for the regulation of actomyosin contractility and cellular traction force generation. In turn, forces acting on the adhesion components are in part regulating adhesion dynamics. To study the effects of talin destabilization on cellular traction force generation, local traction forces were determined by using fluorescent 0.2 µm beads embedded into polyacrylamide gel. Talin-1 in human osteosarcoma U2OS cells was ablated by CRISPR techniques as described by Qi *et al.*[18]. Talin-1 ablation resulted in a large decrease in the average cell area and in a complete loss of cellular traction forces (Fig. 4a–c). Re-expression of GFP-tagged wild-type talin-1 fully rescued cell spreading and largely rescued traction force generation. Re-expression of the destabilized talin proteins rescued cell spreading and traction force generation to a degree dependent on the mechanical stability of the expressed talin protein. Re-expression of the 1S construct fully rescued cell spreading and caused a small, statistically insignificant increase in cellular traction forces as compared to the cells expressing wild-type talin. It is important to notice that although the 1S mutant rescued the total traction force generation to the same level as wild-type talin, its increased accumulation into cell-matrix adhesions (Fig. 3c) most likely leads to a decrease in the forces applied to each individual talin molecule. Re-expression of 2S or 3S forms rescued both cell spreading and traction force generation to slightly lower levels than wild-type talin-1. Re-expression of the 4S form resulted in only a partial rescue of both cell spreading and traction force generation, indicating that drastic talin-1 R3 subdomain destabilization results in severe defects in cellular traction force generation and mechanosignaling.

Fluorescence recovery after photobleaching (FRAP) experiments were performed to analyze how the mechanically destabilizing mutations affect talin and vinculin turnover rates in cell-matrix adhesions. For talin and vinculin FRAP, *TLN1−/−TLN2−/−* cells were either transfected with Tal1-GFP or co-transfected with Tal1-mCherry and GFP-Vinculin, respectively, and imaged on a confocal microscope. Talin destabilization by 1S and 4S mutants increased the mobile fraction of talin localized to cell-matrix adhesions (mobile fractions of 0.33, 0.82 and 0.79 for WT, 1S and 4S, respectively), indicating increased mobility of the 1S and 4S mutants in cell-matrix adhesions (Fig. 4d). Co-expression of destabilized talin proteins also significantly increased the mobile fraction of GFP-vinculin, but the effect was not as large as it was for talin itself (mobile fractions of 0.59, 0.83 and 0.86 for WT, 1S and 4S, respectively) (Fig. 4e). Interestingly, co-expression of destabilized talin proteins also increased the fluorescence recovery half time of GFP-vinculin as compared to co-expression of wild type talin. This indicates

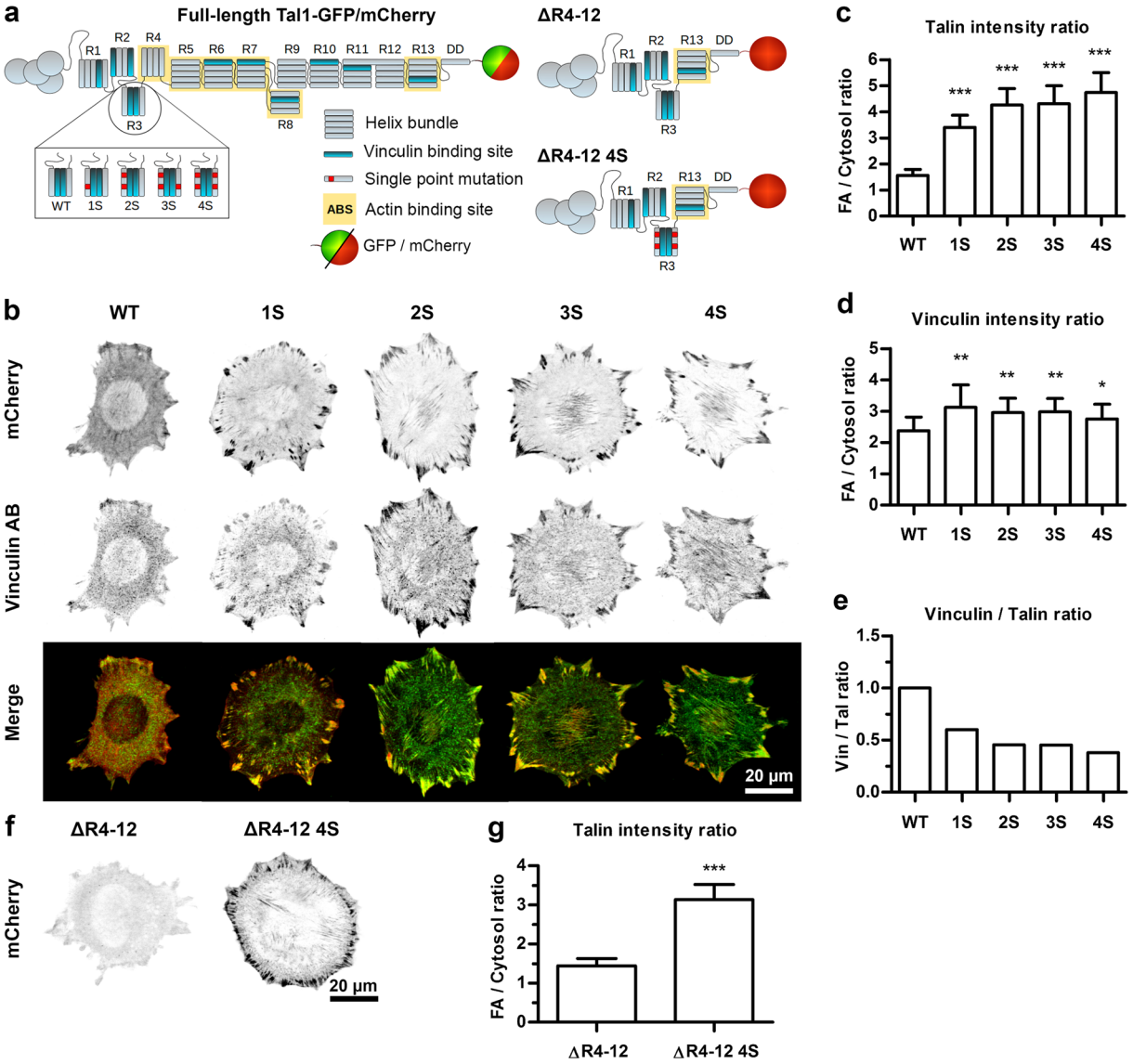

Figure 3. Talin-1 accumulation into cell-matrix adhesions in wild type MEF cells. (**a**) Schematic illustrations of full-length talin-1 constructs and truncated talin-1 constructs lacking rod subdomains R4-R12. The truncated talin ΔR4-12 construct does not contain any destabilizing mutations, while the ΔR4-12 4S construct contains all four point mutations presented in the Fig. 1a. (**b**) Representative images of wild type MEF cells expressing mCherry-tagged talin-1 proteins. In merged images, mCherry signal is shown in red and vinculin antibody staining as green. Colocalization of the two signals is indicated by yellow color. Scale bar is 20 μm. (**c**) Mean ratios of mCherry signal intensities measured from adhesion sites and cytosolic areas in wild type MEF cells expressing mCherry-tagged talin-1 mutant proteins. Error bars represent SD. n = 15 cells for each talin construct. The ratios measured for the talin-1 mutants were compared to mCherry-tagged wild type talin-1 by One-way ANOVA, ***$p < 0.0001$. (**d**) Mean adhesion/cytosolic signal ratios for vinculin antibody staining of cells expressing mCherry-tagged talin-1 forms. Error bars represent SD. n = 22, 20, 15, 15 and 17 cells for wild type talin-1 and 1S, 2S, 3S and 4S mutants, respectively. Comparison to cells expressing wild type talin-1 by one-way ANOVA. **$p < 0.001$, *$p < 0.01$. (**e**) Vinculin/talin-1 ratios for results in (**a**,**b**). (**f**) Representative images of wild type MEF cells expressing truncated mCherry-tagged talin-1 mutant proteins. Scale bar is 20 μm. (**g**) Mean ratios of mCherry signal intensities measured from adhesion sites and cytosolic areas in wild type MEF cells expressing truncated mCherry-tagged talin proteins. Error bars represent SD. n = 15 cells for each construct. Statistical analysis by two-tailed t-test. ***$p < 0.0001$.

that the exchange rate of GFP-vinculin was slower when it was co-expressed with destabilized talin proteins. This could be caused by slower refolding of the destabilized talin proteins, especially when under mechanical force.

To analyze the effects that talin destabilization has on the rate of cell migration, *TLN1−/−TLN2−/−* MEF cells were transfected with wild type and destabilized talin constructs and cultured for 12 h on a fibronectin coated surface. Introduction of a single destabilizing mutation (1S mutant) into the talin-1 R3 domain did not significantly affect the observed rate of migration of talin-1 transfected *TLN1−/−TLN2−/−* MEF cells (Fig. 4f,g).

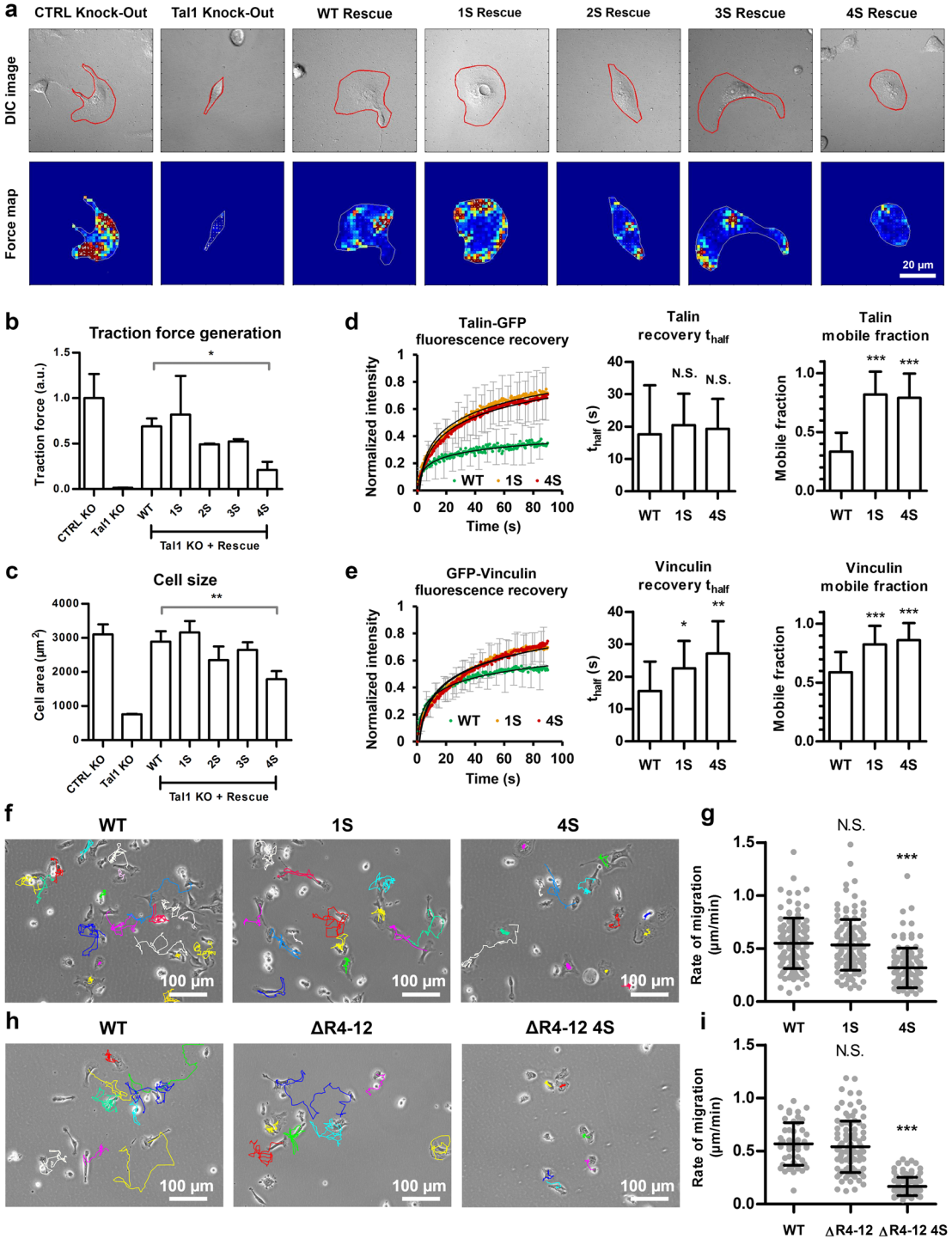

Figure 4. Talin destabilization decreased traction force generation and the rate of cell migration and increased talin and vinculin mobility in cell-matrix adhesions. (**a**) Representative traction force microscopy force maps and DIC images of talin-1 knock-out U2OS cells expressing talin-1 constructs. In the force maps, low local forces are illustrated by blue and green colors, while high local forces are illustrated by yellow and red colors. (**b**) Traction force analysis for talin-1 knock-out U2OS cells. Data are means ± SD. n = 5, 3, 4, 5, 3, 3, 4 for samples named in the graph legend from left to right. Comparison to cells expressing wild type talin-1 by one-way ANOVA and Tukey's test. *$p < 0.05$, Talin-1 WT vs. Talin-1 1S, 2S or 3S were not statistically significant. (**c**) Cell area analysis for talin-1 knock-out U2OS cells. Data are means ± SD, n = 6, 3, 5, 4, 3, 3 and 4 cells for samples named in the graph legend from left to right. Comparison to cells expressing wild type talin-1 by one-way ANOVA. **$p < 0.001$, Talin-1 WT vs. Talin-1 1S, 2S or 3S were not statistically significant. (**d**) Talin-GFP FRAP recovery curve, intensity recovery half time and mobile fraction for wild type talin and destabilized 1S and 4S mutants. Average of 24 cells for each construct from two fully independent experiments. Error bars represent SD. Comparison to cells expressing wild type talin by one-way ANOVA. ***$p < 0.0001$. (**e**) GFP-vinculin FRAP recovery curve, intensity recovery half time and mobile fraction for cells expressing Talin-mCherry constructs.

Average of 29, 24 or 25 cells for WT, 1S and 4S, respectively, from two fully independent experiments. Error bars represent SD. Comparison to cells expressing wild type talin by one-way ANOVA. **$p < 0.001$, *$p < 0.01$. (**f**,**h**) Representative 12-hour migration tracks for *TLN1−/−TLN2−/−* MEF cells expressing EGFP-tagged wild type talin-1 or full-length 1S and 4S talin mutants (**f**) or mCherry-tagged full-length talin and truncated talin forms (**h**). Scale bars are 100 µm (**g**,**i**) Quantification of migration rates for cells expressing full-length or truncated talin-1 constructs. Horizontal lines indicate mean ± SD. For each construct, the results were pooled from two fully independent experiments. n = 116, 122 and 111 cells for wild type talin-1 and full length 1S and 4S talin mutants (**g**). n = 49, 98 and 105 for wild type talin-1 and ΔR4-12 and ΔR4-12 4S mutants (**i**). Other samples were compared to cells expressing wild type talin-1 by one-way ANOVA and Tukey's test. N.S. = Difference not statistically significant, ***$p < 0.0001$.

However, introduction of all four mutations (4S mutant) resulted in a significant decrease in the rate of migration, although it did not completely block migration. To analyze adhesion maturation and disassembly in these cells in detail, we used live-cell fluorescence imaging with cells expressing either GFP-tagged WT talin-1 or talin-1 4S mutant. Although talin-1 R3 subdomain destabilization caused a striking increase in its accumulation into cell-matrix adhesions, no other obvious differences in adhesion formation and disassembly were observed during a 120 min live cell imaging (Supplementary Movie S5). Surprisingly, deletion of the talin-1 rod R4 - R12 subdomains did not significantly affect the rate of cell migration (Fig. 4i). *TLN1−/−TLN2−/−* MEF cells expressing the truncated talin ΔR4-12 protein were still able to polarize and the rate of migration was comparable to that of cells expressing wild type talin-1. On the contrary, cells expressing the 4S-destabilized talin-1 ΔR4-12 construct were able to spread, but their ability to migrate was fully blocked (Fig. 4i). Apart from small movement resulting from seemingly random detachment of lamellipodium on one side of the cell, cells expressing this construct were unable to migrate. This suggests that the correct mechanical stability of the R3 subdomain is indispensable for cell migration in the absence of rod subdomains 4-12, but not in the context of full length talin.

Talin-1 R3 subdomain destabilization affects ECM sensing and talin colocalization with β3 and β1 integrin subtypes. The structure of a cell-matrix adhesion is tightly linked to its function and it is constantly changing as a response to intracellular and extracellular signals. Changes in the structure and function of the intracellular adhesion complex are also reflected on the extracellular side of the plasma membrane, as demonstrated by the different integrins clustered in different adhesion subtypes[19]. To study the nature of cell-matrix adhesions induced by the destabilized mutants, wild type MEF cells expressing GFP-tagged wild type talin-1 or destabilized 1S or 4S mutants were cultured on coverslips micropatterned with fibronectin and vitronectin spatially separated from each other on a subcellular resolution, as described previously in Pinon *et al.*[20]. Imaging with superresolution microscopy (SIM) revealed that in the cells expressing wild type talin-1 adhesions were shorter and more punctuated, as compared to the long, streak-like adhesions seen in the cells expressing 1S and 4S mutants (Fig. 5). To minimize the bias caused by unspecific cytosolic fluorescence signal from the talin-1-GFP constructs, analysis of adhesion localization was limited to areas within a mask based on the paxillin antibody staining (Supplementary Figure S6). Adhesions associated with wild type talin-1 strongly favored vitronectin over fibronectin, with only 26% of adhesion area on fibronectin coated surfaces. Talin-1 destabilization caused a decrease in this preference, as indicated by 31% and 40% of adhesions on fibronectin coated areas for cells expressing the 1S and 4S mutants, respectively.

To study the interactions of integrin subtypes with the destabilized talin proteins, we coexpressed WT, 1S or 4S talins with GFP-tagged β3-integrin on glass coverslips coated with fibronectin (Fig. 5e–l). This analysis revealed that the localization of the talin forms varied so that WT and 1S preferentially accumulated into the cell periphery (Fig. 5e,f), while 4S was mostly found in central adhesions within the cell body (Fig. 5g). The peripheral adhesions containing WT and 1S talins were found to be strongly associated with β3 integrin (Fig. 5e,f,h), while the central adhesions rich in 4S contained only negligible amounts of β3 integrin (Fig. 5g,h). We also studied the colocalization of talin forms with β1 integrin using 9EG7 antibody specific for activated β1-integrin (Fig. 5i–k). Talin 4S mutant showed increased colocalization with β1-integrin as compared to WT, indicating that the stability of talin rod domain can regulate the usage of β-integrin subtypes. These changes in the preference for different ECM proteins and the usage of different β-integrin subtypes suggest that talin-1 destabilization does not only affect adhesion dynamics, but also the protein composition of cell-matrix adhesions and adhesion segregation[19].

Discussion

Talin is a central adhesion scaffold protein and it is intensively involved in integrin-mediated processes. It contains confirmed or putative binding sites for at least ten other adhesion proteins, thus regulating their recruitment and activation. The mechanical properties of the talin rod domain have been proposed to be an important factor in the regulation of mechanosensing and mechanosignalling. The forces needed to unfold the talin rod subdomains *in vitro* cover a wide range, from 5–10 pN for talin R3 to 25–40 pN for R9[9,10]. The working hypothesis of this study was that the mechanical stabilities of the rod subdomains are optimized for cellular mechanotransduction and that the gradual unfolding of talin rod subdomain allows cells to measure small local changes in cellular forces at a high resolution. Despite of the vast amount of talin-focused research, mechanically altered talins have not been thoroughly characterized in previous studies. In particular, the effects of talin destabilization on the regulation of cellular processes are unknown.

Talin-1 R3 subdomain is in many ways unique among the talin-1 rod subdomains. It has binding sites for both vinculin and RIAM and its mechanical stability is the lowest of all rod subdomains[8,13,14]. Because of the low mechanical stability of the R3 subdomain, it may have a key role in the mechanotransduction of low magnitude forces during the maturation of nascent adhesions. If talin acts as a mechanosensor, any alteration to its

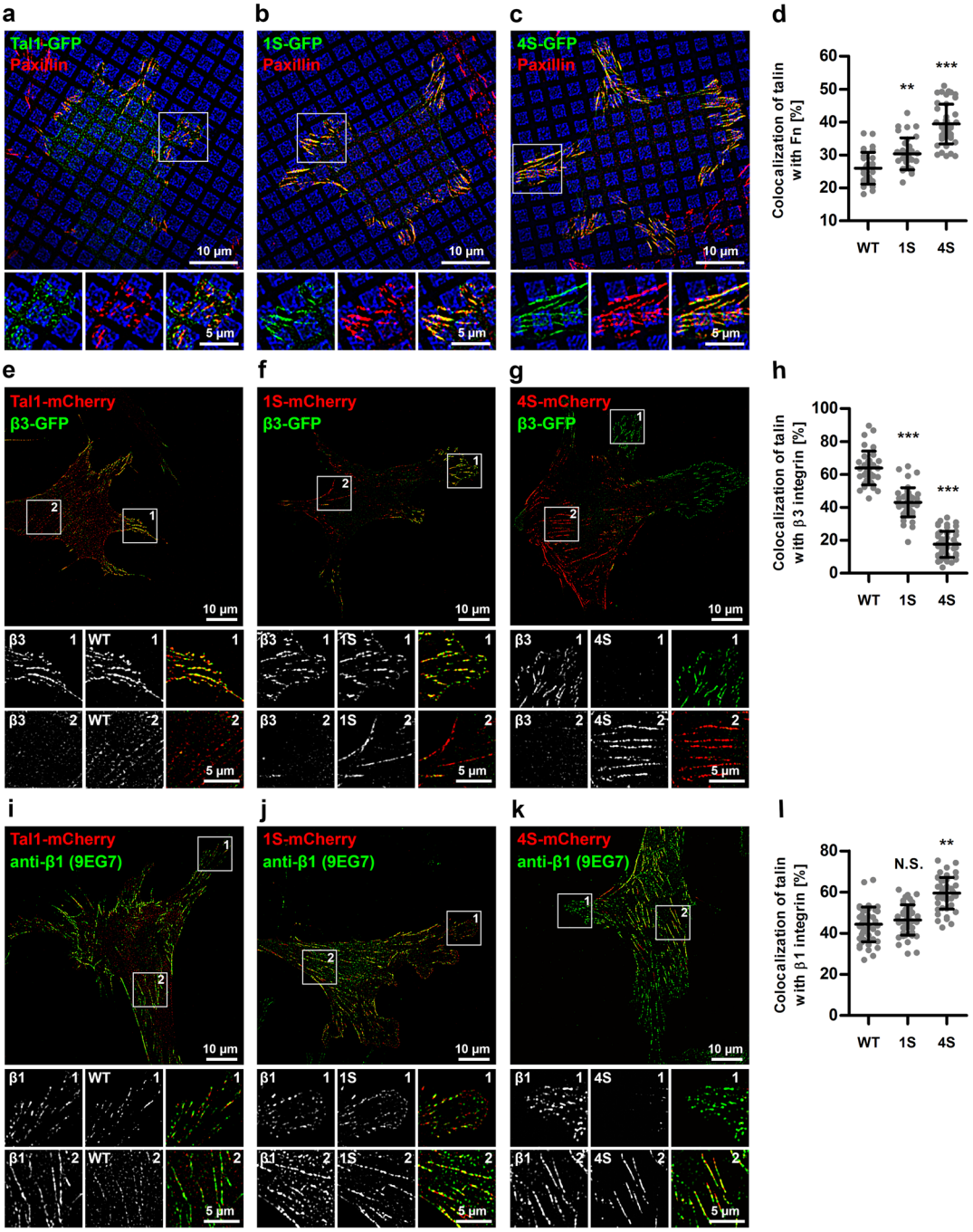

Figure 5. Analysis of talin recruitment to cell-matrix adhesions on Fn/Vn patterned substrates and talin colocalization with β3 and β1 integrin subtypes. (**a**–**c**) Representative SIM images of transfected wild type MEF cells cultured on micropatterned substrates with 56% of area coated with fibronectin (blue squares) and 44% of area coated with vitronectin (black background). Talin1-GFP fluorescence signal is shown as green and paxillin antibody staining used as a reference for cell-matrix adhesion localization is shown as red. (**d**) Quantification of talin recruitment to cell-matrix adhesions on Fn coated areas. Data were pooled from three fully independent experiments, n = 30, 34 and 43 for cells expressing wild type talin-1, 1S mutant or 4S mutant, respectively. Mean ± SD. Statistical analysis by one-way ANOVA and Tukey's test. $^{**}p < 0.001$, $^{***}p < 0.0001$. (**e**–**g**) Representative SIM images of cells cotransfected with talin mutants and β3-GFP and cultured on fibronectin-coated substrate. Notice how talin 4S mostly localized to central adhesions, while β3 integrin only localized to peripheral adhesions. (**h**) Quantification of talin colocalization with β3-GFP. n = 36, 44 and 47 cells for WT, 1S and 4S, respectively, pooled from three fully independent experiments. Mean ± SD. Statistical analysis by one-way ANOVA and Tukey's test. $^{***}p < 0.0001$. (**i**–**k**) Representative SIM images of cells transfected with talin mutants and immunostained with 9EG7 antibody for activated β1 integrin. (**l**) Quantification of talin colocalization with β3-GFP. n = 46, 48 and 47 cells for WT, 1S and 4S, respectively, pooled from three fully independent experiments. Mean ± SD. Statistical analysis by one-way ANOVA and Tukey's test. $^{**}p < 0.001$.

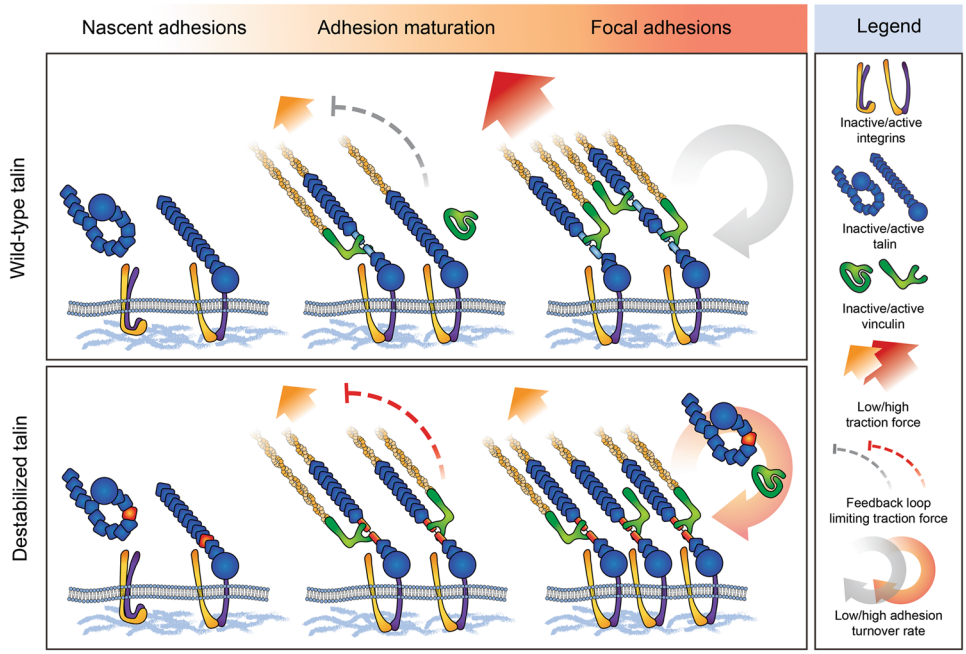

Figure 6. Model for decreased traction force generation and increased talin accumulation after talin rod domain destabilization. Talin is recruited into **nascent adhesions** in its autoinhibited conformation and in the absence of mechanical load. Other adhesion proteins participating in the recruitment of talin are omitted from the schematic representation for simplicity. During **adhesion maturation**, mechanical forces transmitted through the talin rod domain promote unfolding of the rod subdomains. Subdomain unfolding exposes cryptic VBSs and allows vinculin binding. Destabilized talin R3 subdomains unfold at lower force, facilitating subdomain unfolding and vinculin binding. Talin rod subdomain unfolding and vinculin binding initiate negative feedback loops that limit cellular traction force generation and adhesion growth. Decreased unfolding force of the destabilized talin rod R3 subdomain results in the activation of this negative feedback also in adhesions transmitting low magnitude forces, which decreases overall traction force generation. In mature **focal adhesions**, talin rod subdomains unfold at their characteristic threshold forces, creating a heterogeneous pool of talin molecules with rod subdomains unfolded to various degrees. Together with the decrease in cellular traction force generation, the intense accumulation of destabilized talin proteins into focal adhesions results in a large decrease in the force transmitted by an individual talin protein, which increases the mobility of talin proteins within focal adhesions. Decreased traction force generation also affects the unfolding of other talin rod domain bundles, which results in a decrease in the vinculin/talin ratio in these adhesions.

mechanical stability is likely to affect adhesion dynamics and cellular mechanosensing. Accordingly, in a previous study by Elosegui-Artola *et al*., the expression of a mechanically stabilized talin R3 mutant called IVVI was shown to increase the threshold of the substrate rigidity needed for triggering cellular traction force generation and YAP signaling[13]. The likely reason for this increase in the threshold rigidity is that on softer substrates, the tensional forces are not high enough for force-induced unfolding of the stabilized R3 subdomain, which prevents vinculin recruitment to R3 subdomain and downstream signaling. In line with these findings, the destabilizing mutations described in the present study were found to make talin more sensitive for the mechanotransduction of low magnitude forces, as indicated by the observed decreases in both cell migration rate and traction force generation.

Although talin is recruited into nascent adhesions independently of vinculin or transmitted mechanical force, both mechanical stretching of the talin rod domain and recruitment of vinculin are needed for stabilizing talin into cell-matrix adhesions[21,22]. Interestingly, we found that destabilization of the talin R3 subdomain strongly promoted talin accumulation into cell-matrix adhesions (Fig. 3c). Although slightly increased adhesion accumulation was also observed for vinculin, the vinculin/talin ratio was decreased in cells expressing the destabilized talin mutants. This decrease in vinculin/talin-ratio was accompanied by a decrease in the magnitude of cellular traction forces (Fig. 4b). This likely results from facilitated unfolding of the talin R3 subdomain, especially in adhesions transmitting low-magnitude forces. This leads to the exposure of cryptic VBSs in adhesions where the level of mechanical tensions would not normally be sufficient for talin subdomain unfolding (Fig. 6). Such talin unfolding and the resulting vinculin binding possibly trigger downstream signaling cascades that eventually downregulate cellular traction force generation. Decreased traction force generation, in turn, prevents further unfolding of talin rod subdomains and results in a decreased vinculin/talin ratio, as seen for the cells expressing destabilized talin mutants (Fig. 3e).

In the FRAP experiments, talin destabilization vastly increased the mobile fraction of talin localized into cell-matrix adhesions (Fig. 4d). Slightly surprisingly, this suggests that the large and protein-rich adhesions organized around mechanically destabilized talin proteins have a highly dynamic structure. Thus the majority of the

intergrin-bound talin proteins are being constantly exchanged with the cytosolic pool of talin proteins. This finding is in line with the decreased traction force generation observed in this study and highlights the importance of mechanical force as a regulator of adhesion turnover[21]. Similarly to the increased mobile fraction observed for destabilized talin proteins, the mobile fraction of vinculin was increased after talin mutagenesis. However, at the same time we also observed increased FRAP half-recovery time for vinculin. This indicates that despite of the increased mobile fraction, vinculin shows slower initial fluorescence recovery after talin destabilization. This decrease in the vinculin turnover rate may be caused by decelerated dissociation of vinculin-talin complex due to slower refolding of talin rod subdomain after its release from integrin cytoplasmic domain. This is supported by the biochemical analysis of talin R3 mutants, where we found 3S and 4S being rather unstable and poorly folded as isolated domains when compared to WT, 1S and 2S (Fig. 2). Based on these findings, it seems clear that talin destabilization causes defects in cellular mechanosignaling and eventually lowers the force applied on an individual talin protein. This results in increased adhesion protein dynamics and affects the vinculin/talin ratio within cell-matrix adhesions (Fig. 6). The molecular feedback mechanism linking the talin-vinculin interaction to the regulation of applied mechanical load is currently unknown and it may involve several different proteins.

In addition to the increased talin mobile fraction and accumulation into cell-matrix adhesions, R3 destabilization also affected the size, shape and protein composition of cell-matrix adhesions. While wild type talin1-GFP localized mainly into short and roughly circular adhesions at the cell periphery, destabilized talin mutants localized into long, streak-like adhesions that were often found also in the central parts of the cell (Figs 3b and 5). To get a better understanding of the nature of the adhesions formed around the destabilized talin proteins, we analyzed the preference of modified talin proteins to accumulate on fibronectin or vitronectin coated areas. Interestingly, talin destabilization was found to strongly promote adhesion formation on fibronectin (Fig. 5d). In accordance with this finding, we also observed changes in the usage of different β-integrin subtypes after talin rod domain destabilization. These findings indicate that talin rod domain stability is indeed regulating the structure and function of cell-matrix adhesions at the levels of substrate sensing and integrin activation. However, the mechanism that links talin rod domain stability and differential activation of integrin subtypes remains to be found.

In the migration analysis, we observed decreased migration rates for cells expressing destabilized full-length talin-1. Together with the observed accumulation of destabilized talin proteins into cell-matrix adhesions, these results suggest that regulation of adhesion dynamics is controlled by the mechanical stability of talin. These findings are in line with a previous study by Carisey *et al.*, where mutations releasing the vinculin head-tail autoinhibition were shown to lock talin in cell-matrix adhesions, resulting in slower adhesion turnover and decreased cell polarization and migration[21]. In both cases, disturbances in the tight spatial and temporal control of talin-conformation regulated interactions negatively affected the ability of cells to polarize and migrate. It is possible that the defects in cell polarization and migration result from the failure of cells to probe local cellular tension because of the facilitated formation of the talin-vinculin interaction under low force. In this study, we found that neither talin-1 subdomain R3 destabilization nor deletion of the R4-R12 subdomains alone are sufficient to block cell migration. However, together they result in a completely static cell phenotype in talin-null cells (Fig. 4i). The impaired migration of these cells may result from the lack of cryptic and mechano-activatable vinculin binding sites in the talin-1 mutant that is both truncated and destabilized. It is possible that in the context of full-length talin, the defects in mechanosensing caused by the R3 subdomain destabilization can be partly compensated by the presence of other cryptic and mechano-activable vinculin binding sites in the other rod subdomains. We propose that unfolding of mechanosensitive talin-1 rod subdomains results in local differences in the level of talin-initiated signaling in the cell. These local differences in signaling activity are a prerequisite for cell polarization and migration and the lack of them after both truncating and destabilizing talin rod domain would explain the severely impaired cell migration seen for the cells expressing this construct.

Talin R3 subdomain does not only contain two cryptic vinculin binding sites, but it also has a mutually exclusive binding site for a Rap1 effector protein RIAM. RIAM is thought to be an important regulator of talin recruitment to the plasma membrane and it is present mainly in nascent adhesions, while vinculin binding is needed for adhesion reinforcement and locking talin into mature focal adhesions[23,24]. Force-induced unfolding of the R3 subdomain likely acts as a switch releasing RIAM and allowing vinculin binding during adhesion maturation[14]. In the current study, we found that talin R3 subdomain destabilization increased talin and vinculin accumulation into cell-matrix adhesions, which likely indicates a decrease in the threshold force at which the transition from the RIAM-binding conformation to the vinculin-binding conformation occurs. This decrease in the threshold force facilitates the release of RIAM and simultaneously promotes vinculin binding. However, the mutations presented in this study are unlikely to directly affect the formation of the talin-RIAM complex, because they do not directly target the RIAM binding site in talin R3 helices H2 and H3. Moreover, RIAM binding to talin presumably occurs in the absence of mechanical load applied to talin[14]. To study this experimentally, we coexpressed talin mutants and RIAM-GFP and did not observe significant differences in RIAM localization between wild-type and destabilized talin proteins (Supplementary Figure S4). In addition to vinculin and RIAM binding, the R3 subdomain has been suggested to participate in the regulation of actin binding site 2 (ABS2), located in the talin rod subdomains R4 and R8[15]. Interestingly, Atherton *et al.* found that deletion of the R2 and R3 subdomains resulted in the formation of larger and more stable cell-matrix adhesions. Their experiments using talin mutants with reduced actin binding suggested that the R2-R3 region may have a role in the regulation of talin ABS2, which is located in the rod subdomains R4 and R8. Although the destabilizing mutations described in the present study could affect the regulation of ABS2 in an indirect way by promoting forced unfolding of the R3 subdomain, our experiments with the talin ΔR4-12 4S mutant show that the increased talin accumulation into adhesions is independent of the presence of ABS2 (Fig. 3g). Therefore, it seems that the effects caused by talin R3 subdomain destabilization cannot be explained by the released autoinhibition of talin ABS2.

Our study highlights the importance of talin rod domain mechanical stability as a key factor in cellular mechanosensing. We demonstrate that the modulation of the mechanical stability of an individual talin rod subdomain affected a wide range of cellular processes dependent on mechanical signals and cellular mechanosensing. Our results suggest that talin acts as a mechanosensor together with vinculin and is responsible for controlling adhesion turnover, ECM sensing and consequently traction force generation and cell migration.

Experimental procedures. *Sequence analysis and mutation design.* Multiple sequence alignment (Clustal Omega[25]) and conservation analysis for talin-1 R3 domain was performed in order to identify candidates for mutation design (Fig. 1c). The alignment was visualized and analyzed with Jalview[26]. PyMOL, Molecular graphics system, version 1.4.1[27]. Was used for visualization, target residue identification and following mutagenesis of four talin-1 R3 residues.

Molecular dynamics (MD) and steered molecular dynamics (SMD). Gromacs version 4.6.7[28]. On Sisu supercomputer, CSC, Espoo, Finland was used for all MD and SMD simulations. All models were built with explicit TIP3P water model in 0.15 M KCl neutralized solution and placed into a 10 * 10 * 30 nm rectangular box. Each molecule was oriented in the water box so that the d3 vector (vector between V808 CA and G896 CA) was parallel to z-axis; i.e. the pulling direction was perpendicular to the H1-H4 orientation (Fig. 1, Supplementary Figure S1). The system was minimized with 100,000 steps and equilibrated for 10 ns before applying pulling force. Equilibration was performed with 2 fs step size at NTP conditions with v-rescale thermostat at 310 K for protein and solution applied separately and with the Berendsen barostat at 1 bar at isotropic setting. Simulations for domain stability assessment were performed at equilibration conditions for 20 ns. Simulations for domain refolding were performed at equilibration conditions for 20 ns starting from the structure coordinates after 10 ns pulling. Equilibration trajectory was recorded at 100 frames/ns for each analysis.

Pulling simulations were prepared to pull N-terminal helix H1 and C-terminal helix H4 apart in order to follow domain dissociation. Helices were pulled by 4 points in H4 at 150 pN constant force in the z-axis direction. In more detail, the alpha atoms of residues in helix 1 (H1; Q800, T804, V808, S815) were fixed, whilst alpha atoms of residues in helix 4 (H4; Q888, G896, A900 and A904) were pulled with constant force. The use of relatively high force is justified by the limitations in computing resources and based on previous studies suggesting predictive power for SMD simulations carried out using forces higher than observed in nature[6,10]. Pulling simulations were performed with 2 fs step size for 10 ns and recorded at 500 frames/ns. Berendsen thermostat at 310 K was applied for protein and solution separately while Berendsen barostat at 1 bar was used at semiisotropic setting (pressure control was applied in xy coordinates, while pulling was performed in z-axis direction). This setup was selected based on extensive optimization of the parameters (von Essen *et al.*, unpublished data). Equilibration was performed in one simulation experiment for each molecule. Stability and refolding simulations were simulated for wild type R3 subdomain and 4S mutant in one experiment. Finally, pulling simulations were repeated 5 times for each structure. All trajectories were analyzed with VMD[29] at 100 frames/ns.

Protein expression and purification. DNA fragments corresponding to the talin-1 residues 795 – 911 were subcloned into a modified pHis vector to create a construct with N-terminal His6-tag separated from the talin fragment by an 11 residue linker (SSSGPSASGTG). The expression of His6-tagged talin rod domain R3 protein in *Escherichia coli* BL21 Star cells (Invitrogen, USA) was induced by 1 mM IPTG for 5 h at 37 °C. Cell pellets were lysed by homogenization (Emulsiflex C3; Avestin, Inc., Germany) into pH 7.2 sodium phosphate buffer containing 1 M NaCl and 20 mM imidazole. After centrifugation, lysates were loaded into affinity column (HisTrap FF; GE Healthcare, UK) using a liquid chromatography system (Äkta purifier; GE Healthcare, UK). Proteins were eluted with a linear imidazole gradient 0–500 mM. Eluted fractions were run on SDS-PAGE gel. Samples purity were checked on the gels (>90%) and fractions containing proteins were dialyzed by stepwise decrease in imidazole concentration into 50 mM sodium phosphate buffer containing 150 mM NaCl pH 7.2. Dialyzed samples were again analyzed by SDS-PAGE and the concentrations detected by NanoDrop (Thermo Fisher Scientific, USA). Urea-PAGE gel was made in the same standard procedure as for SDS-PAGE gels, except 8 M urea was added. Samples were boiled in the sample buffer for 10 min at 100 °C. After cooling to room temperature, 8 M urea was added to the sample. Electrophoresis was performed at +4 °C, 100 V, for 2–3 hours. Protein concentration was determined by measuring A280 using NanoDrop. 1 mM EDTA and 1 mM DTT were added and protein samples were stored at +4 °C.

Size exclusion chromatography. Analysis was performed using a liquid chromatography instrument (CBM-20A, Shimadzu Corporation, Kyoto, Japan) equipped with autosampler (SIL-20A), UV-VIS (SPD-20A) and Malvern Zetasizer μV SLS/DLS detector (Malvern Instruments Ltd, Worcestershire, UK). Data were processed using Lab Solution Version 5.51 (Shimadzu Corporation) and OmniSec 4.7 (Malvern Instruments) softwares. A sample of the protein (200 μg) was injected on a Superdex 200 10/300 GL column (GE Healthcare, Uppsala, Sweden) equilibrated with 50 mM NaH_3PO_4, 150 mM NaCl pH 7.2 buffer. Runs were performed with flow rate of 0.5 ml/min at 20 °C using a thermostated cabin. The molecular weight of the talin forms were determined using static light-scattering intensity (SLS) and the light scattering detector was calibrated using the monomeric peak of BSA.

Talin fragment CD spectroscopy. CD spectra were recorded on a Chirascan instrument (Applied Photophysics, UK). Spectra were recorded between 200 and 280 nm with sampling points every 1 nm. Three scans were recorded and baseline spectra were subtracted from each spectrum. Quartz cuvettes with a 0.1-cm pathlength were used. Data was processed using Chirascan Pro-Data Viewer (Applied Photophysics, UK), CDNN[30]

written by Gerald Böhm (Martin-Luther Universität Halle-Wittenberg) and Microsoft Excel. The direct CD measurements (θ; mdeg) were converted into mean residue molar ellipticity ($[\theta]_{MR}$) by Pro-Data Viewer. In thermal unfolding experiment a 2 °C step size at 1 °C/min ramp rate with ± 0.2 °C tolerance was used. The melting temperature was analyzed with Global3 (Applied Photophysics).

Mass spectrometry. The purified talin R3 fragments were analyzed by MALDI-TOF instrument (Ultraflex TOF/TOF, Bruker-Daltonics, Germany). A 10 µl aliquot of the protein solution was concentrated using a Millipore µ-C4 ZipTip pipette tip and mixed with a sinapic acid (Sigma Aldrich, USA) matrix. Single and double-charged peaks were detected without signs of significant impurities. The measured masses determined according to most intensive peaks were 14189.7, 14166.6, 14144.7, 14113.8 and 14088.2 (+1) and 7093.8, 7080.9, 7071.5, 7055.6 and 7041.8 (+2) for wild-type talin fragment and 1S, 2S, 3S and 4S mutants, respectively. The determined masses are reasonable when compared to the theoretical molecular weights calculated by Protparam.

Cell lines and cell culture methods. The wild type MEF cell line was a kind gift from Dr. Wolfgang Ziegler and has been previously described by Xu & Baribault, 1998[31]. The *TLN1−/−TLN2−/−* MEF cell line has been previously described by Theodosiou *et al.*, 2016[32]. Both cell lines were maintained in high-glucose DMEM supplemented with 10% FBS and 1% GlutaMax (Thermo Fisher Scientific, USA). A 37 °C incubator with 5% CO_2 was used for culturing both cell lines.

Expression constructs and transfection. C-terminally EGFP- or mCherry-tagged full-length mouse talin-1 expression constructs were created by subcloning talin-1 (1-2541) and EGFP or mCherry DNA fragments into a modified pEGFP-C1 vector backbone (Clontech, USA). Destabilizing point mutations were created with overlapping mutagenesis primers and silent restriction sites in the talin sequence. Centrally truncated and C-terminally mCherry-tagged talin ΔR4-12 and ΔR4-12 4S constructs were created by subcloning mouse talin-1 fragments corresponding to amino acids 1–913 and 2296–2541 into a modified pEGFP-C1 based backbone. All DNA constructs were authenticated by sequencing.

Wild type and *TLN1−/−TLN2−/−* mouse embryonal fibroblast (MEF) cells were transfected with Neon transfection system (Thermo Fisher Scientific, USA). For all constructs, 5 µg of plasmid DNA was used per 10^6 cells. The following electroporation parameters were used for wild type and talin deficient MEF cells: 1350 V, 30 ms, 1 pulse and 1400 v, 30 ms, 1 pulse, respectively.

Immunostaining and imaging of fixed cells. Zeiss high-performance 170 µm thick coverslips were coated with 25 µg/ml human fibronectin (Fn) for 1 hour at 37 °C and washed two times with PBS. Wild type MEF cells were transfected with talin constructs and allowed to recover for 24 h. The cells were trypsinized and plated at low confluency on Fn coated coverslips for 120 min, after which media was aspirated from the wells and the cells were fixed with 4% PFA in PBS (pH 7.4) for 15 min at RT. Fixed cells were washed two times with PBS and permeabilized with 0.2% Triton-X100 in PBS for 5 min at RT. Nonspecific antibody binding was blocked by incubating the samples in 5% FCS, 1% BSA and 0.05% Triton-X100 in PBS for 30 min at RT. Monoclonal anti-vinculin antibody (Clone hVIN-1, V9131, Sigma-Aldrich, USA) was diluted 1:400 in the blocking buffer and incubated on the coverslips for 1 h at RT. Coverslips were washed with PBS (3 × 5 min) before incubation with AlexaFluor-488 conjugated anti-mouse secondary antibody (A21202, Life Technologies, USA) diluted 1:250 in the blocking buffer. Immunostained coverslips were washed with PBS (3 × 10 min) and stored at +4 °C.

Fixed and immunostained samples were imaged with Nikon Eclipse Ti inverted microscope (Nikon Instruments, Japan) equipped with CFI Plan Apo VC 60x/1.40 Oil immersion objective (Nikon instruments, Japan), Yokogawa CSU10 spinning disk confocal unit (Yokogava, Japan) and Andor NEO sCMOS camera (Andor Technology, UK). 488 nm and 651 nm DPSS lasers were used for exciting AlexaFluor-488 and mCherry fluorophores, respectively. The coverslips were mounted to the microscope stage with a detachable steel chamber and kept immersed in PBS during imaging. All imaging parameters were kept constant for all samples to allow quantitative image analysis.

FRAP analysis for talin and vinculin. For FRAP analysis of talin mutants, *TLN1−/−TLN2−/−* cells were transfected with C-terminally GFP-tagged talin constructs. For FRAP analysis of vinculin, cells were co-transfected with C-terminally mCherry-tagged talin constructs and N-terminally GFP-tagged full-length vinculin. Transfected cells were allowed to recover for 24 h and plated on fibronectin coated (25 µg/ml) glass-bottom dishes 2 h before imaging. Samples were allowed to further equilibrate at the microscope stage for 30 min before imaging was started. Zeiss Cell Observer. Z1 microscope equipped with LSM780 confocal unit, 37 °C/5% CO_2 incubator and 63x/1.4 Oil immersion objective was used for imaging. Circular regions with a diameter of 2.6 µm were photobleached with 488 nm argon laser operated at a high intensity. Only one region in each cell was selected to be bleached. Confocal microscope images were captured at 500 ms intervals for 5s before photobleaching and for 90 s after photobleaching. Data was collected from to fully independent experiments using the same bleaching and imaging parameters for all samples. Fluorescence recovery was analyzed by using equation $F = [B(t)/B(t<0)]/[Cell(t)/Cell(t<0)]$, where $B(t<0)$ and $Cell(t<0)$ are the average fluorescence intensities of the of bleached area and the entire cell, respectively, before bleaching and B(t) and Cell(t) intensities of the same regions at each time point after bleaching. The resulting F-values were further normalized to zero. EasyFRAP[33] FRAP analysis software was used to fit single exponential curves to each series individually to calculate mobile fraction and half-recovery times for each region.

Traction force microscopy. Traction force was measured as described previously by Qi *et al.*[18]. Briefly, glass-bottom dishes were silanized by 0.5% (3-Aminopropyl) triethoxysilane and activated by 0.5%

glutaraldehyde. A drop of gel solution containing acrylamide (6%), bis-acrylamide (0.75%), ammonium persulfate, TEMED, and FluoSpheres® carboxylate-modified beads (diameter 0.2 μm, 1:85 dilution by volume) was added to the dishes and covered by a coverslip. The coverslip was removed and the gels were activated with Sulfo-SANPAH under UVA exposure, followed by conjugation with fibronectin (200 μg/ml). Talin1-null US OS cells were transiently transfected with wild type talin-1 or destabilized talin mutants and plated on the gels for 12 h. Traction force was measured as described previously[34], using a Nikon A1 confocal microscope in Lexington VA Medical Center, Kentucky.

Migration analysis. Polystyrene well plates were coated with 10 μg/ml fibronectin at 37 °C for 1 h and washed two times with PBS (pH 7.4). Transfected *TLN1−/−TLN2−/−* MEF cells were allowed to recover for 24 h, trypsinized and plated onto fibronectin coated well plates at a low confluency. Cells were allowed to attach for 1 h, followed by washing the cells with warm PBS (pH 7.4) to remove unbound (non-transfected) cells. The cells were cultured in fresh media for 30 min before imaging was started. Evos FL Auto (Life Technologies, USA) equipped with 37 °C and 5% CO_2 incubator was used for live cell imaging for 12 hours at 120 second intervals. The resulting image stacks were analyzed with ImageJ version 1.50e with MTrackJ plugin[35,36].

Microcontact printing of patterned substrates. Stamps were incubated for 10 minutes with a fibronectin (Fn) solution consisting of 45 μg/ml inactive human Fn (thermal denaturation at 90°), 5 μg/ml active human Fn (Sigma Aldrich) and 1 μg/ml Alexa Fluor 647-labeled bovine Fn (protein-labeling kit; Life Technologies). Fn molecules adsorbed to the stamp were transferred to a glass coverslip for 10 minutes. Stamped structures were incubated with 5 μg/ml human Vn (Sigma Aldrich) for 1 h to coat protein-free regions. Micropatterned substrates were rinsed once with 1 × PBS before they were used for cell culture. Transiently transfected wild type MEF cells were seeded and cultured for 2 h on Fn/Vn substrates in serum-free DMEM. After 2 h of cultivation cells were fixed and immunostained using anti-paxillin primary antibody (BD Bioscience) and Cy3-conjugated secondary antibody (Dianova).

Structured illumination microscopy (SIM) and talin-1 localization analysis. SIM was performed at room temperature on a nonserial prototype microscope (ELYRA PS. 1; Carl Zeiss Microscopy) in superresolution SIM mode using a Plan Apochromat 63 × 1.40 NA oil objective (Carl Zeiss Microscopy). For each image, 15 raw images were processed and reconstructed to extract the superresolution information. Channels were aligned in x,y using predetermined shifts to correct for thermal drift or concussion.

SIM images of talin-1-GFP, paxillin label (Cy3) and labeled Fn (Alexa Fluor 647) were analyzed using Mander's overlap coefficient to determine colocalization of talin-1 with Fn patches. A paxillin mask was created to remove cytosolic fluorescence signal caused by talin expression and to minimize its bias on the quantification (see Supplementary Figure S6). Paxillin masking was done by extending the paxillin SIM signal using Gaussian Blur function in ImageJ and by thresholding the resulting image. This mask was used to calculate Mander's overlap coefficient with manual threshold to determine the degree of GFP fluorescence at sites of Alexa Fluor 647-labeled Fn. Data were obtained from three independent experiments (n = 30–40 cells per condition). For analyzing the colocalization of talin mutants and β3 and β1 integrin subtypes, masks based on widefield fluorescence images was used (see Supplementary Figure S6).

References

1. Schiller, H. B. & Fässler, R. Mechanosensitivity and compositional dynamics of cell–matrix adhesions. *EMBO Reports* **14**, 509–519 (2013).
2. Hoffman, B. D., Grashoff, C. & Schwartz, M. Dynamic molecular processes mediate cellular mechanotransduction. *Nature* **475**, 316–323 (2011).
3. Bate, N. *et al*. Talin contains a C-terminal calpain2 cleavage site important in focal adhesion dynamics. *PLoS One* **7**, e34461 (2012).
4. Rees, D., Ades, S., Singer, S. & Hynes, R. Sequence and domain structure of talin. *Nature* **374**, 685–689 (1990).
5. Calderwood, D. A., Campbell, I. D. & Critchley, D. R. Talins and kindlins: partners in integrin-mediated adhesion. *Nat. Rev. Mol. Cell Biol.* **14**, 503–17 (2013).
6. Hytönen, V. P. & Vogel, V. How force might activate talin's vinculin binding sites: SMD reveals a structural mechanism. *PLoS Comput. Biol.* **4**, e24 (2008).
7. del Rio, A. *et al*. Stretching single talin rod molecules activates vinculin binding. *Science* **323**, 638–641 (2009).
8. Yao, M. *et al*. Mechanical activation of vinculin binding to talin locks talin in an unfolded conformation. *Sci. Rep.* **4**, 4610 (2014).
9. Yao, M. *et al*. The mechanical response of talin. *Nat. Commun.* **7**, 11966 (2016).
10. Haining, A. W. M., von Essen, M., Attwood, S. J., Hytönen, V. P. & del Rio Hernandez, A. All Subdomains of the Talin Rod Are Mechanically Vulnerable and May Contribute to Cellular Mechanosensing. *ACS Nano* **10**, 6648–6658 (2016).
11. Wehrle-Haller, B. Assembly and disassembly of cell matrix adhesions. *Curr. Opin. Cell Biol.* **24**, 569–581 (2012).
12. Jiang, G., Giannone, G., Critchley, D. R., Fukumoto, E. & Sheetz, M. P. Two-piconewton slip bond between fibronectin and the cytoskeleton depends on talin. *Nature* **424**, 334–337 (2003).
13. Elosegui-Artola, A. *et al*. Mechanical regulation of a molecular clutch defines force transmission and transduction in response to matrix rigidity. *Nat. Cell Biol.* **18**, 540–548 (2016).
14. Goult, B. T. *et al*. RIAM and vinculin binding to talin are mutually exclusive and regulate adhesion assembly and turnover. *J. Biol. Chem.* **288**, 8238–8249 (2013).
15. Atherton, P. *et al*. Vinculin controls talin engagement with the actomyosin machinery. *Nat. Commun.* **6**, 10038 (2015).
16. Goksoy, E. *et al*. Structural Basis for the Autoinhibition of Talin in Regulating Integrin Activation. *Mol. Cell* **31**, 124–133 (2008).
17. Goult, B. T. *et al*. The structure of an interdomain complex that regulates Talin activity. *J. Biol. Chem.* **284**, 15097–15106 (2009).
18. Qi, L. *et al*. Talin2-mediated traction force drives matrix degradation and cell invasion. *J. Cell Sci.* **129**, 3661–3674 (2016).
19. Zamir, E. *et al*. Dynamics and segregation of cell– matrix adhesions in cultured fibroblasts. *Nat. Cell Biol.* **2**, 191–196 (2000).
20. Pinon, P. *et al*. Talin-bound NPLY motif recruits integrin-signaling adapters to regulate cell spreading and mechanosensing. *J. Cell Biol.* **205**, 265–281 (2014).
21. Carisey, A. *et al*. Vinculin regulates the recruitment and release of core focal adhesion proteins in a force-dependent manner. *Curr. Biol.* **23**, 271–281 (2013).

22. Missirlis, D. *et al*. Substrate engagement of integrins α5β1 and αvβ3 is necessary, but not sufficient, for high directional persistence in migration on fibronectin. *Sci. Rep.* **6**, 23258 (2016).
23. Humphries, J. D. *et al*. Vinculin controls focal adhesion formation by direct interactions with talin and actin. *J. Cell Biol.* **179**, 1043–1057 (2007).
24. Lee, H. S., Lim, C. J., Puzon-McLaughlin, W., Shattil, S. J. & Ginsberg, M. H. RIAM activates integrins by linking talin to Ras GTPase membrane-targeting sequences. *J. Biol. Chem.* **284**, 5119–5122 (2009).
25. Livingstone, C. D. & Barton, G. J. Protein sequence alignments: A strategy for the hierarchical analysis of residue conservation. *Bioinformatics* **9**, 745–756 (1993).
26. Waterhouse, A. M., Procter, J. B., Martin, D. M. A., Clamp, M. & Barton, G. J. Jalview Version 2-A multiple sequence alignment editor and analysis workbench. *Bioinformatics* **25**, 1189–1191 (2009).
27. DeLano, W. L. The PyMOL Molecular Graphics System. *Schrödinger LLC* Version 1., http://www.pymol.org (2002).
28. Hess, B., Kutzner, C., Van Der Spoel, D. & Lindahl, E. GRGMACS 4: Algorithms for highly efficient, load-balanced, and scalable molecular simulation. *J. Chem. Theory Comput.* **4**, 435–447 (2008).
29. Humphrey, W., Dalke, A. & Schulten, K. VMD: Visual molecular dynamics. *J. Mol. Graph.* **14**, 33–38 (1996).
30. Böhm, G. CDNN: CD spectra deconvolution software version 2.1 (1997).
31. Xu, W. & Baribault, H. Vinculin knockout results in heart and brain defects during embryonic development. *Development* **125**, 327–37 (1998).
32. Theodosiou, M. *et al*. Kindlin-2 cooperates with talin to activate integrins and induces cell spreading by directly binding paxillin. *Elife* **5**, e10130 (2016).
33. Rapsomaniki, M. A. *et al*. easyFRAP: an interactive, easy-to-use tool for qualitative and quantitative analysis of FRAP data. *Bioinformatics* **28**, 1800–1801 (2012).
34. Butler, J. P., Tolić-Nørrelykke, I. M., Fabry, B. & Fredberg, J. J. Traction fields, moments, and strain energy that cells exert on their surroundings. *Am. J. Physiol. Cell Physiol.* **282**, 595–605 (2002).
35. Schneider, C. a., Rasband, W. S. & Eliceiri, K. W. NIH Image to ImageJ: 25 years of image analysis. *Nat. Methods* **9**, 671–675 (2012).
36. Meijering, E., Dzyubachyk, O. & Smal, I. Methods for cell and particle tracking. *Methods Enzymol.* **504**, 183–200 (2012).

Acknowledgements

Academy of Finland supported this research via grants 290506, 273192 and 136288 (for V.P.H). American Cancer Society supported the work by Research Scholar Grant RSG-13-184-01-CSM (for C.H). We thank University of Tampere for the financial support via TGPBB graduate school (for M. v. E). Finnish Cultural Foundation is acknowledged for the grant (for R.R). Swiss Foundation for Research on Myopathies (B. W.-H.), the Swiss National Science Foundation (31003A-130742) (B. W.-H.) and the Ligue Genevoise contre le Cancer are acknowledged (B.W.-H.). We acknowledge CSC for the supercomputing resources and Biocenter Finland for the infrastructure support. The use of the facilities and expertise of the Biocenter Oulu core facility facility and Institute of Biotechnology Proteomics Unit, both members of Biocenter Finland, is gratefully acknowledged and Dr. Hongmin Tu is specially acknowledged for her contribution to CD analysis. Prof. Reinhard Fässler and Dr. Carsten Grashoff are acknowledged for the help with the *TLN1−/−TLN2−/−* cells. Prof. Jinhua Wu is acknowledged for providing us the RIAM-GFP expression construct. We thank Ulla Kiiskinen, Niklas Kähkönen and Merja Jokela for technical assistance.

Author Contributions

R.R., M.v.E. and V.P.H. designed the research. R.R., M.v.E., M.S., L.Q., L.A. and C.K. performed the experiments. R.R., M.v.E., M.S., L.Q., C.K. and L.A. analyzed the data. T.O.I., B.W.H., M.B. and C.H. provided expert opinion, technical support and supervised the experimental work. R.R., M.v.E. and V.P.H. wrote the paper. All authors revised and accepted the final version.

Additional Information

Supplementary information accompanies this paper at doi:10.1038/s41598-017-03335-2

Competing Interests: The authors declare that they have no competing interests.

Publisher's note: Springer Nature remains neutral with regard to jurisdictional claims in published maps and institutional affiliations.

PLOS BIOLOGY

SHORT REPORTS

Mechanotransduction in talin through the interaction of the R8 domain with DLC1

Alexander William M. Haining[1☯], Rolle Rahikainen[2☯], Ernesto Cortes[1], Dariusz Lachowski[1], Alistair Rice[1], Magdalena von Essen[2], Vesa P. Hytönen[2]*, Armando del Río Hernández[1]*

1 Cellular and Molecular Biomechanics Laboratory, Department of Bioengineering, Imperial College London, London, United Kingdom, **2** Faculty of Medicine and Life Sciences and BioMediTech, University of Tampere, Finland and Fimlab Laboratories, Tampere, Finland

☯ These authors contributed equally to this work.
* a.del-rio-hernandez@imperial.ac.uk (ADRH); vesa.hytonen@uta.fi (VPH)

OPEN ACCESS

Citation: Haining AWM, Rahikainen R, Cortes E, Lachowski D, Rice A, von Essen M, et al. (2018) Mechanotransduction in talin through the interaction of the R8 domain with DLC1. PLoS Biol 16(7): e2005599. https://doi.org/10.1371/journal.pbio.2005599

Academic Editor: Carsten Grashoff, University of Münster, Germany

Received: February 3, 2018

Accepted: June 19, 2018

Published: July 20, 2018

Data Availability Statement: All relevant data are within the paper and its Supporting Information files.

Funding: European Research Council (grant number 282051 ForceRegulation) and Academy of Finland (grant number 290506). The funders had no role in study design, data collection and analysis, decision to publish, or preparation of the manuscript.

Competing interests: The authors have declared that no competing interests exist.

Abstract

The mechanical unfolding of proteins is a cellular mechanism for force transduction with potentially broad implications in cell fate. Despite this, the mechanism by which protein unfolding elicits differential downstream signalling pathways remains poorly understood. Here, we used protein engineering, atomic force microscopy, and biophysical tools to delineate how protein unfolding controls cell mechanics. Deleted in liver cancer 1 (DLC1) is a negative regulator of Ras homolog family member A (RhoA) and cell contractility that regulates cell behaviour when localised to focal adhesions bound to folded talin. Using a talin mutant resistant to force-induced unfolding of R8 domain, we show that talin unfolding determines DLC1 downstream signalling and, consequently, cell mechanics. We propose that this new mechanism of mechanotransduction may have implications for a wide variety of associated cellular processes.

Author summary

Mechano-induced conformational changes and the unfolding of protein domains are cornerstones of mechanotransduction and regulate the interaction of proteins with other molecules. Talin is a prominent molecule in focal adhesions and one of the few proteins that simultaneously connects integrin receptors in the cell membrane with the actin cytoskeleton. This bridging position, owing to the cytoskeleton's contractile nature, exposes talin to forces along its length. In this work, we studied the implications of the R8 domain unfolding in the downstream activity of deleted in liver cancer 1 (DLC1), which binds the talin R8 domain and negatively regulates Ras homolog family member A (RhoA). We created a talin mutant with the R8 domain resistant to mechanical unfolding and observed that cells expressing these talin mutants have altered patterns of focal adhesion dynamics and lower levels of actomyosin contraction. This leads to decreased traction forces and diminished cell migration. We propose a novel force-controlled molecular switch that refines the mechanism of talin-mediated focal adhesion activation, providing negative

Abbreviations: a.u., arbitrary unit; DLC1, deleted in liver cancer 1; DTT, dithiothreitol; ECM, extracellular matrix; FRAP, fluorescent recovery after photobleaching; FRET, Förster resonance energy transfer; GFP, green fluorescent protein; GSH, glutathione; MEF, mouse embryonic fibroblast; MFI, mean fluorescence intensity; MLC-2, myosin light chain 2; PDMS, polydimethylsiloxane; RhoA, Ras homolog family member A; RhoGAP, Ras homolog GTPase-activating protein; RMSD, root-mean-square deviation; smAFM, single-molecule atomic force microscopy; SMD, steered molecular dynamics; SMPEG24, succinimidyl-[(Nmaleimidopropionamido) tetracosaethyleneglycol] ester; WT, wild-type.

feedback during focal adhesion maturation. The broader effects of this talin-mediated mechanism need to be elucidated, as it might regulate multiple cellular events.

Mechanical force is increasingly being accepted as a key modulator of cellular behaviour. These forces can be applied externally from the extracellular matrix (ECM) or internally generated from the active actin cytoskeleton pulling against a cell's attachment to the ECM. Unlocking the mechanisms by which cells sense and translate these forces (mechanotransduction) is an active area of research, given its wide-ranging implications. The mechanically induced unfolding of mechanosensitive proteins has provided a new mechanism for force transduction. The disruption of the tertiary structure of these proteins can lead to the exposure of cryptic sites for ligand binding, molecule activation, or cleavage of domains by proteases [1–3]. However, there is still a gap in our understanding of how this mechanically induced protein unfolding triggers distinctive, or alternative, large-scale downstream signalling in cells to differentially control their behaviour. Here, we used single-molecule techniques, combined with protein engineering and cellular biophysical approaches, to characterise how talin mechanotransduction through the interaction of the R8 domain with deleted in liver cancer 1 (DLC1) can regulate cell mechanics.

Talin, one of the most studied mechanosensitive molecules, is a key protein in focal adhesions, where it simultaneously connects integrins in the cell membrane through its N-terminal head domain and the actin cytoskeleton using the C-terminal rod (Fig 1). This bridging position, owing to the cytoskeleton's contractile nature, exposes talin to forces along its length. This tension can subsequently unfold talin domains, changing its affinity for binding partners. Most of the work on talin's mechanosensitivity has focussed on the regions immediately after the head domain—namely, regions R1 to R3—and on its interaction with vinculin, another important structural and signalling focal adhesion protein [1, 4, 5]. Cellular studies utilising Förster resonance energy transfer (FRET) sensors have measured the tension that a single talin linkage experiences [6, 7]. Alongside this, our recent work has demonstrated that this level of tension is sufficient to unfold significant portions of the alpha-helical bundled structure of the talin molecule, in addition to R1-R3, that are between its integrin- and actin-binding sites[8].

These findings open a plethora of possibilities to explore how talin interacts with other molecules to control cell function, given the wide range of proteins that interact with the talin rod. DLC1—a Ras homolog GTPase-activating protein (RhoGAP) that negatively regulates the activity of RhoA-C and is a potent tumour suppressor whose loss has been implicated with numerous cancers [9, 10]—is a notably interesting talin-binding partner. In order for its regulatory role on the Rho family of GTPases to have an impact on cellular function, DLC1 requires to be localised in focal adhesions, and this localisation is mediated by its interaction with talin [11]. DLC1 binds to the R8 helical bundle of the talin rod. This bundle is unique in terms of molecular connections—it does not lie in the chain between two other bundles in the talin rod but exists rather as a protrusion of the R7 bundle (Fig 1). The nature of DLC1's binding to R8 is such that it forms an interaction with two of the helices in R8, effectively creating a 5-helix bundle out of R8's 4 helices and one of DLC1's [12]. This proposed mechanism of interaction suggests that if the R8 bundle structure is disrupted, it would abrogate the binding to DLC1.

Structural in vitro and cellular studies have indicated that such disruption is likely to occur as part of the cell's cycle of adhesion formation and maturation. Previous studies have measured both the length of the talin protein in cells and the internal tension of the rod [6, 13, 14].

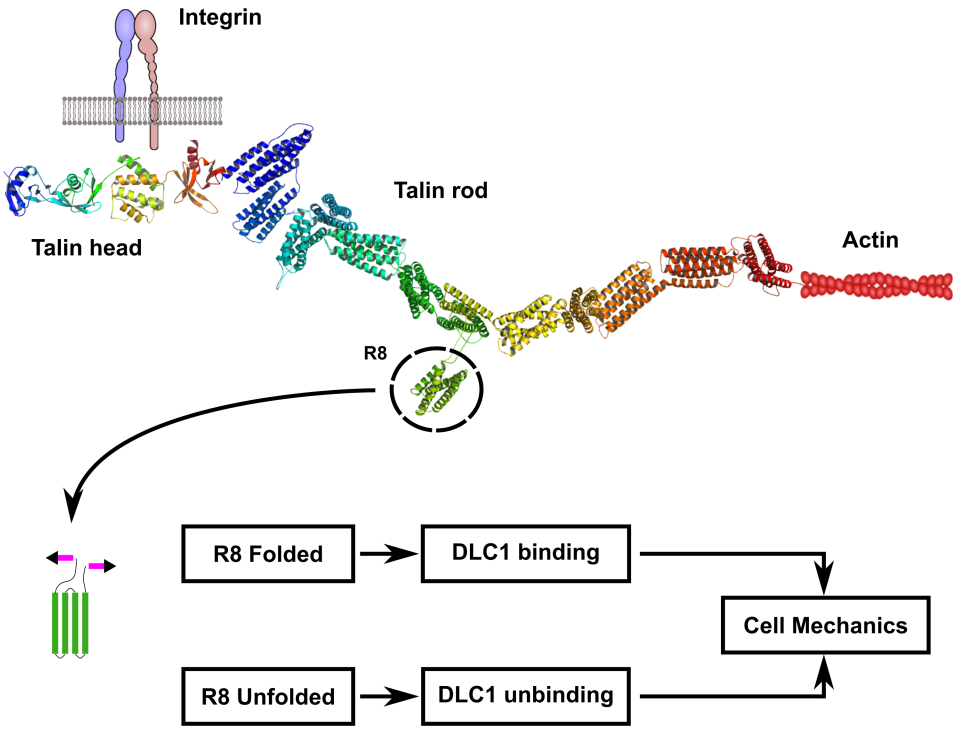

Fig 1. The unfolding/folding state of the R8 region of the talin rod modulates cell mechanics through DLC1 recruitment to focal adhesions. Talin simultaneously links integrins with the actin cytoskeleton. The R8 region protrudes out of the talin molecule structure, and a disulphide bridge was added to the linker area of R7-R8 to prevent R8 unfolding under mechanical load. The folded R8 region promotes DLC1 binding to talin and localisation to focal adhesions. This activates the negative regulation of the RhoA pathway that decreases myosin activation, actomyosin contractility, force generation, and migration. On the other hand, force application on the native talin molecule would unfold the R8 region producing the unbinding and deactivation of DLC1, which does not localise to the focal adhesion and loses its capacity to regulate the RhoA pathway. DLC1, deleted in liver cancer 1; RhoA, Ras homolog family member A.

https://doi.org/10.1371/journal.pbio.2005599.g001

The extension of the molecule varies between 50–350 nm, which would necessitate the unfolding of multiple talin rod subdomains. These extension data were also combined in a previous study with single-molecule data to provide a model of talin subdomain unfolding in cells [15]. This model demonstrated that intramolecular tension, measured in cells at 5–10 pN, is maintained by the dynamic unfolding and refolding of talin rod subdomains. At the higher extensions of the rod, as many as 9 of the 12 α-helix subdomains are unfolded. The R7-R8 bundle is intermediate in stability with respect to the rest of the rod and is likely to unfold over the order of a few seconds at physiological loading rates [8, 15]. Given that myosin-dependent stretching of talin occurs over 6–16 s [14], it is likely that a significant proportion of R7-R8 bundles are disrupted, especially as adhesions mature and develop more stable actin linkages. We hypothesised that unfolding of the R8 region of talin by intracellular tension may modulate DLC1's recruitment to focal adhesions mediated by talin; and this triggers differential downstream pathways in cells (Fig 1).

To experimentally test this hypothesis, we engineered 2 polyproteins amenable to mechanical manipulation using single-molecule atomic force microscopy (smAFM). The first polyprotein (R7-R8) contained the region R7 of the talin molecule and its linked R8 bundle flanked by two units of I27 domains and a HaloTag, as previously reported [8]. Next, we designed a mutant of the R7-R8 subdomain (R7-R8_clamp) to make the R8 bundle resistant to tension-induced unfolding. To do this, we took advantage of the unique structure of the R8 bundle and

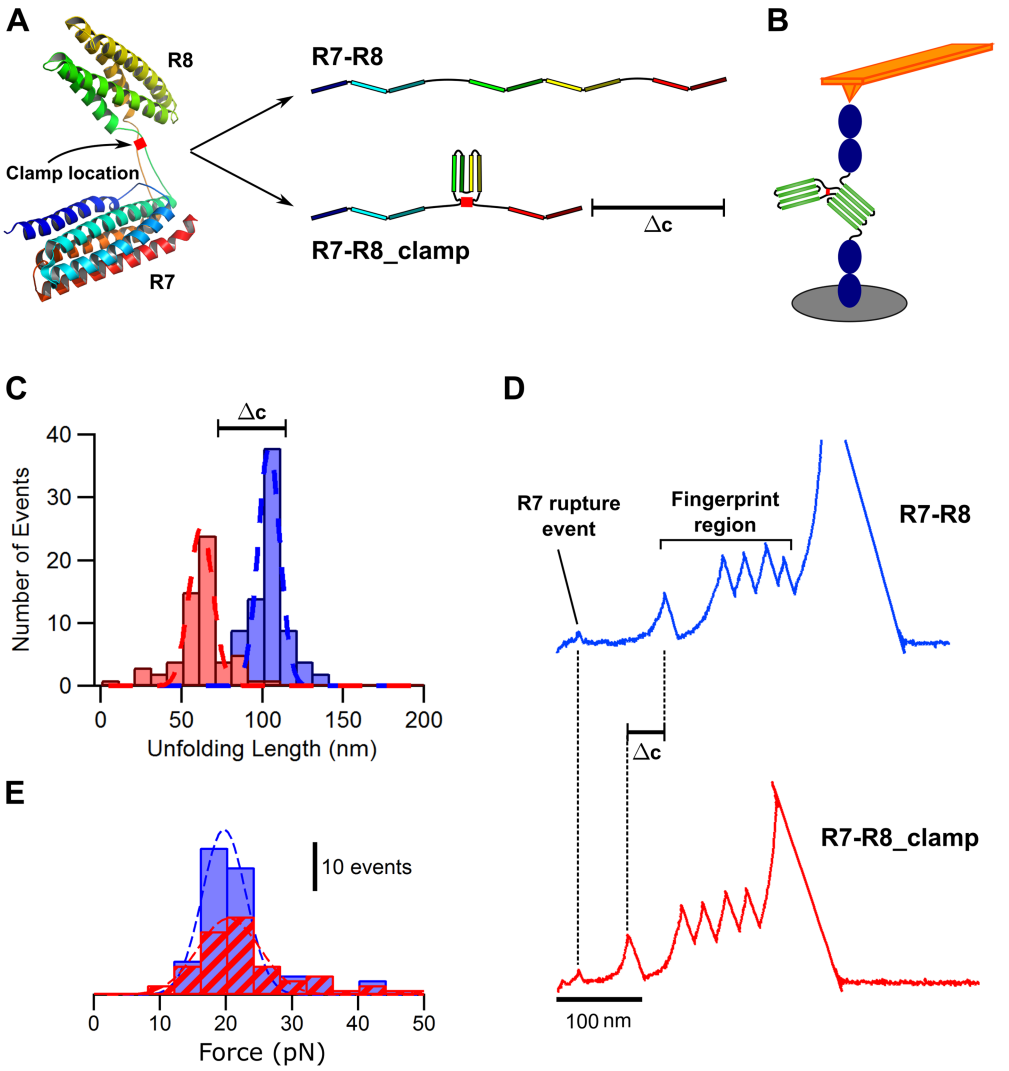

Fig 2. The disulphide clamp inserted in the R8 region of talin prevents R8 subdomain unfolding. (A) Representation of the R7-R8 talin fragment showing the location of the disulphide clamp and how the clamp leads to a difference in unfolding length (ΔC). (B) Schematic of smAFM setup with construct (R7-R8 flanked by fingerprints) extended while trapped between a cantilever and piezo-driven surface. (C) Histogram showing the typical unfolding lengths of the WT R7-R8 (blue) and R7-R8 clamp (red) subdomains. (D) Representative traces highlighting the shortened unfolding pattern of the R7-R8 (blue) and R7-R8_clamp (red) subdomains. (E) Histograms of the unfolding force for R7-R8 (blue) and R7-R8_clamp (red) subdomains. Blue and red dashed lines show gaussian fits applied to the histograms. For panels C and E, $n = 82$ and $n = 56$ traces for R7-R8 and R7-R8_clamp, respectively, taken in more than 5 different experiments. smAFM, single-molecule atomic force microscopy; WT, wild-type.

https://doi.org/10.1371/journal.pbio.2005599.g002

its attachment to the rest of the talin rod. The long linkers that connect the opposite ends of the R8 bundle's amino acid chain to the R7 bundle are in close proximity to one another (<5 Å between the backbone carbons) [16]. We hypothesised that the introduction of a cysteine residue into each linker (by single-point mutation to residues Q1459 and S1583) would create a disulphide bridge between the linkers, creating a clamp to hold the R8 bundle together (Fig 2A). The advantage of the use of this R8 mutant is that it will allow the study of the talin unfolding without abrogating binding sites or removing entire subdomains.

We used a force extension protocol, as previously described, to study the unfolding of both polyproteins (Fig 2B) [8]. The wild-type (WT) R7-R8 form unfolds in a single step, with a total

unfolding length of 104 ± 7 nm, which represents the unfolding length of both bundles. The clamped R8 mutant, by contrast, shows a reduced length of unfolding of 62 ± 6 nm (Fig 2C and 2D and S1 Data). The difference in unfolding length of around 40 nm matches the expected difference from lack of unfolding of the R8 bundle (124 amino acids' removal should result in a 38–50 nm reduction in unfolding length). This confirms that the disulphide clamp introduced in the R8 mutant makes this construct resistant to force-induced unfolding. We also observed that the introduction of the clamp did not significantly alter the unfolding forces of the R7-R8 and R7-R8 clamp domains, as both unfold at forces close to 20 pN (Fig 2E and S1 Data).

We also examined the stability of the R7-R8 domain using steered molecular dynamics (SMD) simulations, as well as investigating the effect of DLC1 binding (Fig 3A) on the stability of the R8 bundle. Previous work has found that 5-helix bundles, such as R7, exhibit higher stabilities than 4-helix bundles, such as R8 [8, 15]. Our SMD analysis with 2 nm/ns constant velocity pulling showed this is the case for the interlinked R7-R8 domain: R7 unfolds first over approximately 15 ns, requiring at least 500 pN of peak force to disrupt the full bundle structure (Fig 3B). After the complete unfolding of the R7 bundle, tension is then transferred to the R8 bundle, which unfolds at peak forces less than 300 pN. This relative instability of the R8 bundle as compared to R7, combined with R7 needing to be unfolded completely before R8 is exposed to tension, leads us to hypothesise that R8's insertion into R7 regulates its unfolding, and thus binding, characteristics.

Given that the binding of DLC1 to R8 takes the form of a '5-helix' bundle arrangement [12], we examined whether the binding of DLC1 alters the stability of the R8 bundle. SMD analysis of the combined DLC1/R8 and R8 alone showed that this interaction does not significantly alter the unfolding characteristics of the bundle (Fig 3C). This is likely due to the nature of the pulling vectors: despite the contribution of an additional helix from DLC1, R8 is still opening in the 'zipper' fashion as opposed to the 'sliding' mechanism that has been postulated as the cause of the higher stability of 5-helix bundles (S1 Fig). These SMD results support the smAFM results and the hypothesis of a mechanically weak R8 bundle whose unfolding characteristics are significantly altered through the addition of the disulphide clamp. More detailed analysis of the SMD data can be found in S1 Text.

We then expressed full-length talin constructs, both WT and with the disulphide clamp (R8), inserted within mammalian vectors, in talin-null mouse embryonic fibroblasts (MEFs) [17], to determine the cellular effects of preventing R8 unfolding. The redox potential inside the cell is not homogeneous and may vary depending on the culture conditions, and consequently, we acknowledge the possibility of low levels of cytosolic disulphides [18]. However, a recent study reported a significantly higher oxidative environment inside cells close to the plasma membrane compared to the inner cytoplasmic milieu, which would favour the disulphide clamp stabilisation in the talin molecule [19].

We first tested the dynamics of focal adhesion–associated DLC1 using fluorescent recovery after photobleaching (FRAP). Along with the talin constructs, the cells were transfected with DLC1 tagged with green fluorescent protein (GFP). A region of the cell containing focal adhesions was then photobleached using a confocal laser. The recovery of the GFP signal into the focal adhesions of the bleached region serves as a measure of the dynamics of the DLC1 in those adhesions (Fig 4A). The recovery curves of the GFP signal show a difference in the immobile fraction between WT and R8 mutant (Fig 4B and S1 Data). Analysis of these curves displays a larger population of immobile DLC1 in the R8 mutant as compared to WT (Fig 4C and S1 Data). This implies a lower turnover of DLC1 in focal adhesions where the R8 bundle is unable to unfold and thus favours DLC1-binding. We created 2 talin constructs, each one harbouring a cysteine residue. These constructs were used as negative controls for our talin R8

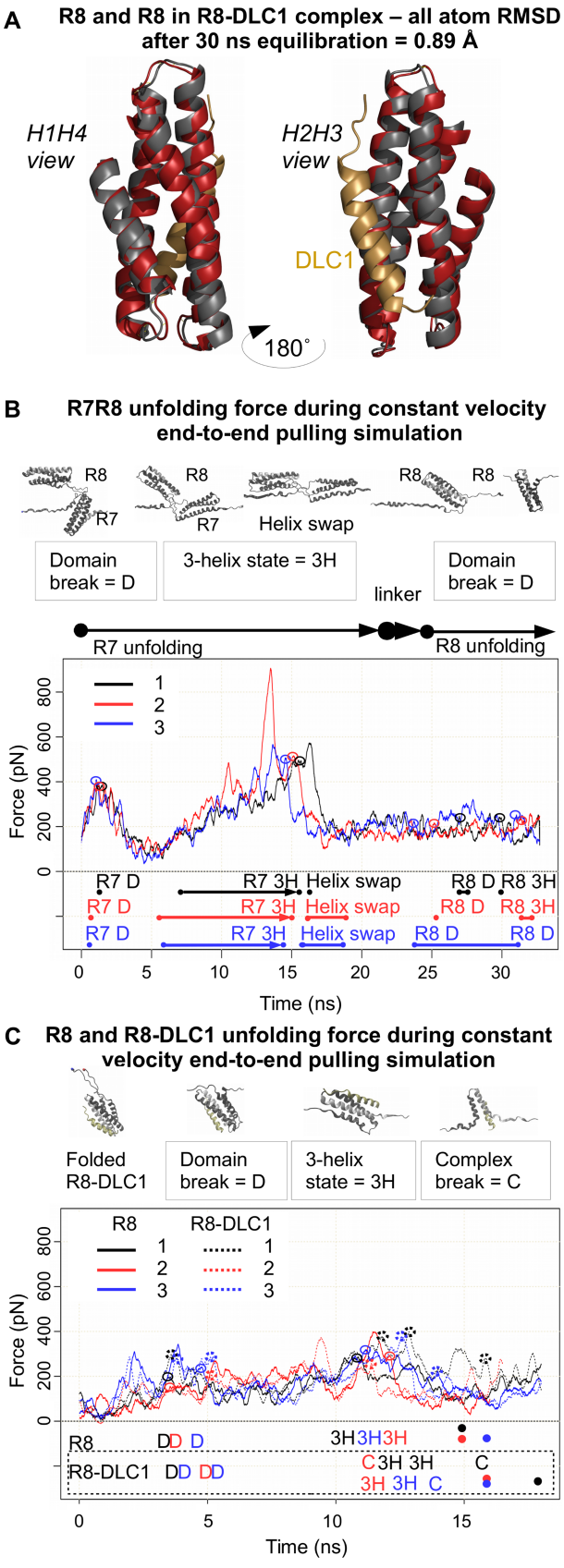
A
R8 and R8 in R8-DLC1 complex – all atom RMSD after 30 ns equilibration = 0.89 Å
H1H4 view
H2H3 view
DLC1
180°
B
R7R8 unfolding force during constant velocity end-to-end pulling simulation
R8
R7
Helix swap
Domain break = D
3-helix state = 3H
linker
Domain break = D
R7 unfolding
R8 unfolding
Force (pN)
Time (ns)
R7 D
R7 3H
Helix swap
R8 D
R8 3H
C
Folded R8-DLC1
Domain break = D
3-helix state = 3H
Complex break = C
R8
R8-DLC1
DD D
3H 3H 3H
C 3H 3H
3H 3H C
DD DD

Fig 3. Unfolding of R7-R8, R8 and R8-DLC1 under mechanical load in SMD simulations. (A) Structural alignment of R8 domain (red) and R8 domain in R8-DLC1 complex (grey) (DLC1 –yellow). (B, C) Unfolding force traces in 3 repetitions, examples of structural changes during the domain unfolding and details of the unfolding events over simulation time; B: R7-R8 double domain, C: R8 domain and R8-DLC1 complex. 'D' = folded domain, '3H' = 3-helix intermediate, Helix swap state = R8-R7H1 complex, 'C' = R8 H2H3-DLC1 complex, 'dot' = unfolded domain. DLC1, deleted in liver cancer 1; RMSD, root-mean-square deviation.

https://doi.org/10.1371/journal.pbio.2005599.g003

clamp, construct C1 with the cysteine residue in position 1459, and construct C2 with the cysteine residue in position 1583. We observed no significant differences in the recovery rates of the GFP signals or in the immobile fraction of DLC1 between cells transfected with either WT, C1, or C2 talin (Fig 4B–4D and S1 Data).

To ensure that this effect was due to the presence of a disulphide bridge in the R8 bundle, we also conducted the FRAP experiment in the presence of dithiothreitol (DTT), a cell-permeable small molecule that reduces intracellular disulphide bonds and thus would disrupt the clamp in subdomain R8. When the FRAP experiments were performed in the presence of DTT, we saw no difference between the recovery curves (Fig 4D and S1 Data), with no significant differences between the immobile fractions as compared to cells expressing WT talin (Fig 4E and S1 Data).

In order to examine if the differences observed in the DLC1 focal adhesion dynamics are present in other focal adhesion proteins, we transfected the MEF cells with either the WT or the R8 talin constructs and GFP vinculin or GFP paxillin. We used the same FRAP protocol and observed no differences in the recovery rates or in the population of the immobile fraction of GFP vinculin between cells expressing WT or R8 (Fig 4F–4H and S1 Data). This is not surprising given that there are 11 vinculin binding sites in the entire talin rod [14], and any potential effect in the binding of vinculin to the R8 domain may be masked or compensated by the entire pool of bound vinculin molecules. In stark contrast, we observed a significant lower recovery rate and significantly larger population of GFP paxillin for MEFs transfected with R8 talin compared to WT cells (Fig 4G and 4H). The recovery curves for paxillin demonstrate a similar difference between WT and R8 as with DLC1. The immobile fraction is greater in R8, again indicating that the disulphide-protected folding of R8 leads to a lower turnover of paxillin (Fig 4H). Paxillin is thought to bind to R8 in an analogous manner to DLC1, with a ΔR8 talin mutant demonstrating reduced levels of paxillin in focal adhesions similar to the reduction in DLC1 [12]. These results indicate that the disruption of the R8 domain abrogates paxillin binding as well as that of DLC1.

Given that the localisation of DLC1 to focal adhesions has been shown to affect downstream cell processes [11], we investigated the effect of the R8 mutant on potentially dependent pathways. Myosin light chain 2 (MLC-2) is downstream of RhoA signalling, and its activation (phosphorylation of serine and threonine residues in the active form—phospho-myosin light chain 2 [pMLC-2]) is proportional to the level of active RhoA [20]. We expected that the greater association of DLC1 with talin in the R8 mutant would down-regulate the activation of RhoA and the downstream effector MLC-2. We used immunofluorescence to quantify the pMLC-2/MLC-2 levels as a surrogate of MLC-2 activation (Fig 4I). We saw a significantly higher pMLC-2/MLC-2 ratio in the WT talin–expressing cells as compared to those with the clamp (R8), indicating greater activation of MLC-2 (Fig 4J, S5 Fig and S1 Data). This difference was abrogated by the addition of DTT but maintained in the presence of glutathione (GSH), a cell membrane–impermeant reducing agent[21]. Furthermore, knocking down DLC1 via small interfering RNA (siRNA) also abolished the differences in the levels of MLC-2 activation between WT and R8 cells. There were no significant differences in the pMLC-2/MLC-2 ratio between WT cells and the cells transfected with either C1 or C2 talin constructs. Taken

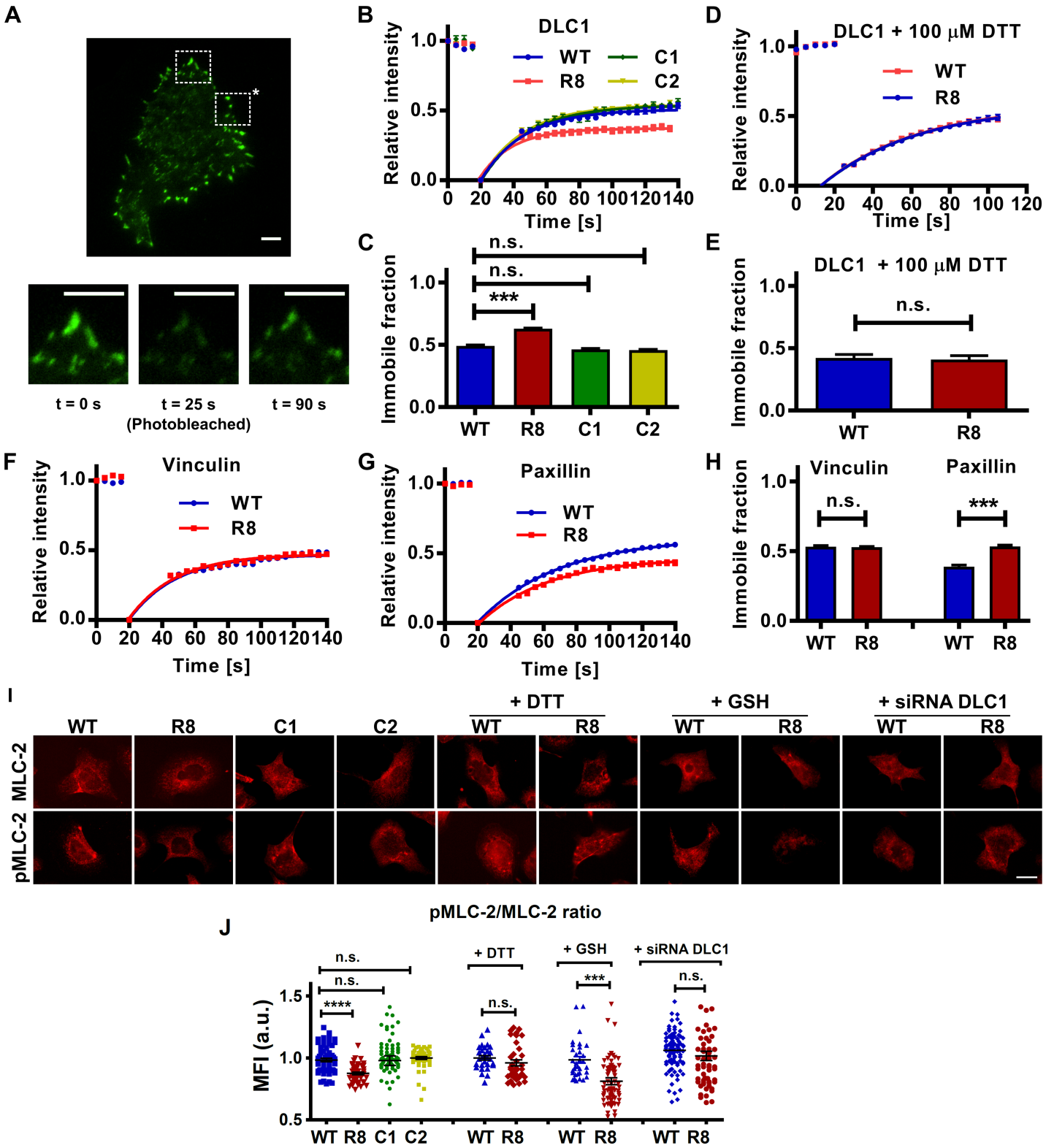

Fig 4. Preventing R8 unfolding increases DLC1 binding and downstream deactivation of MLC-2. (A) Representative images of a cell expressing GFP-DLC1. Insets show the intensity of the focal adhesions at different time points of the FRAP experiments. Region highlighted with asterisk was not exposed to confocal laser (see S2 Fig). Scale bars are 5 μm. (B) FRAP curves for the recovery of GFP-tagged DLC1 for MEFs transfected with either WT talin ('WT'), the clamped R8 mutant ('R8'), construct 1 ('C1'), or construct 2 ('C2'). (C) Immobile fraction data obtained from fit of FRAP curves (n = 25, 32, 26, 28 cells for WT, R8, C1, and C2, respectively). (D)

FRAP curves for MEFs treated with DTT to cleave the disulphide clamp showing no difference in recovery. Errors bars represent sem. (E) Immobile fraction data from fit of FRAP curves in D (n = 14 cells for both WT and R8). (F-G) FRAP curves for the recovery of GFP vinculin (F) or GFP paxillin (G) in MEFs transfected with either WT talin (WT) or the clamped R8 mutant. (H) Immobile fraction data obtained from fit of FRAP curves in F-G (n = 33, 29, 25, 27 cells for WT/vinculin-GFP, R8/vinculin-GFP, WT/paxillin-GFP, R8/paxillin-GFP). (I) Immunofluorescence images of MLC-2 and pMLC-2 staining. Scale bar is 20 μm. (J) Ratio of pMLC-2 staining to total MLC-2 for MEFs transfected with WT talin, the clamped R8 mutant, C1, or C2 constructs. Each dot represents a cell; horizontal lines are mean ± sem. For all panels, histograms represent mean ± sem. All experiments were run in triplicate (t test). a.u., arbitrary unit; DLC1, deleted in liver cancer 1; DTT, dithiothreitol; FRAP, fluorescent recovery after photobleaching; GFP, green fluorescent protein; GSH, glutathione; MEF, mouse embryonic fibroblast; MFI, mean fluorescence intensity; MLC-2, myosin light chain 2; n.s., not significant; pMLC-2, phospho-myosin light chain 2; siRNA, small interfering RNA; WT, wild-type.

https://doi.org/10.1371/journal.pbio.2005599.g004

together, these results show that the presence of the disulphide clamp that makes the R8 region resistant to unfolding and allows DLC1 localisation to focal adhesions was necessary to observe the large-scale downstream effect (Fig 4J).

Higher MLC-2 activation is associated with greater cellular traction force generation [22], and so we next sought to examine the effect of the R8 mutant on generating endogenous forces. We seeded cells expressing either WT, R8 mutant, C1, or C2 talin constructs on top of a substrate consisting of an array of flexible elastic polydimethylsiloxane (PDMS) micropillars coated with fibronectin. The deflection of the pillars is optically monitored and is proportional to the forces applied by the cells on the pillars. We observed that cells expressing WT talin applied significantly higher endogenous traction forces in comparison with the group of cells expressing the R8 mutant talin during the 90 minutes of cell spreading (Fig 5A and 5B and S1 Data). There were no significant differences between the forces applied by cells expressing WT, C1, and C2 talin constructs. The observed differences between the forces applied by WT talin and R8 talin cells were maintained in the presence of the cell-impermeant reducing agent GSH but abrogated when the cell-penetrating reducing agent DTT was added or when the cells were previously transfected with siRNA for DLC1. These data corroborate our previous observations on the MLC-2 activation in cells transfected with WT and R8 talin constructs.

The capacity of cells to apply forces on their substrates correlates with their ability to contract collagen gels and to remodel the ECM [23, 24]. To examine the ability of both groups of cells (containing WT and R8 talin) to deform matrices, we embedded the cells within collagen Matrigel gels and observed that after 48 h, the WT cells contracted the gels to 47% of their initial size, whereas the mutant cells only contracted them to 55% of their initial size. This agrees with the previous results that showed that R8 cells displayed significantly lower traction forces (Fig 5C and S1 Data).

The localisation of DLC1 to adhesions has also been shown to negatively affect the ability of the cells to migrate [11]. The migration speeds of the WT and R8 mutant cells were measured over 12 h, revealing a nonsignificant decrease in migration rate between WT and mutant (Fig 5D). We treated the cells with 50 μM diamide to shift the redox balance towards the oxidative range in the cellular cytoplasm so that more of the mutant protein would exhibit the disulphide bond preventing R8 unfolding and DLC1 unbinding. When the migration speed of these cells was tested, we saw a significant decrease in migration speed in the cells containing the R8 mutant in comparison to WT (Fig 5D, S1 Video, and S1 Data). As a further test of the efficacy of diamide in enhancing the effect of the disulphide clamp, we conducted the pMLC-2/MLC-2 staining for cells treated with diamide. In this case again, we saw that the diamide increases the effect, with a greater decrease in pMLC-2/MLC-2 ratio for diamide-treated R8 mutant cells than for those untreated (Fig 5E and 5F, and S1 Data). A 10 μM diamide concentration had clear effect in this assay. We also confirmed the oxidative effect of the diamide for the disulphides by treating WT MEF cells with diamide and then analysing the cell lysate with 2D electrophoresis (S6 Fig), comparing oxidising and reducing conditions as described in a previous study [18].

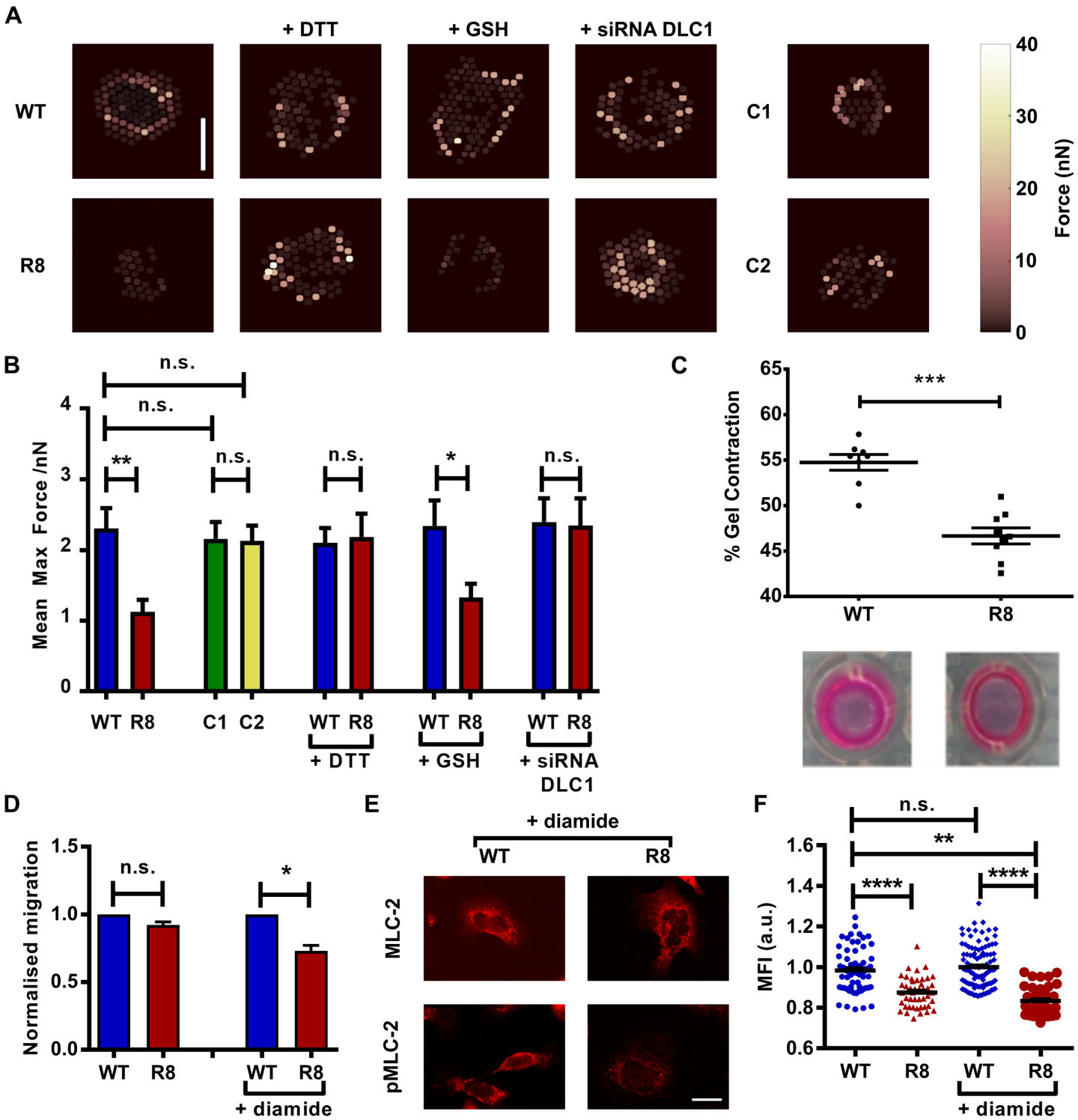

Fig 5. Preventing R8 unfolding reduces force application and cell migration. (A) Heat maps representing forces applied by MEFs on top of the pillars, scale bar = 10 μm. (B) Quantification of average forces applied by MEFs on pillars. (number of analysed cells: 20 WT, 19 R8, 22 C1, 20 C2, 29 WT DTT, 25 R8 DTT, 22 WT GSH, 19 R8 GSH, 27 WT siRNA DLC1, 28 R8 siRNA DLC1). (C) Scatter plot of the percentage change in gel size for collagen Matrigels embedded with transfected MEFs for 48 h (*t* test). (D) Normalised migration rate over 12 h for transfected MEFs, with and without diamide to enhance the disulphide clamp. (Number of cells: 207 WT, 157 R8, 130 WT + diamide, 142 R8 + diamide, *t* test). (E) Immunofluorescence images of MLC-2 and pMLC-2 staining for diamide-treated cells. Scale bar is 20 μm. (F) Ratio of pMLC-2 staining to total MLC-2 for transfected cells, with and without diamide. Each dot represents a cell; horizontal lines are mean ± sem (*t* test). For all panels, histograms represent mean ± sem. All data set in S1 Data. a.u., arbitrary unit; DLC1, deleted in liver cancer 1; DTT, dithiothreitol; GSH, glutathione; MEF, mouse

embryonic fibroblast; MFI, mean fluorescence intensity; MLC-2, myosin light chain 2; n.s., not significant; pMLC-2, phospho-myosin light chain 2; siRNA, small interfering RNA; WT, wild-type.

https://doi.org/10.1371/journal.pbio.2005599.g005

From these results, we have shown how DLC1 localisation to focal adhesions is modulated by the unfolding of talin's R8 domain, constituting a novel force-controlled molecular switch. Through stabilising the R8 bundle in the talin molecule with a disulphide bridge, we altered the dynamics of focal adhesion–associated DLC1 (Fig 4B–4E). This led to downstream reductions in MLC-2 activation (Fig 4I and 4J), force generation (Fig 5A and 5B), and cell migration (Fig 5D).

In the widely accepted model of talin-mediated focal adhesion activation, as force is applied to talin in maturing adhesions by the actin contractile machinery, its helical bundles are disrupted. This allows vinculin to bind, which leads to focal adhesion maturation [4, 25]. It also, based on these findings, disrupts the binding of DLC1, reducing its negative effects on RhoA activity, which enhances the generation of forces at growing adhesions. Thus, in early adhesions, this works cooperatively with the increase in vinculin binding to mature the adhesions. However, the weakness of the model as it stood, with the vinculin-talin interaction at its core, is that it failed to account for any form of negative feedback. As the adhesions grew, talin recruited more vinculin, which increased force generation, which led to greater recruitment of talin and vinculin and so on [26].

Our new model provides a further refined mechanism of talin-mediated focal adhesion activation that works synergistically with its binding to vinculin initially but has a more important role to play in mature adhesions. This is where the mechanical switch involving DLC1 does provide a negative feedback and thus control. In the maturing adhesions, it is as before: force on talin unfolds the R8 domain, reducing DLC1 localisation and increasing RhoA activity. However, as the adhesion matures and recruits more proteins to the complex, the force on individual talin molecules is reduced. This is because, although the total force applied to the adhesion is likely increasing, the presence of an increasing number of mechanical linkages, such as talin and vinculin, means that the force on each linkage is reduced, like springs in parallel. The reduction in force on each linkage has been demonstrated in cellular experiments in which the force on linkages has been measured by FRET tension sensors and shown to be lower in more mature, central adhesions than earlier, peripheral ones [7, 27]. This reduction in force on talin means that our R8 switch now reverts to DLC1 binding. This hypothesis is supported by studies showing a greater localisation of DLC1 to mature adhesions [28].

This reduces force generation and controls the maturation process of the adhesions. This is an attractive model not just in light of the results presented but also when considered with respect to the role of DLC1 deletion in cancers. The role of highly activated and contractile cells in the cancer progression has been investigated before, and it is possible that DLC1's role in cancer (by its absence) is mediated through the subsequent lack of control over focal adhesion activation.

Moreover, when cells are surrounded by stiffer substrates (such as tumours), the talin molecule (anchored to a stiff surface via integrin receptors) would unfold more readily. As can be seen in these results, this will trigger DLC1 deactivation and increased cell contractility, force generation, and migration. Increasing cell contractility in cancer-associated fibroblasts enhances tumour growth via paracrine signalling with the tumour microenvironment [29], and increasing contractility in cancer cells will facilitate the breaching of the basement membrane that surrounds tumours [30]. Furthermore, increasing migration in cancer cells will favour cancer cell invasion. Indeed, the talin molecule has been implicated in diseases that are influenced by mechanical factors, including cancer [31].

The broader implications of the downstream cascades of events resulting from the presented talin mechanotransduction mechanism for the biology of cells need to be established.

For instance, this mechanism could affect actomyosin-dependent fibronectin fibrillogenesis, exerting a direct impact on the regulation of connective tissue homeostasis in health (wound healing) and disease. A fibrotic matrix is a major clinical hallmark of several disorders, such as cirrhosis and pancreatitis, often associated with aberrant mechanotransduction, and this mechanism may provide a potential mechano-therapy target.

As well as these results demonstrating the existence of force-mediated binding between talin and DLC1, it also lays out a method for further investigations of talin or other mechanosensitive proteins. Previously, studies of these types of proteins focussed on the removal of subdomains, whereas here we report a methodology to force these mechanical switches into a particular state. Small differences can also be amplified by the addition of reagents that alter the redox state of the cells to favour the fixed state. In this way, we can establish the local effects of these switches along with the downstream phenomena they control. The regulation of signalling pathways by modulating protein structure and ligand binding may be a cellular adaptation cells have developed for rigidity sensing. Further studies utilizing other mechanosensitive proteins would validate this.

Materials and methods

Generation of polyprotein constructs and smAFM

The smAFM experiments were carried out according to protocols described previously [8]. The talin fragment polyprotein constructs, including flanking I27, were synthesised and cloned into the pFN18a vector. The polyproteins were expressed in *Escherichia coli* BL21-CodonPlus (DE3)-RILP competent cells, using the T7 promoter present in the plasmid. Protein expression was induced with IPTG when the culture reached an OD600 nm of 0.6. Cells were lysed with lysozyme and sonication before protein purification with Ni-NTA beads in a batch process. The eluted proteins were analysed for purity with SDS-PAGE. Final concentration of protein used for experiments was 1–10 μg/ml. Glass coverslips were functionalised with the chloroalkane ligand to HaloTag as previously described [32]. The glass coverslips were first cleaned using Helmanex III (1% in water), acetone, and ethanol washes. The surfaces were then prepped with O2 plasma cleaning for 15 min. Surfaces were then silanised using (3-aminopropyl)trimethoxysilane diluted to 1% in ethanol. Surfaces were then washed with ethanol and then dried with N2. These amine-functionalised surfaces were then incubated with 10 mM succinimidyl-[(Nmaleimidopropionamido)tetracosaethyleneglycol] ester (SMPEG24, Thermo) diluted in 100 mM borax buffer (pH 8.5) for 1 h. The final step involved incubating the surfaces overnight with 10 mM HaloTag Thiol O4 ligand in the same buffer. The surfaces were quenched 50 mM 2-mercaptoethanol in water. We used a commercial AFS-1 from Luigs & Neumann, GmbH, based on a device developed at the Fernandez Lab, Columbia University [33]. The cantilevers used were gold-coated OBL-10 levers from Bruker. The spring constants varied between 4–10 pN/nm as measured by equipartition theorem with the appropriate adjustments for cantilever geometry. Around 20 μl of protein solution was incubated on functionalised coverslips for 30 min prior to the experiments to allow for HaloTag binding. The cantilever was pressed into the surface with a force of approximately 300 pN to bind the cantilever to the polyprotein. Force extension experiments were conducted at 400 nm/s retraction rate. Data analysis was carried out using Igor Pro (Wavemetrics), for which the wormlike chain model was applied.

SMD simulations

The following structures from RCSB Protein Data Bank were used as the protein models for the individual talin rod subdomains: R8 (id 5FZT residues 1451–1588), R8-DLC1 (id 5FZT

talin residues 1451–1588 and DLC1 residues 467–489), and R7R8 (id 2X0C). The talin structures were modified in PyMOL to produce the desired constructs.

MD and SMD simulations were performed using Gromacs ver 2016.1 [34, 35] at the Sisu supercomputer, CSC, Finland. The CHARMM27 force field [36] and explicit TIP3P water model [37] in 0.15 M KCl solution were used, and the total charge of the system was adjusted by K+ and Cl– ions. The energy minimisation of the system was performed in 100,000 steps, using the steepest descent algorithm.

The equilibration was performed with NPT ensemble and was maintained at 310 K using the V-rescale algorithm [38] and 1 atm under Berendsen barostat, as implemented in Gromacs 2016.1. First run of equilibration was performed for R8 and R8-DLC1 with long linkers. These complexes were followed over 30 ns simulation without applied restrictions. Both domains were very stable, with low root-mean-square deviation (RMSD) changes. Major structural changes were observed for the long interdomain linker. In the second equilibration run, the fixed and pulled Cα atoms were restrained with harmonic potential during the 10 ns simulation. The temperature coupling was applied separately for the protein and the solution parts. Each system was equilibrated up to 10 ns, with subsequent monitoring of the RMSDs of Cα atoms. Structures after 10 ns were used as the starting pulling conformation. Pulling vector was set between Cα of the first and the last residue of the appropriate domain parallel to the z-axis of the pulling box. The movement of Cα of N-terminal residue was restrained with harmonic potential, while Cα of C-terminal residue was subjected to the constant velocity pulling. After placing the equilibrated protein in the pulling box and orienting it appropriately in the pulling direction, the water solution was equilibrated as external bath during 1 ns bath equilibration [39]. Furthermore, equilibration was performed at isotropic conditions while pulling at semi-isotropic conditions when pressure control was turned off in the pulling direction (z-axis). The constant velocity pulling SMD simulations were performed at 2 nm/ns with the spring constant set to 1,000 kJ/mol nm^2. All trajectories were produced in 3 repetitions.

Cells and culture conditions

The WT MEF cell line was a kind gift from Dr Wolfgang Ziegler and has been previously described by Xu and Baribault in 1998 [40]. The *Tln1–/–Tln2–/–* MEF cell line has been previously described by Theodosiou and colleagues [17]. Both cell lines were maintained in high-glucose DMEM supplemented with 10% FBS and 1% GlutaMax (Thermo Fisher Scientific, United States of America). A humidified 37˚C incubator with 5% CO_2 was used for culturing both cell lines. Cells were negative when tested for mycoplasma contamination.

Plasmid constructs for use in MEFs

In all cell experiments other than the FRAP, a GFP-Talin1 plasmid was used. The GFP-Talin1 plasmid was a gift from Anna Huttenlocher (Addgene plasmid # 26724) [41]. The GFP-DLC1 plasmid was a gift from Irene Ng [42]. The GFP-vinculin plasmid was obtained from Susan Craig [43]. The GFP-paxillin was a gift from Chinten James Lim (Addgene plasmid # 80023). The talin 1 plasmid (Addgene # 26724) was used as template to generate the R8, C1, and C2 constructs by PCR-based mutagenesis starting construct via 5′ FseI and 3′ ScaI. R8: For the substitution of amino acid glutamine with cysteine at position 1459, CAA was replaced with TGC; and for the substitution of serine for cysteine at position 1583, AGC was replaced with TGC. C1: For the substitution of amino acid glutamine with cysteine at position 1459, CAA was replaced with TGC. C2: For the substitution of serine for cysteine at position 1583, AGC was replaced with TGC.

FRAP

The GFP-DLC1 FRAP experiments were conducted on glass-bottom petri dishes (Mattek) coated with human plasma FN (10 μg ml^{-1}; Sigma) and incubated at 37˚C. For the DTT condition, DTT (Sigma) was added at a concentration of 100 μM 30 min prior to the start of the experiment. Confocal photobleaching and TIRF imaging were carried out using an inverted microscope (Eclipse Ti; Nikon). Five TIRF images were taken at 5 s intervals prior to bleaching for reference. Specified regions of the cells were then bleached using the confocal laser at 100% power. TIRF images were taken at 5 s intervals for 100 s to capture fluorescent recovery. Images were analysed with FIJI, with the fluorescent signal normalised between the prebleach intensity and background. Statistical analysis was then carried out using Prism (GraphPad). Data were pooled from repeats. The significance between curves was measured using extra sum-of-squares F test on the best fit lines.

MLC-2 immunostaining

Immunofluorescence staining was done on coverslips coated with 10 μg/ml fibronectin (Sigma, F0895). Following pertinent treatment, cells were fixed with 4% PFA (Sigma, P6148) in PBS for 10 min and then blocked and permeabilised with 2% BSA-0.1%Triton (Sigma, T8787) in PBS for 30 min. After blocking, cells were incubated with primary antibodies (MLC-2 Millipore MABT180 1/200 and pMLC-2 Thr18/Ser19 Cell Signalling 3674 1/200) prepared in blocking solution for 1 h at room temperature in a humidified chamber. Then cells were washed in PBS and incubated with Alexa Fluor 488 conjugated secondary antibodies and Phalloidin (Invitrogen, A22283, 1/1,000 dilution) prepared in PBS for 30 min at room temperature. Finally, coverslips were washed in PBS and mounted in mounting reagent with DAPI (Invitrogen, P36931). GSH was purchased from Sigma-Aldrich (catalogue 78259) and used at a concentration of 10 mM. DLC1 antibody (clone C-12, catalogue sc-271915, dilution 1/100). siRNA for DLC1 was from Santa Cruz Biotechnology, catalogue sc-72134. Primers used to monitor DLC1 gene expression knockdown: DLC1 (m)-PR, catalogue sc-72134-PR.

Micropillar video microscopy and traction force measurements

The micropillar arrays are based on our protocol as described previously [22]. Pillar arrays were coated with human plasma FN (10 μg ml^{-1}; Sigma) and incubated at 37˚C for 1 h before measurements. Cells that had been trypsinised before measurements were suspended in culture media and plated onto the pillar substrates. Time-lapse imaging of the pillars was conducted with an inverted microscope (Eclipse Ti; Nikon) operating in bright-field mode, with the samples held at an ambient temperature of 37˚C. Image sequences were recorded with a sCMOS camera (Neo sCMOS Andor) at 0.5 Hz using a ×40 (0.6 NA, air; Nikon) objective over 100 min. The position of each pillar in the time-lapse videos was tracked using a custom MATLAB program to track the centre of a point spread function of the intensity of the pillars across all frames. By selecting a location free of cells, tracking of a small set of pillars allowed a measurement of the stage drift to be obtained and corrected for in the data set. The time-dependent displacement of a given pillar was obtained by subtracting the initial position of the pillar (zero force) from the position in a given frame. Traction forces were obtained by multiplying the pillar displacements by the pillar stiffness; the maxima for each pillar were found to obtain the peak forces across the cell.

Gel contraction

To analyse the ECM remodelling ability of MEFs, collagen-I (BD Biosciences, 354249, stock concentration 9.37 mg/ml) and Matrigel (BD Biosciences, 354234, stock concentration 9 mg/

ml) mixture gels were prepared with 10% 10× DMEM (Sigma, D2429) and 10% FBS (Gibco, 10500), yielding to a final concentration of 4.4 mg/ml collagen-I and 2.2 mg/ml Matrigel. The gel mixture was neutralised with 1 M NaOH (Sigma, S8045); then, 5×10^5 cells were embedded in gels in culture media. Eighty μl gel volume was added per well of a 96-well plate, which was pretreated with 2% BSA (Sigma, A8022) for 1 h, washed with PBS, and air dried for 10 min. Gels were set 1 h at 37˚C and then incubated with culture media for 2 d at 37˚C.

Migration assays

Polystyrene 6-well plates were coated with 10 μg/ml fibronectin in PBS (pH 7.4) at 37˚C for 1 h and washed 2 times with PBS. Transfected *Tln1−/−Tln2−/−* MEF cells were allowed to recover for 24 h, trypsinised, and plated onto fibronectin-coated well plates at a low confluency. Cells were allowed to attach for 90 min, followed by replacement of media (2 ml of fresh media) to remove nontransfected cells. For treating the cells with diamide, diamide powder (Sigma-Aldrich D3648) was dissolved in PBS to a stock concentration of 50 mM (8.6 mg/ml) and further diluted with complete cell culture media to 150 μM concentration. One ml of the diamide-containing media was added dropwise to 2 ml of cell culture media in each well 15 min before live cell imaging was started. EVOS FL Auto (Life Technologies, USA) equipped with a 20× objective and 37˚C and 5% CO_2 incubator was used for live cell imaging for 12 h at 120 s intervals. The resulting image stacks were analysed with ImageJ version 1.50e with MTrackJ plugin [44, 45]. For each plasmid construct or diamide treatment, 130–200 individual cells were traced from 3 fully independent experiments.

2D SDS-PAGE analysis

Lysates of diamide-treated WT MEF cells were analysed by 2D SDS-PAGE to confirm the effect of diamide treatment on the level of cellular disulphide bonds. Cells at 80% confluency on 10 cm dishes were washed twice with warm PBS and treated for 120 min with 50 μM diamide dissolved in cell culture media. In negative controls, regular media were used instead. After the diamide treatment, cells were washed with ice-cold PBS and treated with 40 mM iodoacetamide in PBS for 5 min. Cells were lysed with 500 μl of RIPA buffer (50 mM Tris-HCl pH 7.4, 1% NP-40, 0.5% Na-deoxycholate, 0.1% SDS, 150 mM NaCl, 50 mM NaF) supplemented with 40 mM iodoacetamide and Roche complete protease inhibitor cocktail. Cell lysates were incubated on ice for 30 min and centrifuged at 14,000 g for 20 min at 4˚C to pellet cell debris. The concentrations of cleared lysates were determined with BCA assay and matched by diluting the lysates with RIPA buffer. For 2D SDS-PAGE, 120 μg samples of cell lysates were mixed with 2× Laemmli sample buffer without reducing agents, denatured at 95˚C for 5 min, and loaded onto a medium-sized 1 mm thick 10%/4% polyacrylamide gel. The polyacrylamide gels were run at 25 mA current for 5 h, followed by vertical slicing of the gel with a clean scalpel to separate each lane. The gel slices were incubated in SDS-PAGE running buffer supplemented with 100 mM DTT for 20 min at room temperature to reduce disulphide bonds in the lysates. After the treatment, the gel slices were briefly washed with running buffer and treated with 100 mM iodoacetamide in SDS-PAGE running buffer for 10 min. The pieces of gel were placed horizontally on top of 1.5 mm thick 10% polyacrylamide gels and ran at 10 mA current for 14 h. Proteins on the gel were visualised by using silver staining.

Statistical analysis

All statistical analyses were conducted with the Prism graphical software (GraphPad, Software). Data were generated from multiple repeats of different biological experiments in order to obtain the mean values and standard errors (sem) displayed throughout. *P*-values have been

obtained through *t* tests. Significance for the *t* tests was set at $P < 0.05$, for which graphs show significance through symbols (*, $P < 0.05$; **, $P < 0.01$; ***, $P < 0.001$; ****, $P < 0.0001$).

Supporting information

S1 Data. Raw numerical values for all quantitative data. This file has the raw numbers for the following figure panels: Figs 2C and 2E, 4B, 4C, 4D, 4E, 4F, 4G, 4H and 4J, 5B, 5C, 5D and 5F.
(XLSX)

S1 Fig. Unfolding geometry and unfolding force demand. The hypothetical comparison of 4-helix and 5-helix bundles' mechanical stability under end-to-end pulling.
(PDF)

S2 Fig. Comparison of bleached to nonbleached regions of MEF cells in FRAP. (A) Representative images of a cell region exposed to confocal laser during FRAP, demonstrating photobleaching and subsequent recovery. (B) Images of a region of the same cell not exposed to high-power confocal laser, displaying no apparent photobleaching. Scale bar 5 μm. FRAP, fluorescent recovery after photobleaching; MEF, mouse embryonic fibroblast.
(PDF)

S3 Fig. FRAP data for DLC1 GFP. Representative images of a cell region exposed to confocal laser during FRAP, demonstrating photobleaching and subsequent recovery. WT: WT talin, R8: clamped R8 domain in talin, C1: talin control with 1 cysteine in position 1459 of the amino acid sequence, C1: talin control with 1 cysteine in position 1583 of the amino acid sequence. Scale bar is 5 μm. These images correspond to Fig 4 panels B-E. DLC1, deleted in liver cancer 1; DTT, dithiothreitol; FRAP, fluorescent recovery after photobleaching; GFP, green fluorescent protein; WT, wild-type.
(PDF)

S4 Fig. FRAP data for vinculin GFP (two upper rows) and paxillin GFP (two lower rows). Representative images of a cell region exposed to confocal laser during FRAP, demonstrating photobleaching and subsequent recovery. WT: WT talin, R8: clamped R8 domain in talin. Scale bar is 5 μm. These images correspond to Fig 4 panels F-H. FRAP, fluorescent recovery after photobleaching; GFP, green fluorescent protein; WT, wild-type.
(PDF)

S5 Fig. Knockdown efficiency in the DLC1 siRNA cells. PCR levels of DLC1 expression in Tln1−/−Tln2−/− MEF cells transfected with WT and R8 talin constructs. Values are normalised to GAPDH and relative to control. Histogram bars represent mean ± sem, $^{***}P < 0.001$, (*t* test). Three experimental replicates. DLC1, deleted in liver cancer 1; GAPDH, glyceraldehyde 3-phosphate dehydrogenase; MEF, mouse embryonic fibroblast; siRNA, short interfering RNA; WT, wild-type.
(PDF)

S6 Fig. 2D SDS-PAGE analysis of proteins in talin-null MEF cells after treatment with 50 μM diamide revealed a clear increase in the level of disulphide bonds. To confirm the increase in the level of cellular disulphide bonds after a treatment with 50 μM diamide, lysates of diamide-treated MEF cells were analysed with 2D SDS-PAGE. Proteins in total-cell lysates were first separated without reducing agents (horizontal axis), followed by excising each gel lane to separate pieces and treating the gel lanes with DTT to reduce the disulphide bonds. The proteins on the reduced lanes were separated in a second SDS-PAGE run in the other direction

to reveal the differential migration of disulphide-containing proteins in oxidising and reducing conditions. Proteins that do not contain disulphide bonds migrate at similar rates in both gel runs and end up on a diagonal band on the gel. (A) Intra- or intermolecular disulphide bonds affect the rate of protein migration on gel, typically slowing down the rate of protein migration on the gel. Thus, proteins with intra- or intermolecular disulphide bonds migrate at a faster rate after breaking the disulphide bonds by reducing conditions and appear below the diagonal line at the 2D SDS-PAGE analysis. (B) The images presented are representative of two fully independent replicates. DTT, dithiothreitol; MEF, mouse embryonic fibroblast.
(PDF)

S1 Text. Analysis of molecular dynamics simulation data in Fig 3. In the main text, the analyses of the SMD are summarised and presented in full in the section S1 Text. SMD, steered molecular dynamics.
(DOCX)

S1 Video. Migration of talin-null MEFs transfected with WT and R8 (in no diamide condition and when 50 μm of diamide was added). Fifteen frames per second. Scale bar 100 μm. MEF, mouse embryonic fibroblasts; WT, wild type.
(AVI)

Acknowledgments

We thank Irene Ng for GFP DLC1 plasmid. We are grateful to all CMBL members for help and advice throughout this work.

Author Contributions

Conceptualization: Alexander William M. Haining, Vesa P. Hytönen, Armando del Río Hernández.

Data curation: Dariusz Lachowski.

Formal analysis: Alexander William M. Haining, Ernesto Cortes, Dariusz Lachowski.

Funding acquisition: Vesa P. Hytönen, Armando del Río Hernández.

Investigation: Alexander William M. Haining, Rolle Rahikainen, Ernesto Cortes, Dariusz Lachowski, Alistair Rice, Magdalena von Essen, Vesa P. Hytönen, Armando del Río Hernández.

Methodology: Alexander William M. Haining, Rolle Rahikainen, Ernesto Cortes, Dariusz Lachowski, Alistair Rice, Magdalena von Essen.

Project administration: Armando del Río Hernández.

Resources: Vesa P. Hytönen, Armando del Río Hernández.

Supervision: Vesa P. Hytönen, Armando del Río Hernández.

Visualization: Alexander William M. Haining, Ernesto Cortes, Dariusz Lachowski, Alistair Rice.

Writing – original draft: Alexander William M. Haining, Armando del Río Hernández.

Writing – review & editing: Alexander William M. Haining, Rolle Rahikainen, Ernesto Cortes, Dariusz Lachowski, Vesa P. Hytönen, Armando del Río Hernández.

References

1. del Rio A, Perez-Jimenez R, Liu R, Roca-Cusachs P, Fernandez JM, Sheetz MP. Stretching single talin rod molecules activates vinculin binding. Science. 2009; 323(5914):638–41. https://doi.org/10.1126/science.1162912 PMID: 19179532.
2. Maillard RA, Chistol G, Sen M, Righini M, Tan J, Kaiser CM, et al. ClpX(P) generates mechanical force to unfold and translocate its protein substrates. Cell. 2011; 145(3):459–69. https://doi.org/10.1016/j.cell.2011.04.010 PMID: 21529717; PubMed Central PMCID: PMCPMC3686100.
3. Zhang XH, Halvorsen K, Zhang CZ, Wong WP, Springer TA. Mechanoenzymatic Cleavage of the Ultralarge Vascular Protein von Willebrand Factor. Science. 2009; 324(5932):1330–4. doi: 10.1126/science.1170905. WOS:000266635100047. PMID: 19498171
4. Hytonen VP, Vogel V. How force might activate talin's vinculin binding sites: SMD reveals a structural mechanism. PLoS Comput Biol. 2008; 4(2):e24. https://doi.org/10.1371/journal.pcbi.0040024 PMID: 18282082; PubMed Central PMCID: PMC2242828.
5. Yao MX, Goult BT, Chen H, Cong PW, Sheetz MP, Yan J. Mechanical activation of vinculin binding to talin locks talin in an unfolded conformation. Sci Rep-Uk. 2014; 4. Artn 4610 doi: 10.1038/Srep04610. WOS:000333962300004. PMID: 24714394
6. Austen K, Ringer P, Mehlich A, Chrostek-Grashoff A, Kluger C, Klingner C, et al. Extracellular rigidity sensing by talin isoform-specific mechanical linkages. Nat Cell Biol. 2015; 17(12):1597–606. doi: 10.1038/ncb3268. WOS:000365932300012. PMID: 26523364
7. Kumar A, Ouyang MX, Van den Dries K, McGhee EJ, Tanaka K, Anderson MD, et al. Talin tension sensor reveals novel features of focal adhesion force transmission and mechanosensitivity (vol 213, pg 371, 2016). J Cell Biol. 2016; 214(2):231-. doi: 10.1083/jcb.201510012070620 16c. WOS:000380831300012. PMID: 27432899
8. Haining AWM, von Essen M, Attwood SJ, Hytönen VP, del Río Hernández A. All Subdomains of the Talin Rod Are Mechanically Vulnerable and May Contribute To Cellular Mechanosensing. ACS Nano. 2016. https://doi.org/10.1021/acsnano.6b01658 PMID: 27380548
9. Healy KD, Hodgson L, Kim T-Y, Shutes A, Maddileti S, Juliano RL, et al. DLC-1 Suppresses Non-Small Cell Lung Cancer Growth and Invasion By RhoGAP-Dependent and Independent Mechanisms. Molecular carcinogenesis. 2008; 47(5):326–37. doi: 10.1002/mc.20389. PMC2679972. PMID: 17932950
10. Kim TY, Vigil D, Der CJ, Juliano RL. Role of DLC-1, a tumor suppressor protein with RhoGAP activity, in regulation of the cytoskeleton and cell motility. Cancer metastasis reviews. 2009; 28(1–2):77–83. https://doi.org/10.1007/s10555-008-9167-2 PMID: 19221866; PubMed Central PMCID: PMC2757774.
11. Li G, Du X, Vass WC, Papageorge AG, Lowy DR, Qian X. Full activity of the deleted in liver cancer 1 (DLC1) tumor suppressor depends on an LD-like motif that binds talin and focal adhesion kinase (FAK). Proc Natl Acad Sci U S A. 2011; 108(41):17129–34. https://doi.org/10.1073/pnas.1112122108 PMID: 21969587; PubMed Central PMCID: PMC3193248.
12. Zacharchenko T, Qian X, Goult BT, Jethwa D, Almeida TB, Ballestrem C, et al. LD Motif Recognition by Talin: Structure of the Talin-DLC1 Complex. Structure. 2016; 24(7):1130–41. https://doi.org/10.1016/j.str.2016.04.016 PMID: 27265849; PubMed Central PMCID: PMC4938799.
13. Atherton P, Stutchbury B, Wang D-Y, Jethwa D, Tsang R, Meiler-Rodriguez E, et al. Vinculin controls talin engagement with the actomyosin machinery. Nat Commun. 2015; 6:NIL_1–NIL_12. CCC:000367584300001.
14. Margadant F, Chew LL, Hu X, Yu H, Bate N, Zhang X, et al. Mechanotransduction In Vivo by Repeated Talin Stretch-Relaxation Events Depends upon Vinculin. PLoS Biol. 2011; 9(12). ARTN e1001223 doi: 10.1371/journal.pbio.1001223. WOS:000298673000007. PMID: 22205879
15. Yao MX, Goult BT, Klapholz B, Hu X, Toseland CP, Guo YJ, et al. The mechanical response of talin. Nat Commun. 2016; 7. ARTN 11966 doi: 10.1038/ncomms11966. WOS:000380302500001. PMID: 27384267
16. Gingras AR, Bate N, Goult BT, Patel B, Kopp PM, Emsley J, et al. Central region of talin has a unique fold that binds vinculin and actin. The Journal of biological chemistry. 2010; 285(38):29577–87. https://doi.org/10.1074/jbc.M109.095455 PMID: 20610383; PubMed Central PMCID: PMC2937989.
17. Theodosiou M, Widmaier M, Bottcher RT, Rognoni E, Veelders M, Bharadwaj M, et al. Kindlin-2 cooperates with talin to activate integrins and induces cell spreading by directly binding paxillin. eLife. 2016; 5:24. doi: 10.7554/eLife.10130. WOS:000369061200001. PMID: 26821125
18. Cumming RC, Andon NL, Haynes PA, Park M, Fischer WH, Schubert D. Protein Disulfide Bond Formation in the Cytoplasm during Oxidative Stress. Journal of Biological Chemistry. 2004; 279(21):21749–58. https://doi.org/10.1074/jbc.M312267200 PMID: 15031298
19. Hatori Y, Inouye S, Akagi R, Seyama T. Local redox environment beneath biological membranes probed by palmitoylated-roGFP. Redox Biol. 2018; 14:679–85. https://doi.org/10.1016/j.redox.2017.11.015 PMID: 29179107; PubMed Central PMCID: PMCPMC5704182.

20. Wettschureck N, Offermanns S. Rho/Rho-kinase mediated signaling in physiology and pathophysiology. Journal of Molecular Medicine. 2002; 80(10):629–38. https://doi.org/10.1007/s00109-002-0370-2 PMID: 12395147

21. Retamal MA, Schalper KA, Shoji KF, Bennett MV, Saez JC. Opening of connexin 43 hemichannels is increased by lowering intracellular redox potential. Proc Natl Acad Sci U S A. 2007; 104(20):8322–7. https://doi.org/10.1073/pnas.0702456104 PMID: 17494739; PubMed Central PMCID: PMCPMC1895948.

22. Chronopoulos A, Robinson B, Sarper M, Cortes E, Auernheimer V, Lachowski D, et al. ATRA mechanically reprograms pancreatic stellate cells to suppress matrix remodelling and inhibit cancer cell invasion. Nat Commun. 2016; 7:12630. https://doi.org/10.1038/ncomms12630 PMID: 27600527; PubMed Central PMCID: PMC5023948.

23. Calvo F, Ege N, Grande-Garcia A, Hooper S, Jenkins RP, Chaudhry SI, et al. Mechanotransduction and YAP-dependent matrix remodelling is required for the generation and maintenance of cancer-associated fibroblasts. Nat Cell Biol. 2013; 15(6):637-+. doi: 10.1038/ncb2756. WOS:000319804200014. PMID: 23708000

24. Stamenovic D. Effects of cytoskeletal prestress on cell rheological behavior. Acta Biomater. 2005; 1 (3):255–62. doi: 10.1016/j.actbio.2005.01.004. WOS:000235057100002. PMID: 16701804

25. Carisey A, Tsang R, Greiner AM, Nijenhuis N, Heath N, Nazgiewicz A, et al. Vinculin regulates the recruitment and release of core focal adhesion proteins in a force-dependent manner. Curr Biol. 2013; 23(4):271–81. https://doi.org/10.1016/j.cub.2013.01.009 PMID: 23375895; PubMed Central PMCID: PMC3580286.

26. Rahikainen R, von Essen M, Schaefer M, Qi L, Azizi L, Kelly C, et al. Mechanical stability of talin rod controls cell migration and substrate sensing. Sci Rep-Uk. 2017; 7:3571. doi: 10.1038/s41598-017-03335-2. PMC5472591. PMID: 28620171

27. Grashoff C, Hoffman BD, Brenner MD, Zhou R, Parsons M, Yang MT, et al. Measuring mechanical tension across vinculin reveals regulation of focal adhesion dynamics. Nature. 2010; 466(7303):263–6. https://doi.org/10.1038/nature09198 PMID: 20613844; PubMed Central PMCID: PMC2901888.

28. Kaushik S, Ravi A, Hameed FM, Low BC. Concerted modulation of paxillin dynamics at focal adhesions by deleted in liver cancer-1 and focal adhesion kinase during early cell spreading. Cytoskeleton. 2014; 71(12):677–94. https://doi.org/10.1002/cm.21201 PMID: 25448629.

29. Liotta LA, Kohn EC. The microenvironment of the tumour-host interface. Nature. 2001; 411(6835):375–9. https://doi.org/10.1038/35077241 PMID: 11357145.

30. Glentis A, Oertle P, Mariani P, Chikina A, El Marjou F, Attieh Y, et al. Cancer-associated fibroblasts induce metalloprotease-independent cancer cell invasion of the basement membrane. Nature communications. 2017; 8(1):924. https://doi.org/10.1038/s41467-017-00985-8 PMID: 29030636; PubMed Central PMCID: PMCPMC5640679.

31. Haining AWM, Lieberthal TJ, del Río Hernández A. Talin: a mechanosensitive molecule in health and disease. Faseb J. 2016. https://doi.org/10.1096/fj.201500080R PMID: 27252130

32. Popa I, Berkovich R, Alegre-Cebollada J, Badilla CL, Rivas-Pardo JA, Taniguchi Y, et al. Nanomechanics of HaloTag Tethers. J Am Chem Soc. 2013; 135(34):12762–71. doi: 10.1021/ja4056382. WOS:000323876300048. PMID: 23909704

33. Popa I, Kosuri P, Alegre-Cebollada J, Garcia-Manyes S, Fernandez JM. Force dependency of biochemical reactions measured by single-molecule force-clamp spectroscopy. Nat Protoc. 2013; 8(7):1261–76. https://doi.org/10.1038/nprot.2013.056 PMID: 23744288; PubMed Central PMCID: PMC4676941.

34. Berendsen HJC, Vanderspoel D, Vandrunen R. Gromacs—a Message-Passing Parallel Molecular-Dynamics Implementation. Comput Phys Commun. 1995; 91(1–3):43–56. WOS:A1995TF32200004.

35. Van Der Spoel D, Lindahl E, Hess B, Groenhof G, Mark AE, Berendsen HJ. GROMACS: fast, flexible, and free. J Comput Chem. 2005; 26(16):1701–18. https://doi.org/10.1002/jcc.20291 PMID: 16211538.

36. MacKerell AD, Bashford D, Bellott M, Dunbrack RL, Evanseck JD, Field MJ, et al. All-atom empirical potential for molecular modeling and dynamics studies of proteins. The journal of physical chemistry B. 1998; 102(18):3586–616. https://doi.org/10.1021/jp973084f PMID: 24889800.

37. Jorgensen WL, Madura JD. Quantum and Statistical Studies of Liquids .25. Solvation and Conformation of Methanol in Water. J Am Chem Soc. 1983; 105(6):1407–13. WOS:A1983QH26900001.

38. Bussi G, Donadio D, Parrinello M. Canonical sampling through velocity rescaling. J Chem Phys. 2007; 126(1):014101. https://doi.org/10.1063/1.2408420 PMID: 17212484.

39. Berendsen HJC, Postma JPM, Vangunsteren WF, Dinola A, Haak JR. Molecular-Dynamics with Coupling to an External Bath. J Chem Phys. 1984; 81(8):3684–90. WOS:A1984TQ73500045.

40. Xu WM, Baribault H, Adamson ED. Vinculin knockout results in heart and brain defects during embryonic development. Development. 1998; 125(2):327–37. WOS:000072046900017. PMID: 9486805

41. Franco SJ, Rodgers MA, Perrin BJ, Han J, Bennin DA, Critchley DR, et al. Calpain-mediated proteolysis of talin regulates adhesion dynamics. Nat Cell Biol. 2004; 6(10):977–83. https://doi.org/10.1038/ncb1175 PMID: 15448700.

42. Chan LK, Ko FC, Sze KM, Ng IO, Yam JW. Nuclear-targeted deleted in liver cancer 1 (DLC1) is less efficient in exerting its tumor suppressive activity both in vitro and in vivo. PLoS ONE. 2011; 6(9):e25547. https://doi.org/10.1371/journal.pone.0025547 PMID: 21966542; PubMed Central PMCID: PMC3180446.

43. Cohen DM, Chen H, Johnson RP, Choudhury B, Craig SW. Two distinct head-tail interfaces cooperate to suppress activation of vinculin by talin. The Journal of biological chemistry. 2005; 280(17):17109–17. https://doi.org/10.1074/jbc.M414704200 PMID: 15728584.

44. Meijering E, Dzyubachyk O, Smal I. Methods for Cell and Particle Tracking. Method Enzymol. 2012; 504:183–200. doi: 10.1016/13978-0-12-3918574.00009–4. WOS:000303896400009.

45. Schneider CA, Rasband WS, Eliceiri KW. NIH Image to ImageJ: 25 years of image analysis. Nature methods. 2012; 9(7):671–5. PMID: 22930834; PubMed Central PMCID: PMC5554542.

Atherosclerosis 255 (2016) 43–53

Contents lists available at ScienceDirect

Atherosclerosis

journal homepage: www.elsevier.com/locate/atherosclerosis

Talin and vinculin are downregulated in atherosclerotic plaque; Tampere Vascular Study

Magdaléna von Essen [a, 1], Rolle Rahikainen [a, 1], Niku Oksala [b, c], Emma Raitoharju [b], Ilkka Seppälä [b], Ari Mennander [d], Thanos Sioris [d], Ivana Kholová [e], Norman Klopp [f], Thomas Illig [f, g, h], Pekka J. Karhunen [i], Mika Kähönen [j], Terho Lehtimäki [b, 2], Vesa P. Hytönen [a, *, 2]

[a] BioMediTech, University of Tampere and Fimlab Laboratories, Tampere, Finland
[b] Dep. of Clinical Chemistry, Fimlab Laboratories, Tampere University Hospital and School of Medicine, University of Tampere, Tampere, Finland
[c] Division of Vascular Surgery, Department of Surgery, Tampere University Hospital, Tampere, Finland
[d] Heart Center, Tampere University Hospital, Tampere, Finland
[e] Department of Pathology, Fimlab Laboratories, Tampere University Hospital and School of Medicine, University of Tampere, Tampere, Finland
[f] Hannover Unified Biobank, Hannover Medical School, Hannover, Germany
[g] Institute of Human Genetics, Hannover Medical School, Hannover, Germany
[h] Research Unit of Molecular Epidemiology, Helmholtz Zentrum München, German Research Center for Environmental Health, Neuherberg, Germany
[i] School of Medicine, University of Tampere and Fimlab Laboratories, Tampere University Hospital, Tampere, Finland
[j] Department of Clinical Physiology, Tampere University Hospital and School of Medicine, University of Tampere, Tampere, Finland

ARTICLE INFO

Article history:
Received 9 June 2016
Received in revised form
12 October 2016
Accepted 14 October 2016
Available online 15 October 2016

Keywords:
Mechanobiology
Atherosclerosis
Focal adhesion
Talin
Vinculin

ABSTRACT

Background and aims: Focal adhesions (FA) play an important role in the tissue remodeling and in the maintenance of tissue integrity and homeostasis. Talin and vinculin proteins are among the major constituents of FAs contributing to cellular well-being and intercellular communication.
Methods: Microarray analysis (MA) and qRT-PCR low-density array were implemented to analyze talin-1, talin-2, meta-vinculin and vinculin gene expression in circulating blood and arterial plaque.
Results: All analyzed genes were significantly and consistently downregulated in plaques (carotid, abdominal aortic and femoral regions) compared to left internal thoracic artery (LITA) control. The use of LITA samples as controls for arterial plaque samples was validated using immunohistochemistry by comparing LITA samples with healthy arterial samples from a cadaver. Even though the differences in expression levels between stable and unstable plaques were not statistically significant, we observed further negative tendency in the expression in unstable atherosclerotic plaques. The confocal tissue imaging revealed gradient of talin-1 expression in plaque with reduction close to the vessel lumen. Similar gradient was observed for talin-2 expression in LITA controls but was not detected in plaques. This suggests that impaired tissue mechanostability affects the tissue remodeling and healing capabilities leading to development of unstable plaques.
Conclusions: The central role of talin and vinculin in cell adhesions suggests that the disintegration of the tissue in atherosclerosis could be partially driven by downregulation of these genes, leading to loosening of cell-ECM interactions and remodeling of the tissue.

1. Introduction

Atherosclerosis is a disease of the vasculature with a complex etiology. Risk factors include age, sex, family history, dyslipidemia, high blood pressure and high body mass index (BMI), stress and dietary factors. The disease develops over a long time period and may remain asymptomatic over decades. It is characterized by

* Corresponding author. BioMediTech, Lääkärinkatu 1, FI-33520, Tampere, Finland.
E-mail address: vesa.hytonen@uta.fi (V.P. Hytönen).
[1] These authors contributed equally to this work.
[2] These authors contributed equally to this work.

http://dx.doi.org/10.1016/j.atherosclerosis.2016.10.031
0021-9150/

Abbreviations

BMI	body mass index
CAD	coronary artery disease
ECM	extracellular matter
FA	focal adhesion
FC	focal complex
fc	fold change
HUVEC	human umbilical vein endothelial cell
ICAM	intercellular adhesion molecule
LDA	low density array
LITA	left internal thoracic artery
MA	microarray analysis
MΦ	macrophage
PECAM	platelet endothelial cell adhesion molecule
SMC	smooth muscle cell
TVS	Tampere Vascular Study
VBS	vinculin binding site
VCAM	vascular cell adhesion molecule
FFPE	formalin-fixed, paraffin-embedded
HE	hematoxylin-eosin

chronic inflammation of the arterial wall, by infiltration of macrophages (MΦ) and accumulation of oxidized low-density lipoproteins leading to MΦ conversion to foam cells [1].

The vasculature is continuously exposed to cyclical fluctuations of blood flow, pressure and fluid shear stress and also exhibits diurnal variation. The blood mechanical impacts of varying magnitudes exert significant influences on physiological and pathophysiological processes [2–4]. For illustration, veins and arteries are composed of several tissue layers with different cell and extracellular matter (ECM) content. This cell and ECM composition determines the tissue characteristics in terms of physicochemical properties [5,6]. Hence, each vessel layer possesses different ability to withstand, produce or transduce mechanical forces [5]. The mechanical pressure sensed by the endothelial cells is transferred from the extracellular space through the actin cytoskeletal network towards the nucleus [7,8].

To date, a number of genes implicated in cellular mechanostability and their altered expression has been associated with the progress of atherosclerosis. For example, ADAM metalloprotease disintegrins have been linked with cell-cell/surface adhesion and inflammation progression in the atherosclerotic plaque [9]. Moreover, the expression levels of integrin and kindlin family proteins were found to be altered in progressing atherosclerotic plaques [10]. Intergrin and kindlin proteins support leukocyte adhesion, transendothelial migration, platelet aggregation and thrombosis. Furthermore, integrins and kindlins are together with talin and vinculin among the major components of focal adhesions (FA). FAs are key attachments between cells and ECM and play an important role in cell morphology, differentiation, locomotion and intercellular communication. FAs are crucial for the tissue remodeling, integrity and homeostasis through the maintenance of intercellular gaps and cell adhesion supervision.

Talin is a large flexible protein [11] binding to transmembrane integrins (N-terminal FERM domain) [12] and to cytoskeletal actin (C-terminal rod) [13] providing a vital link between the intra- and extracellular space and allowing the communication between the ECM and nucleus [8]. Talin plays a significant role in the actin filament assembly and in spreading and migration of various cell types. During the adhesion maturation, talin recruits vinculin to crosslink with F-actin filaments and stabilize the adhesion complex. For this purpose talin rod contains several binding sites for vinculin [14]. Vinculin binding sites (VBSs) are buried inside the structural bundles and require a major conformational change in the bundle organization prior to vinculin binding [15]. Mechanical force has been suspected to mediate such domain reorganization and talin-vinculin binding [16,17]. Talin interacts with several ligands making it a vital component of numerous mechanosensor and chemical signaling pathways [18–21].

Vinculin is a cytoskeletal protein crosslinking talin and F-actin. Vinculin is ubiquitously expressed with high expression in skeletal, cardiac and smooth muscle. Vinculin head at the N-terminal end binds to talin's VBSs [22]. Vinculin tail at the C-terminal end binds F-actin [23]. Also other important interactions of vinculin have been recognized, for example with paxilin [24] and α-actinin [25]. These ligands make vinculin an important contributor to focal adhesion complex, as well as to the cytoskeletal assembly and stability.

The progress and the causatives of atherosclerosis have been intensively investigated during the past decades. Still, the mechanisms behind the disease development are not fully understood. In more detail, the mechanical impact of shear stress on the cell and tissue integrity has risen to attention only recently. We hypothesize that the cellular mechanostability and maintenance of tissue integrity through focal adhesions is an important factor in all stages of atherosclerotic plaque development. We speculate that the function of focal adhesions is compromised by altered expression of cell adhesion proteins talin and vinculin in atherosclerotic plaque as compared to non-atherosclerotic vessel wall.

In this work, we followed talin and vinculin expression in atherosclerotic plaque samples collected in ongoing Tampere Vascular Study (TVS) series. Gene expression in carotid, abdominal aortic and femoral plaque samples was compared to expression values in left internal thoracic artery (LITA) controls. Expression levels were determined by microarray analysis and low-density qRT-PCR-array. Results are supported by smooth muscle cell (SMC) and macrophage (MΦ) marker co-expression analysis. The tissue localization of talin and vinculin was investigated by confocal immunofluorescence study.

2. Materials and methods

2.1. Vascular samples

Arterial sample series from Tampere Vascular Study (TVS) [9,10,26], including samples from femoral, carotid and abdominal aortic regions, were obtained during open vascular procedures between 2005 and 2015. The patients fulfilled the following inclusion criteria: (1) carotid endarterectomy performed because of asymptomatic or symptomatic and hemodynamically significant carotid stenosis (>70%); (2) femoral or (3) aortic endarterectomy with aortoiliac or aortobifemoral bypass based on symptomatic peripheral arterial disease. The left internal thoracic artery (LITA) controls were obtained during coronary artery bypass surgery due to coronary artery disease (CAD). The samples were collected from patients subjected to open vascular surgery in the Division of Vascular Surgery and Heart Center, Tampere University Hospital. The patient's denial to participate in the study was used as a measure of exclusion. The vascular samples were classified according to American Heart Association recommendation [27]. The type V and VI atherosclerotic lesions were further histologically classified as stable and unstable according to the presence of fissure, rupture, hemorrhage or thrombosis. Gene expression was analyzed from carotid ($n = 29$), abdominal aortic ($n = 15$), and femoral ($n = 24$) plaques (cases) and compared to atherosclerosis-

free LITA samples (n = 28) (controls). The study has been approved by the Ethics Committee of Tampere Hospital District. All studies were conducted according to the declaration of Helsinki, with the informed consent from individual patient involved.

2.2. Whole blood and circulating monocyte fractions

TVS whole blood and monocyte fractions were collected during 2008. The angiographically verified samples were selected from a larger population-based cross-sectional study [28] collected between 2001 and 2004 comprising patients subjected to an exercise test at Tampere University Hospital (treatment according to the Finnish Current Care Guidelines). RNA was isolated from the whole blood and monocyte fractions of individuals with CAD (n = 55) and without coronary artery lesions (n = 45). Patient history data were based on hospital records and patient interviews. These data covered the demographics such as age, sex, weight, lifestyle information and classical cardiovascular risk factors and symptoms.

2.3. RNA isolation and microarrays

The fresh arterial tissue samples were soaked in RNALater solution (Ambion Inc, Austin, TX) and isolated with Trizol reagent (Invitrogen, Carlsbad, CA) and the RNAEasy Kit with DNase Set (Qiagen, Valencia, CA). From the whole blood fraction, the RNA was isolated with PAXgene tubes (BD, Franklin Lakes, NJ) and PAXgene Blood RNA Kit (Qiagen) with DNase Set. Peripheral mononuclear cells were isolated from the whole blood samples by Ficoll-Paque density-gradient centrifugation (Amersham Pharmacia Biotech UK Limited, Buckinghamshire, England). Total RNA was then extracted using RNeasy Mini Kit (Qiagen). Manufacturers' instructions were followed in all isolation protocols. The quality of the RNA samples was evaluated spectrophotometrically and stored at −80 °C.

The expression levels of arterial and whole blood samples were analyzed with Illumina HumanHT-12 v3 Expression BeadChip (Illumina, San Diego, CA) analyzing 47,000 transcripts of all known genes, gene candidates, and splice variants. The microarray experiments for the monocyte RNA were performed using Sentrix Human-6 Expression BeadChips analyzing >46,000 transcripts (Illumina). Both arrays were run according to given instructions by the manufacturer and scanned with the Illumina iScan system. Further details of the methodology can be found in work by Turpeinen et al. [29].

2.4. Microarray data analysis

After background subtraction, raw intensity data were exported using the Illumina GenomeStudio software. Raw expression data were imported into R software, log2 transformed and normalized by the locally estimated scatterplot smoothing normalization method implemented in the R/Bioconductor package Lumi. Locally estimated scatterplot smoothing normalization returned the best accuracy to detect differentially expressed genes in comparison with quantitative reverse transcription polymerase chain reaction using the control artery (LITA) and atherosclerotic plaque samples from the TVS study [30]. All samples fulfilled following data quality control criteria; detection of outlier arrays based on the low number of robustly expressed genes and hierarchical clustering. Probes were considered robustly expressed if the detection was $p < 0.05$ for minimum of 50% of the samples in the data set. *TLN1* (microarray element probe ILMN_1696643), *TLN2* (microarray element probe ILMN_1700042) and *VCL* (transcript variant 1, microarray element probe ILMN_1795429; transcript variant 2, microarray element probe ILMN_2413527) genes were selected for differential expression and correlation analyses. These results were further confirmed by low-density qRT-PCR array.

2.5. Low-density qRT-PCR-array (LDA)

The quantitative real-time polymerase chain reaction (qRT-PCR) was performed with TaqMan low-density array (LDAs; Applied Biosystems) according to the manufacturer's instructions. The functionality of TaqMan assays, the optimal amounts of RNA in cDNA synthesis and optimal amount of cDNA in qRT-PCR were first optimized for functional range and validated for inhibition using several concentrations in separate TaqMan assays. Sufficient RNA was available for 19 out of 24 LITAs (79.2%) and 64 out of 68 plaque (94.2%) samples. 60 (30 cases and 30 controls) out of 96 blood samples (62.5%) were selected for analysis based on pairwise matching according to BMI, age, gender and smoking status. In detail, 500 ng of total RNA per sample was transcribed to cDNA using the High Capacity cDNA Kit (Applied Biosystems). For the qPCR, LDAs were loaded with 7 μl cDNA synthesis product (175 ng of RNA), 43 μl H_2O and 50 μl PCR Universal Master Mix (Applied Biosystems). The array contained technical triplicates. Glyceraldehyde-3-phosphate dehydrogenase (GAPDH, assayID Hs99999905_m1) was used as housekeeping gene control. The qRT-PCR data was analyzed with Expression suite software (Applied biosystems) using the 2-ΔΔCT method.

2.6. Hierarchical clustering and correlation analyses

TLN1, *TLN2*, *VCL* and well-characterized biomarkers of inflammation (cluster of differentiation 68 (CD68) and arachidonate 5-lipoxygenase (ALOX5)), and SMCs markers (calponin 1 (CNN1), smoothelin (SMTN)) [31] were used in the hierarchical clustering analysis to assess whether subgroups of samples had similar marker profiles. Furthermore, similarity of the expression levels (*TLN1*, *TLN2* and *VCL*) across the samples was studied. The procedure was performed using the heatmap.2 function from the gplots R library on all 68 artery samples. Pearson dissimilarity and average linkage were used for the hierarchical clustering of both genes and samples. To further investigate the *TLN1*, *TLN2* and *VCL* genes as measures of plaque cell composition, correlation analyses were performed using previously established macrophage and SMC-rich plaque signatures [31].

2.7. Confocal immunofluorescence study of frozen and paraffin-embedded samples

For immunofluorescence labeling of frozen tissue sections, vascular samples from LITA and from atherosclerotic carotid artery were embedded into TissueTek O.C.T compound (Sakura Finetek, USA), frozen in liquid nitrogen and stored at −80 °C. Leica CM 3050S (Leica Biosystems, Nussloch, Germany) cryostat was used to cut 6 μm sections of the frozen tissues. Before antibody staining, the tissue sections were air-dried at room temperature for 20 min and fixed with acetone at −20 °C for 10 min. Fixed samples were air-dried for 15 min at room temperature, immersed into PBS (pH 7.4) and transferred to Shandon Sequenza (Thermo Shandon Ltd, Runcorn, UK) immunostaining cassettes. Nonspecific antibody binding was blocked by preincubating the tissue sections in blocking buffer containing 1% BSA and 0.3% Triton-X100 diluted in PBS (pH 7.4). All antibodies were diluted into the blocking buffer. The following primary antibodies were used to detect adhesion proteins and vascular cell markers in adjacent sections: mouse-anti-human PECAM-1 antibody (CD31, clone JC70A, Dako Agilent Technologies, Glostrup, Denmark) diluted 1:20 was used as a marker of endothelial cells, rabbit-anti-human Tal1 (clone ab71333,

Abcam, Cambridge, UK) diluted 1:80 was used for talin-1, mouse-anti-human Tal2, (clone 68E7, Cancer Research Technology, London, UK) diluted 1:100 was used for talin-2 and rabbit anti human Vin (clone ab61186, Abcam, Cambridge, UK) diluted 1:50 was used vinculin. Samples were incubated with diluted primary antibodies at +4 °C overnight, followed by washing 3 times with PBS. AlexaFluor-568 labeled goat-anti-mouse IgG (Cat # A11004, Thermo Fisher Scientific) and AlexaFluor-488 labeled donkey-anti-rabbit IgG (Cat # A21206, Thermo Fisher Scientific) antibodies diluted 1:100 were incubated on the samples for 1 h at room temperature to detect the bound primary antibodies. Immunostained samples were washed 5 times with PBS, followed by one wash with deionized water. Glass coverslips were mounted on the samples by using Prolong Diamond (Cat # P36962, Thermo Fisher Scientific) containing DAPI for nuclear staining.

For immunofluorescence staining of formalin-fixed and paraffin-embedded (FFPE) samples, 4 μm sections were cut from paraffin-embedded samples of LITA and healthy carotid artery and abdominal aorta. Samples of LITA were collected from patients diagnosed with atherosclerosis, while the samples of carotid artery and abdominal aorta were collected from a cadaver with no coronary artery disease. Hematoxylin-eosin (HE) stained tissue sections were used to confirm normal tissue morphology of these samples. All tissue sections were deparaffinized and rehydrated by incubating them in xylene and in 99%, 95%, 70% and 50% ethanol solution for 10 min in each. For antigen retrieval, tissue sections were boiled in 10 mM sodium citrate buffer (pH 6) with 0.05% Tween-20 for 20 min in a microwave oven and allowed to slowly cool back to room temperature. Samples were washed 3 times with PBS (pH 7.4) and treated with 0.1% Sudan Black B for 20 min at room temperature to quench tissue autofluorescence. Samples were washed 3 times 10 min with PBS and immunostained using the same methods used for the frozen tissue sections. Antibody specificity was confirmed by using control samples with no primary antibodies.

The immunolabeled sections were examined under a laser scanning confocal microscope (Zeiss Cell Observer.Z1 equipped with a 63x/NA 1.4 oil immersion objective and Zeiss LSM780 confocal unit, Carl Zeiss Microscopy, Jena, Germany). For fluorophore excitation, 480 nm argon laser and 405 nm and 561 nm diode lasers were used together with suitable filter sets. For comparative analysis, the laser intensities, PMT gains and other settings were kept constant for all samples. Serial plane images were collected throughout the whole thickness of the sample at 200 nm intervals. During image processing, maximum intensity projections were used to extract high intensity areas from the image stacks into single images.

2.8. Statistical analyses

Statistical analyses were performed using R version 2.15.0. To estimate fold changes between groups in microarray analysis (MA), differences between medians (in log2 scale) were calculated. The log ratios were back-transformed to fold changes. To ease the interpretation, fold-change values < 1 were replaced by the negative of its inverse. Statistical significance of differences in gene expression was assessed using the nonparametric Wilcoxon signed-rank test and the log-transformed data. For associations between *TLN1*, *TLN2*, *meta-VCL* and *VCL* expression levels and SMC-rich plaque/macrophage markers, the Spearman correlation coefficient was used. To test the effect of covariates on expression levels of *TLN1*, *TLN2*, *meta-VCL* and *VCL*, Wilcoxon rank-sum test and Spearman correlation were used. The associations between covariates and expression levels were tested in the atherosclerotic plaque and LITA samples separately and were considered significant when $p < 0.05/42$ to 0.001 according to the Bonferroni correction for multiple testing. Differences were considered significant when $p < 0.05$.

2.9. Limitations of the study

Due to the poor availability of control arterial samples from healthy persons with no coronary artery disease, LITA samples obtained during coronary artery bypass surgery were used as controls for the studied plaque samples. LITA samples were collected from patients diagnosed with coronary artery disease. Therefore, the levels of talin-1, talin-2 and vinculin transcript expression profiles in LITA may not exactly match their expression profile in artery samples from healthy subjects with no diagnosed CAD. Therefore, immunostaining of talin-1 was used to confirm similar expression pattern of talin-1 in the LITA samples from CAD patients and in artery samples from a healthy subject (Fig. 4). In addition, similar artery morphology for these samples was confirmed by observing tissue sections with HE-staining (Fig. 4). Another limitation of our study is the relatively small sample group size used. The small sample group size results from the poor availability of suitable patient samples and it was taken into consideration in the interpretation of the results.

3. Results

3.1. Characteristics of the subjects and studied samples

The demographics and risk factors of studied population are presented in Table 1. All internal arteries used as controls were verified microscopically as normal. Body mass index, occurrence of hypercholesterolemia, high blood pressure, coronary artery disease and history of myocardial infarction differed significantly between control group and group with atherosclerotic plaques. For mononuclear and whole blood analysis, patients with coronary artery disease considered as case group differed significantly in hypercholesterolemia occurrence, statin medication use and history of myocardial infarction from the control group. Because of these significant differences in the population, the gene expression was analyzed separately between these groups.

3.2. Talin-1, talin-2 and vinculin transcripts are robustly expressed in left internal thoracic artery (LITA) controls with significant reduction in plaques

The gene expression profiles of talin-1, talin-2 and vinculin were investigated to understand the molecular mechanisms behind atherosclerosis. All three transcripts were robustly expressed in LITA samples (Supplementary Table 1A) and in all plaque samples of the three analyzed arterial beds (Supplementary Table 1B). Microarray analysis (MA) and low-density qRT-PCR (LDA) array showed that all tested talin and vinculin transcripts were downregulated in atherosclerotic plaques (fc < −1.6, for all plaques, with MA and LDA, $p < 0.00001$ (Supplementary Table 2, Fig. 1A–D). In more detail, all transcripts were downregulated in plaques of carotid, abdominal aortic and femoral arterial beds in comparison to LITA (Supplementary Table 2, Fig. 1E–H). The downregulation of talin-1 and talin-2 was most substantial in femoral plaques in comparison to LITA, whilst meta-vinculin was most downregulated in carotid plaques and vinculin in abdominal aortic plaques in comparison to LITA.

Table 1
Demographics and risk factors of the study patients included in the Tampere Vascular Study [10].

	Arterial	Plaque	Mononuclear/whole blood	
	Control	Case	CAD Control	CAD Case
No. of subjects	24	68	44	52
Age, y (median, SD)	69.0 (8.6)	70.0 (10.4)	57.0 (8.6)	56.5 (8.6)
Men (%)	82.1	67,6	63.0	61.5
Body mass index, kg/m^2 (median, SD)	28.2 (5.1)	26.0 (4.0)*	27.7 (4.2)	26.9 (4.3)
History of smoking, %	64.3	75.0	53.3	65.4
Diabetes mellitus, %	32.1	23.5	8.7	19.2
Hypercholesterolemia, %	85.7	67.6*	52.2	76.9*
Hypertension, %	100.0	82.4*	84.8	96.2
Antihypertensive medication, %	92.9	80.9	80.4	92.3
Statin medication, %	82.1	73.5	20.4	73.1*
Coronary artery disease, %	100.0	29.4**	0.0	100.0***
Myocardial infarction, %	40.7	13.2*	23.9	57.7***

Pearson Chi-square test and Wilcoxon signed-rank test was used for categorical and continuous risk factors, respectively. $p < 0.05^{*}$, $p < 0.01^{**}$, $p < 0.001^{***}$.

3.3. Expression of talin-1, talin-2 and vinculin transcripts is downregulated in both stable and unstable atherosclerotic plaques

We further characterized the expression profiles as a function of disease progression. According to microarray analysis, all tested transcripts were downregulated in all plaques in comparison with LITA controls (Supplementary Table 2, Fig. 1A–D). Even though no significant reduction was observed between the stable and unstable atherosclerotic plaque, a negative tendency in expression was seen for talin-1, talin-2 and meta-vinculin between the stable and unstable plaques (Fig. 1A–D).

3.4. Talin-1 and vinculin transcripts are expressed in whole blood and circulating monocytes

In order to evaluate if the expression profiles could be monitored using blood samples, whole blood and circulating monocytes were analyzed. Talin-1, meta-vinculin and vinculin were robustly expressed in whole blood samples while talin-2 was not detected in whole blood (Supplementary Table 1A). No significant difference

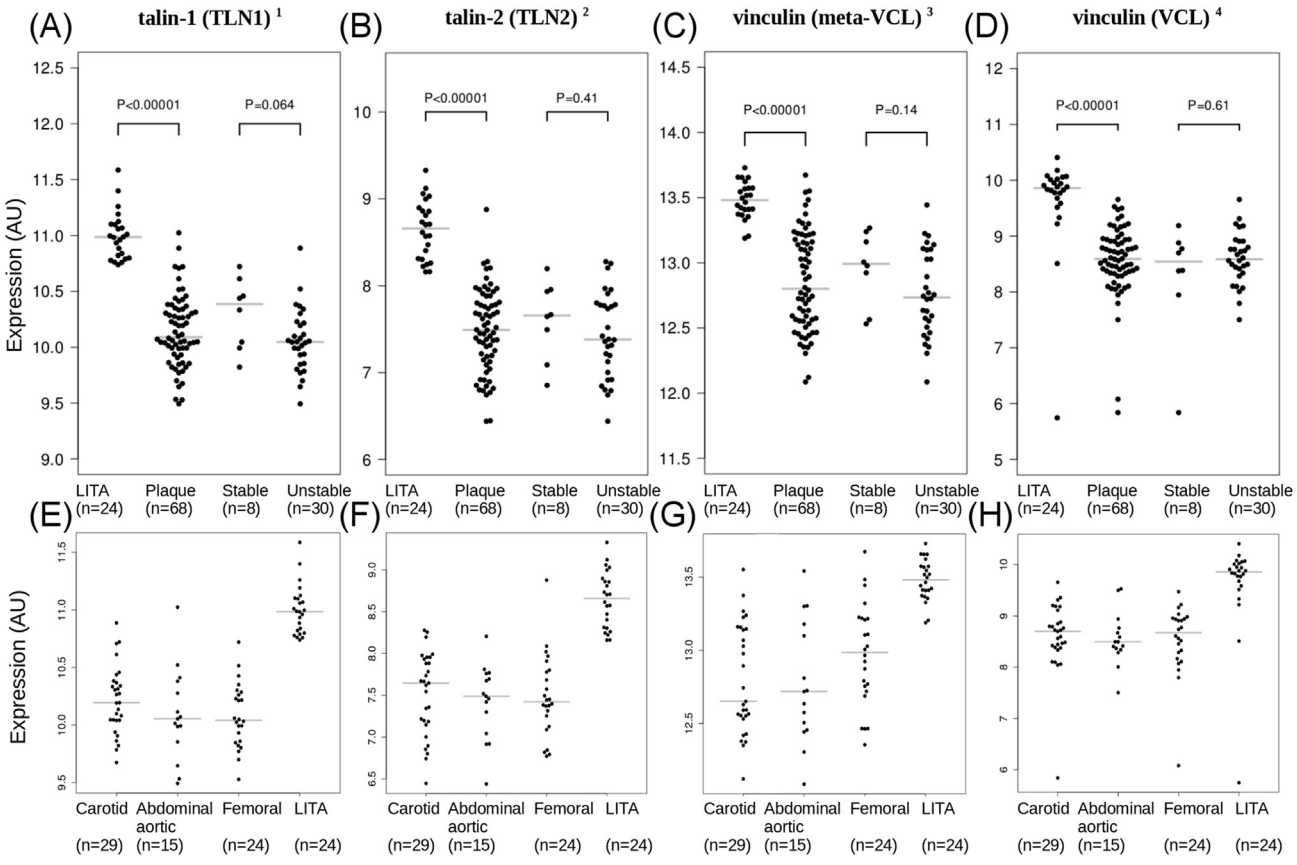

[1] ILMN_1696643, [2] ILMN_1700042, [3] ILMN_1795429, [4] ILMN_2413527

Fig. 1. Expression of talin (*TLN*) and vinculin (*VCL*) transcripts. Results of microarray analysis (MA). (A–D) Expression levels in LITA controls and all, stable and unstable atherosclerotic plaques. (E–H) Expression levels in carotid, abdominal aortic and femoral arterial bed compared to LITA controls.

was observed between patients with history of coronary artery disease (CAD) and controls in the whole blood expression levels of talin-1, talin-2, meta-vinculin and vinculin in MA (fold change (fc) = −1.01–1.03, for all, $p > 0.3$) or in LDA analysis (fold change (fc) = −1.13–1.05, for all, $p > 0.3$). Moreover, no significant differences were observed in the whole blood samples of the patients with hypercholesterolemia, statin usage or patients with myocardial infarction. Expression in circulating monocytes was statistically insignificant between controls and CAD patients for talin-1, talin-2, meta-vinculin or vinculin transcripts. Nominally significantly reduced expression was however observed for patients with myocardial infarction events for talin-1 (fc = −1.13, $p = 0.026$) and for vinculin (fc = −1.12, $p = 0.03$) in circulating monocytes. However, no associations between gene expression and clinical risk factors remained statistically significant after correcting for multiple testing.

3.5. Hierarchical clustering analysis; association of talin-1, talin-2 and vinculin transcripts with SMC and inflammation markers

Hierarchical clustering based on the expression of the two inflammatory and two SMC markers showed distinct separation of plaque samples from the LITA controls. Expression of talin-1, talin-2 and vinculin was dependent on expression of SMC markers (*CNN1* and *SMTN*). Furthermore, high expression of *TLN1*, *TLN2*, *VCL* and SMC markers with low expression of inflammatory biomarkers *CD68* and *ALOX5* was observed in LITA controls (Fig. 2). Also plaque samples of all tested arterial beds separated into two distinct branches of the dendrogram. The samples exhibiting greater reduction in *TLN1*, *TLN2* and *VCL* expression contained mainly carotid arterial samples, whereas majority of femoral arterial beds showed smaller changes in the expression reduction.

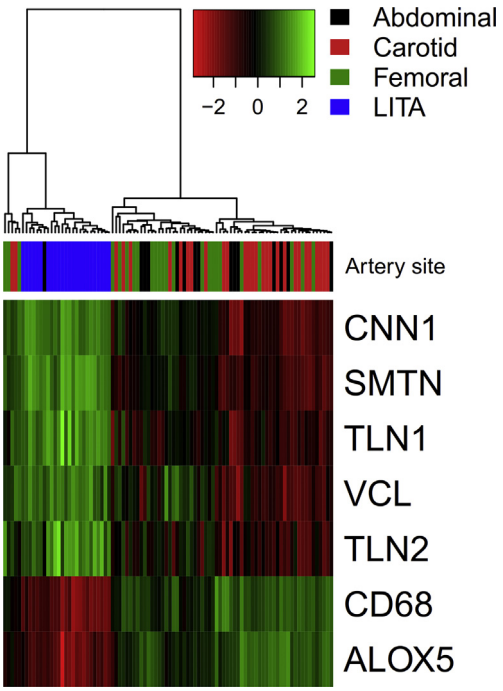

Fig. 2. Heat maps of log2 expression values. Talin-1 (*TLN1*), talin-2 (*TLN2*) and vinculin (*VCL*) co-expression with biomarkers of inflammation (*CD68*, *ALOX5*) and smooth muscle cells markers (*CNN1*, *SMTN*). The expression values of each row (gene) are scaled to z-scores, color-code for expression values and arterial site is presented in the top-right corner. The dendrogram illustrates hierarchical clustering based on the seven robustly expressed genes. The top bar represents the arterial site origin of the sample tissue.

3.6. Talin-1, talin-2 and vinculin transcripts expression levels correlate with SMC-rich atherosclerotic plaque signature

To study the connection between gene expression and plaque composition, the expression profiles were correlated with the known markers of smooth muscle cells (SMC). Utilizing markers of M1 and M2 macrophages and SMC-rich plaque signature, we found that *talin-1*, *talin-2* and both *vinculin* transcripts correlate positively with SMC-rich plaque signature and in majority negatively with M1 and M2 macrophage signatures (Supplementary Fig. 1).

3.7. Talin-1, talin-2 and vinculin localization in the atherosclerotic plaque cells according to confocal immunofluorescence analysis

To get information about the protein localization within the blood vessel samples, immunofluorescence staining of frozen tissue sections from atherosclerotic plaque and LITA controls were used to study adhesion protein localization and expression in advanced disease. Talin-1 was found to be highly expressed in the vascular endothelial cells of LITA samples (Fig. 3A). On the contrary, talin-1 staining was not observed in the endothelial cells of an atherosclerotic artery. Furthermore, in the thickened tunica intima (I) underlying the endothelial cells, gradual increase in talin-1 expression was seen towards tunica media (M).

Antibody staining for talin-2 was observed to only partially colocalize with talin-1 staining in the tunica intima (I) and tunica media (M) in LITA samples (Fig. 3B). Interestingly, in tunica media of LITA controls, talin-2 expression was higher in the luminal side and gradually decreased towards tunica adventitia (A). In plaque samples, talin-2 expression in the endothelial cells was decreased, but not to the same extent as talin-1 expression. In LITA samples, vinculin was found to be expressed in both tunica intima (I) and tunica media (M), but not in tunica adventitia (A).

In tunica media, vinculin expression was higher close to the lumen and lower deeper inside the vessel wall (Fig. 3C). In plaque samples, decreased expression of vinculin in endothelial cells was observed, but in the lower parts of the thickened intima vinculin was still expressed. As expected, the expression of endothelial adhesion molecule PECAM-1 was found to be higher in the endothelium of atherosclerotic plaques compared to the control samples from healthy arteries [32] (Fig. 3A, C).

3.8. Samples from LITA and healthy carotid artery and abdominal aorta show similar tissue morphology and talin-1 expression patterns

To confirm similar tissue morphology and talin-1 expression patterns in healthy carotid artery and abdominal aorta and in the LITA samples used as a control in this study, tissue sections of formalin-fixed and paraffin-embedded (FFPE) samples were stained with talin-1 antibody and hematoxylin-eosin (HE) staining. Immunofluorescence staining of FFPE samples with talin-1 antibody showed strong specific staining of talin-1 in tunica intima (I) and tunica media (M) in samples from LITA and from healthy carotid artery and abdominal aorta (Fig. 4). Similarly to the sections from frozen LITA, the analyzed FFPE sections from LITA or healthy arteries showed uniform talin-1 staining intensity, suggesting that the talin-1 gradient observed in plaque samples is unique feature. In addition, HE staining of the FFPE samples showed similar tissue morphology for samples from LITA and carotid artery and abdominal aorta (Fig. 4). These experiments confirm the feasibility of using LITA samples from CAD patients as negative controls for samples from atherosclerotic plaques when studying expression patterns of focal adhesion proteins.

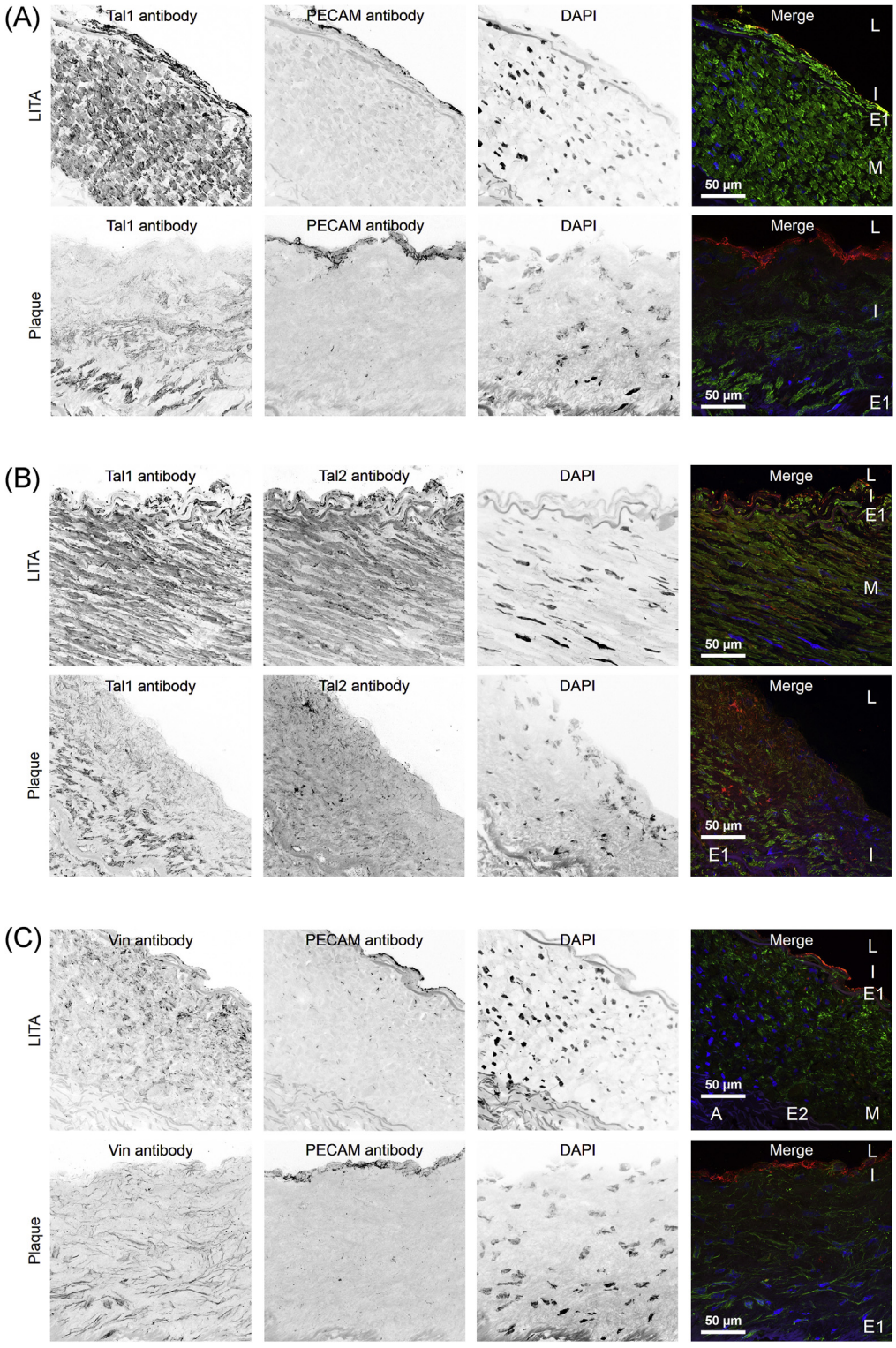

Fig. 3. Tissue localization of talin-1, talin-2 and vinculin in atherosclerotic plaque from carotid artery and left internal thoracic (LITA) control. (A) Talin-1 and PECAM-1, (B) talin-1 and talin-2, (C) vinculin and PECAM-1. Talin-1 was expressed in the endothelial cells of LITA, while talin-1 expression in plaque endothelial cells was not observed (A). Talin-2 expression was decreased in plaque endothelium as compared to LITA, but not as strongly as talin-1 expression (B). In LITA, high vinculin expression was observed in tunica intima and at the lumenal side of tunica media. In plaque samples, decreased vinculin expression was observed in the thickened tunica intima (C). PECAM-1 expression was found to be increased in plaque endothelium (A, C). L, lumen; I, tunica intima; E1, internal elastic lamina; E2, external elastic lamina; M, tunica media; A, tunica adventitia.

4. Discussion

In this study, we show for the first time that the gene expression of talin-1, talin-2, meta-vinculin and vinculin is significantly reduced in atherosclerotic plaques. Significant downregulation of expression was observed in all of the studied carotid, abdominal aortic and femoral arterial beds compared to LITA controls. However, expression of neither gene was changed in circulating

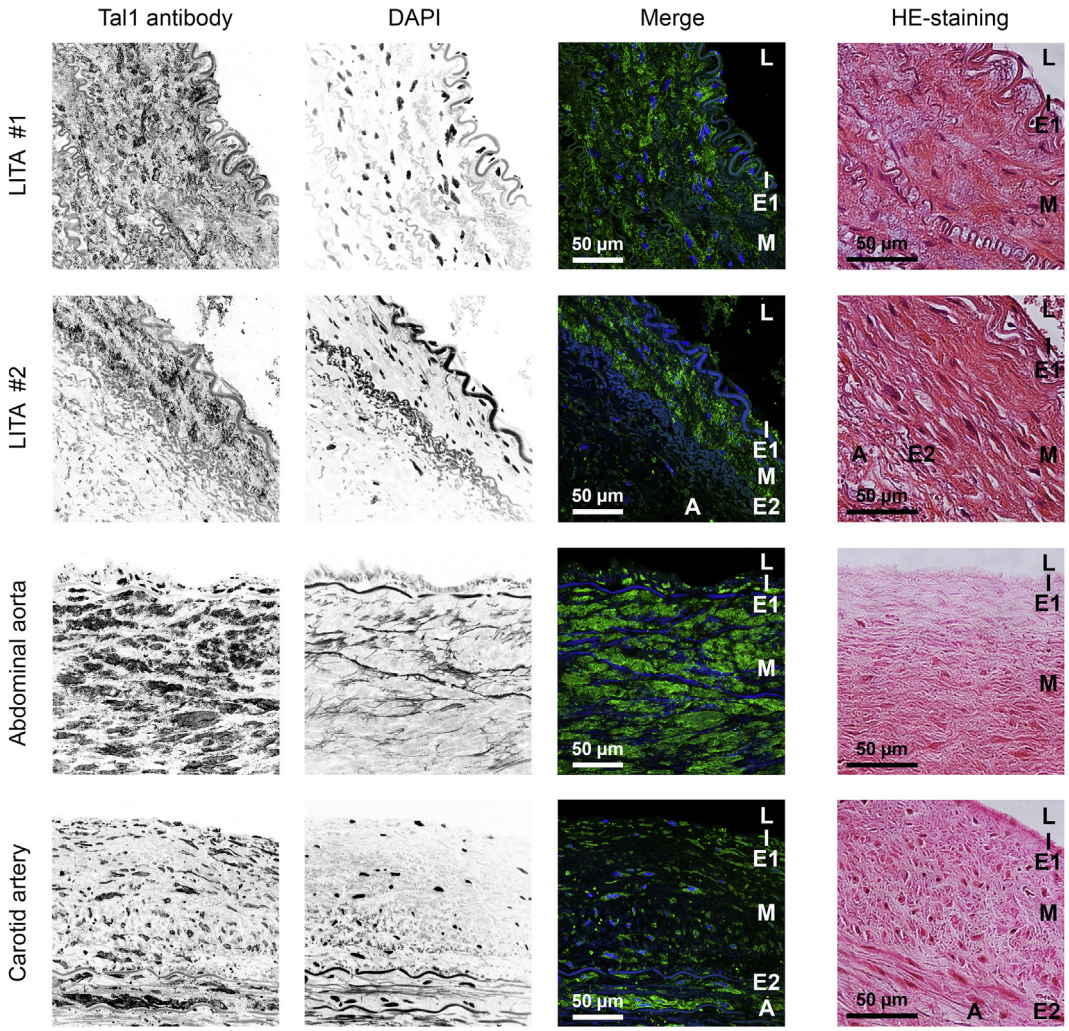

Fig. 4. Tissue morphology and localization of talin-1 in immunostained FFPE sections of LITA from patients with coronary artery disease and in sections of healthy abdominal aorta and carotid artery. Uniform talin-1 immunostaining was observed in tunica intima and tunica media in both immunostained LITA samples, as well as in the samples from healthy abdominal aorta and carotid artery. HE-staining showed normal tissue morphology for all of the analyzed samples. In the merged images, talin-1 immunostaining is shown as green and DAPI chromatin staining as blue. L, lumen; I, tunica intima; E1, internal elastic lamina; E2, external elastic lamina; M, tunica media; A, tunica adventitia. (For interpretation of the references to colour in this figure legend, the reader is referred to the web version of this article.)

monocytes or in whole blood samples in CAD patients compared to controls.

We speculate that reduction in talin-1 expression in the endothelium may be one of the initial triggers for the atherosclerotic plaque formation (Fig. 5). Such downregulation could be caused by an external factor such as altered shear stress and increased blood pressure. It has long been suspected that the mechanosensing and mechanotransduction affects the DNA packing and may contribute to changes in the protein expression in health and in disease [33,34]. Another reason may lie in the mutation affected control of gene expression levels leading to changes in the cell mechanobiology and susceptibility to plaque development. In addition, recently the importance of miRNAs in the regulation of gene expression in endothelial dysfunction has become evident, as discussed by Novák et al. [35]. Furthermore, one of the contributing factors of detected downregulation in this study may be the changed cell composition in the advanced atherosclerotic plaque which can be seen on the confocal images. Changes in acting mechanical force may also alter the signaling pathways related to focal adhesions and affect the expression levels. In connection to atherosclerosis, the magnitude of shear stress was shown to affect the expression of adhesion molecules facilitating endothelial cell-leukocyte adhesion at the vascular lumen (vascular cell adhesion molecule (VCAM), intercellular cell adhesion molecule (ICAM) or platelet endothelial cell adhesion molecule (PECAM) [32,36]. Our previous studies have also shown that the focal adhesions are compromised by reduced expression of integrin family proteins and kindlin-2 in the endothelium and SMCs in the atherosclerotic plaque (*ITGA1*, *ITGAV*, *ITGB1*, *ITGB3*, *ITGB5*, *FERMT2*), while the leukocyte adhesion is accelerated by increased expression of leukocyte integrin-B2 and kindlin-3 [10]. The exact reasons for the observed reduction of the talin and vinculin expression level remain, however, unclear and require attention in future studies.

Altered expression of talin-1, talin-2, meta-vinculin and vinculin may have severe impact on the cell's ability to withstand varying magnitudes of acting mechanical forces, affect cell locomotion, cell/cell and cell-ECM communication since both talin and vinculin are among the major constituents of the focal adhesion complexes and are essential for cellular well-being [37]. Talin acts as molecular scaffolding protein and may contribute to adhesion signaling via its binding partners, converting mechanical signals to chemical cues [38]. Therefore, a reduction in talin-1 expression could render the

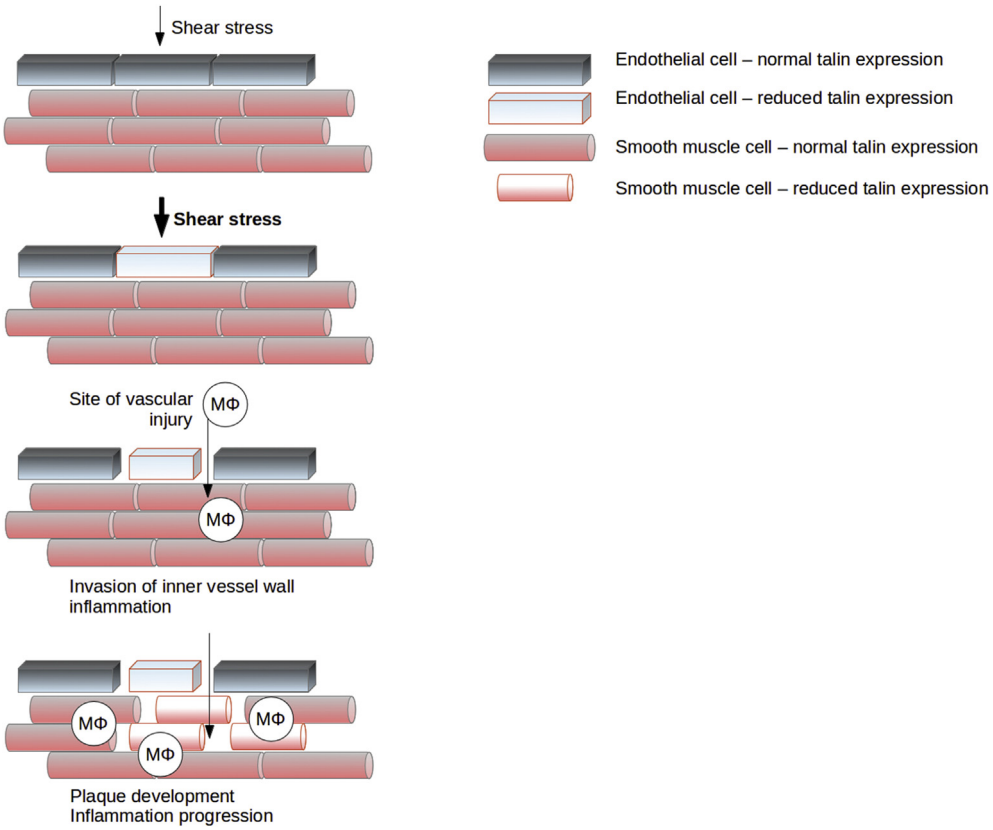

Fig. 5. Simplified speculative model for downregulation of talin expression in vascular endothelium as initial trigger of atherosclerotic plaque formation.

endothelium and the vascular wall prone to endothelial injury compared to mechanically stable endothelial cell [39]. Endothelial injury triggers leukocyte adhesion and promotes inflammatory response at the intima due to exposure of subendothelial collagen and other ECM components. Confocal microscopy images of atherosclerotic plaque show increased PECAM-1 staining in the intima, which points to increased leukocyte adhesion molecules and progression of inflammation at the intima.

In addition, endothelium functions as a barrier for large molecules to enter the vessel wall and trigger pathological processes in the inner vessel layers [40,41]. In other words, the mechanostability of endothelial cells including the endothelial intercellular gap and tight junction maintenance is crucial for healthy vessel wall. Experiments with talin knockout cells show dramatically decreased capability of cells to adhere, revealing the central role of talin in mediating the intracellular-extracellular connection. The reduction in talin-1, talin-2, meta-vinculin and vinculin expression in the endothelium may affect the ability of endothelial cells to adhere to each other and to ECM to form consistent blood-tissue barrier. This could allow the inflammatory agents to progress into the tunica media and trigger macrophage accumulation in the intima and media leading to arterial wall thickening and plaque formation. Such effect can be observed in the presented tissue images where plaque staining shows dramatically thickened intima layer with gross disorganization of the cells and low talin-1 and talin-2 intensity (reduced expression of talin-1 and talin-2 in plaque sample).

Studies by others have also shown the importance of talin-1 and talin-2 for cell, tissue and organ development [42,43]. Such importance of talin proteins on development was illustrated by talin-1 knockout experiments in HUVEC cells [44,45] leading to severe phenotypes in mice embryos. The phenotype is represented by abnormal vascular development affecting the growth of other major tissues [45]. Furthermore, increased talin-1 expression has been detected in aggressive cancers as well as in hypertrophic myocardium and failing heart [46–48]. Even though the downregulation of neither talin-1 nor talin-2 has been to date directly linked to or associated with a disease, the reduced expression may affect the vessel tissue formation, remodeling or healing and recovery. The confocal images of the atherosclerotic plaque show gross disorganization of the cells in the vessel wall. Such additional effects may lead into worsening of the site inflammation and progress of the disease to severe, unstable atherosclerotic plaques. Even though the difference in expression between stable and unstable atherosclerotic plaque reported here was not significant for the investigated transcripts, negative tendency in expression levels was observed for talin-1, talin-2 and meta-vinculin. This suggests that the expression of these genes is further reduced in the advanced disease.

The expression of talin-1 and talin-2 may also differ among the cells depending on the position in the vessel wall layer. As can be seen in the talin-2 LITA staining, the intensity of talin-2 expression in smooth muscle is higher in the layers closer to the intima where the mechanical impacts are expected higher. Similar stratification has not been observed for talin-1 or vinculin in LITA controls. Whether such stratification in healthy tissue is biologically and physiologically important remains open for further investigation.

Talin-1, talin-2, meta-vinculin and vinculin expression is downregulated in atherosclerotic plaque. Downregulation of expression was observed in plaques from all of the studied peripheral arterial beds (carotid, abdominal aortic and femoral).

The central role of talin in cell adhesion proposes that the

disintegration of the tissue in atherosclerosis could be partially driven by downregulation of talin, leading to loosening of cell-ECM interactions and reorganization of the tissue.

In conclusion, we state that proteins contributing to mechanosensing, talin and vinculin, may have important roles in atherosclerotic plaque formation and disease progression.

Conflict of interest

The authors declared they do not have anything to disclose regarding conflict of interest with respect to this manuscript.

Financial support

This work was supported by the Academy of Finland: grants 290506, 273192, 136288 (V.P.H), 286284 (T.L.), 285902 (E.R.), 134309; the Tampere University Hospital Medical Funds (grant X51001 (T.L), 9S054 (E.R) and X51410 (V.P.H)); the Finnish Foundation for Cardiovascular Research (T.L.); the Finnish Cultural Foundation (R.R.); the Tampere Tuberculosis Foundation (T.L. and N.O.); the Emil Aaltonen Foundation (T.L. and N.O.); and the Yrjö Jahnsson Foundation (T.L. and N.O.). This work was also supported by the European Union 7th Framework Programme funding for the AtheroRemo project [201668] and Fimlab Laboratories. We thank the University of Tampere for financial support via the TGPBB graduate school (M.v.E.).

Appendix A. Supplementary data

Supplementary data related to this article can be found at http://dx.doi.org/10.1016/j.atherosclerosis.2016.10.031.

References

[1] A.S. Antonov, F.D. Kolodgie, D.H. Munn, R.G. Gerrity, Regulation of macrophage foam cell formation by alphaVbeta3 integrin: potential role in human atherosclerosis, Am. J. Pathol. 165 (1) (2004) 247–258.
[2] P.F. Davies, Flow-mediated endothelial mechanotransduction, Physiol. Rev. 75 (3) (1995) 519–560.
[3] W.C. Aird, Endothelial cell heterogeneity, Cold Spring Harb. Perspect. Med. 2 (1) (2012) a006429.
[4] W.C. Aird, Spatial and temporal dynamics of the endothelium, J. Thromb. Haemost. 3 (2005) 1392–1406.
[5] J.P. Califano, C.A. Reinhart-King, Exogenous and endogenous force regulation of endothelial cell behavior, J. Biomech. 43 (1) (2010) 79–86.
[6] J.F. Keaney, Atherosclerosis: from lesion formation to plaque activation and endothelial dysfunction, Mol. Asp. Med. 21 (4-5) (2000) 99–166.
[7] T.J. Chancellory, J. Lee, C.K. Thodeti, T. Lele, Actomyosin tension exerted on the nucleus through nesprin-1 connections influences endothelial cell adhesion, migration, and cyclic strain-induced reorientation, Biophys. J. 99 (1) (2010) 115–123.
[8] Z. Jahed, H. Shams, M. Mehrbod, M.R.K. Mofrad, Mechanotransduction pathways linking the extracellular matrix to the nucleus, Int. Rev. Cell Mol. Biol. 310 (171) (2014) e220.
[9] N. Oksala, M. Levula, N. Airla, M. Pelto-Huikko, R.M. Ortiz, O. Järvinen, J.-P. Salenius, B. Ozsait, E. Komurcu-Bayrak, N. Erginel-Unaltuna, A.-P.J. Huovila, L. Kytömäki, J.T. Soini, M. Kähönen, P.J. Karhunen, R. Laaksonen, T. Lehtimäki, ADAM-9, ADAM-15, and ADAM-17 are upregulated in macrophages in advanced human atherosclerotic plaques in aorta and carotid and femoral arteries–Tampere vascular study, Ann. Med. 41 (4) (2009) 279–290.
[10] N. Oksala, J. Pärssinen, I. Seppälä, N. Klopp, T. Illig, R. Laaksonen, M. Levula, E. Raitoharju, I. Kholova, T. Sioris, M. Kähönen, T. Lehtimäki, V.P. Hytönen, Kindlin 3 (FERMT3) is associated with unstable atherosclerotic plaques, anti-inflammatory type II macrophages and upregulation of beta-2 integrins in all major arterial beds, Atherosclerosis 242 (1) (2015) 145–154.
[11] J. Winkler, H. Lünsdorf, B.M. Jockusch, Energy-filtered electron microscopy reveals that talin is a highly flexible protein composed of a series of globular domains, Eur. J. Biochem. 243 (1997) 430–436.
[12] A.R. Gingras, W.H. Ziegler, A.A. Bobkov, M.G. Joyce, D. Fasci, M. Himmel, S. Rothemund, A. Ritter, J.G. Grossmann, B. Patel, N. Bate, B.T. Goult, J. Emsley, I.L. Barsukov, G.C.K. Roberts, R.C. Liddington, M.H. Ginsberg, D.R. Critchley, Structural determinants of integrin binding to the talin rod, J. Biol. Chem. 284 (13) (2009) 8866–8876.
[13] A.R. Gingras, N. Bate, B.T. Goult, L. Hazelwood, I. Canestrelli, J. Gü Nter Grossmann, H. Liu, N. Sm Putz, G.C. Roberts, N. Volkmann, D. Hanein, I.L. Barsukov, D.R. Critchley, The structure of the C-terminal actin-binding domain of talin, EMBO J. 27 (2008) 458–469.
[14] B.T. Goult, A.R. Gingras, N. Bate, I.L. Barsukov, D.R. Critchley, G.C.K. Roberts, The domain structure of talin: residues 1815–1973 form a five-helix bundle containing a cryptic vinculin-binding site, FEBS Lett. 584 (2010) 2237–2241.
[15] E. Papagrigoriou, A.R. Gingras, I.L. Barsukov, N. Bate, I.J. Fillingham, B. Patel, R. Frank, W.H. Ziegler, G.C. Roberts, D.R. Critchley, J. Emsley, Activation of a vinculin-binding site in the talin rod involves rearrangement of a five-helix bundle, EMBO J. 23 (2004) 2942–2951.
[16] V.P. Hytönen, V. Vogel, How force might activate talin's vinculin binding sites: SMD reveals a structural mechanism, PLoS Comput. Biol. 4 (2) (2008) e24.
[17] A. del Rio, R. Perez-Jimenez, R. Liu, P. Roca-Cusachs, J.M. Fernandez, M.P. Sheetz, Stretching single talin rod molecules activates vinculin binding, Science 323 (5914) (2009) 638–641.
[18] B.T. Goult, T. Zacharchenko, N. Bate, R. Tsang, F. Hey, A.R. Gingras, P.R. Elliott, G.C.K. Roberts, C. Ballestrem, D.R. Critchley, I.L. Barsukov, RIAM and vinculin binding to talin are mutually exclusive and regulate adhesion assembly and turnover, J. Biol. Chem. 288 (12) (2013) 8238–8249.
[19] G. Di Paolo, L. Pellegrini, K. Letinic, G. Cestra, R. Zoncu, S. Voronov, S. Chang, J. Guo, M.R. Wenk, P. De Camilli, Recruitment and regulation of phosphatidylinositol phosphate kinase type 1 gamma by the FERM domain of talin, Nature 420 (6911) (2002) 85–89.
[20] G. Luo, A.H. Herrera, R. Horowits, Molecular interactions of N-RAP, a nebulin-related protein of striated muscle myotendon junctions and intercalated disks, Biochemistry 38 (19) (1999) 6135–6143.
[21] N. Sun, D.R. Critchley, D. Paulin, Z. Li, R.M. Robson, Identification of a repeated domain within mammalian alpha-synemin that interacts directly with talin, Exp. Cell Res. 314 (8) (2008) 1839–1849.
[22] R.A. Borgon, C. Vonrhein, G. Bricogne, P.R.J. Bois, T. Izard, Crystal structure of human vinculin, Structure 12 (7) (2004) 1189–1197.
[23] S. Hüttelmaier, P. Bubeck, M. Rüdiger, B.M. Jockusch, Characterization of two F-actin-binding and oligomerization sites in the cell-contact protein vinculin, Eur. J. Biochem. 247 (1997) 1136–1142.
[24] C.K. Wood, C.E. Turner, P. Jackson, D.R. Critchley, Characterisation of the paxillin-binding site and the C-terminal focal adhesion targeting sequence in vinculin, J. Cell Sci. 107 (1994) 709–717.
[25] M. Kroemker, A.H. Rüdiger, B.M. Jockusch, M. Rüdiger, Intramolecular interactions in vinculin control alpha-actinin binding to the vinculin head, FEBS Lett. 355 (1994) 259–262.
[26] N. Oksala, J. Pärssinen, I. Seppälä, E. Raitoharju, I. Kholová, J. Hernesniemi, L.P. Lyytikäinen, M. Levula, K.M. Mäkelä, T. Sioris, M. Kähönen, R. Laaksonen, V. Hytönen, T. Lehtimäki, Association of neuroimmune guidance cue netrin-1 and its chemorepulsive receptor UNC5B with atherosclerotic plaque expression signatures and stability in human(s) Tampere Vascular Study (TVS), Circ. Cardiovasc. Genet. 6 (2013) 579–587.
[27] H.C. Stary, A.B. Chandler, S. Glagov, J.R. Guyton, W. Insull, M.E. Rosenfeld, S.A. Schaffer, C.J. Schwartz, W.D. Wagner, R.W. Wissler, A definition of initial, fatty streak, and intermediate lesions of atherosclerosis. A report from the Committee on Vascular Lesions of the Council on Arteriosclerosis, American Heart Association, Circulation 89 (5) (1994) 2462–2478.
[28] T. Nieminen, R. Lehtinen, J. Viik, T. Lehtimäki, K. Niemelä, K. Nikus, M. Niemi, J. Kallio, T. Kööbi, V. Turjanmaa, M. Kähönen, The Finnish Cardiovascular Study (FINCAVAS): characterising patients with high risk of cardiovascular morbidity and mortality, BMC Cardiovasc. Disord. 6 (1) (2006) 9.
[29] H. Turpeinen, I. Seppälä, L.-P. Lyytikäinen, E. Raitoharju, N. Hutri-Kähönen, M. Levula, N. Oksala, M. Waldenberger, N. Klopp, T. Illig, N. Mononen, R. Laaksonen, O. Raitakari, M. Kähönen, T. Lehtimäki, M. Pesu, A genome-wide expression quantitative trait loci analysis of proprotein convertase subtilisin/kexin enzymes identifies a novel regulatory gene variant for FURIN expression and blood pressure, Hum. Genet. 134 (6) (2015) 627–636.
[30] E. Raitoharju, I. Seppälä, L.P. Lyytikäinen, M. Levula, N. Oksala, N. Klopp, T. Illig, R. Laaksonen, M. Kähönen, T. Lehtimäki, A comparison of the accuracy of Illumina HumanHT-12 v3 Expression BeadChip and TaqMan qRT-PCR gene expression results in patient samples from the Tampere Vascular Study, Atherosclerosis 226 (1) (2013) 149–152.
[31] O. Puig, J. Yuan, S. Stepaniants, R. Zieba, E. Zycband, M. Morris, S. Coulter, X. Yu, J. Menke, J. Woods, F. Chen, D.R. Ramey, X. He, E.A. O'Neill, E. Hailman, D.G. Johns, B.K. Hubbard, P.Y. Lum, S.D. Wright, M.M. DeSouza, A. Plump, V. Reiser, A gene expression signature that classifies human atherosclerotic plaque by relative inflammation status, Circ. Cardiovasc. Genet. 4 (6) (2011) 595–604.
[32] E. Galkina, K. Ley, Vascular adhesion molecules in atherosclerosis, Arterioscler. Thromb. Vasc. Biol. 27 (2007) 2292–2301.
[33] E.K. Yim, M.P. Sheetz, Force-dependent cell signaling in stem cell differentiation, Stem Cell Res. Ther. 3 (5) (2012) 1.
[34] M. Zwerger, C.Y. Ho, J. Lammerding, Nuclear mechanics in disease, Annu. Rev. Biomed. Eng. 13 (2011) 397–428.
[35] J. Novák, V. Olejníčková, N. Tkáčová, G. Santulli, Mechanistic role of microRNAs in coupling lipid metabolism and atherosclerosis, Adv. Exp. Med. Biol. 887 (2015) 79–100.
[36] T. Nagel, N. Resnick, W.J. Atkinson, C.F. Dewey, M.A. Gimbrone, Shear stress selectively upregulates intercellular adhesion molecule-1 expression in cultured human vascular endothelial cells, J. Clin. Investig. 94 (2) (1994) 885–891.

[37] K. Austen, P. Ringer, A. Mehlich, A. Chrostek-Grashoff, C. Kluger, C. Klingner, B. Sabass, R. Zent, M. Rief, C. Grashoff, Extracellular rigidity sensing by talin isoform-specific mechanical linkages, Nat. Cell Biol. 17 (12) (2015) 1597–1606.
[38] V.P. Hytönen, B. Wehrle-Haller, Protein conformation as a regulator of cell-matrix adhesion, Phys. Chem. Chem. Phys. 16 (14) (2014) 6342–6357.
[39] P.F. Davies, Hemodynamic shear stress and the endothelium in cardiovascular pathophysiology, Nat. Clin. Pract. Cardiovasc. Med. 6 (1) (2009) 16–26.
[40] G. Satha, S.B. Lindström, A. Klarbring, G. Satha, S.B. Lindström, A. Klarbring, A. Klarbring, A goal function approach to remodeling of arteries uncovers mechanisms for growth instability, Biomech. Model Mechanobiol. 13 (2014) 1243–1259.
[41] J.M. Tarbell, Shear stress and the endothelial transport barrier, Cardiovasc. Res. 87 (2) (2010) 320–330.
[42] S.J. Monkley, X.H. Zhou, S.J. Kinston, S.M. Giblett, L. Hemmings, H. Priddle, J.E. Brown, C.A. Pritchard, D.R. Critchley, R. Fässler, Disruption of the talin gene arrests mouse development at the gastrulation stage, Dev. Dyn. 219 (4) (2000) 560–574.
[43] F.J. Conti, S.J. Monkley, M.R. Wood, D.R. Critchley, U. Müller, Talin 1 and 2 are required for myoblast fusion, sarcomere assembly and the maintenance of myotendinous junctions, Development 136 (21) (2009) 3597–3606.
[44] P.M. Kopp, N. Bate, T.M. Hansen, N.P.J. Brindle, U. Praekelt, E. Debrand, S. Coleman, D. Mazzeo, B.T. Goult, A.R. Gingras, C.A. Pritchard, D.R. Critchley, S.J. Monkley, Studies on the morphology and spreading of human endothelial cells define key inter- and intramolecular interactions for talin1, Eur. J. Cell Biol. 89 (9) (2010) 661–673.
[45] S.J. Monkley, V. Kostourou, L. Spence, B. Petrich, S. Coleman, M.H. Ginsberg, C.A. Pritchard, D.R. Critchley, Endothelial cell talin1 is essential for embryonic angiogenesis, Dev. Biol. 349 (2) (2011) 494–502.
[46] S. Sakamoto, R.O. McCann, R. Dhir, N. Kyprianou, Talin1 promotes tumor invasion and metastasis via focal adhesion signaling and anoikis resistance, Cancer Res. 70 (5) (2010) 1885–1895.
[47] K. Fang, W. Dai, Y.-H. Ren, Y.-C. Xu, S. Zhang, Y.-B. Qian, Both Talin-1 and Talin-2 correlate with malignancy potential of the human hepatocellular carcinoma MHCC-97 L cell, BMC Cancer 16 (1) (2016) 45.
[48] A.M. Manso, R. Li, S.J. Monkley, N.M. Cruz, S. Ong, D.H. Lao, Y.E. Koshman, Y. Gu, K.L. Peterson, J. Chen, E.D. Abel, A.M. Samarel, D.R. Critchley, R.S. Ross, Talin1 has unique expression versus talin 2 in the heart and modifies the hypertrophic response to pressure overload, J. Biol. Chem. 288 (6) (2013) 4252–4264.